UNIVERSITY OF Hull

Optical sensor for the analysis of biomarkers

Being a Thesis submitted for the Degree of

Doctor of Philosophy (PhD)

In the University of Hull

By

Rana S Al-Shemary

BSc. MSc.

2018

Abstract

The continuous measurement of biomarkers such as proteins and hormones in blood and serum are the cornerstone of healthcare monitoring and optimising treatment plans. Often such biomarkers are present in minute concentrations. Conventional analysis methods involve assays with costly labelled antibodies and lengthy protocols on microtitre well plates. For example fluorescence detection is often favoured for antibody based assays as it is very sensitive, however considerable sample clean-up is required (they will contains interfering materials such as other proteins, salts, etc.) and a protocol is required that requires fluorescence labels. Label-free biosensors are therefore an attractive alternative to improve biomarker analysis. In this work, a label-free optical biosensor was developed based on dye-doped leaky waveguides (DDLW). Chitosan was selected as the porous waveguide material because it has a large surface area, offering the probability of immobilizing a large number of biomolecules, which significantly increases the possibility of capturing target species.

The DDLW biosensor consisted of a 1% of chitosan layer, deposited by spin coating onto a glass substrate from a solution of 0.1 M acetic acid. Reactive Blue 4 dye 100 mM was then incorporated in the chitosan waveguide via reaction with the free amines of the chitosan. The chitosan waveguide on the glass substrate was then sealed within a microfluidics flow cell to allow controlled flushing with reagents. The Reactive Blue 4 dye absorbs light most strongly at the resonance angle and thus generates a dip in reflectivity at that angle which could be used to make measurement

The DDLW sensing mechanism is based on shifts in resonance angle as a result of changes in refractive index in the waveguide, which may change when molecules bind to antibodies immobilised in the waveguide. The surface flatness and thickness of the spin-coated chitosan layer was characterised *via* white light interferometer and a Dektak profiler. The porosity of the waveguide layer is the main factor determining the maximum number of antibodies that can be immobilized in its entire volume. The pore size of the waveguide film needed to be large enough to allow the antibodies to enter the waveguide layer. The pore size of the waveguide layer was tailored using different methodologies. Silica nanoparticles were investigated as well as porogens, but the chemicals required to dissolve the silica nanoparticles and the porogens used were found to damage the chitosan waveguide. Hence, we have developed a facile method of tailoring the porosity of the waveguide layer by controlling a dry time of chitosan to some

extend that can provide a waveguide mode with an enhancement in the porosity of has achieved and shown fascinating results where the pore size was being large enough to different molecular weight of biomolecules. Where we optimised the drying time following different concentrations of chitosan film fabrication by spin coating. The detection method was initially tested using the binding of rabbit IgG to anti-rabbit IgG as a model example. Initially, carboxylic group of the antibody can bind to the amino groups of chitosan film through an activation process using different ratio of EDC-Sulfo-NHS linkage chemistry; the efficiency of immobilisation was investigated with (confocal) fluorescence microscopy, but it was found that the amount of attachment was insufficient. To increase the sensitivity an alternative approach was used in which the antibodies were immobilised into the waveguide layer by first attaching Streptavidin to the amine groups of the chitosan waveguide using glutaraldehyde. Biotinylated anti-rabbit IgG was then immobilised by binding between streptavidin and biotin. Finally, the binding of rabbit-IgG and the immobilised anti-rabbit IgG was studied.

Once the immobilisation chemistry is successfully developed, the waveguide system was intended and used to measure the release of tissue factor (TF) that expressed on pancreatic cell lines. Two types of pancreatic cells (Aspc-1 and Miapaca-2 cells) were used to investigate the concentration of TF in a real-time. There were a strong correlations between the level of TF antigen and activity in these cells, showing that the TF present on the cancer cells was active. The calibration curve of Tissue factor (TF) has been created by preparing a range of TF standard solutions (7.825, 15.65, 31.3, 62.5, 125, 250 pg mL^{-1}) and recorded by ELISA plate reader at 450 nm to inspect the concentration of TF that expressed from unknown sample solutions. The highest expression of tissue factor (107.82 pg mL^{-1}) was recorded on the unknown sample solution of Aspc-1, whereas, TF concentration was very low (57.27 pg mL^{-1}) on unknown sample solution of Miapaca-2 cell lines. A leaky waveguide system was also used to investigate the lowest concentration of TF that released from pancreatic cell lines (7.86 ± 1 pg mL^{-1}) that was expressed on unknown sample solution of Aspc-1 cell lines and (6.89 ± 1 pg mL^{-1}) on unknown sample solution of Miapaca-2 cell lines. Different concentrations of TF standard solutions (0.003, 0.03, 0.3, 3, and 30 pg mL^{-1}) were applied using dye-doped leaky waveguide sensor. Then, the results were compared to the conventional microwell-based ELISA system. In conclusion, when applying lowest concentrations of TF that were expressed on unknown sample solutions of (Aspc-1 and Miapaca-2 cell lines) the degrees of shifting in angles were very close to the shifting in angles of standard solutions TF that were prepared to investigate the detection limit.

Contents

List of Figures

List of Tables

Acknowledgements

Praises to Allah, who made this thesis possible and gave me the ability to proceed successfully. Pursuing a Ph.D. project is a both arduous and enjoyable experience. It's just like climbing a high peak, step by step, accompanied with bitterness, hardships, frustration, encouragement and trust and with so many people's kind help. When I found myself at the top enjoying the beautiful scenery, I realized that it was, in fact, teamwork that got me there. Though it will not be enough to express my gratitude in words to all those people who helped me, I would still like to give my many, many thanks to all these people.

First of all, I'd like to give my sincere thanks to my supervisors Prof. Gillian Greenway, Prof. Nicole Pamme and Dr Ruchi Gupta. They offered me so much advice, patiently supervising me, and always guiding me in the right direction. I've learned a lot from them, without their help I could not have finished my dissertation successfully.

Special thanks are also given to the Iraqi Ministry of Higher Education and Scientific Research (HESR), the Iraqi attaché in London and Ireland, and the University of Babylon for their financial support and encouragement to conduct my study.

I would like to express my sincere gratitude to the Department of Chemistry at the University of Hull for enabling me to pursue postgraduate doctoral training and facilities provided in carrying out this thesis. Special thanks to Sarah Ord for her constant encouragement and support. There are so many friends, both in Iraq and in UK, who offered me so much kindly help. I give my sincere thanks to all these people.

I am very grateful for my parents, their understanding and love encouraged me to work hard and to continue pursuing a Ph.D. They are always let me know they are proud of me, and motivate me to work harder and do my best.

I am greatly indebted to my children (Khaldoon and Redha). They form the backbone and origin of my happiness. Their love and support without any complaint has enabled me to complete this Ph.D. project. Last but not least, I offer my regards and blessings to all family members (my brothers and sisters) to support and the power of love has been providing, it would have been impossible to complete this work; I am happy to say, "Love you too much".

Abbreviations

IUPAC	International Union of Pure and Applied Chemistry
SAW	Surface acoustic wave
BAW	Bulk acoustic wave
APA	Alkaline phosphatase activity analysis.
SPR	Surface Plasmon Resonance sensor
MZI	Mach-Zehnder interferometer sensor
SPW	Surface Plasmon Wave
TIR	Total Internal Reflection
LW	Leaky Waveguide Sensor
FR	Fresnel Reflection
DDLW	Dye-Doped Leaky Waveguide
RB4	Reactive Blue 4 Dye
S	Sensitivity
DL	Detection Limit of a sensor
ELISA	Enzyme-Linked Immunosorbent Assay
TF	Tissue Factor
kDa	kiloDalton
PC	Pancreatic Cancer
TE	Thromboembolism
AA	Amino Acids
MPs	Microparticles
PL	Phospholipid
EMP	Endothelial microparticles
MMP	Matrix Metalloproteinases
TNF-α	Tumour Necrosis Factor Alpha
IL-1	Interleukin-1
TAT	Thrombin - Antithrombin III Complex
CLEIA	Chemiluminescent Enzyme Immunoassay
QCM	Quartz Crystal Microbalance
WLI	White Light Interferometer

BSA	Bovine Serum Albumin
PBS	Phosphate Buffered Solution
PEG	Polyethylene Glycol
PEO	Polyethylene Oxide
NHS-PEG-NHS	N,hydroxysuccinimide-polyethylene glycol- N, Hydroxysuccinimide
EDC	N-(3-dimethylaminopropyl) -N'-ethylcarbodiimide)
Sulfo-NHS	N-hydroxysulfosuccinimide
TF ELISA	Human Coagulation Factor III/Tissue Factor
Anti-IgG	Monoclonal goat anti-rabbit IgG
LED	Light Emitting Diode
TIR	Total Internal Reflection
TM	Light Polarised Perpendicular
TE	Light Polarised Parallel
HEPES	2-[4-(2-hydroxyethyl) piperazin-1-yl] ethane sulfonic acid
FITC	Fluorescein isothiocyanate
TEOS	Tetraethyl Orthosilicate
RT	Room Temperature
DMA	Dimethyl Adipimidate
DMS	Dimethyl Suberimidate
DMSO	Dimethyl Sulphoxide
LVDT	Linear Variable Differential Transformer
DTBP	Dimethyl 3, 3-dithiobispropionimidate
FBS	Fetal Bovine Serum
AsPC-1	Cell Lines generated from Pancreas Ascites from an Adenocarcinoma
Miapaca-2	Cell Lines generated from with a primary adenocarcinoma tumour
O.D.	Optical Density

CHAPTER 1

Theory of Optical Biosensors

Introduction

In the last few years, biosensors have become important bioanalytical tools for environmental monitoring, biotechnology, pharmaceutical, food control and other consumer oriented industries. Using biosensors to measuring chemical species is an exciting prospect because of their high sensitivity, high specificity, low cost, and portable size and ease of use. Important requirements for a sensor for biomaterials detection are high sensitivity and rapid detection. Over several decades, there has been much research to developed fast and sensitive biosensors for different applications. In particular optical techniques have been confirmed to have a high potential due to the possibility of rapid and direct (unlabelled) detection.

There are a number of biosensor devices which have been applied for detecting different biomaterials including various interferometers, surface plasmon resonance sensors and micro ring resonator sensor. Although all of these sensors give sensitive and rapid detection but they are just suitable of objects on a size scale up to 100 nm like, proteins, DNA and viruses. There are still however great opportunities to develop a robust, rapid, sensitive and selective biosensor. In this work a leaky waveguide sensor will be investigated as a relatively inexpensive and easy to use tool for scientific analysis and detection.

1.1 Requirements for biosensors

The following are the important requirements for biosensors

- Ability to provide real-time information at each production step or at various time points throughout a process. This will lead to better monitoring and control, for example of blood sugar levels.
- Many biosensor technologies can be configured to allow continuous flow analysis which is very useful in food production, water supply monitoring, and air quality.
- Biosensors can minimize cost of use through miniaturization and can be integrated into powerful lab-on-a-chip tools which are very capable.
- Biosensors can be used for point-of-care or on-site testing where state-of-the-art molecular analysis is carried out without requiring a state-of-the-art laboratory

1.2 Biosensor

The term biosensor has different meanings depending on what field the user comes from because a biosensor combines fundamental chemical, biological, and physical sciences with computer and engineering sciences to satisfy needs in a wide range of application areas. The International Union of Pure and Applied Chemistry (IUPAC) defined a biosensor as a *"detecting device that uses specific biochemical reactions mediated by isolated enzymes, immunosystems, tissues, organelles, or whole cells to detect chemical compounds by optical, electrical or thermal signals"* [1-2].

A biological recognition element represents the key component of a biosensor, forming a recognition layer which is immobilised on the surface of a suitable transducer (fig.1.1).

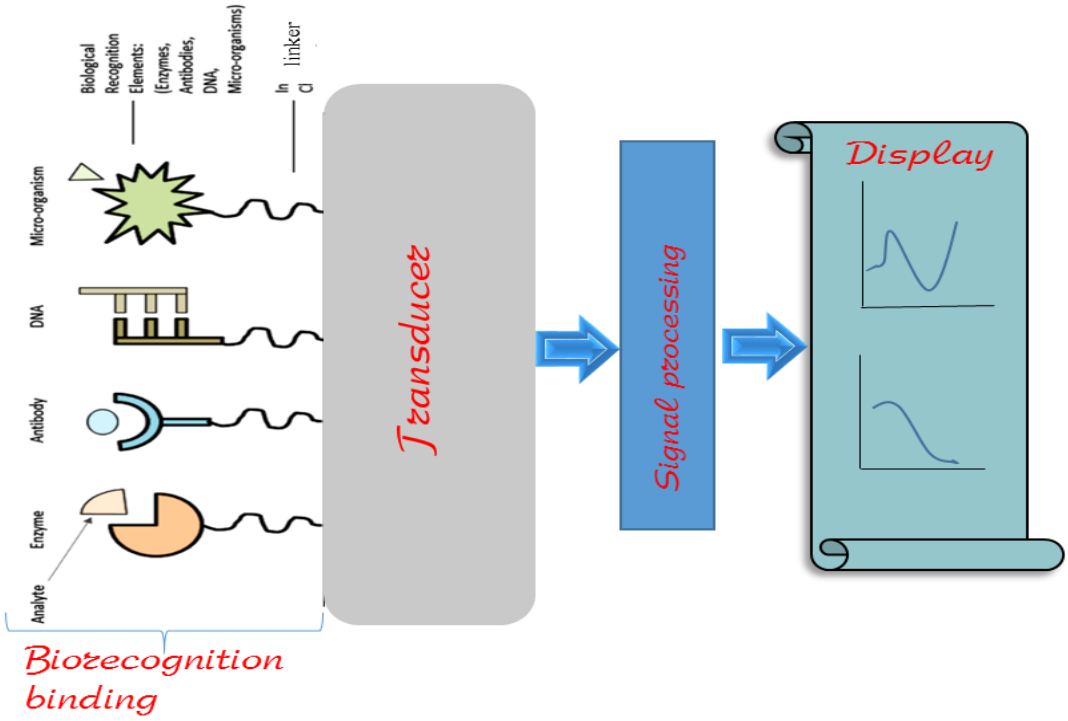

Figure 1.1: General schematic of biosensor set up [3].

The recognition components are biological molecular species (such as enzymes, antibodies, receptors, DNA or even cells such as yeast) which will react with a specific analyte in the sample, generally via the formation of lock-and-key complexes such as antigen-antibody, enzyme-substrate, single-stranded DNA-complementary DNA complexes as in Table 1-1.

Table 1-1: Illustrates the specific molecular interactions to increase specificity and discriminate between different substances in the sample, as commonly used in biosensing devices [4].

Element	Complementary
Antibody	Antigen
Enzyme	Substrate
ssDNA	Complementary DNA
Carbohydrates	Receptors
Cells	Receptors
Drug	Receptors
Metal ions	Amino acids

A physical, chemical or biological change is observed when an analyte (target molecule) interacts with the immobilized biological element (bioreceptor molecules) on a biosensor surface. This change is converted to a measurable signal by a detecting device which is called a transducer [5]. An essential issue in the development of any biosensor is to assure a high functional activity of the immobilized biological element acts on the surface of the transducer. The scale of the transducer surfaces are miniatured to micro- or nanometre size, that's due to the small quantities of biomolecules that can be deposited thereon. (fig.1.2).

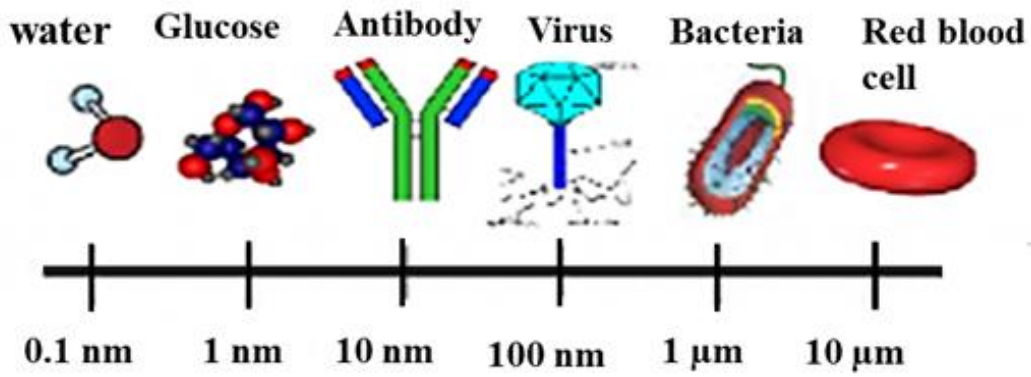

Figure 1.2: Scale size of biorecognition elements [6]

Attaching the biological element directly to the sensor surface, though sometimes possible, is frequently imprudent because the molecule's affinity to the analyte can be affected by the formation of chemical linkages. A linker molecule is commonly used. One

end has a carefully chosen functional group to react with the biomolecule without destroying it, and the other end has a moiety which anchors to the sensor surface [7].

1.3 Biosensor Classification

Essentially, biosensors are classified according to two parameters, the transduction mechanism and biorecognition elements, as shown in fig.1.3 [8].

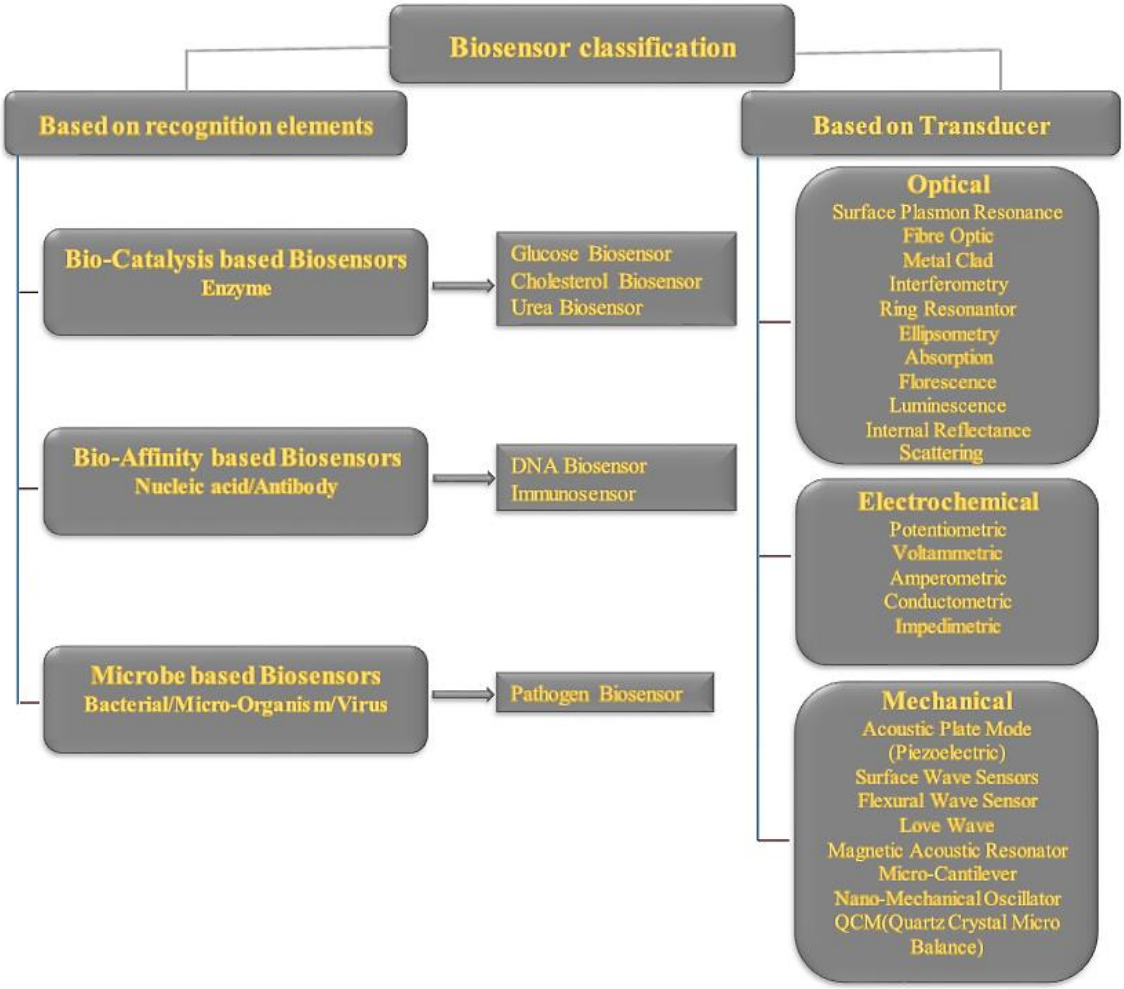

Figure 1.3: Classification of biosensors [9]

1.3.1 Classification of biosensors according to biorecognition elements

1.3.1.1 Biorecognition elements

One way to classify biosensors depends on the biorecognition elements. There are three different groups of biosensors classified depending on the nature of the process and in terms of their biological elements such as bioaffinity (e.g. antibodies and nucleic acid); biocatalytic (e.g. enzymes); and microbial (e.g. bacteria, viruses), as indicated in fig.1.3.

A. Biosensors based on bio-affinity elements

In this type of biosensor, which are also known as immunosensors or DNA biosensors the analyte will specifically bind to the biorecognition elements (antibodies and nucleic acid), that are coated on the surface of the transducer [10]. The mechanism of this type of biosensor depends on the affinity of the biorecognition element and analyte such as between antibodies – antigen pairs and frequently this combination is represented as lock and key fit, as shown in fig.1.4.

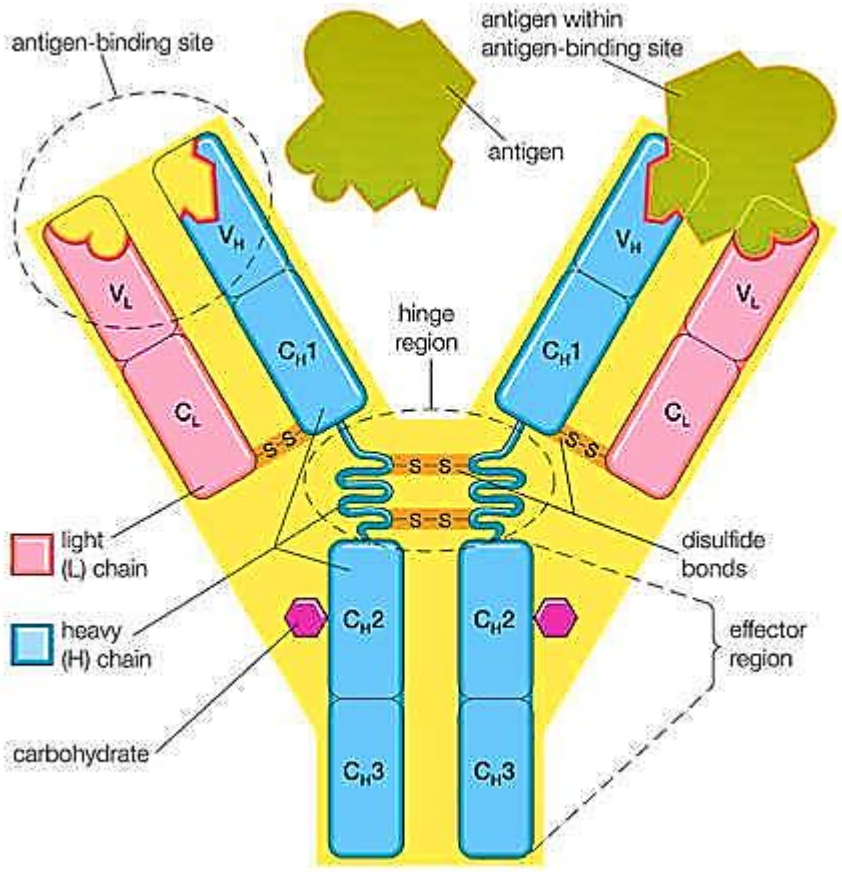

Figure 1.4: Antibody-Antigen Lock & Key Combination [8]

Each antibody can identify its antigen due to the highly selective interaction between them. Antibodies can be coated onto many surfaces, and they can be chemically conjugated onto many different reporter molecules. They can also be developed against nearly any biological element, from single-stranded (ss) DNA to protein. Although these systems are more specific and sensitive than enzyme-based systems, this biosensors face limitations because they are more complicated and need multi-step assay configurations [11].

DNA biosensors systems are based on the immobilization of a single-stranded DNA probe onto the transducer whose sequence is complementary to the target DNA strands. The specificity of these interactions depends on the ability of different nucleotides to form hydrogen bonds with a complementary partner dependent [12].

B. Biosensors based on bio-catalytic elements

In this type of sensor the analyte will undergo a chemical reaction catalysed by the enzymes which are the biological element in these sensors. These enzymes have the ability to recognize their substrates specifically and are termed catalytic biosensors. The chemical change occurring then is detected. Either by monitoring the rate of formation of a product, inhibition of the reaction or loss of a reactant. The equation for the reaction can be seen below [13]:

$$S + E \underset{K_{-1}}{\overset{K_1}{\rightleftharpoons}} ES \xrightarrow{k_2} E + P \quad \text{.....Equation 1.1}$$

Where

S = Substrate

E = Enzyme

ES = Enzyme-substrate complex

P = Product

k_1 = Rate of enzyme-substrate complex formation

k_{-1} = Rate of enzyme-substrate complex dissociation

k_2 = Rate of dissociation of enzyme-substrate complex to products

Another approach involves using the target analyte to investigate the inhibition of the enzymatic activity. This is used mainly to determine the detection limit of these biosensors. The benefits of enzyme-based optical biosensors are that they are highly

selectivity and have high sensitivity, while the major limitations are loss of activity when they have been immobilized on the transducer after a short period; also the stability of the enzyme depends on different conditions like ionic strength, pH, chemical inhibitors, and temperature [13] .

C. Microbial Biosensors

This type of biosensor uses microbes (e.g. bacteria and viruses) as its biological element. The action of microbial sensors depends either on the measurement of the metabolism of the microorganism or on the consumption of carbon dioxide and oxygen. There are several advantages of microbial biosensors, such as that microorganisms are cheaper than enzymes or antibodies; they can be more stable; and they can use enzymes to carry out different complex reactions, although this is less selective than enzymes. Disadvantages include the fact that they may require longer recovery, longer response times and more frequent calibration [14].

1.3.2 Classification according to transducer

The transducer is used to measure the biological event. Transducers show the start of, or alteration in, the biological events in the biosensor depending on the kind of signal or parameter. Thus, biosensors can be classified into four different kinds; electrochemical transducers, optical transducers, thermal transducers and mechanical transducers.

1.3.2.1 Mechanical transducers

A mechanical stress is induced when an electric field is applied through a piezoelectric material, like a quartz crystal, and it creates an oscillating motion of a certain vibrational resonant frequency. This frequency dependent on the mass on the surface of the oscillator and the frequency decreases with increased mass on the surface [15]. Piezoelectric materials can produce and transmit acoustic waves in a frequency-reliant manner. The propagation of these waves occurs on the surface, i.e. surface acoustic wave (SAW), or in the bulk of the resonator, i.e. bulk acoustic wave (BAW). When the surface of the piezoelectric sensor has been coated with a biological substance (such as an antibody) and is placed in a solution containing the analyte an increase in the mass occurs resulting from the attachment of the analyte to the biorecognition element that was coated on the surface giving rise to a corresponding frequency shift [16]. There is another types of mass-sensitive biosensor such as a microcantilever. The main limitation with all types of mechanical transducer sensing is non -selective binding to the transducer surface [17].

1.3.2.2 Thermal transducers

These sensors are also referred to as calorimetric or thermal biosensors. Most biochemical reactions involve the generation or absorption of heat and this can be related to the amount of analyte present [18], which is the principle behind these sensors.

The heat of reaction can be measured when the analyte comes in contact with the immobilized biological element on a temperature sensor. The total heat absorbed or produced is proportional to the molar enthalpy (transfer of heat per mol in a reaction) and the total number of molecules in the reaction. Thermal biosensors are insensitive to the electrochemical and optical properties of the sample and do not require frequent recalibration. Calorimetric biosensors are used for cosmetics, food, and pharmaceutical and other component analysis [19] .

1.3.2.3 Electrochemical transducers

Production or consumption of ions or electrons occurs when an immobilized biomolecule binds with the target analyte onto an electrochemical transducer. This will effect changes in measurable electrical properties of the solution, such as potential or current. There are different methods utilized to detect electrochemical changes with the main techniques being amperometry and potentiometry [20].

i. Potentiometric

A potentiometric sensor measures the potential between the working electrode and the reference electrode at zero current. The relationship between the potential generated at the surface of the electrode, and the activity of the ion of interest is logarithmic. Most electrodes are made from inert materials like gold, stainless steel, silver, platinum, or carbon at the potentials at which the electrochemical reactions are takes place. A selective membrane may be used, or an electron mediator that reacts at lower potential may be incorporated into the immobilization matrix or to the sample containing the analyte, because some species react at potentials where other species are present. The wider detection limits represent the main advantage of these transducers. However, the application is limited due to the requirement of a very stable reference electrode, poor sensitivity. Nearly all potentiometric sensors are commercially available, including metal oxide based sensors, glass electrodes as well as ion-selective electrodes [21].

ii.Amperometric

The principle behind amperometric biosensors is to monitor redox reactions by measuring electric current flowing at a constant potential. A typical examples is where the electrodes are combined with an enzyme which allows the analyte to undergo oxidation or reduction. The concentration of substrate has been shown to be proportional to the magnitude of the catalysis-generated current [21]. Depending on the specificity of the enzyme, the biosensor is designed to detect only one or maybe a few molecular species. The most commonly used biosensor has been developed for diabetic patients and is the single-use amperometric glucose oxidase-based sensor for home glucose assays. Another common type of sensor used in flow systems uses hydrogen peroxidase. Amperometric sensors can also be used with immunoassays, where secondary antibodies are labelled with an enzyme whose product is oxidized at the electrode [22].

The reaction mechanism of all types of electoromechanical sensors takes place at a surface of the electrode causing to a decrease in the selectivity, and this represents one of limitations which has been faced this type of biosensors. One solution has been to develop disposable electrodes, but these then need to be very reproducible.

1.3.2.4 Optical transducers

Optical transducers are the most common type of transducers used in biosensors. They depend on measuring changes in light. Changes in light intensity, phase, polarization, peak position, and angular wavelength will be observed after the interaction of the probe molecules and target molecules, and optical transducers can measure these changes. Mostly, the optical transducer is an optical waveguide (e.g., slot-waveguide, optical fibre, photonic crystal waveguide, photonic nanowire waveguide, and leaky waveguide). Different parallel functions can be performed by this photonic device. The first one will guide the light from the optical source (e.g. laser) into the sensing area. Consequently, the optical waveguide has the rule of transducer, enhancing the interaction between the chemical/biochemical process and the optical signal. By this way, the chemical information can be properly transduced into an optical one. In this context, the transducer can be considered as an engineering prerogative, because several technical solutions have to be implemented in order to maximize the confinement of the optical field in the sensing Compared with other transduction methods, optical sensing encompasses the largest number of sub-categories and can be classified as two major types based on the sensing

mechanism and the sensing architecture. Furthermore, optical biosensors can be categorized according to the detection procedures: label-based detection and label-free detection [23].

1.4 Optical Measurement methods

There are different types of sensing methods

a. Absorption

Simple optical biosensors use the phenomenon of absorption of light from a source, the transducer then transforms the energy of a photon to another form of energy such as heat. Beer Lambert-'s Law is used to determine the concentration of the analyte by measuring the absorbance of a molecule at a specific wavelength. Beer Lambert-Beer's law states.

$$A = log_{10}\frac{I_o}{I} = \varepsilon lc \quad \text{... ... ... } \textit{Equation 1.2}$$

Where I_0 represents the intensity of the incident light, I represents the intensity of transmitted light, $\mathcal{E}$ is a molar extinction coefficient, C denotes the concentration of the absorption of analyte, and l is the path length of absorbing solution (usually 1:00 cm).

This is a very effective and simple method in which the decrease in the intensity of a radiant beam passing through the sample is measured.

The most important benefits of the sensors based on absorption are that they are easy to use, simple and cost-effective [24]. But these sensors have not got a very high sensitivity because the measurement depends on the ratio of intensities of the incident and transmitted beam. The absorption of the light will depend on the concentration of molecules in the solution, and the solution length the light is passing through. They can also be used to sense the concentration of gases such as oxygen or carbon dioxide; biological pathogens; and the pH of solutions.

b. Fluorescence

Sensing by fluorescence usually happens when molecules absorb light at one wavelength which initiates electronic transitions to reach an excited state depending on the wavelength of incident radiation. The molecule then returns to ground state by emttting a photon of light at a longer wavelength as indicated in fig.1.5, is known as fluorescence [25] . Only certain molecules fluoresce so for this method to work fluorescent labels are often added to biomolecules.

The excitation and emission occur only at different energy levels, which leads to each fluorescent molecule having a different spectral fingerprint of fluorescence [26]. Fluorescence in a target molecule mounted on a substrate absorbs a beam of one wavelength and emits another beam, commonly longer, wavelength. The fluorescent label utilizes a reactive derivative of a fluorescent molecule known as a fluorophore which chemically binds a biomolecule such as a protein, antibody or amino acid. The fluorophore selectively connects to a specific functional group or region on the target molecule before being exposed to probe molecules and serves as a marker, tag, or dye, or reporter for peptides, antibodies, and nucleic acids. When a light source is used to excite the fluorophore molecules they absorb photons of the excitation light, which leads to the fluorophore molecules emitting light at a longer wavelength. This is detected by a photodetector, which identifies the presence of the labelled target molecules [27].

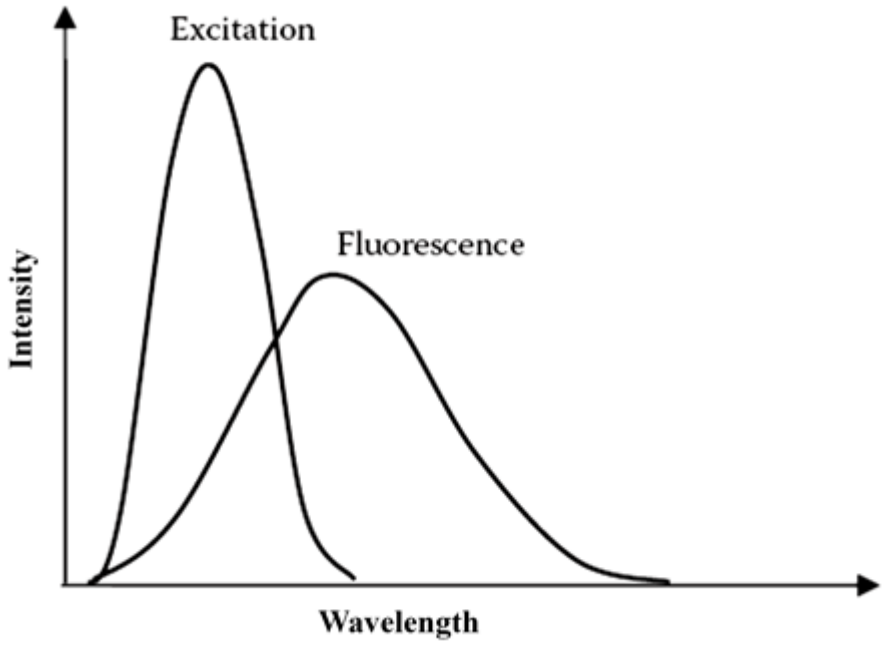

Figure 1.5: Fluorescent light emission [25]

In detection based on fluorescence, each biorecognition element or target molecule has fluorescent tags to label it, such as fluorescent dye (fluorophore) which is a molecule with a rigid conjugated structure (usually a polyaromatic hydrocarbon or heterocycle). The strength of the interaction between the target and the biorecognition elements indicates the emission intensity of the fluorescence as illustrates in the following equation:

$$I_F = \varphi . I_o \left(1 - e^{-K.C.l} \right) = \textit{Fluorescence emission intensity at } \lambda_{EM} \ldots\ldots \quad \textbf{\textit{Equation 1.3}}$$

Where:

I_F is the emitted fluorescent light,

φ is quantum yield (the ratio of the number of photons emitted to the number of photon absorbed),

I_o is the intensity of the incident light,

C is the concentration of the solute,

ε is the molar absorbance,

K is a proportionality constant attributed to the instrument,

and l is the path length of the cell.

The downside for using this sensor is a request of a powerful external light source for labels to provide of the sensitivities needed which can be expensive. Typically, some of these sensors are used to differentiate BaP and benzopyrene (BPT), or in the detection of carcinogens. Also, they are used in quenching DNA, due to their high read-out speed. There are some disadvantages of the technique of bioconjugating fluorophores onto biomolecules, such as that it often results in low yield, and it is time-consuming. Furthermore, the fluorophore modification process can inhibit the efficiency of the bimolecular binding, which causes reduced performance of the sensor. Moreover, since optical detection instruments often must be of high quality, because the fluorescence intensity is typically weak and the lifetime is short, the cost implications can be high.

C. Raman Spectroscopy

The scattering of light, which happens via molecules due to the exchange of energy between an incident photon and scattering molecules, is the principle behind Raman spectroscopy.

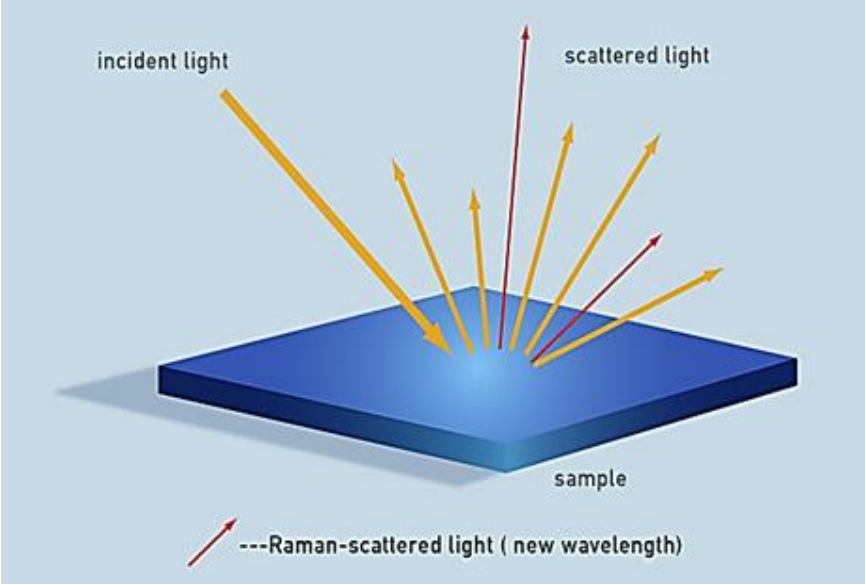

Figure 1.6: Raman Spectroscopy principles

The energy is transported from the incident photon to the scattered photon or vice versa fig.1.6 [28]. When the scattered photon has higher energy than the incident photon, the method is known as Raman anti-Stokes scattering; when the scattered photon has lower energy than the incident photon the method in known as Raman Stokes scattering [29]. A more sensitive technique is Surface Enhanced Resonance Raman Spectrometry (SERRS) The main principle of this technique depends on the use of chromophore as the adsorbate molecule (labels) and tuned the frequency of the chromophore to the excitation wavelength of the light source (laser).

The signals of Raman Spectroscopy are very weak and need power sources and highly accurate optical receptors (biorecognition elements). This kind of sensor is used to overcome some problems of fluorescence sensing: it has the capacity to sense analytes which do not exhibit fluorescence. Raman spectroscopy is commonly used in chemistry that's due to the providing of a fingerprint by which the molecule can be identified via the information is specific to the chemical bonds and symmetry of molecules [30]. In solid-state physics, spontenous Raman spectroscopy is used to characterise materials, measure

temperature, and find the crystallographic orientation of the sample. In addition, Raman spectroscopy can be used to observe other low frequency excitation of the solid, such as Plasmons, magnons, and superconducting gap excitations.

D. Evanescent fields

Other forms of optical biosensors use the evanescent field which is related to the total internal reflection of light when waves travelling through a medium undergo total internal reflection at the boundary. This confines the electromagnetic wave at the boundary between two media of different optical properties, in such a way that this wave will strike the boundary at an angle greater than critical angle, which produces an evanscent field and interact with immobilised biosensing elements. Depending on the sensor configuration, the electromagnetic wave may be in the form of a standing wave or a travelling wave fig.1.7.

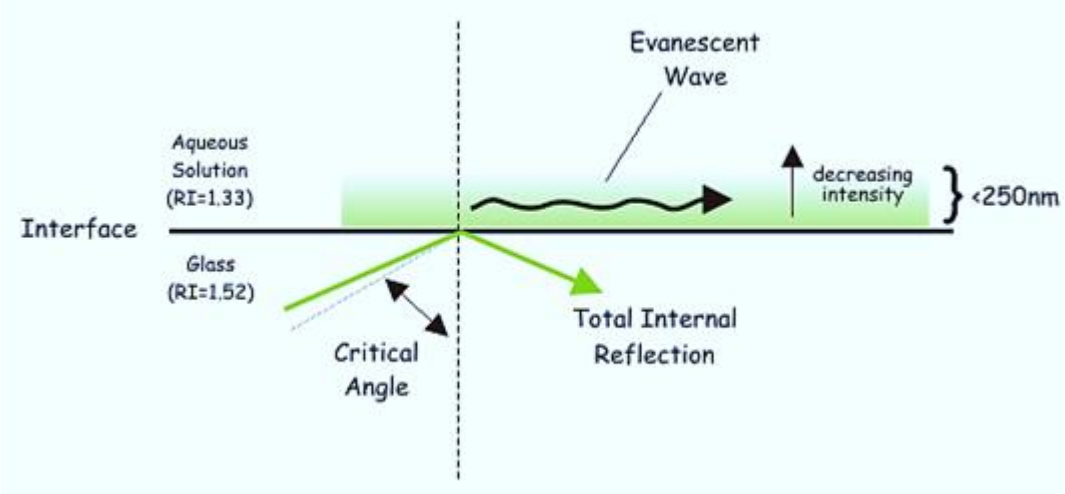

Figure 1.7: The evanescent wave is produce parallel at the boundary of different medium when the incident angle is greater than the critical angle and the majority of the light is reflected during total internal reflection (TIR).

The structure of the sensor must be designed according to the change in the optical properties of the surrounding medium along the waveguide structure. For example, with light, which is guided by the structure of the sensor but interacts at the same time with the exterior environment, the surrounding medium is investigated by the evanescent tail of the mode along the waveguide structure. This interaction will be due to the change in the speed of propagation of the tail, affected by an alteration in the refractive index, and change its attenuation, caused by an alteration in the absorption coefficient. Light is also

detectable from these alterations as a corresponding change in the phase velocity of a waveguide.

The combination of the phase velocity (V_P) and the speed of light (C) introduces a new quantity, the effective refractive index ($neff$).

$$\boldsymbol{Effective\ Refractive\ Index\ (neff) = \frac{speed\ of\ light}{Phase\ velocity}}$$

Or

$$\boldsymbol{neff = \frac{C}{VP}} \quad \textbf{\textit{…….. Equation 1.4}}$$

The interaction between the surrounding medium and the evanescent field will cause a phase velocity v_1 lower than the light speed. The optical properties of the surrounding medium will be changed according to the binding of the antibody with the antigens; this will lead to a change of the phase velocity v_2, which can be compared to v_1 to obtain an alteration in the effective refractive index. For interactions in the close neighbourhood of the sensor surface, the evanescent field sensors have been proved a highly sensitive tool.

Fig.1.8 is a schematic for a conventional evanescent field. Biosensor, which illustrates a change in the effective refractive index N_{eff} of the transmitted light resulting from the interaction of the bimolecular, that's on the waveguide surface inside the evanescent area. The phase velocity of the guided mode will be shifted and there will be a change in the local refractive index felt by the evanescent field of the optical waveguide when the target molecules binds to the receptor molecules at the sensor window.

Fig.1.8. a, and b indicates the upper and lower extents of the waveguide core represented by dashed lines. The chemical reactions occur on the upper surface of the waveguide at x=0 μm.

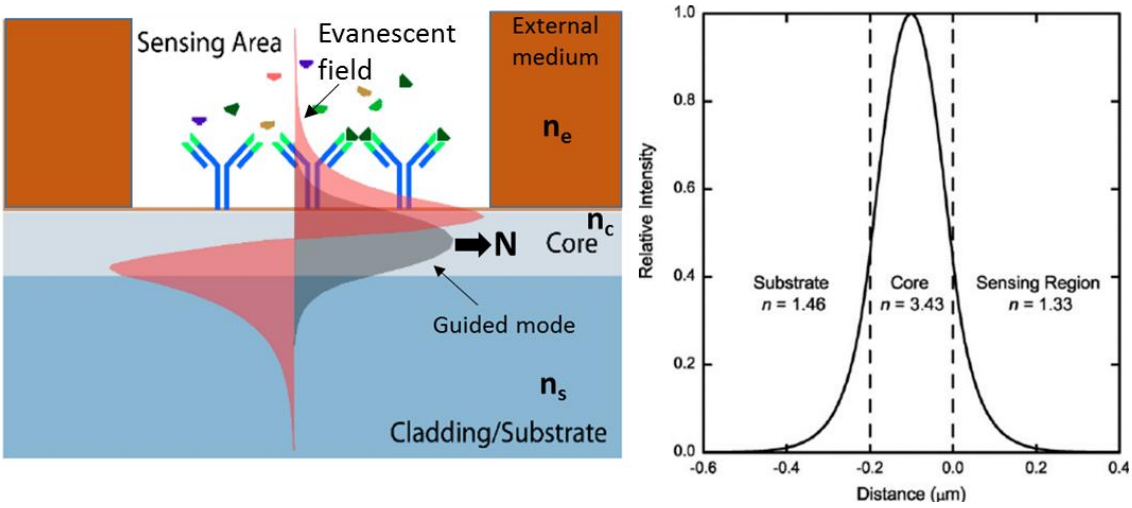

Figure 1.8: (a) Scheme representing evanescent field sensing, the cross-section of a waveguide and the optical electric field distribution of the vertically polarized mode; (b) The cross-sectional plot of the evanescent field intensity of optical waveguide [31]. ns: Substrate, ne: External, n: Refractive index, and nc: Core.

If we suppose the typical wavelength of light for optical biosensors lies in the range of λ=600-1550 nm, the evanescent field will extend into the test sample around 100-250 nm fig.1.9a. The distance of the evanescent field is therefore very short, so only material directly near the surface, such as antibodies, DNA, and proteins which are chemically attached to the surface, interact with the biosensor; the biosensor is not influenced by unbound material like eukaryotic cells or bacteria suspended in solution. Different designs of optical biosensors can manipulate the features of the evanescent field: it is either confined tightly to the sensor surface, or it penetrates deeply into the test sample [32].

There is one key to designing a sensor with high sensitivity, which is matching the regions of the highest evanescent field intensity with the regions of greatest biochemical binding (fig.1.9b). Many label-free optical biosensors depend on the change in the refractive index obtained from the interaction of biomolecules with evanescent waves. For example, the most commonly used, the surface plasmon resonance (SPR) sensor utilizes the evanescent wave of a surface plasmon resonance method present at the interface between dielectric materials and metal as a collective electron oscillation wave[33], when the incident light is totally reflected at the prism–metal interface and generates an evanescent field penetrating into the metal layer. At the resonant angle or resonant wavelength, the propagation constant of the evanescent field matches that of the surface plasmon waveguide (SPW) and as a result, the photon will be coupled into the SPW. Another type of biosensor is based on the evanescent wave established on silica or silicon platforms,

such as planer waveguide sensors, fibre optic sensors, and, lately silicon nanowire sensors, slot-waveguide micro-ring resonator, and leaky waveguide sensors.

For example the silicon nanowire waveguide design can enhance sensitivity over traditional slab waveguide sensors by using a thinner waveguide core. With biomolecules immobilized on the core a larger portion of the electric field will leak out and interact with a biomolecule immobilized on the core surface. Coordinated in a match-Zehnder configuration, there's an advantage in silicon wire waveguides from longer field molecule interaction lengths. In the slot-waveguide micro-ring resonators, the interaction between analyte molecules and the surface of the waveguide in the slot region has improved sensitivity detection, and design of very high quality factor resonant structures will allow the interaction of the evanescent field with biomolecules over the multiple cycles of the confined wave [34].

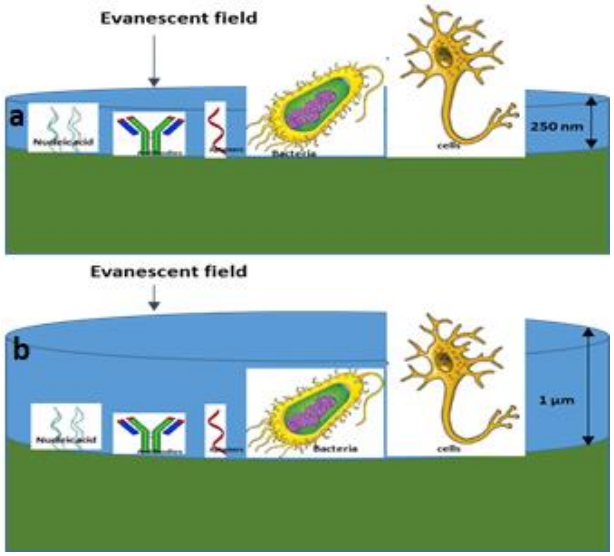

Figure 1.9: (a) Limited evanescent field of the conventional evanescent field sensors of 250 nm (b) Increase in evanescent field of the deep-probe evanescent field biosensor of 1µm [35]

1.5 Labels and Label-free detection techniques

In label-based systems labels (probes) are attached to the molecule of interest. Labels are small modifying agents which can be used to tag probe proteins and dye, nucleic acids, antibodies and other molecules [36]. Often these compounds include groups which supply sensitive detectability by an atomic property or intrinsic chemicals such as radioactivity, visible chrogenic character, fluorescence, or bioaffinity for another protein. Accordingly, most probes contain a reactive protein capable of coupling with the functional groups of biomolecules, which can be designed through modification of a protein. Through this

reactive portion, the probe is being covalently attached, consequently permanently tagging it with a unique detectable property. Subsequent interactions can be followed through the tag's visibility which the labelled protein is allowed to undergo. The most traditional label-based methods obtainable are radioactivity, chromogenic and fluorescence-based detection systems.

In the radioactivity system certain elements emit energy in the form of particles or waves by disintegrating the unstable atomic nuclei into a more stable form[37]. Different applications have been studied for several interactions: protein-protein, protein-RNA, protein-DNA, and antigen-antibody interactions that give out radiation on binding to the corresponding target molecule by utilizing the radio-labelled query protein on an antigen[38].

The chromogenic detection of antigen-antibody can be easy to detect. The substrate used in chromogenic detection is a molecule which is stimulated via connecting the enzyme to the antibody to provide a coloured product [39].

Label-free biosensors which do not need fluorescent molecules for biomolecule detection have the advantage of improving reliability and eliminating complex sample preparation techniques. The basic principles of operating optical label-free biosensors depend on the change in the refractive index due to the affinity binding of biomolecules, such as antigen-antibody binding or DNA hybridization. The labelling of biomolecules often changes the characteristics of surface and natural activities of the query molecule and exhibit interface of the binding site. Also the labelling procedure is lengthy, laborious and limits the types and number of query molecules. Thus, Label-free detection biosensors have a significant advantage in overcoming the problems with label detection biosensors [40].

Label-free detection techniques avoid interference via the tagging molecules, provide quantitative information for the binding kinetics, and simplify the bioassays by eliminating the need for secondary reactants. Label-based detection methods are not appropriate for hand-held or portable diagnostic devices because binding the dyes is very complex. Detecting the fluorescence needs expensive lab-based equipment. Label-free methods of biosensing, on the other hand, can detect the binding of complex biomolecules by utilizing hand-held or portable devices. This is less costly and does not require expertise [41].

1.5.1 Sensitivity

In the development of sensors, sensitivity is an important parameter in evaluating sensor performance, which is determined via interaction strength between the sample and light. There are several factors affecting the sensitivity of optical biosensors including depth of penetration of the evanescent field, electromagnetic field strength, geometric factors which involve the thickness, length and diameter of core or the waveguide, and optical power contained in the sensing region. The sensitivity is the magnitude of sensor transduction signal change in response to the change in the analyte. The sensitivity of most evanescent wave-based sensors is determined via the fraction of light in solution or the light intensity at the sensor surface [42].

Sensitivity is defined as the proportion of the alteration in transducing optical parameters (ΔI in the intensity variation scheme and $\Delta\lambda$ in the resonant wavelength shift scheme) to the alteration in the waveguide parameters affected by the analytes. Table 1.2 lists four different combinations according to the definition of the sensitivity S, which can be divided into two parts from the mathematical expressions of sensitivity. These are named device sensitivity and waveguide sensitivity respectively.

A. Device sensitivity

Device sensitivity depends only on the difference of optical transduction parameters, which depends on the transducing method. Therefore, device sensitivity can be defined as the ratio of the change in the transducing optical parameter to the change in the effective refractive index. Device sensitivity is expressed for the shift in the resonant wavelength scheme as;

$$\boldsymbol{S = \frac{\partial \lambda}{\partial n_{eff}}} \text{ ……. } \textbf{\textit{Equation 1.5}}$$

$$\boldsymbol{\partial \lambda = \frac{\partial n_{eff}.\lambda_{res}}{n_g}} \text{ … … … …. } \textbf{\textit{Equation 1.6}}$$

Where $\partial\lambda$ is the shift of the resonant wavelength, ∂n_{eff} is the change in the effective refractive index caused by the analyte attaching, λ_{res} is the resonance wavelength, and n_g is the group index.

In the intensity scheme this will become:

$$S = \frac{\partial I}{\partial n_{eff}} \text{ ..... } \textit{Equation 1.7}$$

According to the above equations, device sensitivity will be increased by using a smaller effective refractive index or longer resonant wavelength for each case.

B. Waveguide sensitivity

The sensitivity of the waveguide is related to waveguide structures regardless of the type of sensor, therefore it can be defined as the ratio of the change of the effective index(∂n_{eff}) to the change in the waveguide parameter (∂n_c) affected by the analytes. By changing the effective refractive index, the sensitivity of the waveguide can be determined, resulting from the changing of the analyte - induced by a change in waveguide parameters [43]. The change in the refractive index is caused either by a change of the refractive index of a cover medium or by a change of sensing the thickness (∂t) of a layer immobilized on the surface of a waveguide layer. It differs according to the sensing mechanism which is used and is expressed as:

$\partial n_{eff}/\partial n_c$ *(Homogenous sensing) ……. Equation 1.8*

$\partial n_{eff}/\partial t$ *(Surface sensing) ……. Equation 1.9*

Table 1-2: Overall sensitivity based on the sensing mechanisms and transducing schemes of sensors.

		Sensing scheme	
		Intensity variation	**Resonant wavelength shift**
Sensing mechanism	**Homogenous**	$s = \frac{\partial I}{\partial n_c} = \frac{\partial I}{\partial n_{eff}} . \frac{\partial n_{eff}}{\partial n_c}$	$s = \frac{\partial \lambda}{\partial n_c} = \frac{\partial \lambda}{\partial n_{eff}} . \frac{\partial n_{eff}}{\partial n_c}$
	Surface	$s = \frac{\partial I}{\partial t} = \frac{\partial I}{\partial n_{eff}} . \frac{\partial n_{eff}}{\partial t}$	$s = \frac{\partial \lambda}{\partial t} = \frac{\partial \lambda}{\partial n_{eff}} . \frac{\partial n_{eff}}{\partial t}$

C. Surface sensing

For surface sensing the external surface is treated with a selective layer for attracting the analytes. For this reason, the analytes will be bound to the waveguide surface, which will increase the thickness of the waveguide: this layer of analytes is known as the addlayer (∂t) fig.1.10 [44-45]. Thus, the definition of the sensitivity of surface sensors is a ratio of change in addlayer thickness (∂t) to the change in resonance wavelength ($\partial\lambda$).

$$S = \frac{\partial\lambda}{\partial t} \ldots\ldots\ldots\ldots \textit{Equation 1.10}$$

There are several biochemical applications of surface sensing, such as antigen-antibody reactions, DNA sequencing by hybridization or measuring the concentration of pollution in water, which depends on the immobilization of an ultra-thin layer of receptor molecules on the surface of a guiding film. This interaction will cause a change in thickness of molecular addlayer, which affects the effective index of the propagating optical mode[46].

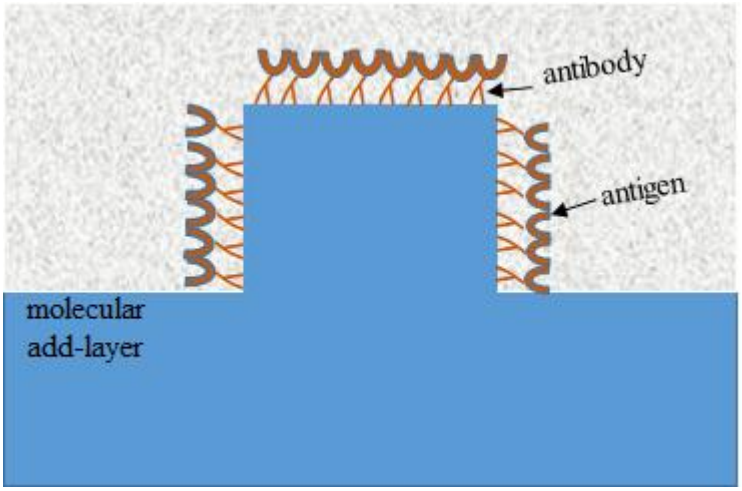

Figure 1.10: Adsorption of analyte molecules on the surface of the sensor as an ultrathin film.

D. Homogeneous sensing

In this kind of sensing, the analyte molecules are suspended in a fluid medium (liquid or gaseous), which exists around the waveguide surface, fig.1.11. This will lead to a change in the amount of homogeneously present analytes and as a result, this will change the cladding index. This in turn will change the effective refractive index of the guided mode and move the resonance wavelength. Thus, all materials either the detected molecules or the sensing layer in the solution can participate in a shift in the effective index, and this will lead to non-specific interaction. Surface sensing can be utilized to solve this

problem[42]. The sensing of the homogeneous sensor can be defined as the ratio of a cladding index change (∂n_c) to the resonance wavelength change ($\partial\lambda$), as expressed by the following equation;

$$\boldsymbol{S = \partial\lambda/\partial n_c} \text{ ... ...} \textbf{\textit{ Equation 1.11}}$$

Represents homogeneous sensing, that enables an observer to measure the concentrations of various chemical kinds usually present in a solution such as ethanol or glucose, as well as enabling such an observer to appreciate the change of concentration of some gases. This is because the refractive index sensitivity for several polymeric materials is specific to gas concentrations. In all of these cases, the change in the concentration of chemical analyte will induce change in the refractive index of a solid or liquid serving as cover in the guiding structure. For instance, changing the concentration of glucose in an aqueous solution will induce a change in the refractive index of this solution [43].

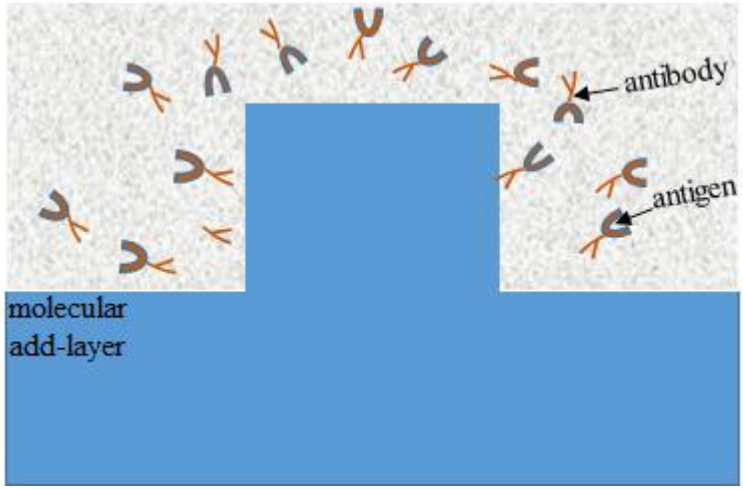

Figure 1.11: Homogeneous sensing: this shows analyte molecules existing in the surrounding aqueous medium that serves as the top cladding.

1.5.2 Limit of Determination (or Resolution)

Limit of determination is a critical criterion of performance for detection of adsorbed molecules with low molecular weight or detection of analyte molecules existing at low concentrations. To do this it is necessary to determine the noise. At a basic level noise can be easier to characterize by allowing the sensor to reach a steady-state condition and recording the measured output in sequence many times without any intended change to the sensor. The noise can be defined as the standard deviation, σ, of all the repeated measurements. And if the signal has a magnitude 3σ, and is defined as a detectable signal,

then the limit of detection can be defined as a change of the smallest measurable mass density of the sensor, expressed as:

$$LOD = 3\sigma/S \quad \text{..... Equation 1.12}$$

One can use sensitivity to define the smallest value determined over zero concentration, while using resolution to describe the lowest resolvable differentiation between two measurements at any concentration. Consequently, sensitivity and the resolution are related but are quite different of merit figure [47].

1.5.3 Limit of Detection

The detection limit of a sensor (DL) is an important parameter to describe its performance. The limit of detection (LOD) can be derived by taking the lowest resolvable signal, or by taking the noise in the transduction signal (σ) into account:

$$DL = \sigma/s \quad \text{..... Equation 1.13}$$

Where S indicates the sensitivity. The DL may be improved by increasing the sensitivity or by decreasing the noise level. One may enhance the sensitivity by increasing the interaction of the light with the solution. Typically, the noise parameter is more commonly seen. It is produced from temperature fluctuations or thermal expansion in both the buffer solution and substrate of a sensor. The change of the refractive index results from temperature dependency. One may enhance the performance of a sensor and overcome noise that's related to the temperature fluctuation by using various methods of controlling and employing non-specific binding and bulk the change of refractive index. One may reduce thermally stimulated noise by implementing a temperature control, like a thermoelectric cooler. There is another method of reducing noise by balancing the thermo-mechanic and thermo-optic effects. The third method is called common mode noise, which employs a reference channel constructed into the same sensor or into a different sensor nearby to decrease the temperature effect [48-49].

1.5.4 Sensor Cost

In most diagnostic or pharmaceutical applications, the cost of an individual assay is estimated for comparison. To bring the cost of the assay to appropriate levels, two major methods have been applied. First, if the fabrication and packaging of the sensor are very expensive they can be regenerated and used for various successive assays. The second method is designing sensors using inexpensive materials and processes suitable for mass production which before disposal can be used only once, like a typical labelled assay.

Label free optical biosensors do not require tag reagents which reduces the cost and consequently any compensation for the cost of the additional reagents. The transducer cost in each assay must be low. The large challenge to acceptance for optical biosensors is due to the cost challenges which consist of high-accuracy optical components fabricated by using highly exacting processes such as metal deposition, photolithography, dielectric or plasma etching from costly materials such as optical fibre, glass or silicon. Moreover, if the fabrication of the sensor is low-cost, the cost of testing and packaging must be more efficient.

1.6 Further Biosensor Detection Modes

There are different constructions which are widely used in the development of optical label-free sensors:

- Interferometer-based biosensors
- Surface Plasmon Resonance-based biosensors
- Fibre optic-based biosensors
- Micro ring resonator-based biosensors
- Waveguide layer-based biosensor

1.6.1 Interferometer-Based Biosensors

This type of sensor occurs through the change in the effective refractive index of mode when the sample interacts with the guided light propagated in the sensor to detect the phase shift. The Mach-Zehnder method represents one of the interferometer constructions which has a high sensitivity for label-free optical biosensing [50]. In these sensors, the analyte will interact with the evanescent field of the guided light or, when a hollow or slot waveguide is employed, the analyte will propagate light in the core of the waveguide. The

Mach-Zehnder interferometer is composed of an incident waveguide, which is divided into two branches of a single mode waveguide including a reference arm and a sensing arm as indicated in fig.1.12 [51].

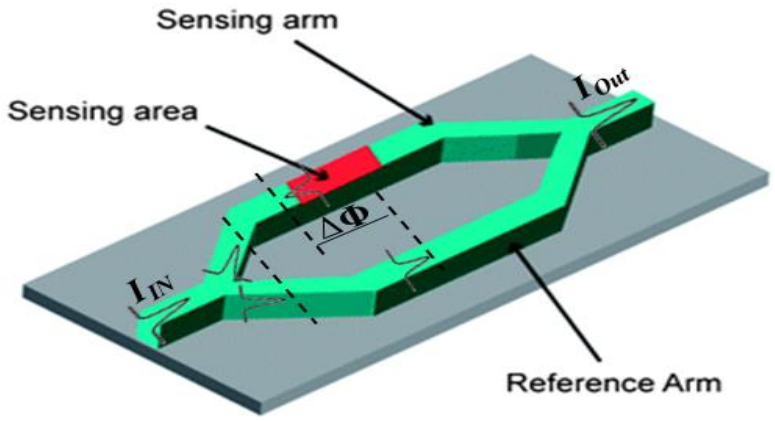

Figure 1.12: A schematic of an integrated Mach–Zehnder interferometer, where I_{out} represents the optical output intensity, I_{IN} incident light intensity, and $\Delta\Phi$ represents the difference between phases [52].

The reference arm is one of these waveguides, isolated from changes in the surrounding medium by cladding, while the other waveguide - the sensing arm - has no cladding. The effective refractive index (Δn_{eff}) will change in the sensing region (e.g. the addition of a thin biolayer, or changes in the bulk superstrate index) this will affect the evanescent field of the waveguide mode, which introduces in this arm a phase shift of the travelling light ($\Delta n_{eff}\ k_0\ L$), where L is the sensor window length, k_0 is the wavenumber of the free space ($k_0=2\pi/\lambda$) [53].

At the MZI output, where the sensing and the reference arms are recombined, interference occurs due the relative phase shift ϕ induced by the difference of the effective indices. The interference translates this phase shift into a modulation of the optical output intensity satisfying the condition. The MZI sensor is a cosine-dependent intensity function that changes according to the signal change, which is very difficult to resolve close to the maximum and minimum of the cosine function.

The sensitivity of the Mach-Zehnder architecture depends on the length of the sensing arm (L). An effective refractive index of the undesired shift in propagating mode may be introduced due to change of temperature that can affect the sensitivity. A trade-off has therefore usually to be achieved between the sensitivity and the length of the device. Lately the MZI has been developed for optical sensing by employing a nanowire sensor

in a wire assembly. Different types of nanowire, either pulled from bulk glass, or metallic, as well chemically grown nanoribbons, have been used as building blocks after fabrication for applications in micro- or nano-photonics such as nonlinear and biosensing optics for future potential. Silica nanowires offer several advantages over other types of nanowires since they are based on materials used in the most important photonic and optoelectronic applications within the visible and the near-infrared ranges and as a result their optical properties are familiar. As a result, they offer many advantages over other types of nanowire. The nanowire sensor has high sensitivity to the changing of the surrounding medium index as a result of leaving a large portion of the guided field outside the wire as evanescent waves [54-55].

1.6.2 Surface Plasmon Resonance

Surface Plasmon Resonance (SPR) is a successful optical transduction method, which is used commercially for chemical and biochemical sensing [56]. Surface Plasmon is a longitudinal charge density wave along the interface of two media, where one is metal and other is dielectric. The working principle depends on transverse magnetic polarized light leading to the excitation of oscillations of electron density at the metal dielectric interface (need a metal surface), which produces a wave known as a surface plasmon wave (SPW). A sharp dip in the reflected light intensity occurs when the incident light (which carries momentum as well as energy) and the wave of surface plasmon match a resonance at the metal surface (non-magnetic), surface plasmon wave is p-polarized, and due to its electromagnetic and surface propagating nature, creates enhanced evanescent wave, as illustrated in fig.1.13a, and b.

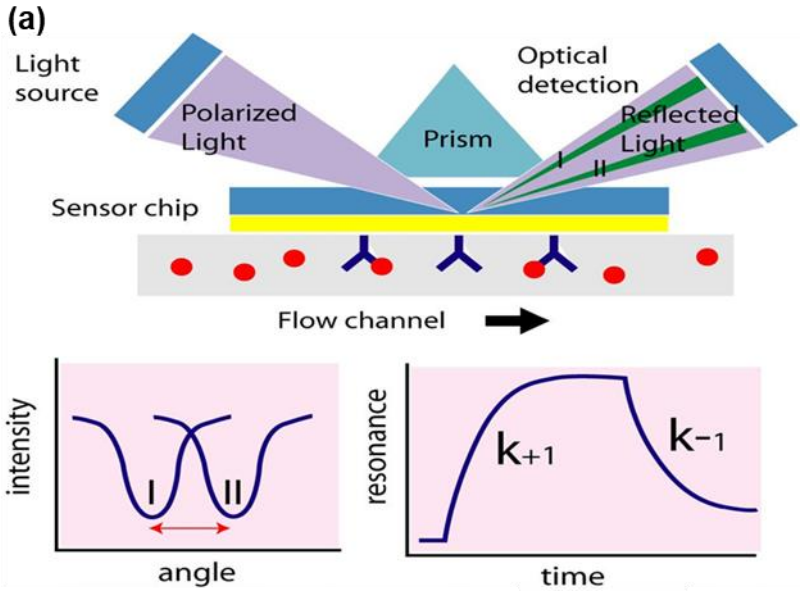

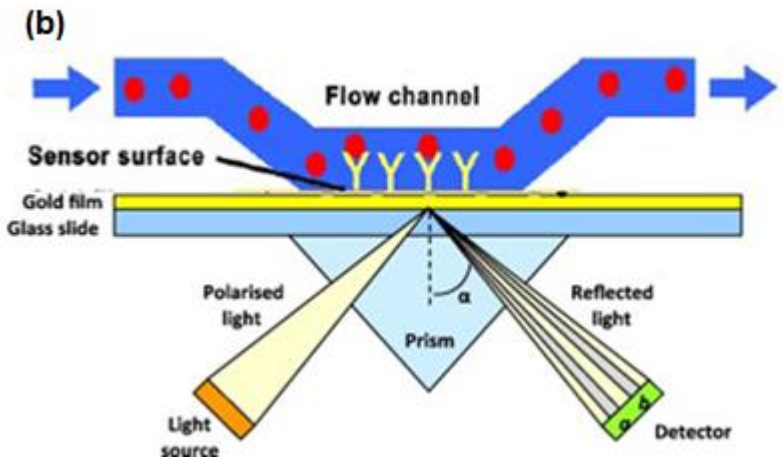

Figure 1.13: a: typical surface plasmon resonance principle K_{+1} indicated association constant for the reactants and k_{-1} indicates dissociation constant the products ; and b: Detecting the changes of the refractive index in the frontal closeness of a surface layer with a sensor chip. A sharp shadow has been observed of the plasmonic resonance in the reflected light at an angle (this angle will be shifted if biomolecules bind to the surface), which depends on the material mass at the surface [57-58].

There are several resonance conditions, which depend on the light wavelength, the incident angle, and the dielectric properties of the substrate as well as the metal. An angular interrogation takes place when the wavelength is kept constant and the angle of incidence is varied which results in a sharp dip at the particular angle. A spectral or wavelength interrogation takes place when the angle of the incident beam is kept constant and the wavelength is varied which results in resonance at a particular wavelength.

The changes in refractive index will change the value of the incident angle or the wavelength because the incident angle and the wavelength depend on the refractive index of the dielectric medium. Generally, a prism is employed to excite surface plasmons using a light source. There are different types of shortcoming in the prism-based SPR sensing device, such as: no remote sensing; large size; and the presence of varied mechanical and optical moving elements. As described below an optical fibre can be used instead of the prism to overcome these shortcomings. The optical fibre SPR probe can be miniaturized, which can be useful for samples, which exist in tiny quantities and are costly [59-60].

1.6.3 Fibre optic SPR

In this type of sensor, the evanescent wave will be produced due to total internal reflection (TIR) is the reflection of the total amount of incident light at the boundary between two media, at the core-cladding interface, as indicated in fig.1.14a. A fibre optic based SPR sensor is built by replacing the silicon cladding of the fibre with a thin layer of metal, which is further surrounded with the sensing layer. To produce the evanescent field, the light is guided into one end of the optical fibre to excite the surface plasmons at the interface of the metal-dielectric sensing layer, as shown in fig.1.14b. The strength of the combination between surface plasmons and the evanescent field depends on fibre diameter, probe geometry, wavelength, and metal layer properties. The intensity of transmitted light (fig.1.14c) is detected at the other end of the fibre after passing via the SPR sensing region as a function of the wavelength.

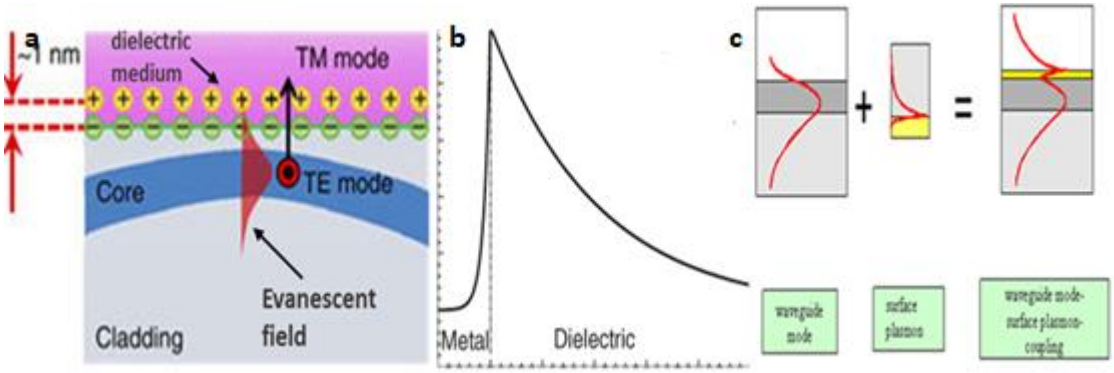

Figure 1.14: (a) the evanescent field corresponding with a TM-mode, which propagates along the interface of a dielectric and a metal, where (b) the electric field declines exponentially. (c) The distribution of the magnetic intensity at the interface between metal and a dielectric for a surface plasmon The possibility of a combination between surface plasmon and waveguide modes [61].

At the metal surface, when biorecognition elements immobilized onto the metal surface recognize and bind with an analyte, which exists in a liquid sample, this leads to an increase in the refractive index. This increase leads to an increase in the propagation constant of the surface plasmon wave (SPW), which propagates along the surface of the metal and can be measured by an optical transducer. The increase in the propagation constant of the SPW is the underlying physical principle of affinity SPR biosensors fig.1.15 [62].

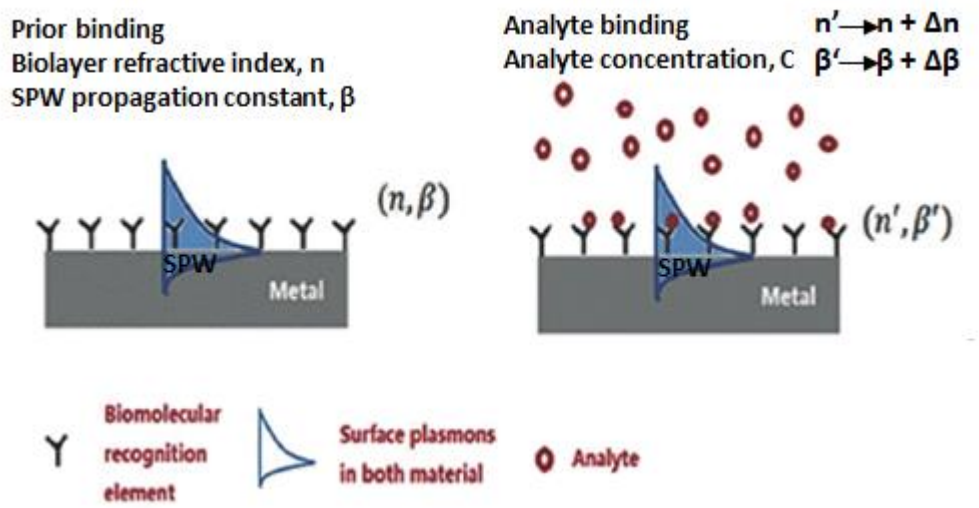

Figure 1.15: Main principles of Surface Plasmon Resonance biosensors [63].

Designs of SPR probe

There are many designs to achieve high sensitivity, reproducibility, detection accuracy and operative range of a fibre optic SPR probe, the sensitivity and the detection accuracy are determined in the same way as determined in the case of angular interrogation.

Metals Selection

For coating, silver or gold is selected for the surface of the fibre core. These have a dielectric constant of both the real and imaginary parts that plays a critical role in achieving detection accuracy and sensitivity. Gold has a higher parameter for the shift of resonance due to the higher value of the real part of the dielectric constant which results in a change of the refractive index of the sensing layer. Silver, on the other hand has higher value of the imaginary part of the dielectric constant which results in a narrower width of the SPR curve causing a higher SNR or detection accuracy.

Gold is chemically stable whereas chemical stability of silver is poor due to its oxidation. The chemical stability of gold is higher than that of silver, due to the tendency of silver to oxides when exposed to air, and especially to water which makes it very difficult to get reproducible results. Therefore a silver-plated sensor isn't reliable for practical applications. There are other metals used for SPR sensor applications such as copper (Cu), and aluminium (Al). Copper is limited in use as the metal for an SPR sensor because it's chemically vulnerable to corrosion and oxidation [63].

Dopants effect

To evaluate the effect of dopants on the sensitivity of the SNR, a theoretical modelling and analysis of SPR based fibre optic sensor was carried out. Phosphorus pentoxide (P_2O_5), germanium oxide (GeO_2), pure silica, and boron oxide (B_2O_3) are commonly used as dopants to enhance the sensitivity of the sensor [64]. The principles simulation of this technique depends on the interaction between several small molecules and various graphene sheets. The model systems are carefully chosen to cover several basic issues. The gas molecules, CO, NO, NO_2 and NH_3, are all of great practical interest for industrial, environmental and medical applications. Meanwhile, NO_2 and NH_3 represent typical electron acceptors and donors, which may undergo charge transfer with graphene. The graphenes are doped by boron and nitrogen atoms, representing the most widely used p- and n-type dopants that the sensitivity and selectivity of graphene-based gas sensors could be significantly improved by introducing dopants or defects into the graphenes.

Polished of side fibre

A common configuration of the sensor among fibre optic SPR probes uses a single mode of side-polished optical fibre and a thin metal layer. Fig.1.13. indicates this configuration, where propagating the guided mode in the fibre will excite the surface plasmon wave at the boundary surface between the sensing medium and a metal. The resonance will occur when the two modes are in a closely matching phase. Thus, the interaction between biomolecule recognition elements and target molecules will induce variations in the refractive index at the sensor surface. For example, immobilisation of antibodies on the surface of a sensor will be observed as a change in the resonant wavelength. Fig.1.16. illustrates the single mode optical fibre based SPR sensor, which is more accurate and sensitive. In recent years, studies of SPR sensing systems have been focused on the attenuated-total reflection geometry obtained by use of prism-coupling optics and the systems of optical fiber sensors that need some bulky structures or complicated signal processing to improve their high sensitivity [65].

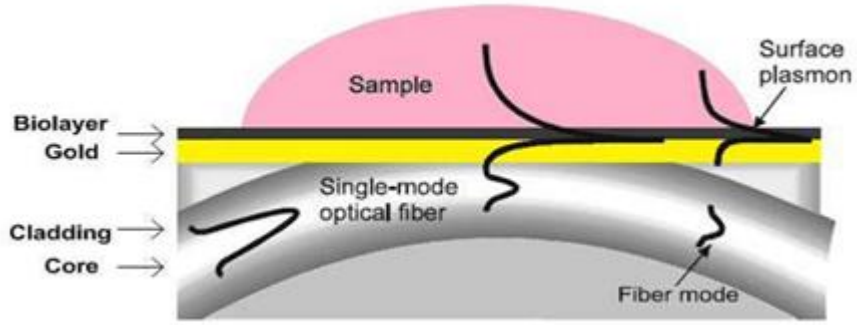

Figure 1.16: A side-polished single mode fibre SPR sensing structure

This type of sensor increases the sensitivity of the sensing area as a result of the side-polish of the fibre. There is another sensor fabricated from D-type single-mode optical fibres using the SPR technique with improved sensitivity for sensing applications. There are SPR designs based on a fibre optic sensor containing the reflecting end face to face with an SPR probe at one of the ends of the fibre. Also, other types of SPR based fibre optic sensors such as side polished multimode optical fibre sensor, and photonic gap fibre sensor have recently been reported that's due to the fabrication of this sensor is very complex compared with multi-mode optical fibre based SPR sensors [66].

1.6.4 Micro-ring resonator optical biosensor

The optical micro-ring biosensor is an emerging technology for achieving high sensitivity, which has recently been under intense investigation to find applications in multiplexed analysis. The size of the device has been reduced by some orders of magnitude without compromising its sensitivity. Micro-ring sensors represent an ideal optical biosensor due to long photon lifetime within the resonator provides a large interaction length at resonance which achieves a highly detectable phase shift. Lately it has been found that a larger light-analyte interaction occurs when the measurement is carried out in a slot-waveguide biosensor with a flow through system for the biomolecules. This means that a slot waveguide-based micro-ring resonator has had a huge impact among biosensors. By applying the proper surface chemistry to a waveguide surface a slot waveguide-based micro-ring resonator is prepared which will result in a thin layer on the top surface of the waveguide, which includes specific receptor molecules for the analyte. The analyte will bind to the specific receptor molecules at the top surface of the waveguide and when the resonator is brought into contact with a fluid including this analyte, this leads to a change of the thickness of the surface of the waveguide layer. This binding will also change the

local refractive index that causing a change in the effective refractive index of the optical mode, as well as the resonance wavelength shift.

To improve the detection limit of the sensor, there are two significant routes. One of these routes is to decrease noise in the determination of the resonance wavelength to increase the quality of the resonator. The other route is involves increasing the interaction of biomolecules attached to the waveguide surface and the light, to increase the average resonance wavelength shift. Only the tail of the evanescent waveguide mode will interact with the biomolecules when using a normal photonic waveguide with a rectangular cross-section [67]. To increase the interaction binding of the analyte molecules to the waveguide surface and improve the sensitivity of the sensor, a narrow slot should be etched in the middle of the waveguide. A large fraction of the quasi-TE mode will be concentrated in that slot.

Light is coupled into a slot-waveguide ring (W_{ring}) by using a straight slot-waveguide (W_{in}), coupled with only one wavelength of light called the resonance wavelength (R), as indicated in fig.1.17a and b, shows a schematic cross-section of the coupling region into the straight-ring of slot-waveguides. There are two strips (rails) on a bottom cladding layer which is straight and ring-slot-waveguides. The top surface of the whole device will expose to the environment, and the refractive index of this region forms the sensing region (S).

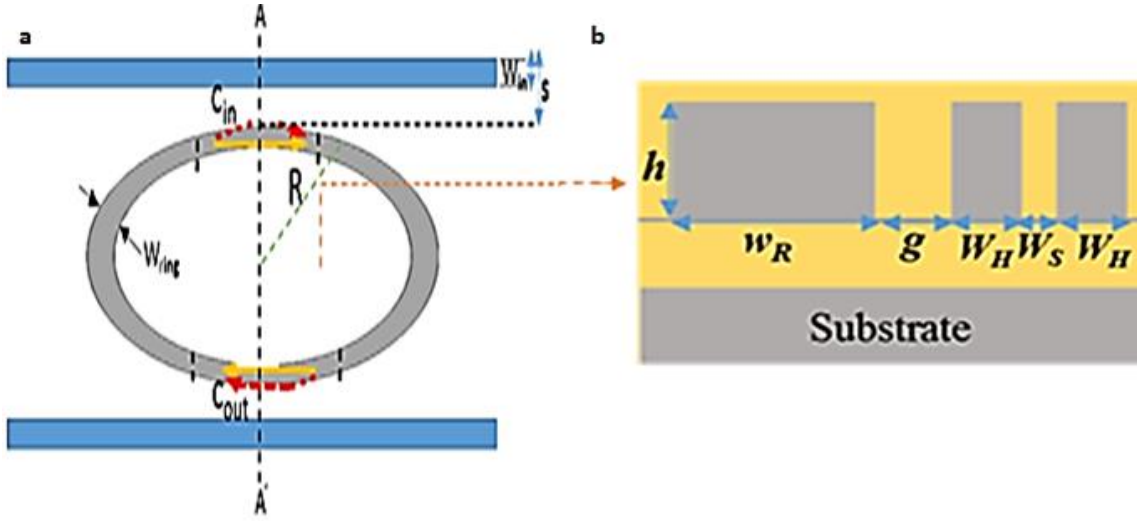

Figure 1.17: (a) A Schematic view top of the slot-waveguide based micro ring resonator, (b) Cross-sectional view of coupling region in the slot-waveguide based micro ring resonator [68-69].

1.6.5 Planar Waveguide optical biosensor

During the last years, optical sensor-based waveguide layers have attracted interest because of the sensor's versatility, sensitivity, small sample requirement, high throughput applications and real-time measurement capabilities. Waveguides that is made of high refractive index materials such as glass, quartz, polymer films and fibres, which is surrounded on all sides by a lower refractive index, like substrate. Planar optical waveguides consist of a transparent waveguide layer with a refractive index that is higher than the substrate layers. At a critical angle of incidence, light is coupled into the waveguide layer and propagated by total internal reflection (TIR), creating an electromagnetic wave (the evanescent field) fig.1.18.[70]. The evanescent field is generated at the waveguide sensor due to the excitation of the light itself in the dielectric layer. This method is highly sensitive to change in the evanescent field; Therefore, it has shown to be an excellent technique for the investigation of surface bound-biorecognitions.

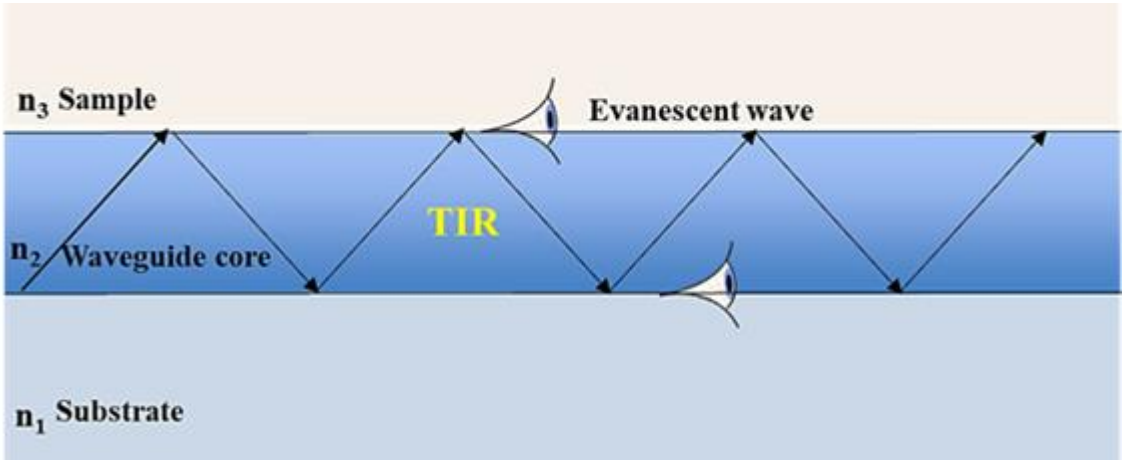

Figure 1.18: Diagram representing the waveguide mode sensor (when $n_2 > n_1$ and $n_2 > n_3$) where n_1, n_2 and n_3 are represent the refractive indices of the light in the different materials). The light is confined into the waveguide layer at a critical angle and travels under total internal reflection (TIR), producing an evanescent field at the boundary.

This was historically explained by Snell's law of refraction as indicated in the following equation:

$$n_1 \sin\theta_1 = n_2 \sin\theta_2 \quad \text{.... ....} \textit{Equation 1.14}$$

Where θ_1 and θ_2 represent the incidence and refraction angles respectively of a ray crossing the interface between two media with refractive indices n_1 and n_2 .

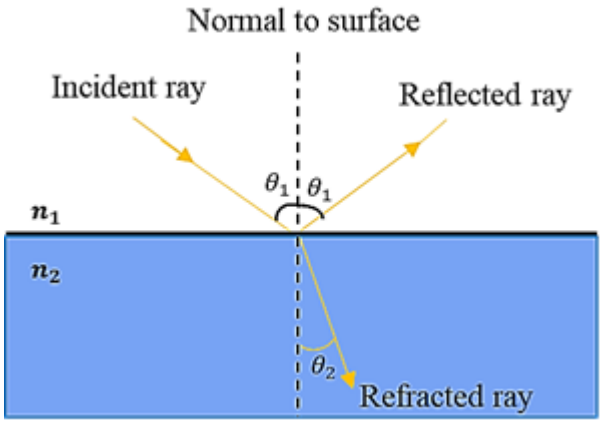

Figure 1.19: The propagation of light through two media ($n_1 \neq n_2$)

The waveguide sensor uses the changes in the refractive index and the intensity of the reflected light that will happen once biomolecules are adsorbed into the waveguide surface and the angle at which the coupling occurs changes fig.1.19 [71].

However, most of the light is confined into the waveguide layer. A small portion of the evanescent field will be extend out of the substrate and into the sample. The evanescent field will be equal to zero at a distance less than one-half the wavelength of the coupled light because it has decayed from the waveguide surface. Hereby a large distinction between contaminates within the sample solution and molecules captured by immobilized bio-recognition species will be obtained, thus obtaining highly sensitive measurements. Different techniques have been used for coupling the light into the waveguide layer such as End-fire coupling via either optical fibre or lens which is considered suitable for a remote sensing application due to the high efficiency of the light transmission. However, the drawbacks of this method may be illustrated by the vulnerability to variation present in a sensing system and the low efficiency of coupling with the nanometre scale core. The grating coupler technique implements the optical diffraction stimulated by periodic patterns engraved on a waveguide layer. Its straightforwardness and stability are the advantages of this method while, due to a narrow band of coupling angles, it suffers from low coupling efficiencies.

By utilizing a prism, the light is coupled into a waveguide layer at a higher refractive index than that of a thin tunnelling substrate. This is preferable for coupling light in optical sensing due to its easy coupling operation and simple configuration [72].

1.6.5.1 Leaky Waveguide Sensor

The leaky waveguide sensor (LW) technique is an alternative way to confine the light into the waveguide layer by total internal reflection (TIR) at the interface between the waveguide and cover interface (sample) being sensed. In this case the light is not completely reflected at the boundary between the substrate and the waveguide and some of the light is leaked fig.1.20 [73].

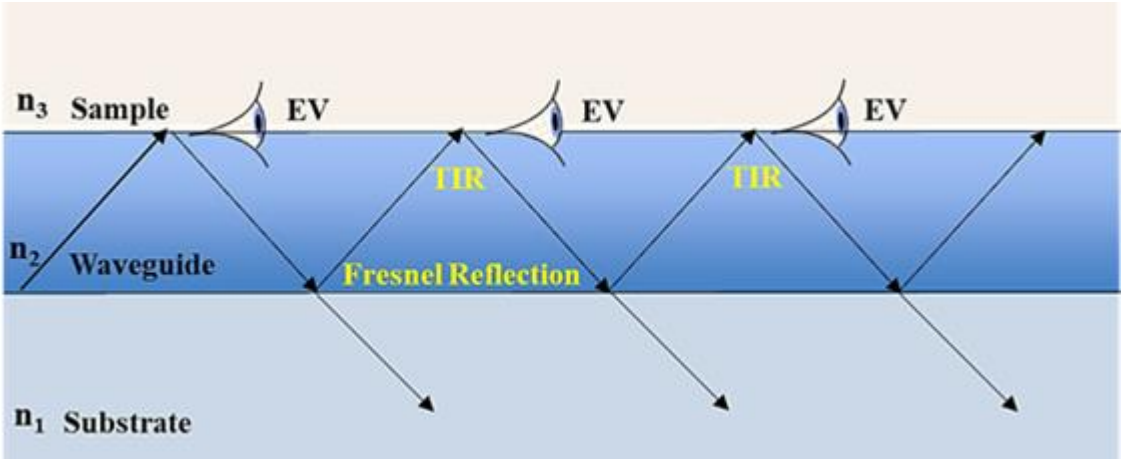

Figure 1.20: Diagram representing a leaky waveguide sensor principle where $n_1 > n_2$ and $n_2 > n_3$ where n_1, n_2 and n_3 are represent the refractive indices of the light in the different materials. Total internal reflection (TIR) occurs at the boundary between the sample and the waveguide creating an evanescent field (EV). The Fresnel reflection is present at the interface between the waveguide and the substrate.

The Fresnel Reflection (FR) is a mechanism for confining light at the interface between waveguide-substrate. FR occurs at any interface between materials with different refractive indices. There is no evanescent field on the other boundary because some of the light is being leaked, and this is different from total internal reflection, although the light is gradually lost from the waveguide either by radiation loss or by absorption. The leaky waveguide technique indicates a typical propagation distance from a few millimetres to a few centimetres, which is appropriate for sensing in most applications [74].

A variety of advantages has been shown for the leaky waveguide sensor over the conventional waveguide, which can be due to TIR no longer being applied at the waveguide-substrate and this leads to greater flexibility in the of choice of waveguide materials. Materials such as silica sol-gels and hydrogels, like agarose can be used as there is no longer requirement for them to have a refractive index higher than that of the substrate. The smaller difference of the refractive index between the waveguide and the sample will generate a higher penetration depth of the evanescent field into the sensing

region which leads to the fact that the leaky waveguide sensor is more sensitive than SPR and a conventional waveguide techniques. The penetration depth of the evanescent field into the leaky waveguide coated with the dye as a reflective layer is 1.5 µM that has been shown to be around 150-200 nm [75].

Specifically, the DDLW in this project consists of a chitosan waveguide doped with reactive blue 4 dye (RB4) on a glass substrate. There are two reasons for immobilizing RB4 dye. First of all, it allows the imaging of the resonance angle in the reflectivity curve as a dip at a wavelength away from the absorption of the antibody. Secondly, RB4 dye contains a sulphonate group, which will react with the amino groups in chitosan under acidic conditions, prevents the dye from leach out the waveguide layer. The immobilisation of RB4 dye into the waveguide layer offers some advantages: first, the coloured product is unable to diffuse away from the sensing region, because it's still immobilized in the waveguide layer; otherwise this would lead to a rapid loss of absorbance signal. Secondly, the experimentally determined sensitivity is higher than total internal reflection (TIR), because of maximisation of the interaction between the optical mode and the immobilized product in the waveguide layer[74]. Third, the small size of the waveguide will focus a high concentration on the small amount of the substrate; this is very low compared with the concentration of the substrate solution present in a flow cell of typical dimensions. And last a high rate of product formation depends on the concentration of the target molecules in the waveguide layer. Therefore the local concentration of the substrate should be high. The DDLW has potential applications in drug discovery, clinical diagnostics and industrial biotechnology fig.1.21 [76].

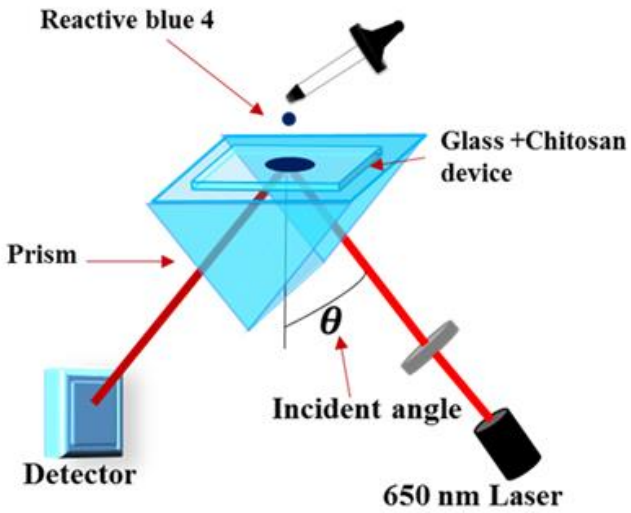

Figure 1.21: The schematic of purpose-built optical set-up used to examine glass slides with reactive blue 4 dye.

1.6.5.2 Materials for Porous Waveguide

In the last twenty years there has been a focus on hydrogel materials because of their range of important properties, for instance biocompatibility, responsive behaviour (volumetric changes), storage capacity and the ease with which they can be modified [77]. This project includes the creation of responsive hydrogel thin films by using chemical crosslinking of reactive blue 4 dye (as a reagent). Hydrogel thin films have attracted interest as their advantages include a method to produce responsive surfaces and interfaces, as they have a broad selection of activation/immobilization chemistries associated with the higher density of immobilization sites and basic surfaces. Hydrogel materials are immobilized on a range of different substrates, including chitosan, agarose, silica sol-gel, polyacrylamide, HEMA, etc. (The substrates often have surfaces modified with an adhesion organiser to increase the stability of the films e.g., self-assembled monolayer or polymer brush) [78].

Chitosan is a derivative of chitin. It is one of the most plentiful natural polysaccharides and its nontoxic. It has some interesting unique properties such as its antimicrobial action which prevents the growth of many varieties of fungi, yeasts, and bacteria, which can be useful for use in the biomedical field, air cleaning and water purification applications. It binds with toxic metal ions and it has a refractive index of 1. 338. Furthermore, chitosan has a pH-dependent solubility: its primary amine groups have a pka value of 6.5 and are positively charged at a lower pH. Chitosan becomes soluble at a higher pH as the amines are deprotonated. This therefore facilitates the deposition of chitosan stable film on different surfaces under neutral and basic pH conditions. All these properties are created as a result of protonation of NH_2^+groups on the skeletal structure of chitosan [79] as indicated in fig.1.22.

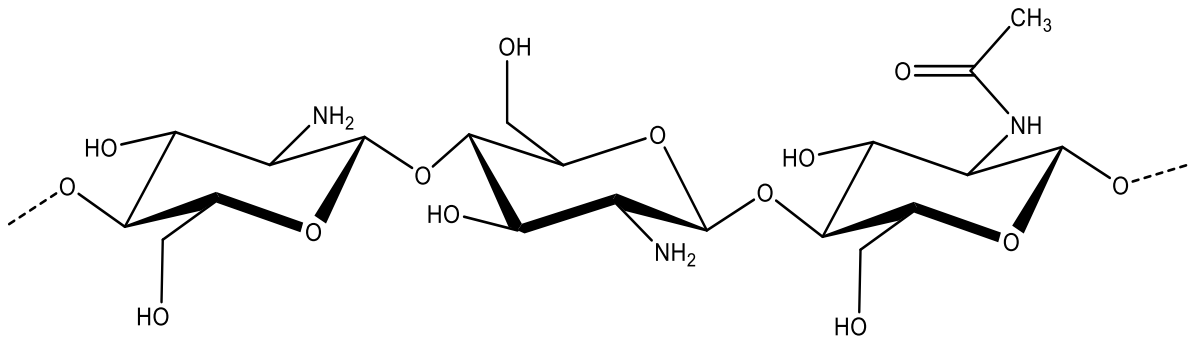

Figure 1.22: Chemical structure of chitosan.

Furthermore, the positively charged amines can be used for the attachment of biomolecules such as antibodies, enzymes and DNA through covalent bonding. The attachment can also carried out through physical interaction such as entrapment and surface absorbance when the substance carries a negative charge. The chain of chitosan polymer may also be crosslinked through an amine group, enhancing the strength and chemical resistance of the film. Chitosan film without any modification is transparent and thus can be used in optical sensors [80].

1.7 Differentiation of performance

Section 1.5 compares the advantages and disadvantages of different sensor architectures. The sensitivity of Mach-Zehnder sensors is high but they are not as compact as micro-ring resonators [81], which require short lengths of three orders of magnitude and will exhibit the sensitivity whereas the Mach-Zehnder based biosensors need long structures. Their sensitivity is similar to that of Micro-ring resonator-based sensors, which depends on the length of the sensing arm L. A change in temperature can introduce an undesired shift in the propagating mode of an effective index, and the sensitivity in a Mach-Zehnder sensor can be affected as a result of such a change. The sensitivity that can be achieved with optical nanowires is much higher when sensing is about 7.5 μm, in comparison with that of a conventional Mach-Zehnder based on integrated planar waveguides, which is below 0.7 μm [50].

The most important advantage of configurations of Micro-ring resonator-based sensors is related to the reduction of dimension without significant effect on the sensitivity of the device. This is due to the large photon lifetime provided at the resonance over a long interaction length which interacts with biomolecules to obtain a detectable phase shift. Therefore, silicon slot waveguides have appeared very attractive nanometre ultrasensitive optical biosensors. The refractive index (RI) sensitivity of a slot waveguide ring resonator is over 298 nm RIU and a D.L of $4.2*10^{-5}$ RIU, and an estimated D.L of protein 20 pg mm^{-2}, whereas in a normal waveguide based ring resonator sensitivity is about 70 nm/RIU[68].

The resonance wavelength is monitored when the micro-ring resonator acquires a source of a tunable laser; this will lead to increased instrumentation costs, which is also why this project does not offer internal referencing for wavelength drifts, temperature drifts and nonspecific binding of molecules. Mach-Zehnder interferometer based sensors can be

utilized with a fixed wavelength diode laser source over a large dynamic range at low cost, and offer internal referencing efficiency for the above parameters by using the reference arm [52].

The Surface Plasmon Resonance (SPR) is commonly used as an evanescent wave sensor It has outstanding performance in evaluating the interactions of complex biomolecules, as a result of which it has been used commercially [50]. However, the sensitivity of the SPR sensor is limited to the nanomolar range, which is not enough for applications needing lower detection levels such as in clinical practice, although it's useful in various other applications. Furthermore, Surface Plasmon Resonance has a relatively large size, which is very complex to miniaturize in a lab-on-a-chip [52].

To overcome these drawbacks, the configurations of Surface Plasmon Resonance-based optical fibre sensors allow for a compact sensing element as well as sensing of sample volume, the potential for disposable miniaturized sensing devices, and the capacity for remote sensing. Therefore these sensors have attracted significant attention, and lead to proposing and demonstrating use SPR based optical fibre sensors, which include single mode fibres or multimode fibres [82].

1.8 Immobilization of Biorecognition Receptors

Immobilization represents a critical step in improvement of any type of optical biosensors: it makes detection more sensitive and easier. A broad range of biomolecules can be used as bioreceptors, such as peptides, antibodies, enzymes, nucleic acid sequences, cell receptors and many more. The immobilization procedure needs to maintain, the bioavailability of the bioreceptors to target molecules in a solution [49]. The chemical and physical properties of the interface plays the main role in realizing optimum recognition of the target molecules and reducing nonspecific adsorption. There is no generic immobilization method because of the variability and complexity of biorecognition molecules. Therefore, the choice of immobilization method depends on the specific properties of the chosen biorecognition molecules.

Different methods have been used to biofunctionalize the sensor surface: (i) Physical adsorption causes by direct deposition of biomolecules; (ii) physical entrapment in a polymer layer; (iii) Covalent bonding of the bioreceptor to the surface; (iv) Non-covalent bonding either by non-affinity binding (such as biotin-avidin systems) or by non-specific electrostatic interactions [83].

1.8.1 Physical Adsorption

In this process the interaction of the molecules with the surface by attractive reactions will lead to adsorption on the surface from solution. A dynamic equilibrium is created between the molecules adsorbed on the surface and the molecules in solution. The system reaches equilibrium when the adsorption rate is equal to the desorption rate. The surface concentrations are related to the residual concentrations, i.e. the high concentration in solution means a high adsorbed amount. The surface excess is called 'on the surface concentration', which is expressed in mol m^{-2}. Some prefer a thermodynamic explanation at the surface the standard chemical potential of the molecule is lower than that in the solution, which represents at the same time a more appropriate environment for these molecules. However, there are many disadvantages for immobilization by adsorption methods only [84].

Adsorption methods are based on the interaction between biomolecules and the surface. Thus the number of the adsorbed molecules will differ from spot to spot. When the solid support is submerged in the solution, release of the adsorbed molecules is more likely: this will cause loss of the signal and cross-contamination of the spots. So, the immobilization process will happen again because of the reversal of the roles of probes and target, which allows for this.

Physical adsorption of biomolecules to a surface depends on the nature of the surface of the substrate and the sorbent, which occurs through van der Waals forces, dipole-dipole interactions and hydrogen bonding. In general, physical adsorption is affected by variations of the surrounding conditions, such as the solvent used, pH, and as well may be a reversible process. On the other hand, physical adsorption may not give as high density of the immobilization of biomolecules as covalent immobilization. So physical adsorption is more often than not specific, and multi-oriented, and often causing inaccessibility of the active binding site. Moreover, the immobilization of proteins on the solid surface by physical adsorption is affected by the chemical and physical characteristics of the sample being analyzed such as urine, blood, and waste water, etc. Also, several factors can cause desorption of the adsorbed proteins such as ionic strength, pH or particular additives in the sample. By using covalent coupling methods these problems can be overcome [85].

1.8.2 Physical Entrapment

The physical entrapment method involves entrapping the biorecognition element in the structure of a substrate such as sol-gel processed glass. The sol-gel process is a powerful method for immobilization of heat-sensitive and fragile biorecognition elements such as antibodies, enzymes, proteins etc. This is because immobilization is straightforward, the simplicity of preparation and the chemical inertness of the sol gel, negligible swelling behaviour, optical transparency and mechanical stability. Two further advantages of a sol-gel process are: that it can keep a large amount of water, making the encapsulated enzyme catalytic centres or biorecognition agents stable for longer; and the method can be carried out at room temperature. Moreover, using a porous substrate such as a sol-gel processed glass offers the opportunity to insert size-dependent specificity towards analytes, due to the fact that the size of porosity can be tailored. One disadvantage of this process is the random orientation of biomolecules. This can mean the active sites are not easily accessible within the matrix, thus making them unavailable [86].

Under basic or acidic conditions, the sol-gel method includes hydrolysis of alkoxide precursors, followed by condensation and polycondensation of the hydroxylated units; this will lead to forming of a porous gel. The resulting sol-gel is a polymeric chain whose average length is greater than a micrometre. Biorecognition elements entrapped in sol-gel have been used in the forms of coatings, films, or monoliths. The surface of an optical sensing element such as waveguide, fibre, or a surface plasmon resonance device can be been coated by a sol-gel processed film [87-88].

1.8.3 Covalent Immobilization

Currently there is more interest in covalent coupling of proteins to solid substrates is due to the greater strength of this approach. In immunosensor applications the transducer surface is usually activated before the attachment of proteins.

This method consists of forming a covalent bond between the biorecognition element, such as antibody, protein, enzyme, or DNA, and the sensor surface. A chemical modification should be performed to the surface before the biomolecule immobilization step because the biorecognition elements cannot couple directly to the surface. The modification of the surface often involves at least two steps. The binding of the biomolecule represents the difficult step of the grafting process [89].

Indeed different constraints have to be accommodated in the process such as low temperature, low concentration, and aqueous solvent etc. The process for attaching the reactive biomolecule to the surface is devised when the chemical functionality of the surface is chosen. The next constraint, the surface chemistry of the transducer should be managed. Indeed, the transducer should be chosen according to its sensitivity to the chemical signal, not for its ability to be grafted. Inorganic materials are used for typical surfaces such as glass, silica, gold etc., but these have limited capability for reacting with the biomolecules.

The chemistry involved is often quite strong and often a coupling agent is used which is a bifunctional molecule. It may be either a homodifunctional agent if the two reactive functions are similar (e.g. phenylenediisothiocyanate), or heterodifunctional if they are different. One end of a coupling agent reacts with the functionalized surface while the second end will further react with the biomolecules. The coupling agent is used either for the chemical modification of the biomolecules or surface functionalization fig.1.23. [90].

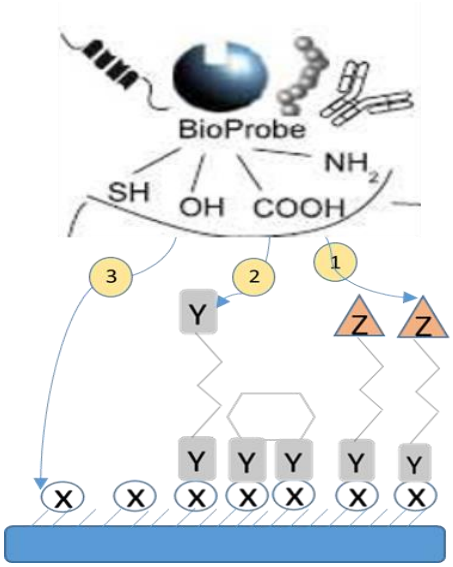

Figure 1.23: Main strategies of chemical grafting; (1) activation of the surface with heterodifunctional linker, (2) activation of the surface with homodifunctional linker, and (3) direct reaction to active surface.

1.8.3.1 Main Coupling Methods

In general, there are three kinds of coupling chemistry: amines, aldehydes, or thiol functional groups on glycoproteins. In all types of coupling, strategies use free carboxymethyl groups on the surface of a sensor. Therefore, they can be utilized for any chips of the sensor which have such carboxymethyl groups. The method of choice is probably ligand-thiol coupling when the protein is to be immobilized on a surface on which a free cysteine or disulphide function group is exposed. If this is unsuccessful,

amine coupling should be tried for. If this coupling method inactivates the protein, aldehyde coupling can be attempted , provided that the protein is glycosylated [91].

(a) Amine Coupling

The most applicable covalent coupling method used for protein immobilization is amine coupling. Immobilization of the protein is via free amine groups that are abundant in most proteins, or the N-terminus of peptides and proteins as indicate in fig.1.24 [92].

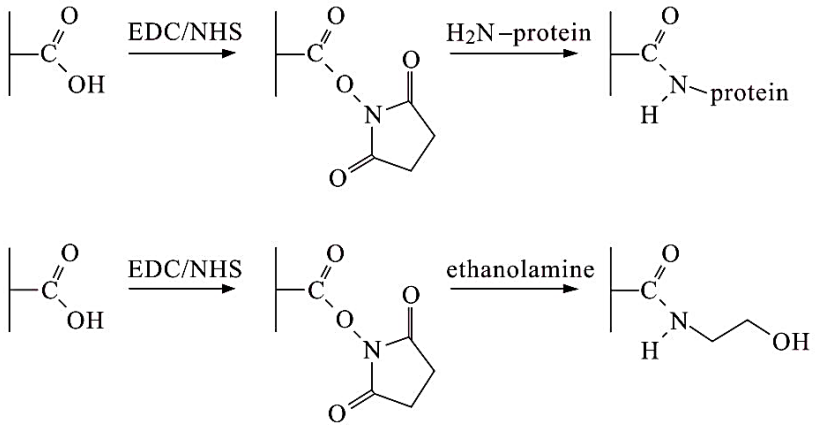

Figure 1.24: Scheme of the covalent coupling of the amino groups of proteins to a carboxylic-terminated surface.

This approach has many advantages including:

- It is highly adaptable, as the huge majority of biomolecules may be immobilized without requiring tags, or without derivatization.
- It produces a highly stable covalent bond which prevents the leaching of ligand from the surface.
- It is very effective through a wide pH range.
- A biomolecule is not exposed to harsh conditions.
- The preparation and reagents may be stored frozen for a long time, may be a few months.
- Immobilization conditions can be controlled easily to decrease cross-linking with the surface.

(b) Aldehyde Coupling

Aldehyde coupling requires forming a hydrazone bond through condensation of hydrazide groups on the surface of a sensor with aldehyde groups on the ligand molecule. Aldehyde coupling is very useful for a specific orientation of protein immobilization that contains functional groups and which may be converted to aldehyde moieties and also may be useful for site-directed immobilization of glycoproteins and polysaccharides. These aldehyde moieties may be introduced through mild oxidation of cis-diols present in the ligand molecule or native to the protein [93].

(c) Thiol Coupling

Thiol coupling via covalent coupling strategies allows site-specific reactions. Forming a sulfhydryl (or thiol) group may be via the sulphur atom of cysteine. The low possibility of cysteine's existence or availability of proteins restricts thiol group immobilization to the natural molecules. This indicates that it is very useful for inserting solvent-reactive groups on the surface of proteins. Cysteine residues involved in disulphide bonds before a subsequent reaction with activated surfaces can be cleft chemically or enzymatically. Because the reaction of a thiol group is very specific, therefore, it is very quick to react with various chemical functions that are highly stable in water fig.1.25 [94].

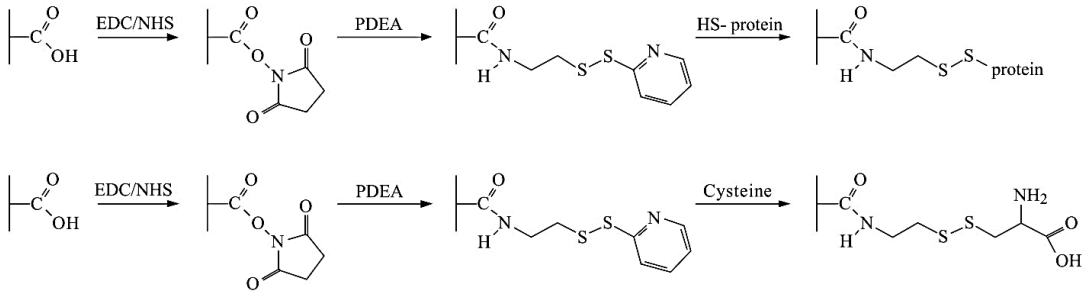

Figure 1.25: Scheme of the covalent coupling of the thiol groups of proteins to a carboxylic-terminated surface.

The reaction of a thiol group onto supported thiol groups via forming of disulphide linkage is the simplest approach. Under reducing conditions, disulphide bonds are unstable. Formation of stable thioether bonds via reaction with haloacetamide groups, or by Michael addition on maleimide groups represents alternative approaches. Thiols are

exposure to self-oxidation. The reactions of oxygen with thiols in aqueous solution give disulphides quite easily (pH 7–9), whole covalent methods are represented in fig.1.26 [95].

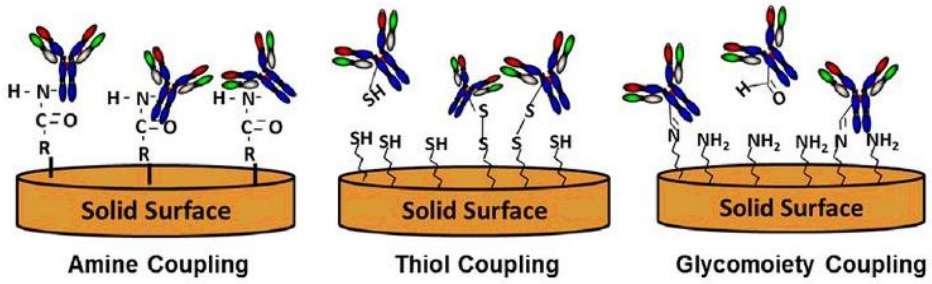

Figure 1.26: Schematic representation covalent coupling immobilization.

1.8.4 Non-covalent Immobilization (Streptavidin-Biotin System)

As early as 1941, the strong interaction between avidin and biotin was discovered [96]. Avidin is a protein usually purified from chicken egg white whereas biotin is a vitamin that can be extracted from all cells. Streptavidin is a bacterial homologous protein to avidin, separated from the actinobacterium Streptomyces avidinii. It is commercially available and more frequently used than avidin because of the number of engineered forms.

The interaction between avidin/streptavidin and biotin has been regarded as the strongest, biological interaction known, with a dissociation constant (Kd) 4 x 10^{-14} M [97].

The formation of a bond between avidin/streptavidin and biotin is very rapid. When it is formed, it is unaffected by extremes of organic solvents, temperature, and other denaturing agents. A large number of research and diagnostic applications using the strong interaction between avidin/streptavidin and biotin have been published. In biotechnology, the strength and reliability of this interaction is very important, and it also serves as a model for high-affinity receptor-ligand binding. In most assays, Streptavidin is bound to a solid phase such as a biosensor chip, whereas biotin is bound to the moiety of interest, often a nucleic acid, proteins or antibody [98], as explained in section 2.14.

Streptavidin has four high-affinity binding sites for the small vitamin biotin that is easily soluble in water. Many biotin molecules can be linked to a single molecule of protein and biotin can be bound to different biomolecules involving antibodies as shown in fig.1.27.

This immobilization approach is utilized in this research to apply with the antibody Tissue Factor (TF) as explained in the experimental section [88].

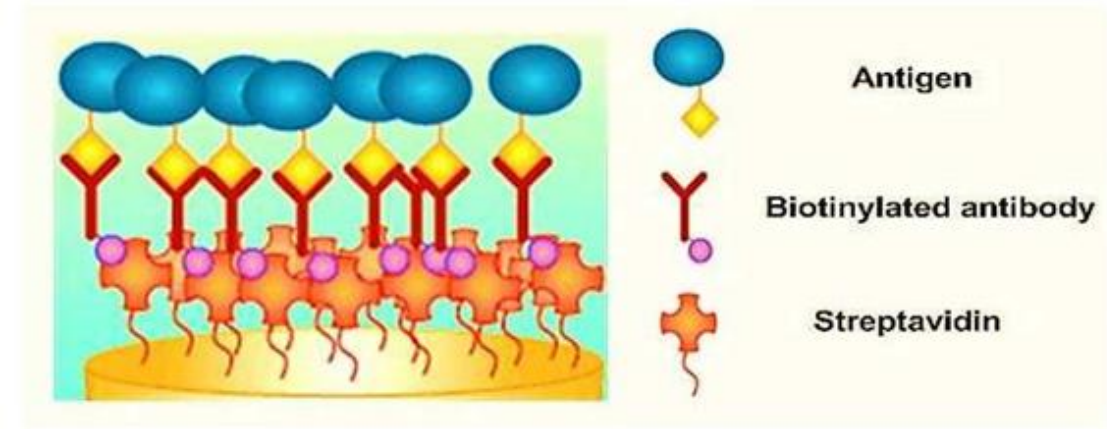

Figure 1.27: Schematic drawing of streptavidin-biotin immobilization [99]

1.9 Application of method - Tissue Factor (TF) analysis

Tissue Factor (TF) is an initiator of the external coagulation cascade which is expressed in different types of cancer cells and has an important function in angiogenesis, progression and metastasis of cancer and embryogenesis. Some call it by different names, such as differentiation CD-142; thromboplastin; or factor III. It has a molecular weight 47 kiloDalton (kDa) of glycoprotein receptor. Recently, it has been shown that TF plays a vital role during fetus formation as insufficiency of TF in transgenic mice causes weakening of vascular function and unusual development of the yolk sac, causing death by day 10.5 [100].

TF is expressed in essential organs including the heart (myocardium), brain (meninges and cerebral cortex), kidney (glomeruli), lung (bronchial mucosa, alveolar epithelial cells, aleveolar macrophages and alveolar septa), placenta and blood vessels (adventitial cells surrounding the blood vessel walls). Expression of TF on these organs has a protective effect in impeding or stopping bleeding that has dangerous sequelae for these organs [101].

Moreover, TF is expressed in non-vital organs such as the gut (mucosa), the peripheral nerve (Schwann) cells, skin (epidermis), and spleen (trabeculae and capsule). Furthermore, TF is usually expressed in host cells such as monocytes, macrophages and fibroblasts, endothelial cells but only in remodelling signals in malignant cases or in response to inflammatory stimuli [102]. The amount of biologically active TF is relatively minor in the plasma of healthy individuals, but this amount increases in different

conditions such as cancer. Pancreatic Cancer (PC) displays high plasma TF concentration that is positively correlated with the occurrence of thromboembolism (TE) [103].

There are 3 distinct domains of this factor, which is composed of 295 amino acids (AA): a 32 AA leader sequence (264-295), which is split to yield the protein, 263 AA which is formed of three domains (cytoplasmic, transmembrane and extra-cellular) that have recognizable roles. The extra-cellular N-terminal domain (AA 1-219) includes two domains of fibronectin type III, which react with FVIIa for initiation of the coagulation cascade and are attached to factor Xa and factor VIIa; while the transmembrane domain comprises 23 AA (220-242), and the short C-terminal cytoplasmic domain 21 AA (243-263) includes three serine residues as indicated in fig.1.28. [104]

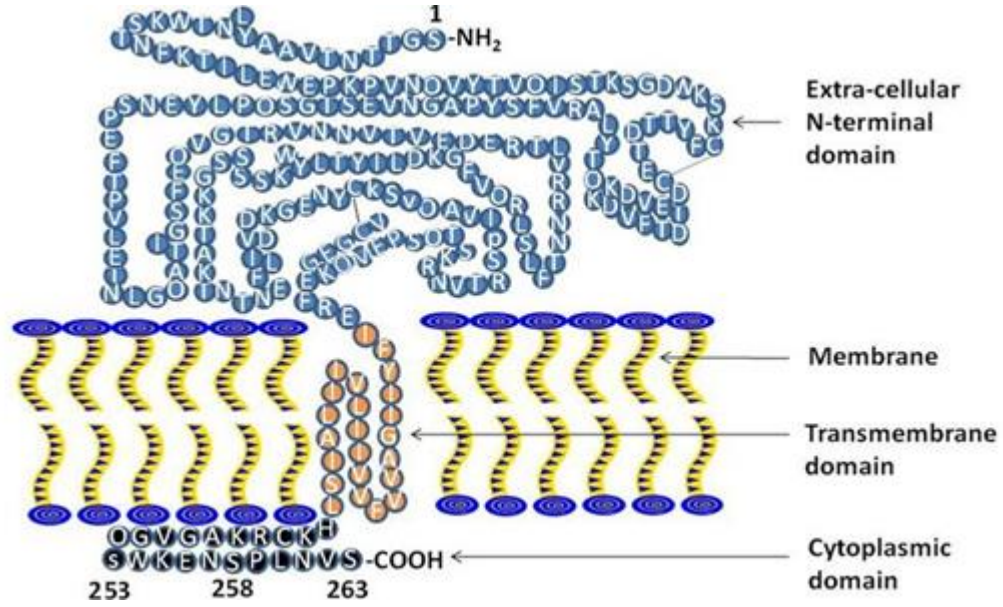

Figure 1.28: Schematic representation three intracellular serine residues of tissue factor

TF appears to have the symmetry of a class II cytokine receptor [105]. However, it does not display all the conventional features of a cytokine receptor, due to the fact that the C-terminal intracellular domain of TF is very short and needs the membrane-proximal design for attaching of the non-receptor Janus kinases (JAKs). The cytoplasmic domain can be phosphorylated by the effect of phorbol ester, when incubated in the synthetic cytoplasmic domain with cell lysate that has been phosphorylated at multiple sites and through a mechanism including protein kinase which can be phosphorylated at serine 253 and serine 258. This phosphorylation is very necessary for cancer metastasis which increases the chemotaxis ability of malignant cells via involvement of the cytoplasmic domain of TF in TF-VIIa signalling [106].

The behaviour of cells through FVIIa/TF signalling alters the tendency for aberrant expression of TF on the tissue. Moreover, high expression of TF is related to greater growth of primary pancreatic cancer (PC) and consecutively more with FVIIa/TF signalling [107]. Another source of TF in the blood is circulating microparticles which will be discussed in detail.

1.9.1 Microparticles

Microparticles (MPs) can be defined as membrane vesicles which have a diameter around 0.1-1 μm and are shed from the plasma membrane of apoptotic and stimulated cells and healthy cells. Microparticles were discovered in 1967 by Wolf, but he considered them as "platelet dust" [108]. The sources of different types of microparticles can include platelets, monocytes, tumour cells, granulocytes, endothelial cells, and smooth muscle cells. Tumour cells are considered the main source of TF-bearing MP. The structure of microparticles consists of a cytoplasmic constituent and membrane components such as phospholipids (PL) and cell surface receptors. Following stimulation, the plasma membrane is rearranged resulting in an outer leaflet rich in phosphatidylserine, essential for TF activity. This is followed by release of MP into the circulation. Furthermore, p-selectin dependent interaction among platelets, macrophages and granulocytes determines expression of TF activity. Moreover, MP express antigenic markers distinctive of the parent cell fig.1.29 [109]. MP might express P-selectin glycoprotein ligand-1 on their surfaces. Endothelial MP (EMP) are also known to contain matrix metalloproteinases (MMP) in addition to procoagulants that are involved in angiogenesis. MMP play an important role in the cell invasion processes. MMP degrades the basement membrane allowing the invasion of the interstitial stroma by migrating endothelial cells [110].

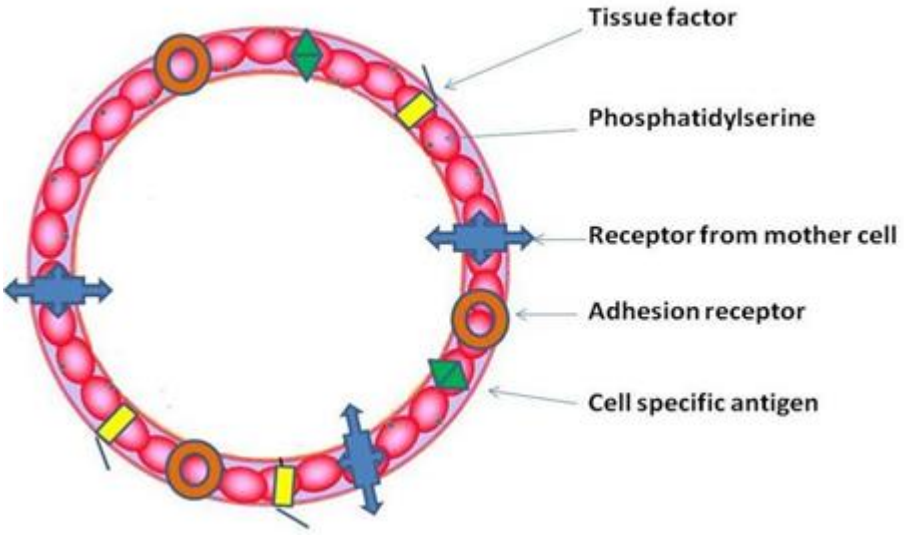

Figure 1.29: Schematic representation of Microparticle.

In vitro, using chemical stimuli such as incubation with Interleukin 1 (IL-1), tumour necrosis factor alpha (TNF-α), and bacterial polysaccharides has led to the induction of microparticles, as also have external causes such as oxidative injury, hypoxia, and chemotherapy caused by the damage to endothelial cells [111].

The activity of pro-coagulant in cancer patients mostly relies on the number of MP circulating bearing PL and TF, and these factors (PL and TF) are essential for transforming FVII to FVIIa which is very important for the external pathway of coagulation. Additionally, enough evidence is accumulating of a relation between the activity of TF expressed on MP and thromboembolism (TE) in cancers [112]. Some investigators have reported that MP bearing TF are necessary for coagulation causing growth and increase of blood clot size instead of initiating coagulation, because the level of TF within the MP is thought too low to trigger the formation of the clot itself, or to be encrypted; however, other investigators suggested that MP bearing TF initiate coagulation and affect vascular function. The TF+MP may both initiate and increase the clot when MP bear a high level of TF. Furthermore, the highest levels of TF activity can be found in pancreatic cancer patients while levels of MP can be increased in patients with some cancer types. Finally, a literature review on MP has supported the idea that is a relation between an increase in the number of MP with the activity of TF in several types of cancer including pancreatic cancer [113].

1.9.2 Correlation between Thrombosis and Cancer

Trousseau described thrombosis in 1865 as a main complication of cancer. The risk of thrombosis in patients with cancer is increased 2-7 fold by comparison with people without cancer [114]. Furthermore, the rate of recurrence of thromboembolism (TE) has been noted as higher in cancer patients than in those without cancer (1.9% vs. 5.4%). In many patients with malignancy, aberrant coagulation was detected, especially in advanced levels or disseminated stages. Moreover, when increasing the prevalence of abnormalities in coagulation, the likelihood of a recognisable haemostasis-related clinical syndrome will increase [115].

That has been supported by a seminal post-mortem study in 1938 which showed that TE is the main complication of pancreatic cancer, related to the high incidence that has been found in pancreatic tail tumours [116]. Pancreatic cancer (PC) has been proved in many recent studies to be one of the malignancies with the highest spread of thromboembolism (TE) (it occurs in more than 57% of pancreatic cancers), and developing thrombosis in a patient's cancer is increased with chemotherapy treatment. Thromboembolism (TE) in pancreatic cancer (PC) patients is related to a short survival period, and the associated early mortality may be directly correlated to the occurrence of thromboembolism (TE)[117]. There are three explanations for the correlation between thrombosis and reduced survival in Pancreatic cancer (PC). First, the thrombosis itself is potentially fatal, and this risk increases directly with the use of many of the conventional therapies, involving erythropoietin, chemotherapy, and anti-angiogenic drugs. Second, malignant cells exhibit increased ability to shed microparticles (MP) and induce thrombosis as they are inherently more aggressive. Lastly, sustaining a continuous loop of factors that promote trafficking and anchoring, tumour growth, invasion and metastasis or a combination of one or more processes causes the targeting of aberrant coagulation which exacerbates the malignant phenotype [118].

1.9.3 Methods Used to Measure TF (III)

Many studies have demonstrated that the major physiological effectors of the initiation of coagulation in blood are pre-existing TF on circulating microvesicles and exposed on the surface of activated platelets. In addition, TF has lately been suggested to be the principle initiator of pathological thrombosis and physiological coagulation, existing in human blood: the location and functional significance of intravascular TF is unknown [119]. The majority of studies using commercial assays report high concentrations of Tissue Factor present in plasma or in microparticles and blood cells. Tissue Factor (III) was detected by different methods under all conditions in plasma, in whole blood, and in suspensions of isolated blood components. To induce the TF-dependent activation of coagulation that were found in microvesicles and activated platelets which should be required substantially to contribute for thrombogenesis. In line with this view, no TF-dependent fibrin formation was measurable, without platelets and microvesicles [120].

Another study in patients with metastatic breast and pancreatic cancer who presented with thrombosis found that that blood coagulation was initiated after isolation of MP in vitro because of the existence of active TF on their membranes. Aspc-1 cells containing high TF antigen levels were assessed by flow cytometry and relative mean fluorescence determined in comparison with Miapaca-2 contained 0.0017 pM of TF[121].

Furthermore, TF expression was determined in pancreatic tissues with pancreatic adenocarcinoma by immunofluorescence. These were investigated for soluble TF levels and coagulation activation markers [thrombin-antithrombin III complex (TAT), prothrombin fragment 1 + 2 (F1 + 2)]. The expression of TF assessed in pancreatic cancer cell lines (Aspc-1 and Miapaca-2) were 357 pg mL^{-1} and 178 pg mL^{-1} respectively[122].

A new chemiluminescent enzyme immunoassay (CLEIA) has been constructed using an anti-human TF monoclonal antibody. Moreover, the CLEIA automated method is more effective than traditional methods such as enzyme-linked immune sorbent assay (ELISA). In addition, the CLEIA method seems to be a simple and quick method with higher sensitivity than the ELISA kit. The detection limit of the CLEIA method was determined to be 0.02 pM of TF expressed from Miapaca-2 cell lines, whereas the detection limit using the ELISA kit was 4.2 pM [123].

Another study has reported that this is related to investigate expression of tissue factor (TF) on pancraeatic cell lines. This was evaluated using optical biosensor interaction

analysis. Fragments of TF were found to bind to plasminogen in a dose-dependent manner, with a detection limit of 10^6 pM. Using optical biosensor analysis (SPR), this study reported whether plasminogen had an effect on the binding of factor F (VII) and F (VIIa) to TF apoprotein. Plasminogen and FVII were found not to block each other's binding to TF and probably bind at an independent site [124].

Furthermore, the quartz crystal microbalance (QCM) sensor was found to be capable of detecting different TF concentrations responsible of clot formation. This technique has been used to obtain substantial information about the clotting process when a potential is applied to the system there is a point where the redox species is oxidised or reduced, when this happens there is a change in current and this current can then be measured to determine the concentration of analyte within the sample. In addition, QCM has many advantages such as it has the potential to be used for point-of-care diagnostics and easy to operate for real-time analysis of blood coagulation. This method requires the use of an electrochemical label. The detection limit of tissue factor by QCM technique was 0.35 pM [125].

Generally, through the last ten years, many conflicting studies have been published related to the concentration, presence, and functional activity of TF in various blood cells and platelets, circulating in blood as a soluble protein. A number of researchers have reported a high concentration of TF antigen circulating in blood at a particle size of 5-10 nm, and this active protein can be reaching (sub)-nanomolar concentrations.

On the other hand, other groups of researchers published some data indicating that the concentration of active protein does not exceed 0.02 pM of TF-related activity either in plasma or in blood from healthy humans. Furthermore, depending on the experience collected from several laboratories, sub-picomolar concentrations of functional TF existing in blood or plasma may be activated within several minutes.

Most studies that have reported high concentrations of TF in platelets and blood cells and the presence of TF in plasma have used commercial assays such as ELISA, Flow cytometer, and Confocal laser scanning microscopy, etc[126].

This sensing system have been used to measure smallest concentrations of Tissue Factor (III), and table1.3, shows limit of detection and sensitivity for the whole methods.

In this work, we are developing a label-free optical biosensor based on dye-doped leaky waveguides (DDLW). Label-free optical sensors are an attractive technology because

they do not require fluorescent dyes or radioactive isotopes for detection, thereby reducing cost and measurement time. Our group is developing dye-doped leaky waveguide (DDLW) system for label-free sensing featuring a thin hydrogel layer as porous waveguide material (chitosan) as the porous waveguide material. The porous hydrogel layer is advantageous as a waveguide because the bio-recognition molecules can be immobilised in its entire volume. The previous work has focussed on agarose as waveguide material for enzyme assays [127]. Here, we investigate chitosan, since it features functional amino groups, and is thus amenable for tethering of bio-recognition elements. We have chosen Anti-IgG as bio-recognition elements as an initial example application. Biotinylated anti-rabbit IgG was immobilised by binding between streptavidin and biotin. The binding of rabbit-IgG and the immobilised anti-rabbit IgG was studied. Once the immobilisation chemistry is developed, the waveguide system is intended to be used to study the release of tissue factor (TF) from pancreatic cells in real-time, and compared to the conventional microwell-based ELISA system. Different TF concentrations (0.003, 0.03, 0.3, 3, and 30 pg mL^{-1}) were investigated.

Table 1-3: Sensitivity and detection limit of Tissue Factor (III), which expression on pancreatic cell lines.

Method	Pancreatic cells	LOD	LOD (pg mL^{-1})
Flow Cytometry	Miapaca-2	0.0016 pM	0.0004
Immunofluorescence	Aspc-1, Miapaca-2	1310 pM 653 pM	357 178
Chemiluminescent Enzyme Immunoassay (CLEIA)	Miapaca-2	0.02 pM	0.005
Optical Biosensor Interaction Analysis	Miapaca-2	10^6 pM	10^6 pM
Quartz Crystal Microbalance (QCM)	Aspc-1	0.35 pM	0.0953
ELISA kit	Aspc-1, Miapaca-2	4.2 pM	1.144

This table indicates some methods required a long-time (> 1 day) to get results, while others needed several hours, also detection limit different for all methods.

Aim and objectives

The aim of this thesis is to develop a dye-doped leaky waveguide (DDLW) system for label-free sensing featuring a thin hydrogel layer as porous waveguide material for detection of biomarkers at pg mL^{-1} levels. Chitosan was selected for the waveguide, since it features functional amino groups, and is thus amenable for tethering of bio-recognition element. Anti-IgG was selected as a model bio-recognition elements for an initial example application. Biotinylated anti-rabbit IgG was immobilised by binding between streptavidin and biotin. Once the method was demonstrated for the model compound the aim was to study a real application. This would be based on the release of tissue factor (TF) from pancreatic cells in real-time.

The objectives of this project were:

- Optimisation the concentration and the thickness of a waveguide layer by using different concentrations (1%, 1.5% and 2%) of porous materials (chitosan) at different spin speeds (2000, 3000, and 4000 rpm).
- Calculation of the available amino groups on chitosan waveguide that would be available for attachment of biorecognition elements.
- Optimisation of the porosity of the chitosan waveguide.
- Optimisation of the immobilisation of rabbit IgG and the binding of rabbit-IgG based on chemistry attachment, concentration of IgG and anti-IgG, type of buffer used and finally incubation time of blocking molecules.
- Investigation of a real application. The release of tissue factor (TF) that has been expressed from pancreatic cell lines (Aspc-1 and Miapaca-2 cells) will be studied with results to be compared with the conventional microwell-based ELISA system.

CHAPTER 2

Experimental Methodology

In this chapter, the utilised equipment and material are described, processes to optimise the waveguide layer are laid out, and experimental methods for enhancement of thin polymer waveguide film porosity are given. The aim of these methods to get a waveguide thin film, smooth and uniform. Moreover, characteristics of a waveguide film and investigate the porosity, all of which have been done through describe tool and materials which are used to optimize and characterize the waveguide layer in order to immobilize biorecognition elements into the waveguide film.

2.1 Materials

The reagents used during the project are shown in table 2.1. Reagents were analytical grade, unless otherwise stated. Reagents were used as supplied unless otherwise stated. Deionised water was obtained from tap water via a water purification system (Elga Ltd., UK).

Table 2-1: List of materials and companies they were obtained from grouped by type of experiment.

Material	Purity %	Companies
Solvents		
Ethanol	> 99.5	Sigma-Aldrich, UK
Chitosan film preparation		
Acetic acid (0.1 M)		Sigma-Aldrich, UK
Chitosan low MW ~ (50-190 kDa)	75-85	Sigma-Aldrich, UK
Chitosan high MW ~ (310-375 kDa)	98	
Glutaraldehyde	25	Sigma-Aldrich, UK
Reactive Blue 4 dye (RB4)	< = 100	Sigma-Aldrich, UK
Buffers and pH adjustment		
HEPES buffer (pH 7.4)	> 99.5	Sigma-Aldrich, UK
Phosphate buffered saline (PBS) tablets		Sigma-Aldrich, UK
Sodium phosphate monobasic dehydrate ($NaH_2PO_4 \cdot H_2O$)	> 99.0	Sigma-Aldrich, UK
Sodium phosphate dibasic (Na_2HPO_4)	> 98.5	Sigma-Aldrich, UK

Sodium hydroxide (NaOH)	> 97	Sigma-Aldrich, UK
Monopotassium phosphate (KH_2PO_4)	> 99	Sigma-Aldrich, UK
Silica nanoparticle experiments		
Ammonium hydroxide (NH_4OH)	35%	Sigma-Aldrich, UK
Silica nanoparticles (100 nm) 10 % (w/v) in ethanol	10% w/v	Sigma-Aldrich, UK
Silica nanoparticles (200 nm) 10% (w/v) in ethanol	10% w/v	Sigma-Aldrich, UK
Tetraethyl Orthosilicate (TEOS)	98	Sigma-Aldrich, UK
Chitosan film characterisation		
Fluorescein isothiocyanate isomer (I) (FITC)		Sigma-Aldrich, UK
Glycerol	> 99	Sigma-Aldrich, UK
Polyethylene glycol (PEG) MW (40 kDa)		Sigma-Aldrich, UK
Polyethylene oxide (PEO) MW (100 kDa)		Sigma-Aldrich, UK
Polyethylene oxide (PEO) MW (200 kDa)		Sigma-Aldrich, UK
Polyethylene oxide (PEO) MW (400 kDa)		Sigma-Aldrich, UK
Linking proteins to film		
N, hydroxysuccinimide-polyethylene glycol- N, hydroxysuccinimide (NHS-PEG-NHS) (500 Da)		Sigma-Aldrich, UK
NHS-PEG-NHS (2000 Da)		
NHS-PEG-NHS 3000 Da)		
NHS-PEG-NHS (10,000 Da)		
(N-(3-dimethylaminopropyl)-N'-ethylcarbodiimide) (EDC)	> 99	Sigma-Aldrich, UK
Sulfo-(N-hydroxysulfosuccinimide) Sulfo-NHS	> 98	Sigma-Aldrich, UK
Reagents for IgG assays		
Bovine serum albumin (BSA)	> 98	Sigma-Aldrich, UK
Monoclonal goat anti-rabbit IgG		Abcam plc, Cambridge, UK

Polyclonal goat anti-rabbit IgG		Abcam plc, Cambridge, UK
Biotinylated goat anti-rabbit IgG		Abcam plc, Cambridge, UK
Rabbit IgG (HRP)		R&D system Europe, Ltd. Abingdon, UK
Streptavidin		Sigma-Aldrich, UK
Tissue factor (TF) assay reagents		
Duo Set ELISA Ancillary Reagent Kit 3		R&D system Europe, Ltd. Abingdon, UK
Human Coagulation Factor III/Tissue Factor (TF) KIT		R&D system Europe, Ltd. Abingdon, UK
Cell line experiments		
AsPC-1 (Cell Lines generated from Pancreas Ascites from an Adenocarcinoma)		ATCC, Teddington, UK
MIA-PaCa-2 (Cell Lines generated from with a primary adenocarcinoma tumour)		ATCC, Teddington, UK
RPMI-1640 (Roswell Park Memorial Institute, medium culture human leukemic cells)		PAA the cell culture company, Yeovil, Somerset, UK
Trypan blue solution ($C_{34}H_{24}N_6Na_4O_{14}S_4$) in water, <0.1 mg/mL		Sigma-Aldrich, UK
DMEM High Glucose Without L-Glutamine		PAA the cell culture company, Yeovil, Somerset, UK

2.2 Waveguide Fabrication and Characterisation

2.2.1 Concept of Optical Setup

The concept of the dye-doped leaky waveguide (DDLW) has been laid out in detail in section 1.6.5.1). Briefly, a glass substrate of high refractive index (n = 1.51) is coated with a fairly thin chitosan layer (*ca.* 500 nm) of medium refractive index (n ~ 1.338); the

top layer of aqueous sample or buffer solution features a lower refractive index (n ~ 1.333) (fig.2.1). When coupled into the waveguide above a critical angle (θ_c), light travels along this waveguide based on total internal reflection (TIR) and Fresnel reflection/refraction (fig.2.2a and c). The waveguide is doped with an absorbing dye (RB4) which causes a dip in the reflectivity curve at a resonance angle (θ_r). The chitosan layer can be modified with biomolecules such as antibodies through its entire volume to allow specific binding for immunoassays. Such binding events cause a change in refractive index within the waveguide layer and thus a shift in the resonance angle (dip). This is used for quantification of the binding events occurring in the waveguide layer (fig.2.2b and d).

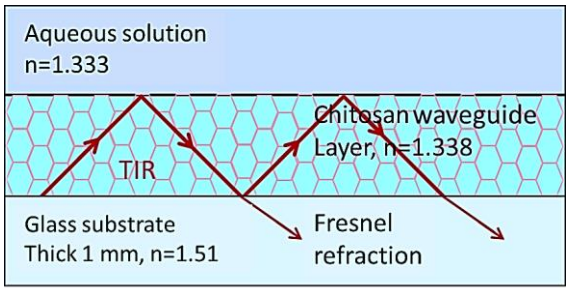

Figure 2.1: Glass substrate 1 mm thick (n = 1.51), coated with chitosan layer of chitosan (n = 1.338), the 'cover' are the aqueous solution (water n=1.333). When irradiated above a critical angle, light propagates through the chitosan layer by total internal reflection (TIR) and Fresnel reflection/refraction.

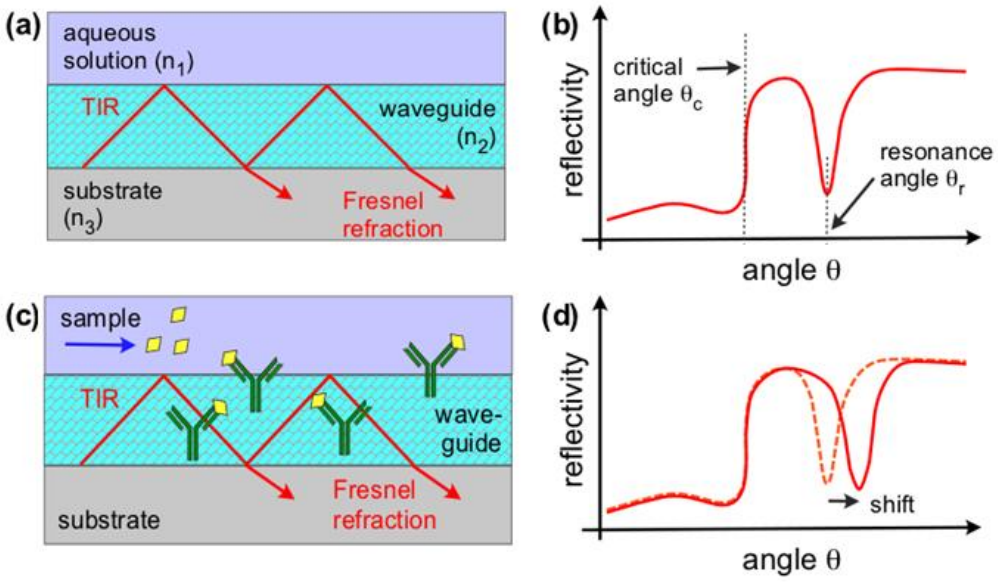

Figure 2.2: a- Coupled the light into the waveguide layer above critical angle, b; The waveguide is doped with an absorbing dye (RB4) which cause a dip in the reflectivity curve at resonance angle, c; The waveguide layer can be modified with biomolecules through its entire volume to allow specific binding for immunoassays; d; A shift in the resonance angle (dip) that's due to the change in the refractive index when binding events of biomolecules within the waveguide layer.

To conduct measurements with this concept, the chitosan film needed to be deposited a substrate and interfaced to a flow cell to allow fluid delivery. The flow cell is then mounted onto an optical setup to introduce light at a given angle and detect the light exciting the waveguide via a suitable detector (fig.2.3). The data then needs to be processed. These are described in the following sections.

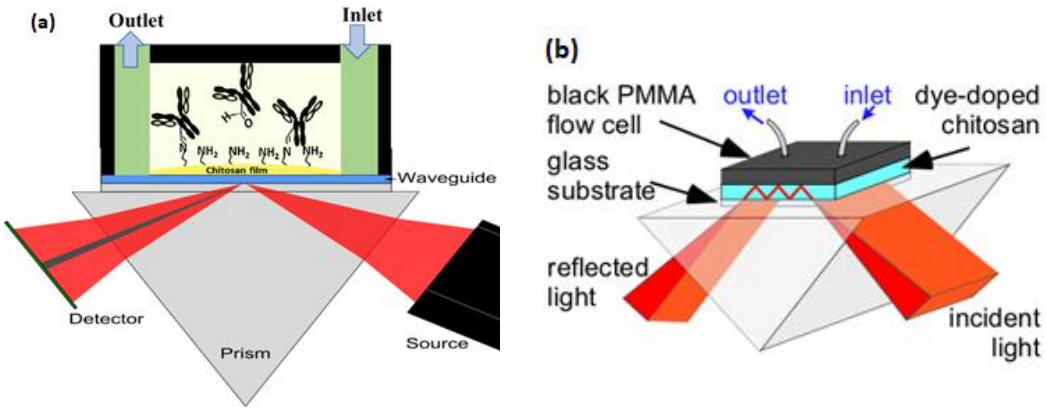

Figure 2.3: Schematic representation of (a) an optical setup that was used to optimise and characterise the waveguide film and to investigate the binding reaction of biorecognition elements and (b) It consists of the light source, detector, and the device.

2.2.2 Glass Substrate Cleaning

To get good adhesion between the substrate and the waveguide film, the substrate should be treated to render it hydrophilic. Glass microscope slides of dimensions 25 mm x 75 mm (VWR Leicestershire, UK) and 1 mm thickness were cut into 25 mm x 25 mm squares using a diamond scribe and a ruler for guidance. The glass squares were cleaned in three steps: firstly, using tap water with soap, secondly, in de-ionised water and, finally, in ethanol (>99.5%), each in an ultrasonic bath (Buckinghamshire, UK) for 30 min.

2.2.3 Preparation of Chitosan Solutions

Chitosan was obtained as a powder. A range of chitosan solutions were made up with concentrations of 1.0%, 1.5%, 2.0%, 3.0% and 4.0% (w/v%). These were prepared by weighing an appropriate amount of chitosan and dissolving it in 10 mL of 0.1 M aqueous acetic acid. Dissolution of the chitosan was achieved by magnetic stirring for 90 min. Immediately following this, 12.5 µL of 50% (v/v %) glutaraldehyde in water was added as a crosslinker and left to react for 15 min. This was used straightaway for spin-coating.

2.2.4 Spin Coating Chitosan on the Glass Substrate

For spin coating, a clean glass slide substrate was mounted on the chuck of a spin coater with Norland Optical Adhesive (NOA, 13685, Tech Optics, UK). A vacuum of ~10 psi was used to hold the glass substrate on the chuck. About 2 mL of chitosan solution was dispensed onto the glass substrate such that it was flooded and spread out uniformly covering entire the surface (fig.2.4). The substrates were spun at a range of spin speeds (2,000, 3,000 and 4,000 rpm) for 30 s. Excess solution was thus removed from the glass substrate surface leaving a thin film. Following spin coating, the film was left to dry on the bench for about half an hour. At this stage reactive-blue-4 (RB4) dye was added to obtain a 'dye-doped' waveguide. This doping procedure was optimised as outlined in section 2.3.1. The chitosan films were characterised as outlined in section 2.4. Photographs of the substrate before and after film coating are shown in fig.2.5.

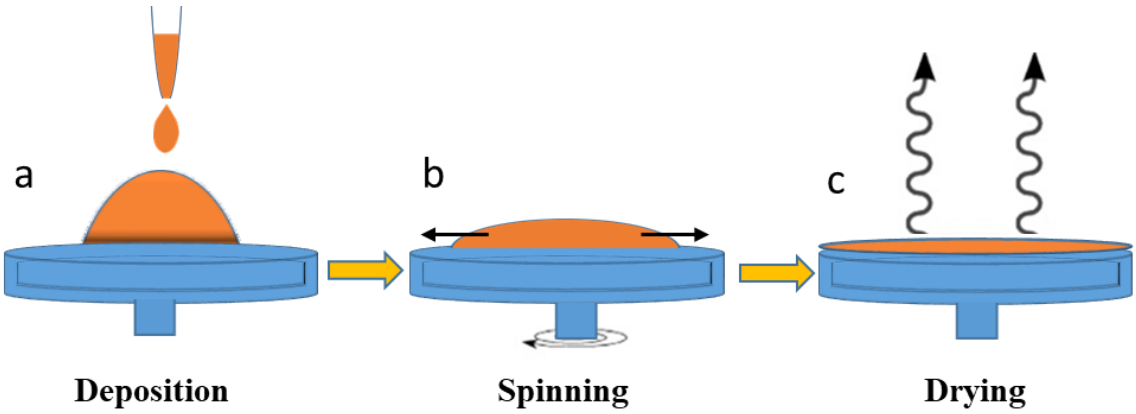

Figure 2.4: Process of spin coating the glass substrate with chitosan solution. (a) Dispensing 2 mL of chitosan solution onto the substrate, (b) spinning at 2000 – 4000 rpm for 30 s to achieve a uniform spread out thin film and (c) film drying at room temperature on the bench.

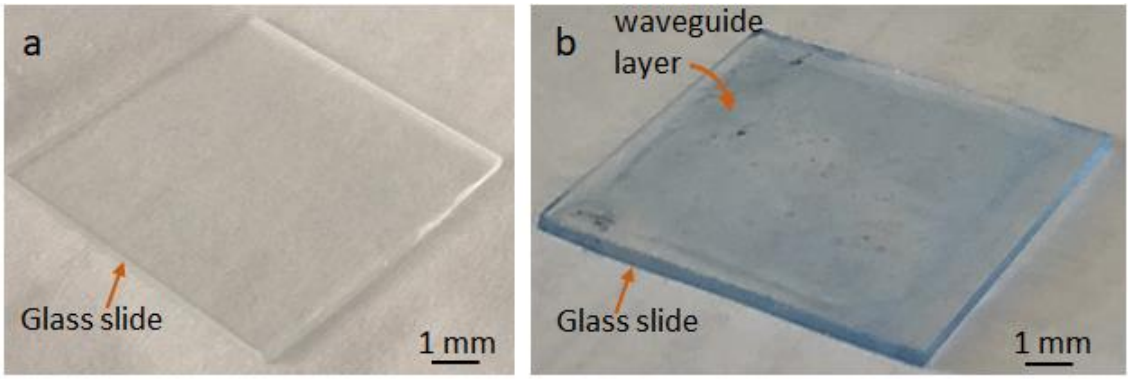

Figure 2.5: Photographs of glass substrates coated with chitosan (a) before and (b) after staining with RB4 dye.

2.2.5 Optical detection setup

A schematic of the instrumentation used for the leaky waveguide experiments is shown in fig.2.6. A BK7 equilateral prism of 30 mm by 30 mm (Qioptic Photonics, UK) was used to couple light in and out of the DDLW device. Two different sets of light source and detector were used.

(1) To obtain reflectivity curves as function of angle of incident light, the light source was a red laser (RS components, UK, λ= 650 nm, power output 5 mV), and the detector was a photodiode (OSD100-6, Centronic, Surrey, UK) (fig.2.7a). (2) To monitor the shift in dip as a function of time, a red LED (RCLED, PR65-F1P0T, Roithner Lasertechnik, Austria) was employed as light source. A collimating lens (30 DQ 25, Comar Optics, UK) and a cylindrical lens (100 mm YD 25, Comar Optics, UK) were positioned in front of the LED to obtain a collimated and wedge shaped beam. For detection a monochrome CMOS camera (PL-B781, Pixelink, Ottowa, Canada) with 2,208 pixels by 3,000 pixels (6.6 mega pixels) was employed (fig.2.7b).

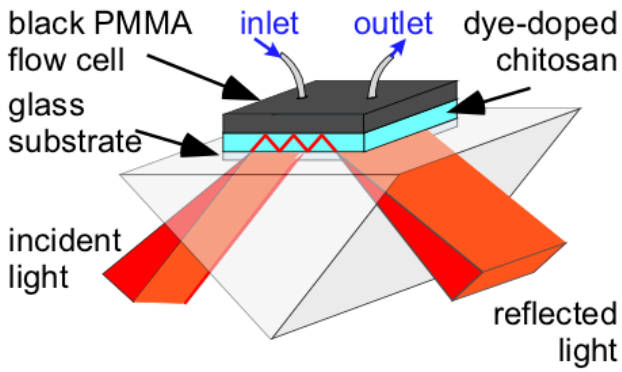

Figure 2.6: Conceptual drawing of setup showing the flow cell, waveguide in the chitosan layer. (a) A circular laser beam with photodiode was used for measuring reflectivity curves and (b) a wedge shaped beam from a red LED in combination with a CMOS camera was used to carry out measurements to record the shift in dip.

This was accomplished by using an adaptor and passed through a variable diameter iris (Comar Instruments, Cambridge, UK). The iris was positioned between the source light and the prism end and a collimating achromatic doublet lens (Comar Instruments, Cambridge, UK). The lens had a diameter of 25 mm and a focal length of 63 mm. The output beam from the Leaky Waveguide (LW) was focused on a plano-convex lens with a diameter of 6.3 mm and a 10 mm focal length.

The light source and detector were mounted on rails, which were connected to two goniometers (fig.2.7); the angular position was controlled via a computer interface through a program by Dr Gupta's collaborator.

The goniometers provided high angular precision, one controlled the position of the light source and the other was used to synchronise the detector to the corresponding specular reflection angle. The whole system was encased in a light tight box with door (fig.2.8).

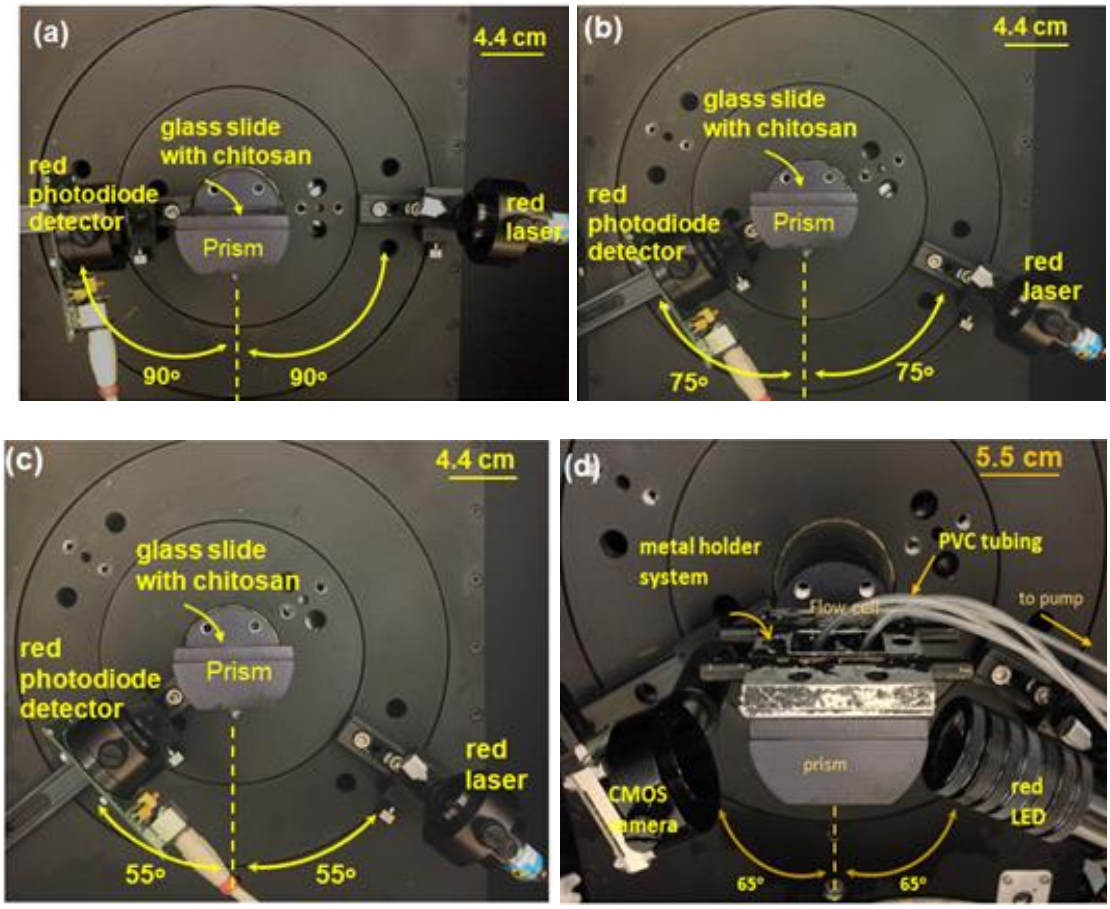

Figure 2.7: (a) Setup featuring laser light source and photodiode detector at home position 90°, (b) at 75° angle and (c) at 55° angle (d) Setup featuring red LED as light source and CMOS camera as detection at 65 ° angle.

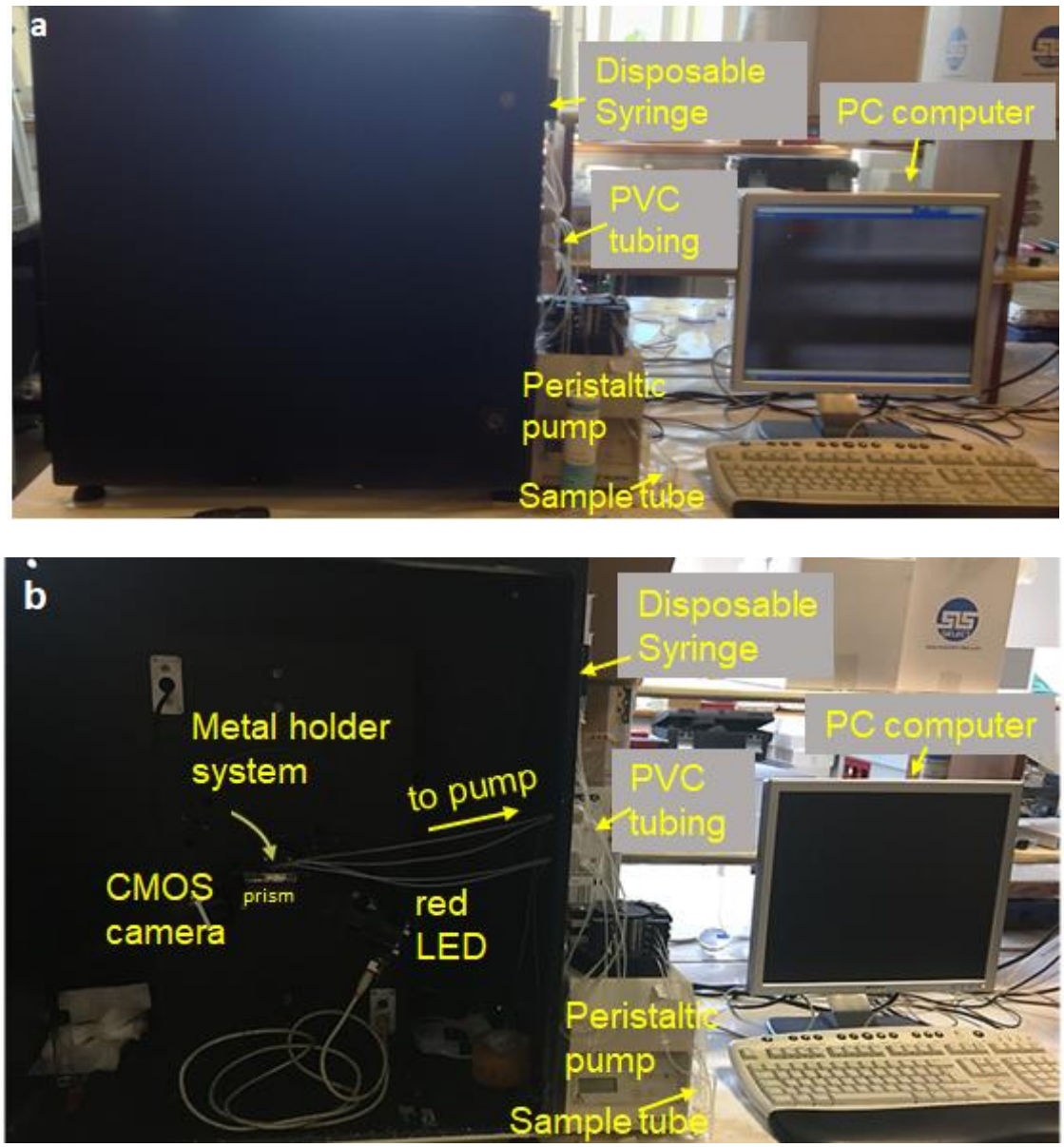

Figure 2.8: Photograph of full setup encased in light tight box (a) with closed door, (b) with open door.

Procedure for measuring absorbance spectra in cuvettes or glass substrates

To produce simple absorbance measurements, (fig.2.9), a polymer cuvette (12.5 mm x 12.5 mm x 45 mm, 2.5 mL internal volume, 10 mm pathlengh, Brand, Germany) was mounted into a holder. For absorbance measurements through chitosan coated glass substrates, the glass slide was fixed in the holder with BlueTac. The holder was fixed in the centre of the setup. The laser was used as light source and the photodiode as detector, these were attached to the rails at 90°with respect to the normal to the base of the prism. The acquisition time of the photodiode was set to 25 ms. The output was recorded in mV.

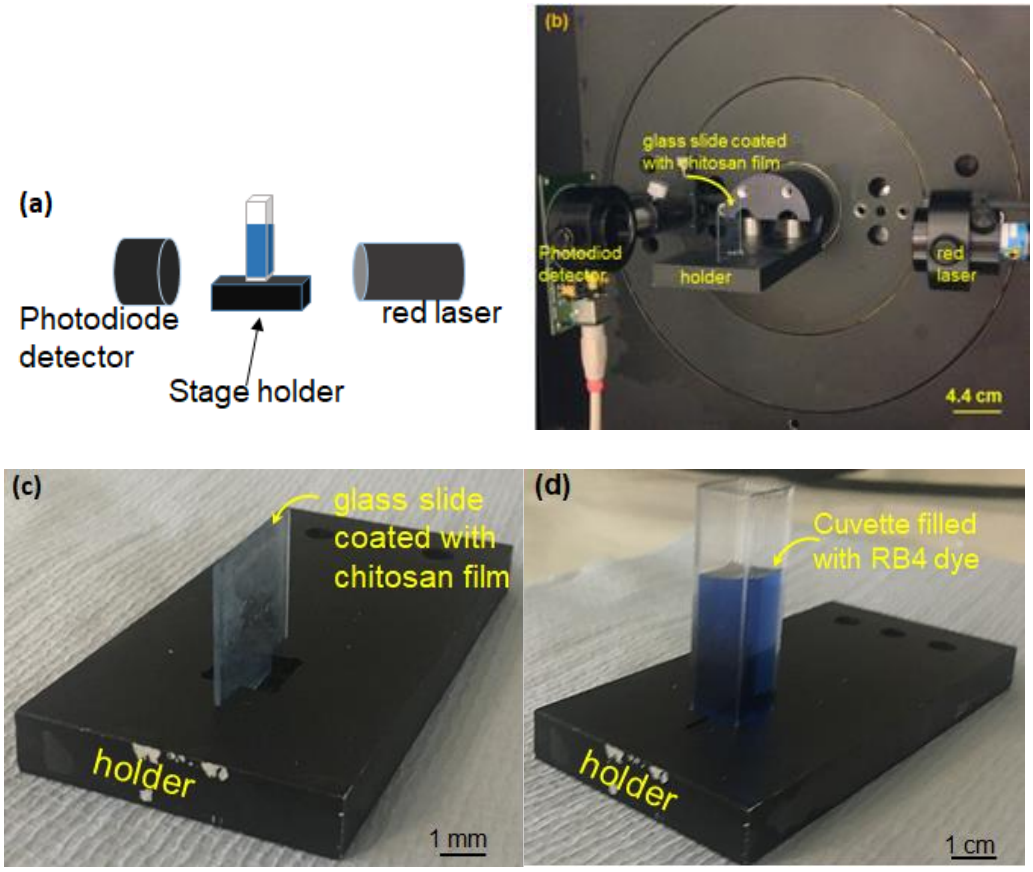

Figure 2.9: (a) Schematic of absorbance measurement setup. (b) Photo of absorbance measurement setup with light source and photodiode detector featuring mounted glass substrate. (c) Photograph showing detail of glass substrate mounted on stage, (d) photograph of cuvette mounted on stage.

Procedure for taking reflectivity curves

To produce reflectivity curves (fig.2.11), the laser was used as light source and the photodiode as detector. These were mounted onto the rails (fig.2.10). Angular scans were typically performed from 75° to 55° with respect to the normal to the base of the prism. This was processed with a measurement time of 30 s. The acquisition time of the photodiode was set to 25 ms. The output was then in the form of a reflectivity curve (fig.2.11) showing amount of light picked up by the photodiode in mV as a function of incident angle. A typical shape would show low reflectivity at low angles. When the incident angle is above the critical angel (θ_c), the reflectivity rises sharply and remains high. However, when RB4 dye is present, due to absorbance of light at a certain resonance angle (θ_r), a reduction in reflectivity is observed around this resonance angle. This reduction is reflectivity is referred to as 'dip' in reflectivity.

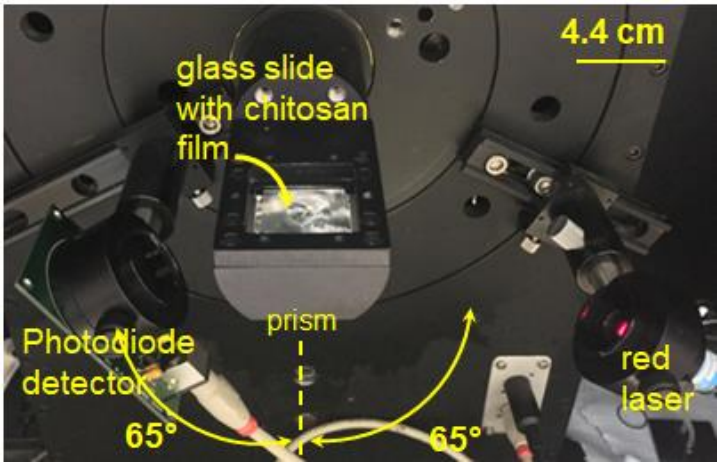

Figure 2.10: Photograph of laser light source and photodiode detector at 65 ° angle.

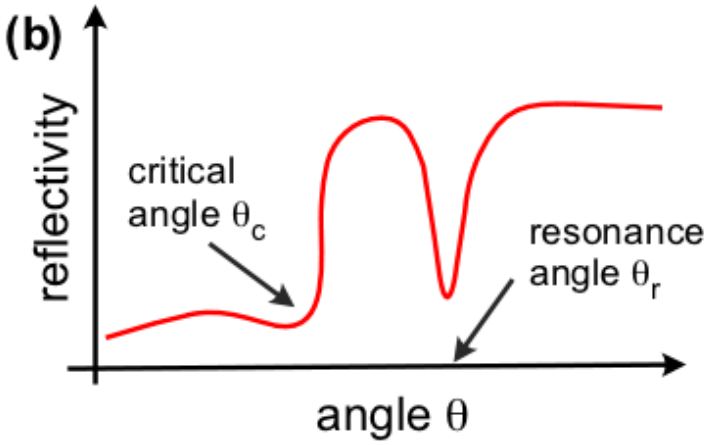

Figure 2.11: Reflectivity curve of the output light that picked up by the photodiode in mV as a function of incident angle.

Procedure for measuring shift in dip

For quantitation of binding events, curves were obtained showing the shift in dip as a function of time (fig.2.13). It is the shift in angle for the dip before and after a binding event that is recorded to obtain information on amount of binding. The red LED was used as light source and the CMOS camera as detector. These were held at a fixed position, *i.e.* 65°, with respect to the normal of the prism base, which is close to the resonance angle for the chitosan waveguide (fig.2.12b). The CMOS camera captures a two-dimensional image (fig.2.12c), the y axis represents a certain width of the flow cell (i.e. a distance measurement), whereas the x-axis represents an angular reading. The dip in reflectivity is recorded as a dark line on this image. If the dip in reflectivity shifts, the dark line moves along the x-axis of these images. These shifts in darkness are recorded and tracked. Initially a shift in pixels is obtained from the image, which is converted into a shift in degrees as outlined in below.

The CMOS camera was interfaced to a computer via USB 2.0. The camera settings were controlled via PixeLINK capture OEM (Pixelink, Ontario, Canada). The data was recorded through a program called GetFrame V8.

The software opens a menu (fig.2.12a), which allows the user to select number of bits (8 bit or 16 bit capture), brightness and also allows the user to start measurement. The image obtained from the CMOS camera is also displayed on the screen, (fig.2.14). The image is 3,000 pixels (x-direction) and 2,208 pixels (y-direction). This represents a reading in distance on the y-axis and a reading in angle in the x-direction. 'Boxes' for data capture could then be drawn around the dip region (fig.2.12e) which resulted in a plot of distance versus grey scale intensity being displayed (fig.2.12d). It was important to start and end the boxes in the light regions around the dip. The software allowed automatic tracking of any shift in the dark region using a center of gravity algorithm and a threshold of 60% of the depth of the dip which was captured over time showing data for all the boxes drawn (fig.2.15). When a measurement was started, the time plot would start from zero seconds and continue saving data until such a time when the measurement was stopped. This data was saved as csv file and later processed with Microsoft Excel. Typically, about 20 boxes would be processed in parallel.

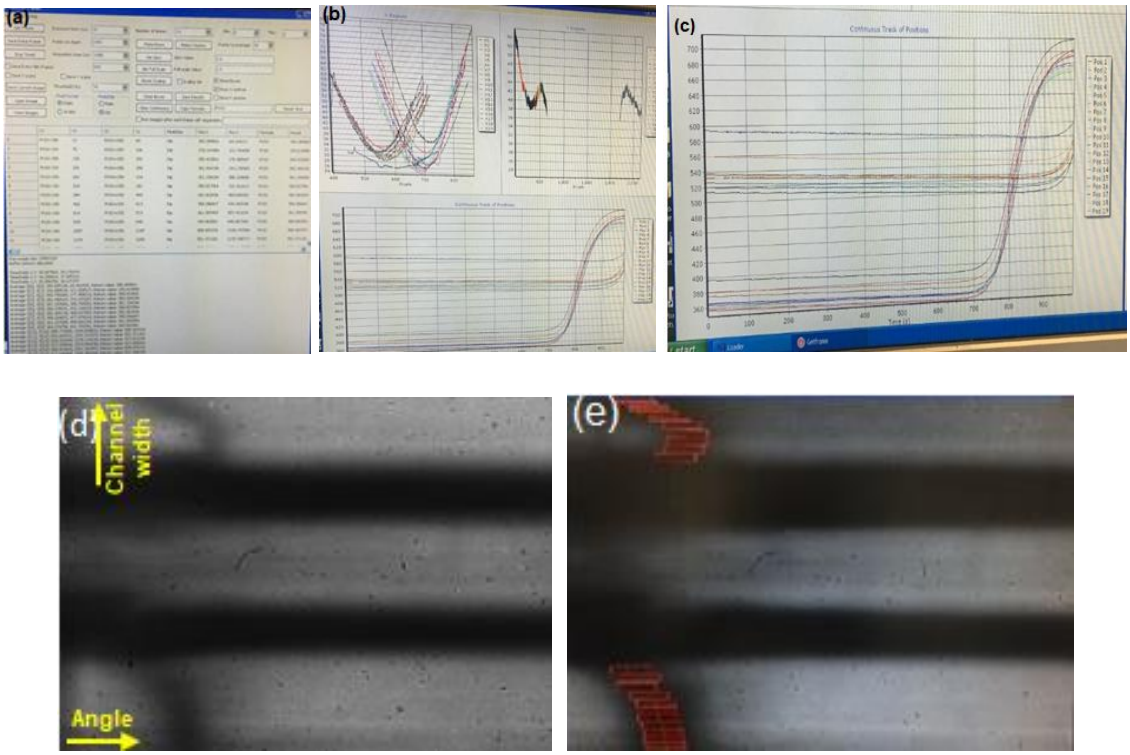

Figure 2.12: (a) Screenshot of window for menu selection, (b) shift in dip versus time, (c) pixels versus darkness plot, (d) screenshot of CMOS image, (e) Screenshot of CMOS image with boxes.

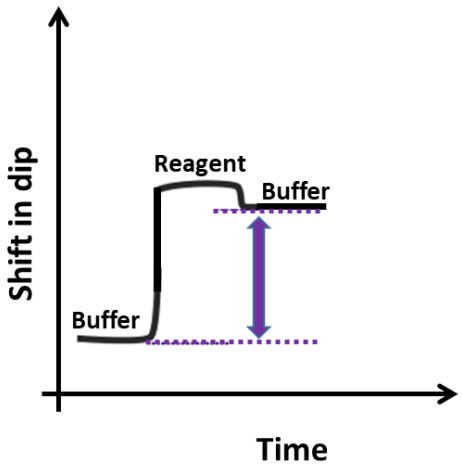

Figure 2.13: Concept of quantitation of shift in dip versus time.

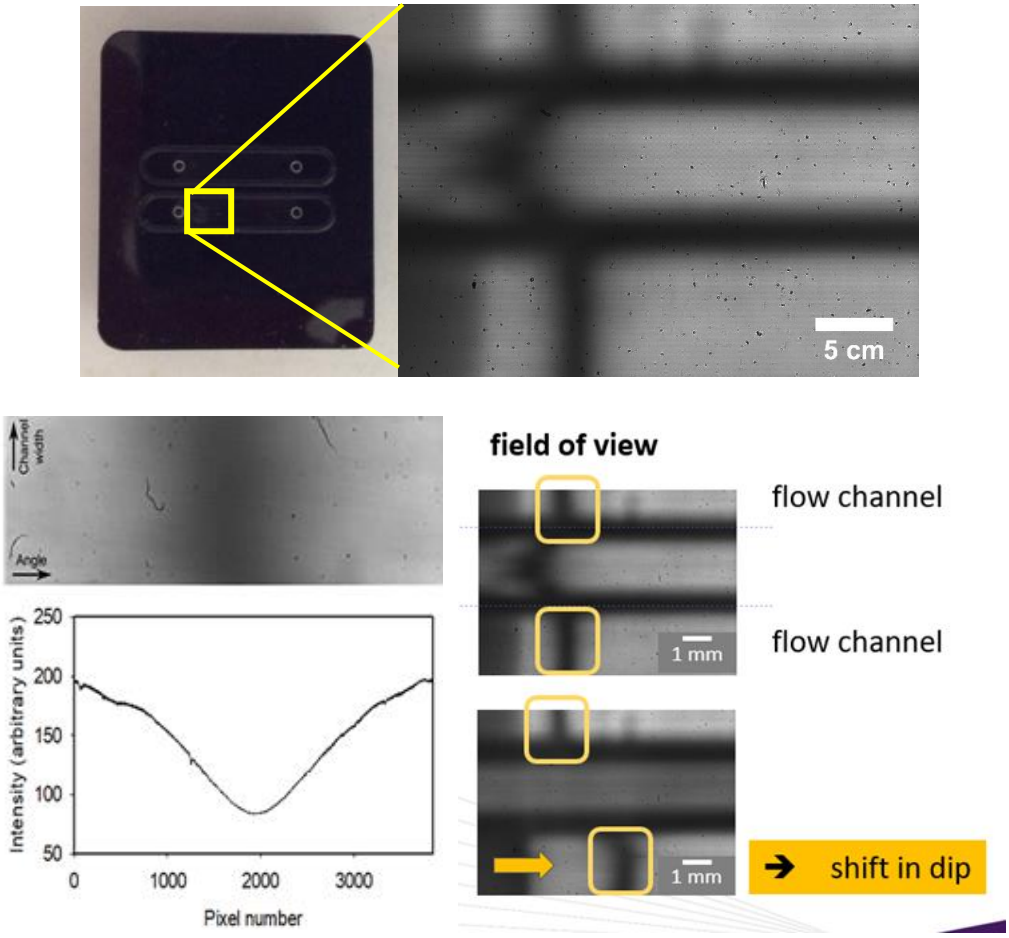

Figure 2.14: Examples of an image obtained from the CMOS camera. The x-axis corresponds to an angle, the y-axis to the interrogated width on the flow cell.

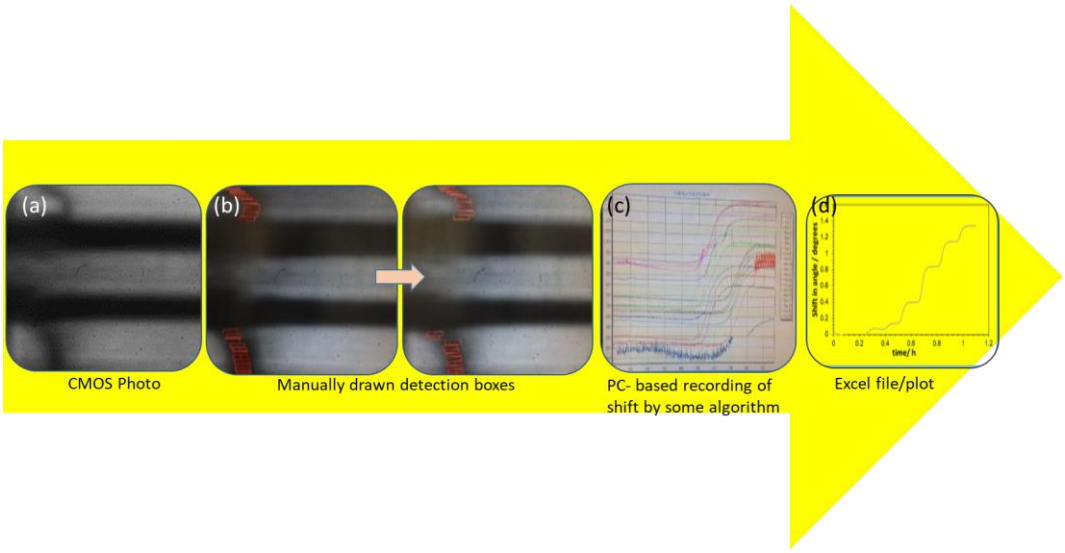

Figure 2.15: (a) box diagram (1 CMOS photo to 2 manually drawn detection boxes to 3 PC – based recording of shift by some algorithm to (4) excel file/plot) (b) Photos from computer monitor showing the boxes for measurement drawn around the dark dip region, (c) photo of computer monitor show time/shift plot. (d) How the data is captured as position of the box as a function of time.

The calibration curve has been obtained by taking the reading of the dip position in pixel that is provided by CMOS camera. This pixel is corresponding to the specific angle of incident light. By changing the incident angle to different degree, a reading in pixel would be different thus a calibration curve can be gained fig.2.16.

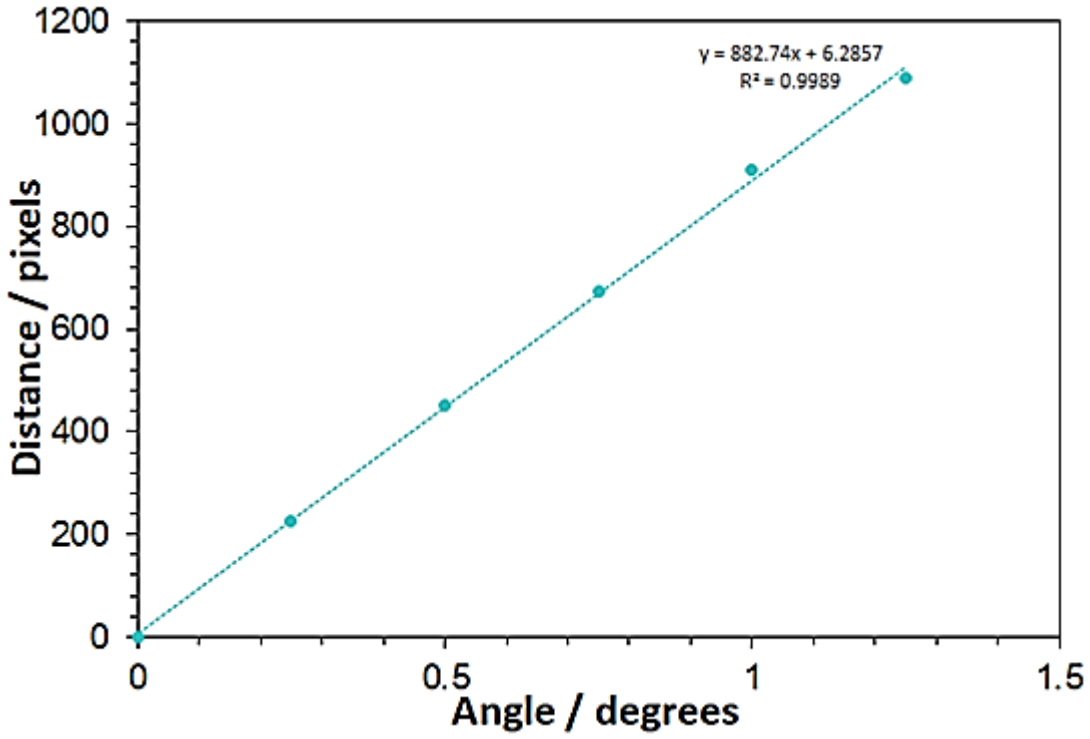

Figure 2.16: Example of a calibration curve by taking the reading of the dip position in pixel with changing the incident angle to different degree.

Light was passed through an assembly of achromatic doublet and cylindrical lens to obtain a wedge-shaped beam, which permit illuminating the DDLW with a range of angles of incidence simultaneously. The beam width at the waveguide was 0.5 mm. The focal length of the cylindrical lens used was 100 mm, which resulted in light of wedge angle of ∼14◦in air or ∼9◦in the prism.

The output of the DDLW was passed through a transmission grating (Thorlabs GT25-03, 300 lines mm−1, blaze angle 17.5◦) to disperse the output light and then an achromatic doublet (Comar Optics100 DQ 25) to focus it onto the camera. The camera integration time was 7 ms. the relationship between camera pixel and wavelength was determined by introducing interference filters of known wavelength in the path of incident light and recording the corresponding position of reflected light on the camera. The output is captured by a camera that is connected to a program called GetFram V8 in PC where the movement of the dip can be monitored.

Flow Cell Design 1

Flow Cell 1 was constructed from (1) an injection moulded black piece of PMMA featuring access holes, (2) pressure sensitive adhesive double sided tape (3M) with a channel structure cut out via laser cutter (at University of Manchester, courtesy of Dr Gupta) and (3) the glass substrate with chitosan waveguide fig.2.17a. The two channels cut into the in the adhesive tape (3M, 467MP, 50 µm thickness, obtained from Viking Industrial Products, UK) were 5 mm wide and 8 mm long fig.2.17b. The black PMMA piece featured four holes (1.5 mm diameter) fig.2.17c. Crimp Bootlace Ferrules (RS Components) with 8 mm pin length and 1.5 mm pin diameter) were glued to the PMMA to allow interfacing to tubing fig.2.17d. The fully assembled flow cell is shown in fig. 2.17e.

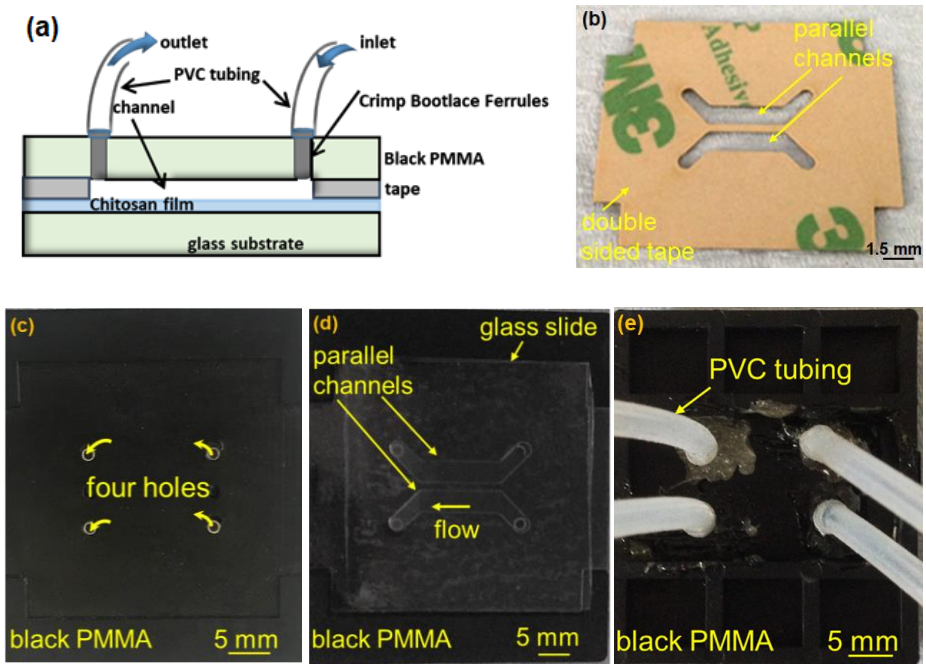

Figure 2.17: (a) Schematic of flow cell 1, (b) photo of laser cut 3M tape, (c) photo of bottom of black PMMA piece, (d) bottom view of device with 3M tape and chitosan-coated glass substrate attached and (e) top view of fully assembled device with tubing.

Flow Cell Design 2

Flow cell 2 fig.2.18 consisted of (1) a piece of black PMMA (0.2 mm thick) with a milled circular section, 0.2 mm deep and 4 mm wide diameter. This device was fabricated in fabricated by Nick in Manchester. The waveguide instrument was also designed and made by him. An O-ring was used for sealing. The PMMA piece with the O-ring was then directly mounted on (2) the chitosan coated glass substrate.

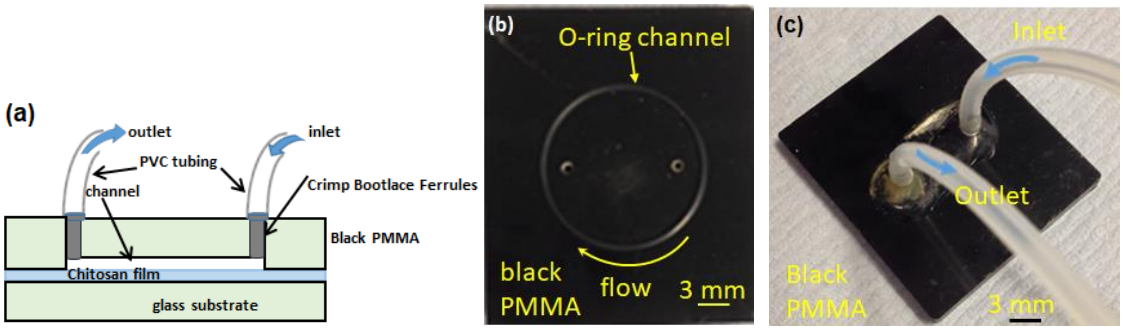

Figure 2.18: (a) Schematic of flow cell 2, (b) photo of milled black PMMA piece, (c) photo of fully assembled device.

Flow Cell Design 3

Flow cell 3 featured (1) a CNC milled black piece of PMMA mounted onto (2) the chitosan coated glass substrate. The milling as shown in fig.2.19 was carried out by Dr Iles at the University of Hull. The design featured two channels with a recess for an O-ring for sealing (, 0.2 mm deep and 4 mm wide diameter). Photographs of the milled PMMA and the fully assembled flow cell are shown in fig.2.20.

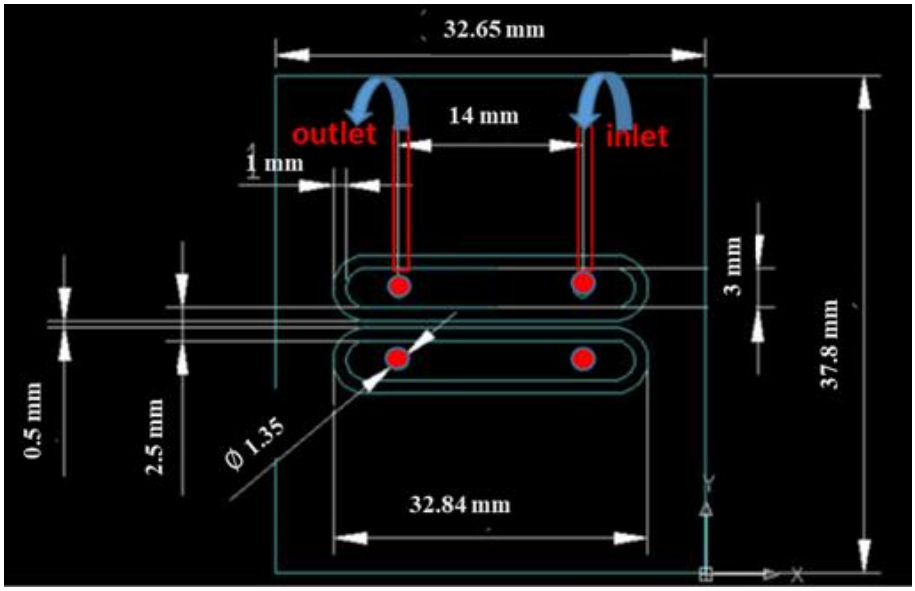

Figure 2.19: Schematic diagram illustration of the polystyrene flow-cell design.

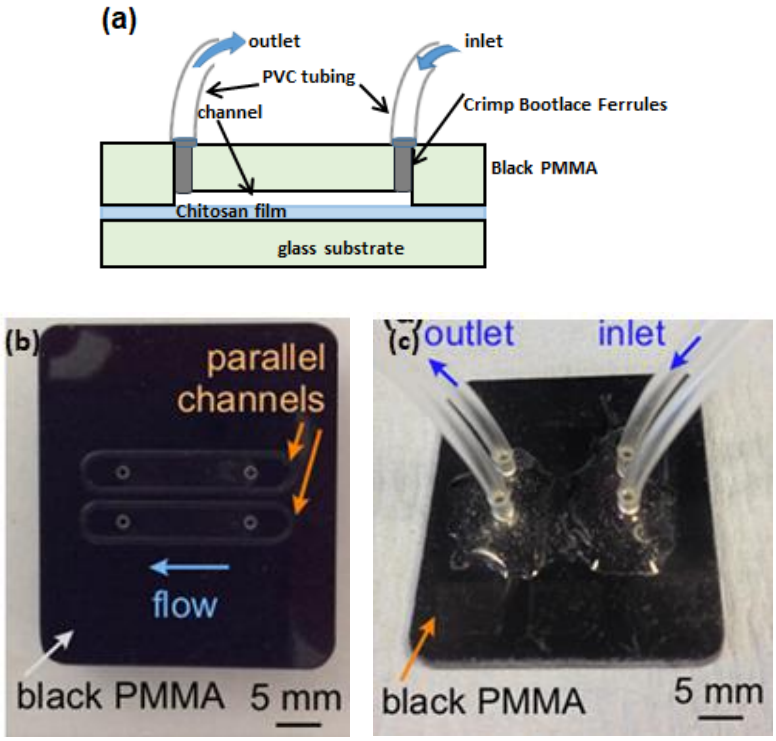

Figure 2.20: (a) Schematic of flow cell 3, (b) photograph of milled PMMA piece, (c) photograph of fully assembled flow cell.

The flow cell was positioned on the prism with refractive index matched oil (Series A, Cargille Labs, New Jersey, USA) and clamped into a custom-made metal holder system fig.2.21, to ensure the glass substrate was fixed in place fig.2.22.

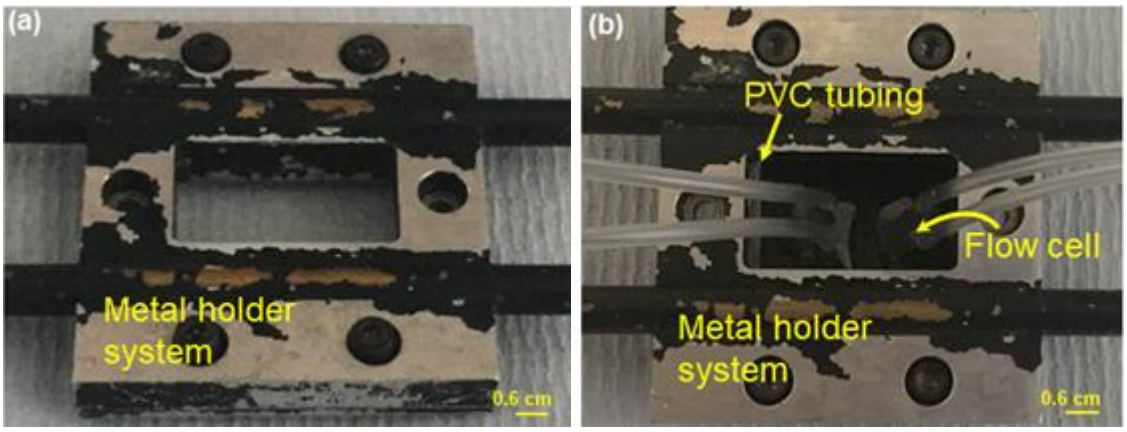

Figure 2.21: Photograph of (a) metal holder system that (b) a flow cell is positioned on the prism and clamped with it to ensure the glass substrate was fixed in the place.

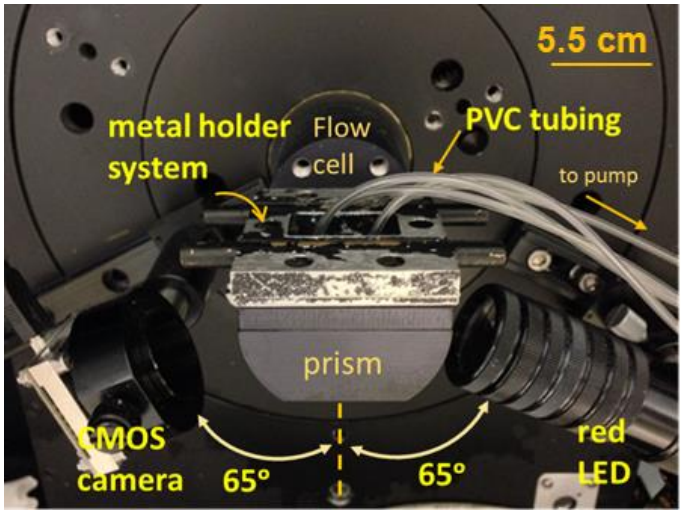

Figure 2.22: Photograph illustrations of the polystyrene flow-cell design consist of red LED light source and CMOS camera detector fixed at resonance angle 65°.

Interfacing flow cells, pumping of liquids

For all three flow cells, pumping was achieved with a peristaltic pump (Minipuls®, 3 Gilson, UK). Ferrules (Crimp Bootlace Ferrules, RS Components) of 8 mm pin length and 1.5 mm pin diameter, were glued into the inlet holes in all three types of PMMA devices used for the three types of flow cell. Loctite Double Bubble 2-Part Epoxy Glue was used throughout. Elkay PVC tubing (i.d. 0.76 mm, o.d. 2.438 mm) was pushed over the ferrules fig.2.23a and, at the other end, placed into vessels with buffer or solutions for pumping as required fig.2.23b. To change from one solution to another, the tubing was manually dipped into the relevant vessel. Liquid from the output was collected in a petri

dish. In order to allow efficient flushing of the system, for example to remove air bubbles, syringes (HENKE SASS WOLF, Keltenstrabe 1, D-78532 Tuttlingen/ Germany) were connected to the main tubing via T-pieces fig.2.24a, b, and c.

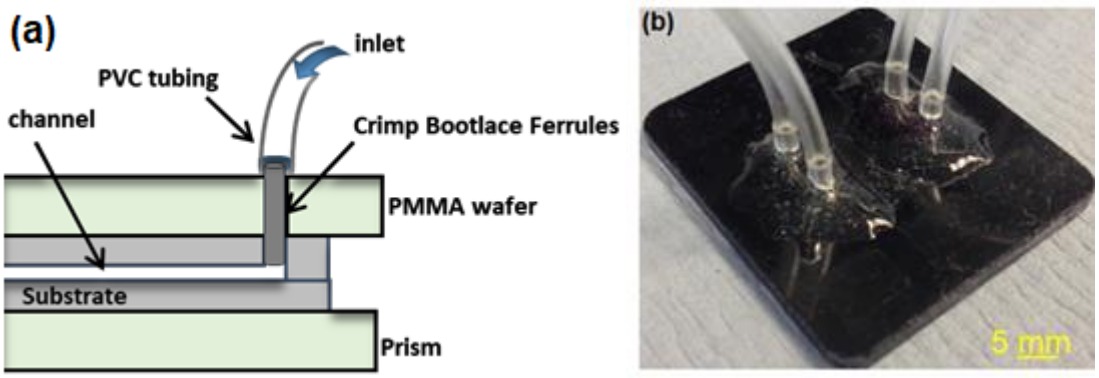

Figure 2.23: (a) Schematic illustration of interfacing to tubing, (b) example photograph of ferrules with tubing and glue.

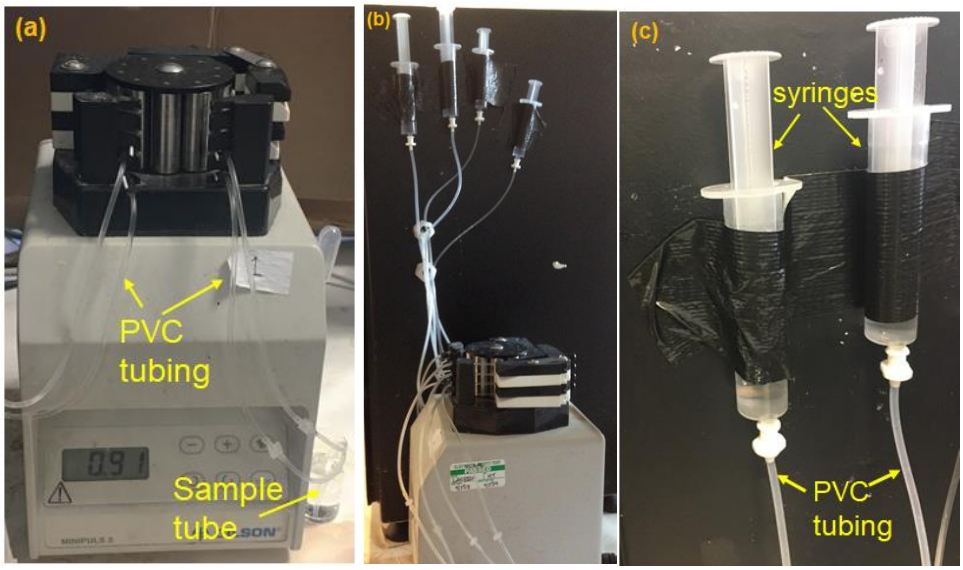

Figure 2.24: (a) Schematic of tubing and pumping setup, (b) photo of peristaltic pump and (c) photo of syringes connected with T-pieces for manual flushing.

2.3 Waveguide Film Optimisation

2.3.1 Concentration of a Reactive Blue 4 Dye (RB4)

Chitosan was deposited on the glass substrates by spin coating as outlined in sections 2.2.2 to 2.2.4. A dye, Reactive Blue 4, needed to be immobilised in the entire volume of the waveguide to obtain a dip in reflectivity fig.2.25a. The chemical structure of RB4 is shown in fig.2.25b. RB4 was chosen for its light absorption properties and also for it has

a functional group that reacts with the amino groups in the chitosan under acidic conditions via electrostatic interaction fig.2.26. This allows bonding of the RB4 molecules in the entire waveguide volume and prevents the dye from leaching out of the waveguide film.

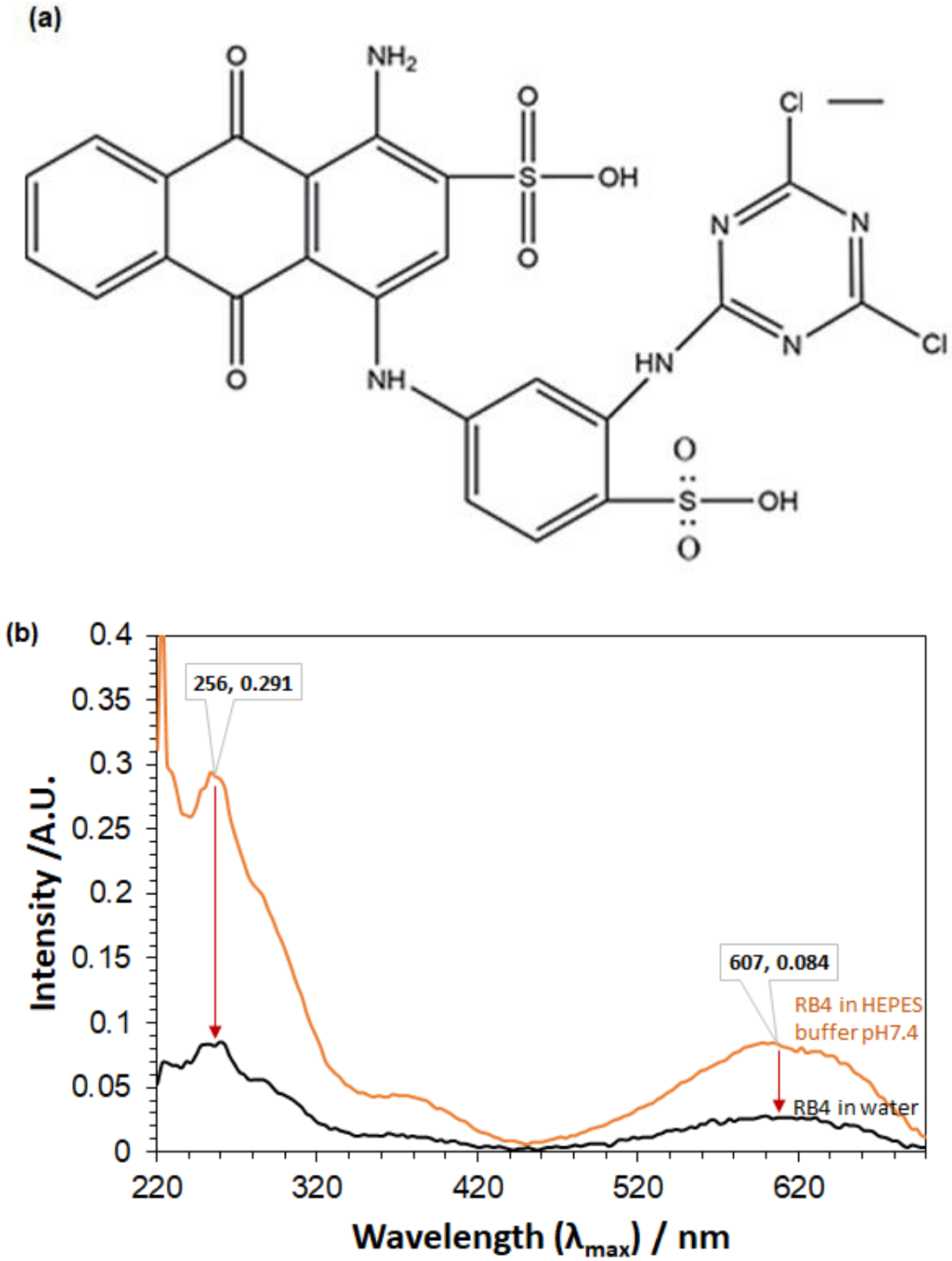

Figure 2.25: (a) Chemical structure of RB4 dye, (b) UV/vis absorbance spectrum of RB4 dye (100 mM) between 200 nm and 800 nm.

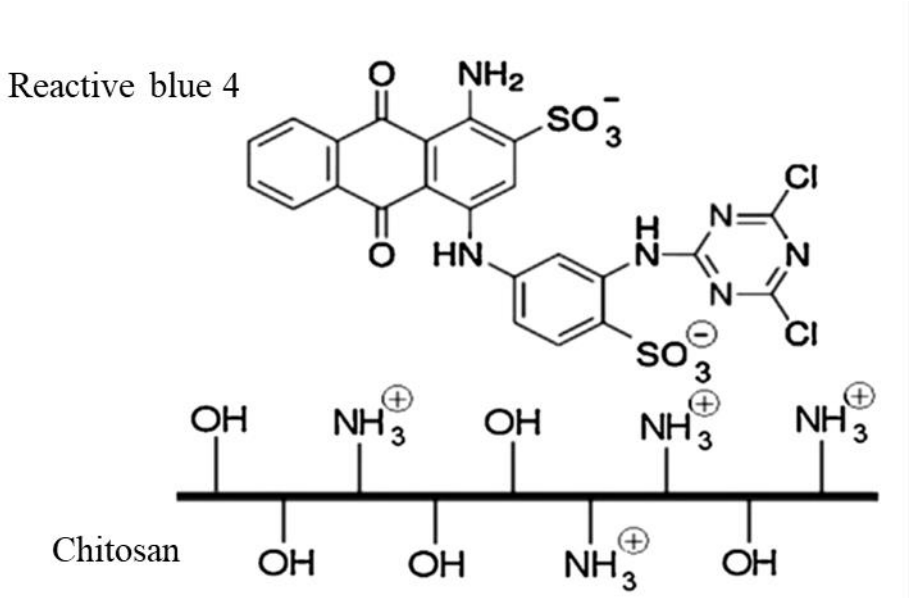

Figure 2.26: Electrostatic attraction between sulphate groups of RB4 and amino groups in chitosan film.

After optimizing spin speeds and concentration of chitosan (section 2.2.2-2.2.4) a range of RB4 solutions in water were prepared with concentrations of 1.5, 2.5, 5.0, 7.5, 10 μM in order to study the effect of concentration of the dye on the chitosan layer. A blank solution of water was also tested. These solutions were pumped through the flow cell 1manually with a 5 mL disposable syringe. To avoid any air bubbles, water was injected into the flow cell before testing each dye solution. The order of measurement of solutions was from low to high dye concentration. Reflectivity curves were measured using the setup described in section 2.2.5 for angles between 55° and 75°.

2.3.2 Effect of Different pH

The effect of pH of utilized buffer on the waveguide performance was investigated by preparing buffer solutions from phosphate salts and phosphoric acid in deionized water. Table.2.2, summaries the amounts used to obtain buffers with pH 4.0, 5.0, 6.0, 7.0, 8.0, 9.0 and 10. All were made up to 1000 mL with deionized water. The pH was verified with a pH meter (HI 2210. Hanna Instruments Ltd. UK) and adjustments made by adding 0.1 M phosphoric acid (85%).

Table 2-2: Preparation of phosphate buffer solutions with pH 4.0, 5.0, 6.0, 7.0, 8.0, 9.0 and 10.

pH	Volume of Na_2HPO_4 (0.2 M) / mL	Volume of NaH_2PO_4 (0.2 M) / mL	Volume of H_3PO_4 (0.1 M) / mL
4	19.3		30.7
5	25.7		24.3
6	12.3	87.7	
7	61.0	39.0	
8	94.7	5.3	
9	955		45.0
10	966		

The chitosan (2.0%) was spin coated (3,000 rpm) onto the glass substrate and stained by manually flushing 5 mL of 10 µM RB4 dye solution through the flow cell (flow cell 1). The flow cell was then flushed with 5 mL of buffer solution, and reflectivity was measured as function of incident angle in the range 55° – 75° using the setup described in section 2.2.5. The flow cell was then washed with 5 mL water before the next buffer solution was introduced and the next reflectivity measurement was taken. Each buffer solution was flushed three times.

2.4 Waveguide Film Characterisation

2.4.1 Determination of Amino Groups in Waveguide

To calculate the number of moles (n) of amino groups in the chitosan layer, the concentration (c) of amino groups as well as the volume of the sample (v), need to calculate the thickness of the layer (l) and the area (A_{il}) of incident light need to be obtained, as expressed in equation 2.1.

$$n = c \cdot V \qquad with \qquad V = A_{il} \cdot l$$ **……Equation 2.1**

The concentration (c) can be calculated from the total concentration of RB4 dye bound to the waveguide layer, which can be determined via absorbance spectroscopy and applying

Beer-Lambert law (equation 2.2), with I_0 and I as the intensities of light in the absence and the presence of the sample, respectively. Absorbance (A) at 650 nm was measured using two different setups, namely (1) a conventional UV/vis spectrophotometer, USA (model Bio Lambda 10) and (2) the optical setup with cuvette holder as described in section 2.2.5, fig.2.9b. On the conventional UV/vis system, absorbance (A) is measured directly.

On the waveguide system, I_0 and I represent the depth of the dips of the reference and the sample solution, respectively. ε is the wavelength-dependent molar extinction coefficient; c is the sample concentration, and b is the optical path length through the sample.

$$A = log\frac{I_0}{I} = \varepsilon \cdot b \cdot c \ldots\ldots\ldots\ldots$$ **Equation 2.2**

To carry out this study, 0.038 g of RB4 dye was dissolved in 20 mL water to make a 1 mM stock solution. This stock solution was diluted with deionized water to obtain working solutions ranging from 0.1 μM to 100 μM. For UV/vis absorbance measurements on the conventional system, the solutions were placed into a cuvette and absorbance was recorded at 650 nm. Measurements were taken in triplicate. For measurement with the custom-built optical system, the sample solutions were placed in a cuvette (12.5 mm x 12.5 mm x 45 mm, 2.5 mL volume, 10 mm path length, Brand, Germany), that was placed into a holder as shown in fig.2.9c. The obtained signal (in mV) for the blank was taken as I_0, the obtained signals for the samples solutions (in mV) were taken as I to calculate the absorbance as per equation 2.2.

Following the measurement of the aqueous RB4 solutions, different concentrations of chitosan were prepared at 1.0%, 1.5% and 2.0% (w:v%) in 10 mL of 0.1 M acetic acid. These solutions were transferred to a stirring device until the chitosan was fully dissolved. Following this, 12.5 μL of 50% (v:v) glutaraldehyde was added to each solution and left stirring for 15 min. These chitosan solutions were then spin-coated onto cleaned glass substrates at 3,000 rpm for 30 s, as described in section 2.2.4. The absorbance of these unstained spin-coated films with different concentrations of chitosan were measured for reference. To study the uptake of RB4 by the chitosan films and thus estimate the number of available amino groups, the chitosan films were stained in an incubation bath (Petri dish) with 100 μM RB4 solution for different periods of time starting from 10 min up to 280 min. Every 10 min, the glass was taken out of the incubation bath and washed with deionised water to remove any unbound molecules. The absorbance at 650 nm of the stained chitosan films was then measured both on conventional UV/vis spectrometer and

on the custom-built optical setup with laser light source and photodiode detector by positioning the glass substrate on the respective holders and fixing it with BlueTac adhesive. Measurements were carried out in triplicate.

2.4.2 Thickness Measurement

The thickness of the deposited chitosan film was measured with a white light interferometer (Wyko NT1100, Veeco, USA). Chitosan solutions of 1.0%, 1.5%, 2.0% w/v% were prepared in 10 mL of 0.1 M of acetic acid and 12.5 µL of 50% (v/v%) glutaraldehyde were added as before. The WLI can visualize a surface area, any steps on the imaged surface can be quantified in height. To measure the chitosan layer thickness, half of the glass substrate was covered with a piece of masking tape. The chitosan gel solution was then spun onto the glass substrate at 3,000 rpm for 30 s as before. For measurement of dry chitosan layers, the films were dried at room temperature for about 30 min prior to measurement on the WLI. For measurement of wet films, the coated glass substrates were kept in a Petri dish with deionized water until immediately prior to measurement. The tape was removed, leaving half of the substrate covered with chitosan film and the other half void of the chitosan film to allow for the film thickness to be measured. Measurements of film thickness were by a member of staff in Physics.

2.5 Waveguide Sensitivity to Changes in Refractive Index

Quantitative measurement of binding events in the waveguide depends on changes in refractive index. It was therefore important to establish the sensitivity of the developed chitosan waveguide sensor with respect to changes in refractive index. To this end, a series of glycerol solutions of known refractive index was prepared. A 10% (v/v) stock solution of glycerol in water was prepared from which dilutions in water were made up with concentrations of 0.1%, 0.5%, 1%, 2.5%, 5%, 7.5% and 10% (v/v). The refractive index of these solutions was measured by refractometer (M 46.317, Hilger & Watts, UK). A 2% (w/v) chitosan solution was prepared as before and spin coated onto the glass substrate. The coated glass slides were then incubation with a RB4 dye (10 µM) for different amounts of time, namely 10 min, 30 min, 60 min and 130 min. A flow cell (design 1) was put onto to coated glass substrates and the assembly was placed on the BK7 prism. The different concentrations of glycerol were pumped through the flow cell via the peristaltic pump at a flow rate 0.25 mL min^{-1} for a period of about 10 min.

For these measurements the incident angle was fixed at the resonance angle for the chitosan, i.e. at 65°. The setup as described in section 2.2.5, fig.2.7d was used, featuring a red LED light source and a CMOS camera to capture an image of a section of the waveguide layer. The dip in reflectivity is presented as a dark line on the image. The dark line shifts when the refractive index of the waveguide layer changes. This shift is monitored by the custom-written software, using a center of gravity algorithm and a threshold of 60% of the depth of the dip, and translated to a shift in pixels, which can later be converted into a shift in degrees.

The optimum time of incubation with dye was selected (10 min) as a result of these experiments. In addition to making up glycerol solutions between 0.1% and 10% in water, two different buffer systems were also studied, namely PBS (phosphate buffered saline) at pH 7.4 and HEPES (2-[4-(2- hydroxyethyl) piperazin-1-yl] ethane sulfonic acid) buffer at pH 7.4. These buffers were chosen as they are commonly used in biological research. PBS is a salty solution containing sodium chloride, sodium phosphate, and, in some formulations, potassium chloride and potassium phosphate. It is isotonic and non-toxic to cells. HEPES 4-(2-hydroxyethyl)-1-piperazineethanesulfonic acid, pH 7.4. is a common buffering chemical and is classified as a "Good's buffer" for the following reasons:

- It is easy to prepare
- It has pKa values between 6.0 and 8.0
- It has limited effect on biochemical reactions
- It has very low visible and ultraviolet light absorbance
- It is chemically and enzymatically stable

The refractive index of glycerol solutions made up in PBS and HEPES was measured using the refractometer (M 46.317, Hilger & Watts, UK) as described above. The shift in dip as these different glycerol solutions in PBS and HEPES buffer are pumped over the chitosan waveguide were then recorded as described above. For these experiments flow cell 1 was used.

2.6 Porosity of the Waveguide Film

The porosity of the waveguide film is crucial: it determines the available surface area for binding of biorecognition elements; the pore size need to be sufficiently large to allow the recognition molecules as well as sample components to penetrate into the film and thus give a fast response time; the 3-dimensional network structure of the film should also be fairly stable to avoid excessive swelling or components of the film layer being carried away with the flow.

2.6.1 Investigation the Porosity using the DDLW optical setup

To investigate the pore size of the waveguide layer, the effect of two components of different molecular weight on the shift in dip was initially studied, namely glycerol as an example of a low molecular weight compound (MW = 92.1 g mol^{-1}) and BSA (bovine serum albumin) as an example of a higher molecular weight and thus larger compound (MW = 66.463 kDa).

Glycerol solutions (0.5%, 1.0%, 2.5%, 5.0%, 7.5% and 10%) were prepared in PBS buffer as before. A BSA stock solution of 10% (w/v %) was prepared by dissolving 1 g of BSA in 10 mL of PBS buffer. A series of working solutions was then prepared by diluting the stock solution with PBS to obtain BSA concentrations of 0.5%, 1.0%, 2.0%, 3.0%, 4.0% and 5.0%. The refractive index of these solutions was determined with the refractometer (table 2.3).

Table 2-3: Refractive indices of Glycerol and BSA solutions.

Glycerol in PBS (v/v %)	**R.I**	**BSA in PBS (w/v %)**	**R.I**
0.5	1.3355	0.5	1.335
1	1.336	1	1.336
2	1.3385	2	1.3375
3	1.3405	3	1.3395
4	1.3435	4	1.340
5	1.348	5	1.341

Chitosan waveguides were prepared as before from 2.0% chitosan solution and glutaraldehyde. The chitosan film was stained with 10 μM RB4 dye solution for 10 min.

After that, these slides were washed with distilled water and dry on a hotplate at 40 °C, for a couple of minutes.

In these experiments, flow cell 1 was attached to the substrate with waveguide. The flow cell assembly was placed on the prism and the shift in dip was measured as described before (section 2.2.5) using an angle of 65° for the incident light and CMOS detector. Solutions were pumped via peristaltic pump at a flow rate of 0.25 mL min^{-1}. Following flushing with deionised water, the glycerol solutions with increasing concentrations were consecutively pumped through the device, each for 10 min. This was followed by a flush with buffer. Subsequently, the BSA solutions were pumped through the chip, from the lowest BSA concentration to the highest, each for 10 min. This was again followed by a wash with PBS buffer.

To study the porosity of the waveguide film further, polymers of different molecular weights were also tested. PEG (polyethylene glycol) and PEO (polyethylene oxide) were purchased with different molecular weights, specifically 40 kDa (PEG), 100 kDa (PEO), 200 kDa (PEO) and 400 kDa (PEO). These were dissolved in PBS to obtain 1% (w/v) concentrations. A 1% glycerol was also utilised in these experiments for comparison as it has the same refractive index as the polymer solution (n = 1.3355). The workflow involved pumping at 0.25 mL min^{-1} of PBS, then glycerol, then PBS again and then the polymer solutions with increasing concentrations for 10 min each. Following pumping of each polymer solution, the flow cell was flushed with PBS for 10 min. Importantly, for these polymer experiments, flow cell design 2 was utilised, which only features one circular measurement 'channel' and no reference channel.

2.6.2 Investigation Waveguide Porosity using Fluorescence

Fluorescence analyses was carried out to investigate and quantify the binding of fluorescently labelled BSA protein to the chitosan hydrogel.

A 2 % (w/v) chitosan solution with glutaraldehyde was prepared as described previous (section 2.2.3). 1 mL of the chitosan solution then was poured into cuvettes and left to dry at room temperature for 24 h. The dried chitosan gel in the cuvette was then measured by fluorimeter at λ_{ex} = 490 nm and λ_{em} = 525 nm (Perkin Elmer LS 55 Fluorescence Spectrometer (Perkin Elmer LS 55 Fluorescence Spectrometer Bio Lambda 10, USA) as a blank.

A 0.05% (w/v) solution of bovine serum albumin (BSA) conjugated with FITC (Fluorescein isothiocyanate) (BSA-FITC) was prepared in 10 mL of PBS (pH 7.4). Separately, a 0.05% (w/v) FITC solution was also prepared in 10 mL of PBS (pH 7.4). Two mL of each solution was pipetted into different cuvettes and left 2 h for to incubate. The fluorescence was then measured as above. Following this, the cuvettes were washed three times with 2 mL PBS buffer and the fluorescence intensity of the gel in the cuvette was measured again. Each test was run in three cuvettes (n = 3).

2.7 Enhancement of Waveguide Porosity

The pore size of the waveguide film is a fundamental factor which determines whether biorecognition elements such as antibodies can to penetrate into the film for their immobilisation. If the pore size is too small, the antibodies will simply adsorb on the surface of the waveguide layer or become only partly entrapped in the pores. The pores also need to be sufficiently large to allow analytes of interest from the sample to penetrate into the waveguide film for binding. In order to enhance the porosity of the waveguide film, a number of approaches were investigated as outlined below.

2.7.1 Incorporation of Silica Particles as Porogens

Silica nanoparticles (NPs) were envisaged as poregens. The idea was to incorporate them during the waveguide film deposition and then to dissolve them with sodium hydroxide (NaOH) in order to obtain pores of the size of the silica particles.

Initially, commercially available silica nanoparticles (100 nm) obtained from Sigma Aldrich as 10 % (w/v) suspension in ethanol were investigated. A working suspension of 1% silica NPs was prepared by diluting with deionised water. To study the solubility of these particles in NaOH 5, 10 and 15% (w/v) aqueous solutions of NaOH were prepared. A series of tubes were then charged with 20 µL of the 1% silica suspension with different volumes (5, 10, 20, 30, 40 µL) of the different concentrations of NaOH. After a short manual shaking to induce mixing, the tubes were left for various times, *i.e.* 2 h, 4 h and 17 h at room temperature. The solubility of the silica nanoparticles was then studied by visual inspection.

Dissolution with NaOH of silica nanoparticles embedded in chitosan gel was then studied. The stock suspension with 10% of silica particles was diluted in water to 5%. The suspension was placed in ultrasonic bath for 60 min to ensure the particles are uniformly

dispersed. A 2.5% (w/v) solution of chitosan was prepared by dissolving 0.25 g of chitosan powder in 10 mL (0.1 M) acetic acid for 3 h under continuous stirring. At this point, 15.62 μL of aqueous glutaraldehyde (50% (v/v)) was added and stirred for 15 min. Then 320 μL chitosan solution was mixed with 160 μL of the 5% silica NP (2:1 ratio) to have a gel mixture with a final concentration of 1% silica NPs. This was mixed for 30 min under magnetic stirring and poured into cuvettes. The cuvettes were left standing for 24 h to form chitosan gel with embedded silica nanoparticles.

After the gel had formed, the dissolution of the silica nanoparticles with NaOH was studied. A 10% (w/v) NaOH solution was prepared, 400 μL of this was added to the cuvettes containing the chitosan gel. They were placed on a hot plate at 80°C and left reacting for different times starting from 10 min to 100 min. Following this, the gel was washed with 2 mL deionised water to remove the sodium hydroxide. At this point, 2 mL of a 0.05% aqueous BSA-FITC solution was added and left to incubate for 2 h. The fluorescence intensity of the gel inside the cuvette was measured via fluorimeter (λ_{ex} = 490 nm, λ_{em} = 525 nm). Following this, the gel in the cuvettes was washed three times with 2 mL of PBS buffer and the gel was again measured on the fluorimeter.

In a following series of experiments, different ratios of chitosan solution to silica nanoparticles were investigated. The same procedure as above was followed, with the exception that the ratio of silica nanoparticle suspension to chitosan solution was varied, 2:1, 1:1, 1:2 and 1:3 ratios were prepared in the cuvettes and left for 24 h at room temperature to form a chitosan gel with embedded silica nanoparticles. For dissolution of the silica particles, 400 μL of the 10 % NaOH solution was added and kept for 17 h at room temperature. The cuvettes with the gel were then washed with deionised water as described above and measured on the fluorimeter (λ_{ex} = 490 nm, λ_{em} = 525 nm). Following this, the gels were incubated with 0.05% BSA-FITC for 2 h and measured on the fluorimeter. Then BSA-FITC solution was decanted and the gel fluorescence was again measured on the fluorimeter. Finally, the gel was washed to remove excess BSA-FITC solution with 2 mL of PBS.

Because the commercial nanoparticles are somewhat expensive, the in-house synthesis of silica nanoparticles via the Stöber Method was investigated next.

2.7.2 Synthesis of Silica Nanoparticles via Stöber Method

The Stöber Method is the standard method to prepare monodisperse uniform-sized silica nanoparticles by hydrolysis of tetraethyl orthosilicate (TEOS) in ethanol medium in the presence of ammonium hydroxide [128]. The reaction scheme is shown in fig.2.27, the process is divided into a hydrolysis (eq.2.3) and polymerisation reaction (eq.2.4).

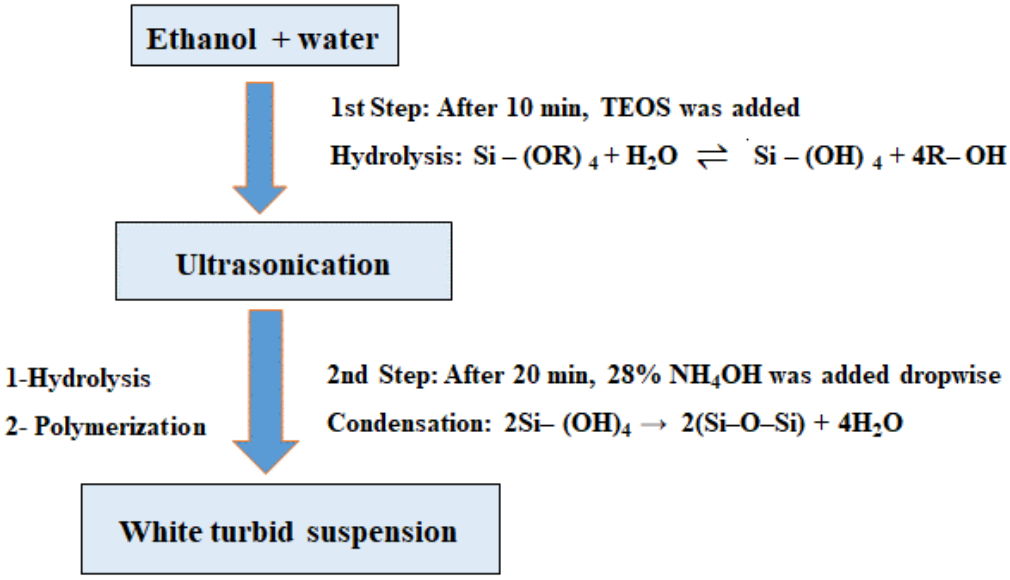

Figure 2.27: Preparation of silica nanoparticles by sequential addition method.

$Si\ (OC_2H_5)_4 + 4\ H_2O \rightleftharpoons Si\ (OH)_4 + 4\ C_2H_5OH$**…….Equation 2.3**

$2\ Si\ (OH)_4 + x\ H_2O \rightarrow (OH)_3\ Si\text{-}O\text{-}Si\ (OH)_3 + H_2O$**….....Equation 2.4**

The Stöber Method is based on hydrolysis of alkyl silicates, following condensation of silicic acid in alcoholic solution using ammonia as catalyst. The hydrolysis and condensation reactions provide precursor species and the necessary super-saturation for the formation of particles. The reaction mechanism is summarized in eq.2.3 to 2.4[129]. During the hydrolysis reaction (eq.2.5), an intermediate [$Si\ (OC_2H_5)_{4-x}\ (OH)_x$] is produced with hydroxyl groups substituting the ethoxy groups, which resulted from the reaction of the ethoxy groups on the TEOS with water molecules. This reaction initiated when hydroxyl anions attacks on TEOS molecules as well ammonia works as a basic catalyst to this reaction.

$Si\ (OC_2H_5)_4 + x\ H_2O \rightarrow Si\ (OC_2H_5)_{4-x}\ (OH)_x + x\ C_2H_5OH$…….**Equation 2.5**

After that, the condensation reaction occurs immediately, the hydroxyl group of the intermediate reacts with either the ethoxy group of the TEOS eq.2.6. or the hydroxyl group of another hydrolysis intermediate eq.2.7.to form Si–O–Si bridges. As the rate of water condensation is thousands of times faster than the alcohol condensation, silica particles form and precipitate.

$\equiv Si–OC_2H_5 + HO–Si\equiv \rightarrow \equiv Si–O–Si\equiv + C_2H_5OH$**……..Equation 2.6**

$2 \equiv Si–OH + HO–Si\equiv \rightarrow \equiv Si–O–Si\equiv + H_2O$**……..Equation 2.7**

The overall reaction is expressed as shown in eq.2.8.

$Si\ (OC_2H_5)_4 + 2H_2O \rightarrow \quad SiO_2 + 4C_2H_5OH$**……..Equation 2.8**

Absolute ethanol (2.339 mL) was mixed with 2.52 mL of deionized water and sonicated at room temperature for 10 min to remove any air bubbles. Next, 600 µL of TEOS (0.0042 M) was added and sonicated for 20 min. A known volume of 14 M ammonium hydroxide solution (0.5 mL, 0.6 mL, 2.7 mL, 3.0 mL and 5.2 mL) was added to yield final concentrations in the reaction vessel of 0.86 M. 1.01 M, 1.15 M, 1.30 M and 1.44 M. The ammonium hydroxide acts as a catalyst to promote the condensation reaction (see figure 2.27). Sonication was continued for a further 60 min to yield a turbid white suspension. This was centrifuged (Sorvall LEGEND X1, Thermo scientific) and the particle size was measured via zeta sizer (ZEN1002 Zetasizer Nano series Malvern). Following this procedure, the size of silica particles produced was larger than 100 nm, therefore, another protocol was also investigated to obtain smaller silica nanoparticles.

An alternative method that has been reported to produce smaller sized silica nanoparticles[129], via a variation of the Stöber Method was investigated next. Volumes of absolute ethanol (between 100 µL and 1 mL) were mixed with 380 µL ammonium hydroxide (0.2 M) and 180 µL deionized water and let stirring for 5 min. Then 8.860 mL of TEOS (0.4 M in absolute ethanol) was added to the above solution using a syringe pump over a period of about 10 min to allow self-aggregation and precipitation of the of silica nanoparticles. The mixture was left to react at room temperature under continuous stirring for 24 h. Afterwards, the obtained colloidal suspension was centrifuged at 5,000 rpm on a high-speed centrifuge (Sorvall LEGEND X1,Thermo scientific), and the silica particles were washed with absolute ethanol three times. This was followed by drying in oven at 100 °C for 2 h to prevent continued reaction. The size of the obtained particles was measured using the zeta sizer.

2.7.3 Porosity measurement via fluorimeter

The effectiveness to use the 50 nm silica particles, prepared via the Stöber Method, as porogens for chitosan was investigated. A 2.5% (w/v%) solution of chitosan was prepared in 10 mL aqueous acetic acid (0.1 M) by stirring for 3h. As before, 15.62 µL of aqueous glutaraldehyde solution (50% (v/v)) was added to the chitosan solution and left to stir for 15 min. A 10% suspensions of the 50 nm silica nanoparticles was prepared in absolute ethanol and placed in an ultrasonic bath for 1 h to obtain a uniform dispersion. Then, different ratios of chitosan solution to silica nanoparticles were prepared, namely 2:1, 1:1, 1:2 and 1:3. These were stirred for 1 h to ensure complete mixing. The mixtures were then poured into cuvettes and left to gel for 24 h at room temperature. To dissolve the silica nanoparticles, 400 µL of sodium hydroxide solution (10 %) was added to the cuvettes with the gels and left to incubate for 17 h at room temperature. The gels were then washed with 2 mL of deionised water to remove sodium hydroxide. Finally, 2 mL of aqueous BSA-FITC (0.05 vol %) was added and left to incubate for 2 h. The excess was then removed by decanting and the gels in the cuvettes were washed with 2 mL of PBS. The fluorescence intensity from these cuvettes was measured at λ_{ex} = 490 nm and λ_{em} = 525 nm for the gel before BSA-FITC addition, the gel with BSA-FITC, the gel following decanting of excess of BSA-FITC and the gel following washing with PBS buffer.

2.7.4 Performance of porogen treated waveguide on DDLW system

The performance of spin-coated leaky waveguide layers with enhanced porosity through silica nanoparticle incorporation as porogens was investigated with both, commercially available 100 nm silica NPs and the synthesised 48 nm ± 25 nm silica NPs.

A 2.0% (w/v%) solution of chitosan was prepared in 10 mL acetic acid (0.1 M) and left to stir for 90 min to ensure dissolution. Then 12.5 µL of aqueous glutaraldehyde (50%) was added and the mixture was stirred for 15 min.

For both silica nanoparticle types, the 10% particle suspensions were diluted in deionized water to yield a 1% concentration and ultra-sonicated for 1 h. The chitosan mixture and silica particle suspensions were combined in a 2:1 ratio and left to stir for 60 min. The mixture was then spin coated onto the glass substrates at 3,000 rpm for 30 s. Following spin coating, the slides were left to ‘gel’ for 1 h. Then, 40 µL of aqueous sodium hydroxide (10%) were added to the top of the substrate by pipetting and left to incubate

17 h at room temperature and washed by immersion in deionised water to remove any remaining aqueous NaOH[157] .The chitosan gel layer was stained by immersion in 10 μM RB4 for 10 min. The glass substrate was fixed onto flow cell 2 and interfaced to the peristaltic pump. The flow cell was placed on the prism setup with the red LED as light source and CMOS camera for detection as described in section 2.2.5 with an angle of 65°. PBS buffer was pumped at a flow rate of 0.25 mL min^{-1}. This was followed by a 10% of glycerol solution in PBS and then followed by solutions of the different molecular weight polymers from 10 kDa to 200 kDa (see section 2.6.1).

2.7.5 Drying a Waveguide Film

The purpose of drying a film is to remove the solvent slowly enough from the waveguide film produced from spin coating particularly in the initial stage of drying, firstly to make sure the film without microbubbles, which is effect on the uniform of the film, Secondly, in this stage the film is still wet and has been controlled by different dry times, that can provide a waveguide mode with an enhancement of the porosity, and also to reduce violent changes in surface tension that may causes cracks in the film, this experiment was suggested by Dr. Ruchi Gupta (University of Hull/Chemistry department). Different concentrations of chitosan (0.5, 1, and 1.5 w/v %) were prepared in 10 mL of (0.1 M) acetic acid, and transferred into stirring device for 1 h to dissolve totally. The solutions were coated on cleaned glasses by spin coating at different spin speed (500-1500 rpm). The substrate chips were left on the bench for drying under different times (1, 2, 3, 4, 5, and 10 min), then they were incubated with RB4 dye (100 μM, prepared 100 mM of HEPES buffer pH7.4) for 5 min. Chitosan layer was irradiated with TE- polarized laser at different angles between (55º-75º), the optical output was captured by a photodiode detector showing a reflective curve.

2.8 Characterisation of a Film Porosity

There are several procedures has been done to investigate the porous of a waveguide film in order to obtain an appropriate microporous structure for immobilisation biorecognition species (goat anti-rabbit IgG as a model of the antibody).

2.8.1 Different Molecular Weights of Polymers

The optimum conditions were selected and injected into a flow cell through a peristaltic pump, and irradiated by red LED and the output was monitor by CMOS camera in order to investigate the porous of a waveguide film. 1% of glycerol (v/v), and polymers different molecular weights were prepared in HEPES buffer (100 mM pH 7.4), and were made up with the same refractive index, and injected through a pump to the polystyrene flow cell at a flow rate 0.25 mL min^{-1}.

2.8.2 Different concentrations of bovine serum albumin BSA protein

The experimental procedure of using bovine serum albumin (BSA) and glycerol solution was described previously in section 2.6.1 to investigate the pore size of the waveguide layer for immobilisation step they have a molecular weight (66 kDa, and 92.09 $g.mol^{-1}$) respectively.

By using 1% of chitosan was dissolved in 10 mL of 0.1 M acetic acid and left on stirring device till totally dissolved, then coated cleaned glass slides (that prepared as mentioned previously) by using a spin coater for the 30 Sec at 900 rpm left 3 min dry time then incubated with HEPES buffer (100 mM and pH 7.4). These slides were incubated with RB4 dye (100 μM) for 5 min.

Subsequently, this experiment was done by putting the coated slide on the polystyrene flow cell was placed on a prism for coupling the light inside a waveguide layer by using a waveguide setup that mentioned before, the incident light was fixed at an angle of 65° to cover the dip at the image sensor. The output is captured by a camera that is connected to a program called GetFram V8 in PC where the movement of the dip can be tracked. A peristaltic pump was used to pump distilled water firstly at flow rate 0.25 mL min^{-1} through silicone tube, then pumped series concentrations of glycerol, and BSA solution starting from lower to higher concentration having slightly higher refractive index than water. The source light is was red LED and the output was monitored by CMOS camera providing a real time measurement for tracking the position shift of a dip.

2.8.3 Effect of pH Buffer

Effect pH buffer on the porous of a waveguide film was investigated by preparing different solutions of HEPES buffer (4-(2-hydroxyethyl)-1-piperazineethanesulfonic acid).

That have different pH (8.4, 7.4, 6.4, 5.4, and 4.4). All buffer solutions were prepared using 18.2 deionised water. The flow cell was mounted onto a glass substrate that is coated with 1% (w/v) of chitosan solution in 10 mL of (0.1 M) acetic acid and left for 3 min dry time, then incubated with HEPES buffer (pH 7.4) overnight. RB4 dye (100 mM) was used to incubate the waveguide film for 5 min and a cross linker (NHS-PEG-NHS) (Mwt.3000 Dalton) (0.1 mM) also for 5 min, these solutions of different pH buffer (HEPES) were injected to the channel in flow cell by peristaltic pump at flow rate of 0.25 mL min^{-1} using silicone tube. The flow cell was washed with HEPES buffer (pH 7.4) before and after each measurement with buffer. The output is captured by CMOS camera that is connected to a program called GetFram V8 in PC where the movement of the dip can be monitored. This experiment was repeated without a cross linker to compare between the results for all measurements.

2.9 Effect of Crosslinker

To study the effect of cross linker on the porous of chitosan film, different molecular weights (500, 2000, 3000 and 10000 Dalton) of (NHS-PEG-NHS) (0.1 mM) has been used in this experiment. 1 % (w/v %) of chitosan was prepared in 10 mL of 0.1M acetic acid where are then transferred into a stirring device for one hour till totally dissolved. The cleaned glasses that were prepared for coating with chitosan solution by using a spin coater for 30 Sec at 900 rpm and left it to dry for 3 min then put in HEPES buffer (pH 7.4) and left overnight. After that the glass slides placed in solution of (NHS-PEG-NHS) (0.1 mM) different molecular weight (500, 2000, 3000 and 10000 Dalton) dissolved in 2 mL of HEPES buffer for 5 min, then washed with buffer also and incubated these slides with RB4 dye (100 mM) for 5 min. then left it to dry for half an hour. A resonant cavity light emitting diode (RCLED, PR65-F1P0T, Roithner, Lasertechnik, Vienna, Austria) and a camera (PL-B781, pixelink, Ontario, Canada) with an integration time 25 ms have been used for tracking position of the dip. The flow cell was placed on a prism for coupling the light inside a waveguide layer. Red LED with a high resolution CMOS camera are placed on rails and connected to goniometers. The incident light was fixed at

angle of 65° in order to cover the dip at image sensor. The output is captured by CMOS camera that is connected to a program called GetFram V8 in PC where the movement of the dip can be monitored. HEPES buffer (100 mM) was first pumped to the channel in flow cell by peristaltic pump at flow rate of 0.25 mL min^{-1} using silicone tube. Then 0.5% of glycerol solution was prepared in 10 mL of HEPES buffer and injected after HEPES buffer, then different molecular weights of polymers were injected from (40-400 kDa) to compare the results for all of these solutions.

2.10 Surface Characterization of a Waveguide Film

Different concentrations of chitosan (0.5, 1, and 1.5%) have been investigated by using various instruments in order to check the porous of a waveguide film. White light interferometer (WLI) has been used to investigate the thickness of the waveguide layer (chitosan), different concentrations of chitosan were prepared in 10 mL of 0.1 M of acetic acid where are then transferred into a stirring device till totally dissolved. The cleaned glasses that were prepared half covered with a tape then it coated with chitosan solution by using a spin coater for 30 Sec at 900 rpm and incubated with HEPES buffer (100 mM, pH 7.4) . The tape was then removed from the contact surface after sign on the back of these slides. These glasses were measured their thicknesses by a white light interferometer (WLI) was used for measuring the thickness of chitosan layer, above procedure has been followed for preparation of chitosan solution and coated the substrate but without using a tap to cover a half of the substrate to measure by Dektak instrument to profile surface of the waveguide layer, the work has been done in the physics department at Hull University. Moreover, the porosity of a waveguide film was measured by Confocal Microscope for different concentration of chitosan with different dry time (1, 2, 3, 4, and 5 min) cover slip has been coated with chitosan solutions instead of glass microscope substrate. Furthermore, ImageJ was used to characterise a surface of a waveguide thin film (1, 1.5, and 2 %), which were spin coated onto glass slides at different spin speed.

2.11 Immobilisation of Biorecognition Species

A biosensor device is an analytical device consist of biorecognition sensing elements (antibody, enzyme, and DNA) in close contact with a physical transducer (mass, optical, or electrochemical) which both relate to convert the concentration of the analyte to optical

output signal. In this research the biorecognition element -Goat anti-rabbit IgG- has been immobilised in a waveguide thin film as a model of the antibody.

The experimental of antibody immobilisation was performed by preparing a waveguide film of chitosan with an optimum condition as described in section 3.6.2. The antibody solutions of polyclonal anti-rabbit IgG (0.5 mg mL^{-1}), which prepared in 2 mL of HEPES buffer (100 mM pH 7.4) to get ($2.5*10^{-9}$ M), the first solution was prepared without EDC-Sulfo-NHS and the second solution was prepared with EDC (4 mg in 100 mM of HEPES buffer pH 7.4) and-Sulfo-NHS (11 mg in 100 mM of HEPES buffer pH 7.4) and left 15 min to react before pumped, and 0.5% of BSA has been used as a blocking molecules after immobilise the antibody . All prepared solutions were injected via a peristaltic pump to the flow cell and the optical output was detected by CMOS camera. This experiment has been done to compare between the results of the antibody immobilisations with and without using EDC-Sulfo-NHS.

2.11.1 Antibody Immobilisation Using EDC- Sulfo-NHS

There are a wide range of strategies for antibody immobilisation such as covalent binding, site-specific binding, biotin-streptavidin interactions, intermediate proteins, and affinity tags. The most prominent strategies that are based on the covalent binding of antibodies as they are rapid, highly stable antibody binding, leach-proof with high immobilisation density. The heterobifunctional is used most widely of the covalent binding strategy for crosslinking of the carboxyl groups on the antibody to the free amine groups into the waveguide thin film using EDC along with Sulfo-NHS.

2.11.2 Using Ratio (4:1) of EDC- Sulfo-NHS

Using various ratios EDC-Sulfo-NHS of EDC-based crosslinking strategies this led to the activation of carboxyl groups on anti-rabbit IgG antibody and react with the amino groups into the waveguide film which involved. Sequentially the cleaning of chitosan chip with previous procedure of cleaning glass slides. Immobilisation of anti-rabbit IgG antibody using several of EDC- Sulfo-NHS based crosslinking strategy, blocking with 0.5% BSA, and detection rabbit IgG (10^{-7} M).

Initially, the cleaned chip was coated with 1% of chitosan that was prepared in 10 mL of 0.1 M of acetic acid and incubated with HEPES buffer (100 mM and pH 7.4) overnight. The EDC-Sulfo-NHS-activated anti-rabbit IgG antibody was prepared with ratio (4:1)

(0.008 g of EDC and 0.022 g of Sulfo-NHS in 2 mL of HEPES buffer pH 7.4) by the procedure mentioned in Section 3.7. The flow rate used for all the process steps was 0.118 mL min^{-1}. The antibody immobilization was done by injecting 2 mL of EDC-Sulfo-NHS activated anti-rabbit IgG ($2.5*10^{-9}$ M) antibody over all the two channels of flow cell of a waveguide sensor. The anti-rabbit IgG antibody bound chitosan film was then blocked by injecting of 0.5% (w/v) BSA was prepared in HEPES buffer. Subsequently, the dilution buffer of HEPES, pH 7.4 was passed through two channels of flow cell and the optical output was detected by CMOS camera. Finally, 2 mL of rabbit IgG (10^{-7} M) was passed through the flow cell.

2.11.2.1 Using Ratio (1:1) of EDC- Sulfo-NHS

This experiment has been done with the optimum conditions were mentioned in 3.7.1.1 but the difference with the ratio of EDC-Sulfo-NHS (1:1).

2.11.2.2 Using Ratio (1:4) of EDC- Sulfo-NHS

As described in section 3.7.1.2, the process of antibody immobilisation has been done by the optimum conditions which are used in the detection of rabbit IgG with the ratio (1:1) of EDC-Sulfo-NHS.

2.12 Optimisation of Antibody Immobilisation

2.12.1 Effect of a Cross Linker

A cross linker (NHS-PEG-NHS) (Mwt.3000 Dalton) (0.1 mM) was prepared in 2 mL of HEPES buffer (100 mM pH 7.4), and used to incubate a cleaned glass slides for 5 min, which were coated with 1% (w/v%) of chitosan that which prepared in 10 mL of 0.1 M acetic acid and left 3 min to dry then incubated with HEPES buffer (100 mM and pH 7.4) overnight.

RB4 dye (100 mM) was used to incubate cleaned glasses for 5 min and left for drying at room temperature. The EDC-Sulfo-NHS-activated anti-rabbit IgG antibody was prepared with ratio (4:1) (0.008 g of EDC and 0.022 g of Sulfo-NHS in 2 mL of HEPES buffer pH 7.4) by the procedure mentioned in Section 3.7. The flow rate used for all the process steps was 0.118 mL min^{-1}. The antibody immobilization was done by injecting 2 mL of EDC- Sulfo-NHS-activated anti-rabbit IgG ($2.5*10^{-9}$ M) antibody over all the two channels of flow cell of a waveguide sensor. The anti-rabbit IgG antibody bound chitosan

film was then blocked by injecting of 0.5% (w/v) BSA was prepared in HEPES buffer. Subsequently, the dilution buffer of HEPES, pH 7.4 was passed through two channels of flow cell and the optical output was detected by CMOS camera that is connected to a program called GetFram V8 in PC where the movement of the dip can be monitored. Finally, 2 mL of rabbit IgG (10^{-7} M) was passed through the flow cell. To study the effect of using cross linker in the antibody immobilisation into the waveguide layer of chitosan, this experiment has been done with cross linker and without cross linker.

2.12.2 Effect of pH

Effect of pH buffer on the antibody immobilisation into a waveguide film was investigated by preparing all the materials with HEPES buffer that have pH (6.4). The flow cell was mounted onto a glass substrate that is coated with 1% (w/v) of chitosan solution in 10 mL of (0.1 M) acetic acid, spin coated at 900 rpm and left to dry for 3 min, then incubated with HEPES buffer (pH 7.4) overnight. RB4 dye (100 mM) was used to incubate the waveguide film for 5 min, The EDC- Sulfo-NHS-activated anti-rabbit IgG antibody was prepared with ratio (4:1) as mentioned in Section 3.7 but with (pH 6.4) of HEPES buffer then blocked by injecting of 0.5% (w/v) BSA was also prepared in HEPES buffer (pH 6.4). The prepared solutions were injected to the channel in flow cell by peristaltic pump at flow rate of 0.25 mL min^{-1} using silicone tube. The flow cell was washed with HEPES buffer (pH 6.4) before and after each measurement with buffer. The output is captured by CMOS camera that is connected to a program called GetFram V8 in PC where the movement of the dip can be monitored.

2.12.3 Optimise concentration of detection IgG

In order to optimise a concentration of detection IgG, a stock solution of antigen (10^{-7} M) was prepared in HEPES buffer (100 mM pH 7.4), and series concentrations (10^{-7}-10^{-11} M) were obtained by dilution with HEPES buffer, which were injected through a peristaltic pump into the flow cell at flow rate 0.25 mL min^{-1}, that was passed on the cleaned glass slide that was coated with 1% (w/v) of chitosan dissolved in 10 mL of 0.1 M acetic acid at spin speed 900 rpm, left for 3 min dry time and incubated with HEPES buffer (100 mM pH 7.4) overnight then following day incubated with RB4 dye (100 mM) for 5 min. The

EDC- Sulfo-NHS -activated anti-rabbit IgG antibody was prepared with ratio (4:1) as mentioned in Section 3.7 that was injected then blocked by injecting of 0.5% (w/v) BSA was prepared in HEPES buffer before series concentrations of detection IgG, the measured signal was captured by CMOS camera that is connected to a program called GetFram V8 in PC where the movement of the dip can be monitored.

2.13 Enhancement of the Interaction Sensitivity

There are various experiments has been done to obtain a high interaction sensitivity between anti-rabbit IgG antibody and detection IgG.

2.13.1 Increase an Interaction Time between the Antibody and Antigen

The optimum conditions were obtained from previous experiments will be applied to enhance the interaction sensitivity between the anti-rabbit IgG antibody and detection IgG. Firstly, the cleaned chip was coated with 1% of chitosan that was prepared in 10ml of 0.1 M of acetic acid at spin speed 900 rpm and left 3 min to dry, after that incubated with HEPES buffer (100 mM and pH 7.4) overnight. Coated glass slide was incubated with RB4 dye (100 mM) for 5 min and left to dry at RT (room temperature).

The EDC-Sulfo-NHS-activated anti-rabbit IgG antibody was prepared with ratio (4:1) (0.008 g of EDC and 0.022 g of Sulfo-NHS in 2 mL of HEPES buffer (100 mM, pH 7.4) by the procedure mentioned in Section 3.7. The antibody immobilization was done by injecting 2 mL of EDC-Sulfo-NHS-activated anti-rabbit IgG ($2.5*10^{-9}$ M) antibody over one channel of flow cell and the second channel was only used to inject HEPES buffer (100 mM pH 7.4) at a flow-rate (0.25 mL min^{-1}) of a waveguide sensor. The anti-rabbit IgG antibody bound chitosan film was left overnight then blocked by injecting of 0.5% (w/v) BSA was prepared in HEPES buffer. Subsequently, the dilution buffer of HEPES, pH 7.4 was passed through two channels of flow cell and the optical output was detected by a camera. Finally, 2 mL of rabbit IgG (10^{-7} M) was passed through the flow cell. The movement of the dip can be monitored by CMOS camera that is connected to a program called GetFram V8 in PC. This procedure has been repeated two times with the same conditions one time, detection IgG was injected overnight instead of anti-IgG antibody, and secondly, anti-rabbit IgG was injected for 10 min then pause (stop the pump) the pump for one hour then repeated three times, then which was injected overnight in order to enhance the interaction sensitivity.

2.13.2 Increasing incubation time of blocking molecules

The EDC-Sulfo-NHS-activated anti-rabbit IgG antibody was prepared with ratio (4:1) (0.008 g of EDC and 0.022 g of Sulfo-NHS in 2 mL of HEPES buffer (100 mM, pH 7.4) by the procedure mentioned in Section 3.7, blocked with 0.5% of BSA for longer time 2 h. till get base line ,then detection IgG (10^{-7} M) was injected via the peristaltic pump to the flow cell at a flow-rate 0.25 mL min^{-1}, the immobilisation process has been done by using coated glass slides with 1% (w/v) of chitosan was completely dissolved in 10 mL of acetic acid (0.1 M),spin coated at 900 rpm for 30 Sec then left with HEPES buffer (pH 7.4) to incubate overnight, then incubated with RB4 dye (100 mM) for 5 min to dry at RT. The optical output was captured by CMOS camera that is connected to a program called GetFram V8 in PC where the movement of the dip can be monitored.

2.13.3 Reducing of the flow-rate

To increase the interaction sensitivity of a waveguide film for antibody immobilisation by a similar procedure described in section 3.7 by immobilising EDC- Sulfo-NHS-activated anti-rabbit IgG antibody ($2.5*10^{-9}$ M) overnight, blocked with 0.5% of BSA, and which was reacted with detected IgG (10^{-7} M) with reducing the flow-rate of the peristaltic pump at 0.118 mL min^{-1}. The antibody immobilisation was performed by using coated glass slide with 1% (w/v) of chitosan, which was totally dissolved in 10 mL of (0.1 M) acetic acid and spin coated at 900 rpm for 30 Sec, then dried for 3 min at RT, incubated with HEPES buffer (100 mM, pH 7.4) overnight.

RB4 dye (100 mM) was used to incubate coated glass slides for 5 min then left to dry at RT. Afterward, the dilution buffer of HEPES, pH 7.4 was passed through two channels of flow cell and the optical output was detected by CMOS camera. Finally, 2 mL of rabbit IgG (10^{-7} M) was passed through the flow cell. The movement of the dip can be monitored by a camera that is connected to a program called GetFram V8 in PC.

2.13.4 Flowing Effect

Initially, the cleaned glass slides were coated with 1% of chitosan that was prepared in 10 mL of 0.1 M of acetic acid, spin coated at 900 rpm for 30 Sec, and incubated with HEPES buffer (100 mM and pH 7.4) overnight, and with RB4 (100 mM) dye for 5 min.

After that, EDC-Sulfo-NHS-activated anti-rabbit IgG antibody ($2.5*10^{-9}$ M) was prepared with ratio (4:1)(0.008 g of EDC and 0.022 g of Sulfo-NHS in 2 mL of HEPES

buffer (pH 7.4) by the procedure mentioned in Section 3.7,the flow rate used for all the process steps was 0.118 mL min^{-1}. The antibody immobilization was done by injecting 2 mL of EDC- Sulfo-NHS-activated anti-rabbit IgG ($2.5*10^{-9}$ M) antibody over all the two channels of flow cell for 10 min then pause one hour, then injected for 10 min and pause also for one hour repeated three times then Anti-IgG was left overnight. The anti-rabbit IgG antibody bound chitosan film was then blocked for 2 hrs by 0.5% (w/v) BSA was prepared in HEPES buffer. Subsequently, the dilution buffer of HEPES (pH 7.4) was passed through two channels of flow cell and the optical output was detected by CMOS camera. Finally, 2 mL of rabbit IgG (10^{-7} M) was passed through the flow cell, the optical output was captured by a camera that is connected to a program called GetFram V8 in PC where the movement of the dip can be monitored.

2.13.5 Ionic strength of HEPES buffer

HEPES (4-(2-hydroxyethyl)-1-piperazineethanesulfonic acid) is a common buffering chemical and is classified as a "Good's buffer" which has been derived from a set of buffers described by Dr. Norman Good and his colleagues in 1966. There are various reasons for using HEPES buffer in the chemical reactions:

- Easy to prepare.
- pKa values between 6.0 and 8.0
- Limited effect on biochemical reactions.
- Very low visible and ultraviolet light absorbance.
- Chemically and enzymatically stable.

Therefore, it was used to keep the pH of the reaction at a certain value. This experiment was performed in order to increase of the interaction sensitivity by adding salt of sodium chloride (100 mM, 150 mM, 200 and 250 mM) to HEPES buffer (100 mM pH 7.4) [121] , and this buffer has been used to prepare the whole solutions which were injected through the peristaltic pump to immobilise EDC- Sulfo-NHS-activated anti-rabbit IgG antibody ($2.5*10^{-9}$ M) and detection IgG (10^{-7} M). The immobilisation process has been done using DDLW sensor.

2.14 Investigation of the Antibody Immobilization

There are several detection methods commonly used for biomolecular process to characterize and quantify a biorecognition elements such as fluorescence microscope, confocal microscope, and a waveguide sensor... etc.

2.14.1 Fluorescence Microscopy

Fluorescence detection method is more preferred to detect biorecognition elements because of its high safety, sensitivity and relative ease of use and for an increasingly large selection (in biocompatibility, physiochemical/structural properties) of labelling agents involving green fluorescence protein, fluorophores, metal cages, phytochrome proteins, semiconductor quantum dots, and others. Experimentally,1% (w/v) of chitosan was dissolved completely in 10 mL of 0.1 M acetic acid, coated by using cleaned glass slides at spin speed 900 rpm, left for 3 min to dry at RT, then incubated with HEPES buffer (100 mM pH 7.4) overnight. Coated glass slides with chitosan were incubated with EDC-Sulfo-NHS-activated anti-rabbit IgG-FITC antibody ($2.5*10^{-9}$ M) overnight, following day some of these slides were washed with fresh HEPES buffer for 5 min. and others still without washing with HEPES buffer, and the rest were placed on the prism to perform the immobilisation process by using DDLW and the optical output was captured by CMOS camera that is connected to a program called GetFram V8 in PC where the movement of the dip can be monitored at different flow-rate 0.25 mL min^{-1}, and 0.118 mL min^{-1}. Finally, all these slides were detected by fluorescence microscope.

2.14.2 Confocal Microscope

Laser scanning confocal microscopy, differs from fluorescence microscopy, can be collect the light from a single focal plane. It collects the pixel information into one image after scans the sample point by point and line by line, and can put together a single images or optical slices to build up a three-dimensional stack by moving the focal plane in axil (z) dimension. The experimental method was similar to section 3.10.1 cover slips were coated with 1% (w/v) of chitosan was prepared by dissolving totally in 10 mL of 0.1 M acetic acid, spin coated at 900 rpm for 30 sec and left to dry for 3 min, then incubated with HEPES buffer (100 mM pH 7.4) overnight. Activated EDC-Sulfo-NHS-goat anti-rabbit IgG-FITC antibody ($2.5*10^{-9}$ M) was used to incubate these cover slips overnight. following day some of these slips were washed with fresh HEPES buffer for 5 min and

others still without washing with HEPES buffer, and the rest were placed on the prism to perform the immobilisation process by using DDLW and the optical output was captured by CMOS camera that is connected to a program called GetFram V8 in PC where the movement of the dip can be monitored. Finally, all these slips were detected by laser scanning confocal microscopy.

2.14.3 Dye doped leaky waveguide sensor (DDLW)

This experiment has been performed in order to investigate of the antibody immobilisation by using 1 % (w/v) of chitosan was dissolved in 10 mL of acetic acid (0.1 M), cleaned glass slides were spin coated at 900 rpm for 30 Sec and dry it for 3 min, incubated with HEPES buffer (100 mM pH 7.4) overnight. RB4 dye (100 mM) was used to incubate coated glass slides for 5 min. The antibody immobilization was done by injecting 2 mL of EDC- Sulfo-NHS-activated goat anti-rabbit IgG ($2.5*10^{-9}$ M) antibody was injected via one channel to track the immobilisation of the antibody, and second channel was used to inject (Antibody and antigen), goat anti-rabbit IgG antibody was blocked by 0.5% (w/v) BSA which was prepared in HEPES buffer. Subsequently, the dilution buffer of HEPES (pH 7.4) was passed through two channels of flow cell and the optical output was detected by CMOS camera. Finally, 2 mL of rabbit IgG (10^{-7} M) was passed through the second channel of the flow cell. The optical output was captured by CMOS camera that is connected to a program called GetFram V8 in PC where the movement of the dip can be monitored.

2.15 Immobilization of the Antibody using a linker (Glutaraldehyde)

It is important before starting with experiments of crosslinking, should select essential linker for optimal reaction with the proteins. Some features should be taken in the consideration such as membrane permeability, solubility, and reversibility of cross-links, in addition that it can be conducted under natural conditions of temperature and pH to maintain the original structure of the protein. Some Homo-bifunctional reagents are work very well with chitosan's amines such as DMA (dimethyl adipimidate), DMS (Dimethyl suberimidate), and glutaraldehyde.

This experiment procedure was done by using glutaraldehyde as a linker that it should be conducted in buffers free from amines like HEPES buffer at pH 7.5 to 8.0 is suitable. For

glutaraldehyde solution, different concentrations of glutaraldehyde (0.3, 0.6, and 1%) were prepared in 2 mL of HEPES buffer pH 7.4 for 2 to 5 min at 37^{o}C. It was injected via cleaned glass slides were coated by 1% (w/v) of chitosan was dissolved in 10 mL of acetic acid (0.1 M), spin coated at 900 rpm for 30 min and left to dry for 3 min, then incubated with HEPES buffer pH 7.4 overnight. Next, RB4 dye (100 mM) was used to incubate coated glass slides for 5 min. Firstly, the dilution buffer of HEPES (pH 7.4) was passed through two channels of flow cell, then different concentrations of a cross linker was injected through one channel. Subsequently, 2 mL of EDC-Sulfo-NHS-activated goat anti-rabbit IgG ($2.5*10^{-9}$ M) antibody was injected via one channel to track the immobilisation of the antibody, and second channel was only used to inject (HEPES buffer), goat anti-rabbit IgG antibody was blocked by 0.5% (w/v) BSA which was prepared in HEPES buffer. Finally, 2 mL of rabbit IgG (10^{-7} M) was passed to interact with goat anti-rabbit IgG until get straight line then injected HEPES buffer. The optical output was captured by CMOS camera that is connected to a program called GetFram V8 in PC where the movement of the dip can be monitored.

2.16 Immobilisation of the Antibody using Biotin-Streptavidin

One of the most popular protocol of the antibody immobilization via using biotin-streptavidin system to enhance the stability of the interaction (antibody-antigen), and the output signal. The binding of biotin - streptavidin is well established for both with high affinity and high specificity, strongest, and noncovalent interaction, therefore making them a popular nano-”adhesive”. Streptavidin, a bacterial homologous protein to avidin, is more used than avidin, and is isolated from the actinobacterium Streptomyces avidinii. An important detail of these two experiments was that the waveguide film (1% w/v of chitosan was dissolved totally in 10 mL of acetic acid 0.1 M, spin coated at 900 rpm for 30 Sec and dry it for 3 min. then incubated with HEPES buffer pH 7.4 overnight. RB4 dye 100 mM was used to incubate of the waveguide film for 5 min) is functionalized with 0.3% of glutaraldehyde 25 µL of 50% (v/v%) in 2 mL of HEPES buffer, then injected 1 µM of streptavidin 20 µL in 2 mL of HEPES buffer, next the waveguide film was blocked by 0.5% (w/v) BSA which was prepared in HEPES buffer, later biotinylated goat anti-rabbit IgG ($2.5*10^{-9}$ M) was injected through a peristaltic pump. Finally, 2 mL of rabbit IgG (10^{-7} M) was passed to interact with biotinylated goat anti-rabbit IgG until get straight line then injected HEPES buffer. The optical output was captured by CMOS camera that is connected to a program called GetFram V8 in PC where the movement of the dip can

be monitored in first experiment , whereas in the second experiment was performed without glutaraldehyde. Different concentrations of Streptavidin were used to attach biotinylated goat anti-rabbit IgG and increase the stability of the interaction between the antibody and the antigen.

2.17 ELISA quantification of Tissue Factor (III)

2.17.1 Culture of the Cell Lines

All experiments has been performed in sterilized environment in a class II biological safety cabinet provided with UV that was switched on before 30 min of work. Moreover, the culture hood, water path and incubator was cleaned by using Virkon disinfectant. 70% ethanol was used for cleaning all surfaces the hood, weared gloves, media bottles and everything needed to be used within the laminar before commencing work. All media were pre-warmed by placing in a water bath at 37ºC for 30 min before start and a sterile 75 mL plastic flasks were used for all cells. Furthermore, all cell lines were maintained at 37º in 5% CO_2 within sterile incubator. In term of defrosting, all vials of cell lines were kept in frozen in liquid nitrogen. Then, there were directly thawed in 37º water path for 2 minutes. The 1 mL of vial defrosted cells was added to 9 mL of pre-warmed media. After finishing the experiments, the cells were stored. However, the viability was tested before and if it is >90% the cells would be stored. Viability test will be explained later. In order to store the cells, the cells were harvested and pelleted by the centrifuge for 5 min at 400 x g. After that, cells were cultured in freezing media [10% Dimethyl sulphoxide (DMSO) + 90% FBS], cell vials were kept in -80º freezer.

2.17.2 Maintenance and adaptation of cell lines to serum free media

2.17.2.1 Maintenance

Two types of pancreatic cell line were used in this research, (Aspc-1, and Miapaca-2) were cultured in PRMI-1640 and DMEM media respectively. Aspc-1 cells were supplemented with 1% L-glutamine, 1% sodium pyruvate, 1% streptomycin/penicillin, 10% foetal bovine serum and 25 μM of glucose concentration (FBS). Whereas, Miapaca-2 cells were maintained within a DMEM media comprising 25 μM of glucose concentration, 1% sodium pyruvate, 1% L-glutamine, 10% FBS and 1% streptomycin/penicillin.

2.17.2.2 Passaging

The pancreatic cells were split up in 3-well plates and allowed to adhere. Before activation and harvesting of all cell lines should incubated overnight and pre-adapted to respective free medium of conditioned media ,and which were grown in 75 mL tissue culture flasks were suitably labelled with the cell line, passage number then incubated at 37ºC with 5% CO_2 atmosphere. On the following overnight incubation, the cell lines will be observed by utilizing a phase contrast microscope for a monolayer growth of about 70-80% and to ensure of the absence of fungal and bacterial contaminates, Depending on observations cells were either seeded or left for growing especially for slow growing cell lines, the culture media was replaced every 48 h after incubation to confirm sufficient nutrients for cell growth. Time-course measurements were performed by collecting conditioned media at various recovery periods (0, 1, 2 and 72 h) incubated at 37º C with 5% CO_2 atmosphere for experiments concerning TF expression by ELISA. After that, the pancreatic cells were adherent cells, therefore, a cell scraper was used to detach the cells from the flask's surface. Next, the cells were pelleted by the centrifuge for 3 min at 400 x g. Fresh media was added following the discarding of the supernatant and then transferred into a new) polycarbonate centrifuge tubes freezing and storage at -80ºC. The passaging was carried out when the cells reached 80–90% confluence on the flask's surface.

2.17.2.3 Cell Counting

This assay was performed by mixing 10 µL of trypan blue and 10 µL of the cell suspension to the pellet re-suspended in a 1ml centrifuge tube and mixed by lightly pipetting. The number of viable cells were counted by filling of the chamber with 10 µL of cell suspension / trypan blue solution were prepared using slight pressure for ensuring no air bubbles were present, and for attaching a cover slip until Newton's refraction rings appeared (rainbow-like rings under the cover-slip), The principle behind the use of the trypan blue is that living cells will appear to be transparent because the dye cannot enter their cellular membrane. However, the dye will enter dead cells due to their cell wall being damaged and hence they will appear to be a blue colour. samples watched (seen as bright cells) under a light microscope using 10X magnification, and counted in the central square (gridded 5 x 5 squares) and the 4 squares left and right , above and below of the central square as indicate in fig.2.28, followed by calculation of the average number of cells per large square.

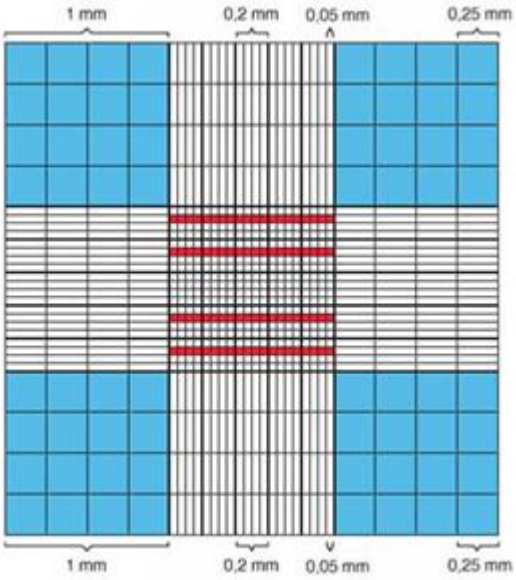

Figure 2.28: Haemocytometer the blue areas indicate the counting areas of the chamber [130].

The average number = x 10^5 and equalled the number of cells per 1 mL within the cell suspension / trypan blue solution. The dilution factor was calculated using the following equation:

$$\textit{Dilution factor} = \frac{Concentration\ of\ original\ cell\ suspension}{Concentration\ of\ required\ cell\ suspension}\ \textit{x Volume}\ldots\ldots\ldots\textit{Equation 2.9}$$

2.17.3 Tissue Factor (TF) ELISA method

2.17.3.1 Principle of (TF) ELISA

This test was done to measure the TF concentration in the PC, and control samples (fig.2.29.shows R&D systems 96-well ELISA plates (Costar EIA Plate) was coated with anti-TF antibodies. After that, a TF secondary antibody labelled with an enzyme (peroxidase) was added to the wells. Finally, TMB substrate was added and, according to the colour density, the amount of TF in the sample was calculated by using a standard curve of known values.

	1	2	3	4	5	6	7	8	9	10	11	12
A	Standard1	Standard1	Standard1	Sample1	Sample1	Sample1	Sample9	Sample9	Sample9			
B	Standard2	Standard2	Standard2	Sample2	Sample2	Sample2	Sample10	Sample10	Sample10			
C	Standard3	Standard3	Standard3	Sample3	Sample3	Sample3	Sample11	Sample11	Sample11			
D	Standard4	Standard4	Standard4	Sample4	Sample4	Sample4	Sample12	Sample12	Sample12			
E	Standard5	Standard5	Standard5	Sample5	Sample5	Sample5	Sample13	Sample13	Sample13			
F	Standard6	Standard6	Standard6	Sample6	Sample6	Sample6						
G	Standard7	Standard7	Standard7	Sample7	Sample7	Sample7						
H	Blank1	Blank2	Blank3	Sample8	Sample8	Sample8						

Figure 2.29: The plate map for the ELISA test, the samples were triplicated. The colour yellow represents the standard samples, while green colour represents the blank samples, orange represents the PC samples, Standard 1= 500 pg mL^{-1}, Standard 2= 250 pg mL^{-1}, Standard 3= 125 pg mL^{-1}, Standard 4= 62.5 pg mL^{-1}, Standard 5= 31.25 pg mL^{-1}, Standard 6= 15.62 pg mL^{-1}, Standard 7= 7.81 pg mL^{-1} .

2.17.3.2 Method of TF ELISA

Before starting with the experiment, the samples were taken from the -80°C freezer and they were kept at RT to thaw. Firstly, the plate was coated with 100 µL/well with capture antibody (mouse anti-human Coagulation Factor III) diluted 5:1000 in PBS buffer, sealed, and incubated overnight at 4°C. The coated plates were aspirated, and washed three times with 400 µL of wash buffer (20 mL was diluted with deionised water to prepare a total volume of 500 mL) by using a plate washer, after the last wash removed any remaining wash buffer by inverting the plate and blotting it against clean paper towels, then blocked each well with 300 µL of reagent diluent (2 mL of reagent diluent + 36 mL of DW) and incubated at room temperature for a minimum of one hour. The plates were washed three times and 100 µL.

TF standard and samples were reconstituted with 0.5 mL of reagent diluent to form a stock solution (85000 pg mL^{-1}) which was then sit for 15 min with gentle agitation prior to making dilutions with reagent diluent to give a range of standards: 500, 250; 125; 62.5; 31.3; 15.6 and 7.8 pg mL^{-1} were added in triplicate, and incubated at RT for 2 hrs and subsequently washed three times with wash buffer, 100 µL/well of biotinylated goat anti-human coagulation Factor III detection antibody was reconstituted to a working

concentration (36000 pg mL^{-1}) with 1 mL of reagent diluent (diluted 5:1000) was added to each well and plates incubated at RT for one hour, the plate is covered with adhesive film. Plates were then washed three times.

Then 100 µL of TF conjugate (which is streptavidin conjugated to horseradish peroxidase) was added and plates were incubated for 20 min at RT in the dark place, the wash was repeated three times as described previously, 100 µL of substrate solution [colour reagent A (H_2O_2) and reagent B (Tetramethylbenzidine) were mixed together in equal volumes was added and incubated for 20 min at room temperature in the dark and the plate was covered with adhesive film, during this time a blue colour appeared, at which time the reaction was stopped by adding 50 µL stop solution (2 M H_2SO_4) to each well, gently tap the plate to ensure thorough mixing. The density of the obtained colour (when the blue colour was changed to yellow) was measured using an ELISA plate reader at 450 nm wavelength and the blank samples were used as negative samples for zeroing the reading.

2.18 Conclusion

In the previous chapter, we have seen it is possible to enhance the sensitivity of a leaky waveguide sensor through immobilization very little concentrations of biorecognition elements into the leaky waveguide film.

In this chapter, we have presented in detail the fabrication, characterisation, and investigation the porosity of a leaky waveguide film by using different methodologies. These optimisations are make doped dye leaky waveguide sensor very appropriate in the detection of large particles like Antibody.

In the following chapters, we will show all of these optimisations and the application into the leaky waveguide film by monitoring the position of the dip via the change in the refractive index.

CHAPTER 3

Optimisation & Characterization

Of Waveguide Film

In order to guide light thought the chitosan waveguide layer by total internal reflection (TIR) and Fresnel reflection, the waveguide film should be uniform, smooth and fairly thin (sub-µm).The conditions for the deposition of the polymer film on the glass substrate were optimised and the waveguide film thickness was examined. Furthermore, the porosity of the film was investigated by analysing the uptake of materials of different refractive indices and molecular weights.

3.1 Initial Waveguide Optimisation

Parameters to optimise the waveguide film included the concentration of the polymer solution, the concentration of the reactive blue 4 dye (RB4) to enable the absorbance of light within the waveguide film, and the speed of the spin coater to achieve a uniform film with a thickness of about 1 µm or less.

3.1.1 Optimisation of Chitosan Concentration and Spin Speed

Chitosan was chosen as a waveguide material, as it is a porous material that can provide a large surface area and as it features functional groups for electrostatic interaction of the dye (RB4) as well as covalent bonding of biorecognition molecules (antibodies). Depending on the porosity of the chitosan the sample molecules can diffuse into the layer and interact with all the light in the waveguide. This is in contrast to non-porous materials because in these materials binding only occurs at the surface.

Chitosan solutions (1%, 1.5%, and 2% w/v) were prepared as outlined in section 2.2.4 and spin coated onto the glass substrate at speeds ranging of 2,000, 3,000 and 4,000 rpm. These films were dyed by adding a few drops of reactive blue dye (100 µm) manually. Reflectivity curves for angles between 55° and 75° were measured as described in section 2.2.5. It was expected that there is low reflectivity at low angles of incidence. Above a critical angle the reflectivity should generally be high and fairly stable over the range of angles, but at the resonance angle there should be a sharp dip in the reflectivity since light is absorbed by the RB4 dye (see fig.3.1). Each of these experiments was repeated three times for each concentration of chitosan and each spin speed.

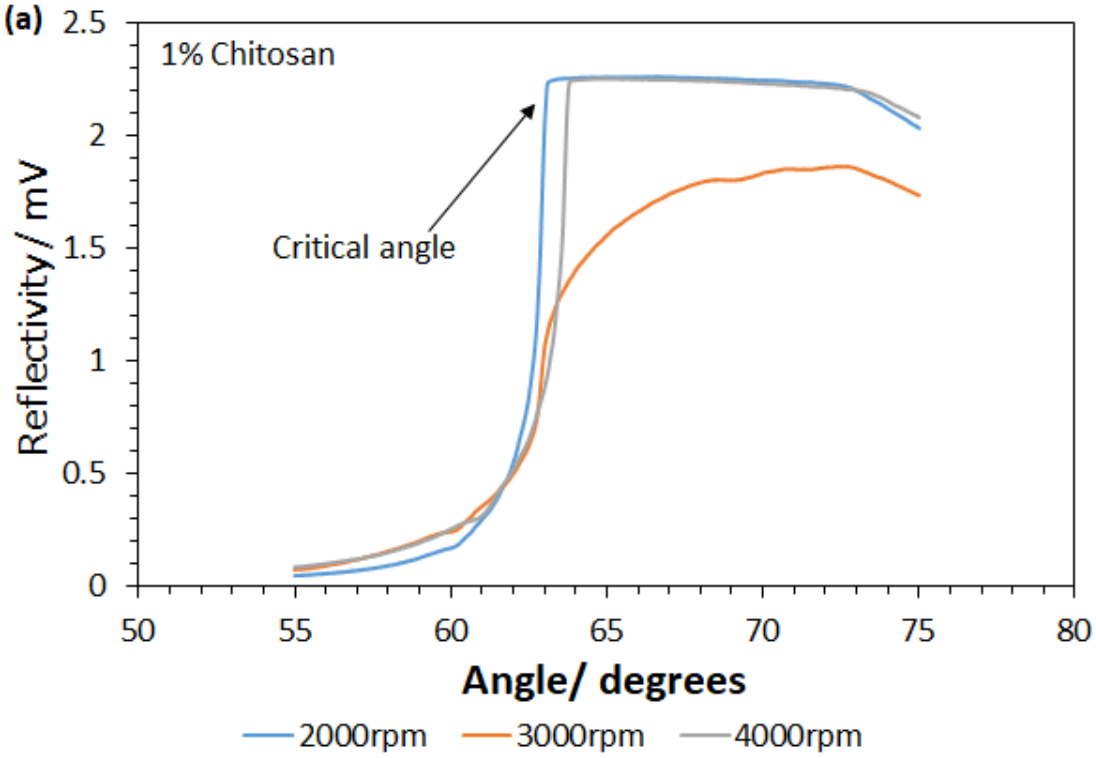
(a)
1% Chitosan
Critical angle
Reflectivity / mV
Angle/ degrees
2000rpm
3000rpm
4000rpm

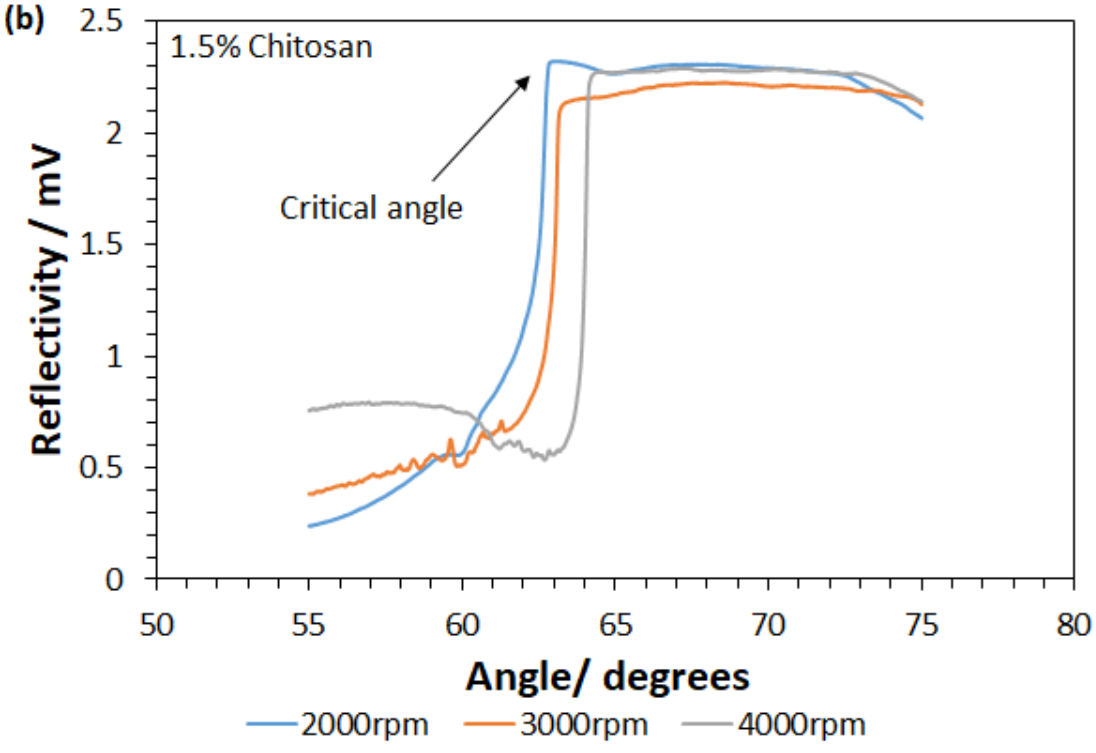
(b)
1.5% Chitosan
Critical angle
Reflectivity / mV
Angle/ degrees
2000rpm
3000rpm
4000rpm

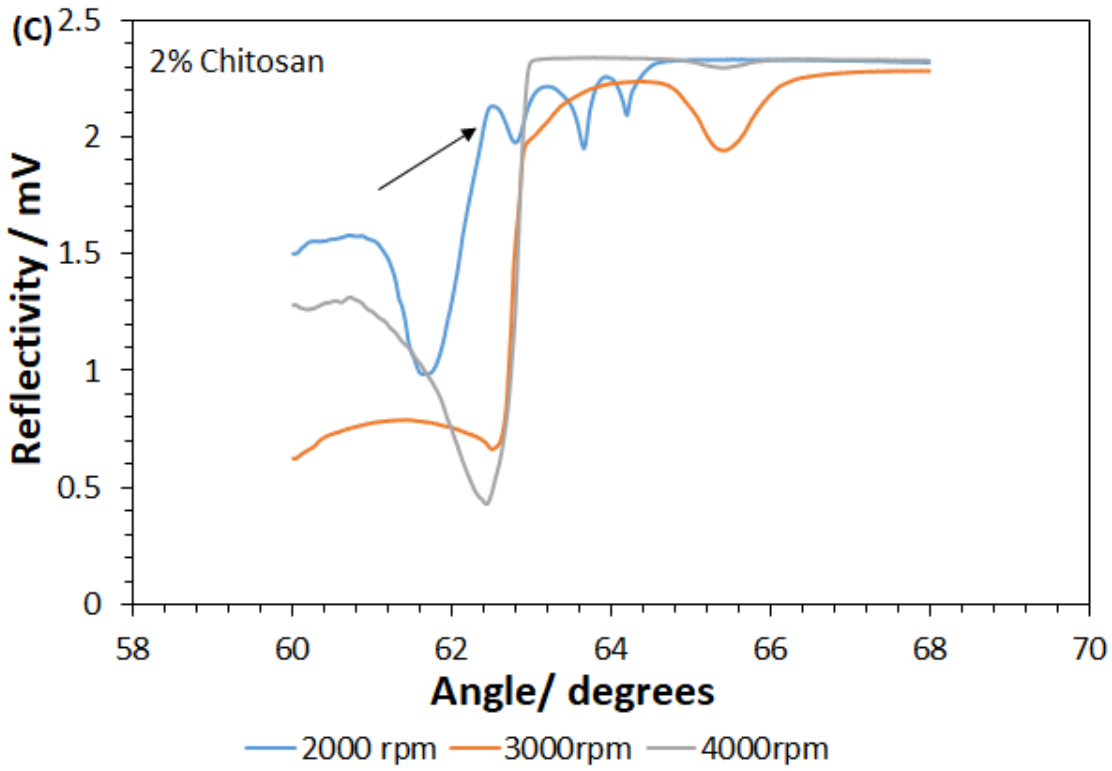

Figure 3.1: Reflectivity as a function of angle from chitosan films stained with (10 µM) reactive blue dye of (a) 1.0%, (b) 1.5% and (c) 2.0% concentrations (n=3).

For the 1.0% chitosan solution (figure 3.1a), the intensity of the reflected light measured in mV detected on the photodiode increased steadily starting from 0.24 mV at 55°. When the incident angle reached the critical angle at around 63°, total internal reflection occurred, and the intensity of the reflected light rose sharply to >2 mV and then remained steady at that level. However, the anticipated dip in reflectivity due to absorbance by the RB4 was not observed. This may be because chitosan is too thin to support an optical mode or too low a chitosan concentration. Varying the concentration of chitosan and thickness of the film may address these issues. For the 1.5% chitosan solution (figure 3.1b), also no apparent dip was observed. However, when a 2% chitosan solution was spun at 3,000 rpm (fig.3.1c), a dip in reflectivity was observed at around 65°. Whilst the dip was relatively shallow, it demonstrated the principle that a small amount of the light confined is the waveguide is absorbed by the RB4. At 2,000 rpm three dips were observed at different resonance angles. At this lower spin speed, the chitosan layer is likely to be thicker which provided multiple optical modes that could be absorbed by the dye molecules at the incident angle. At 4,000 rpm no dip was observed, possibly because the layer was then too thin to provide sufficient dye material to achieve a dip. This means the high chitosan concentration (2.0% chitosan) at medium spin speed (3,000 rpm) gave best results, but further optimisation was required to obtain a sharp dip in reflectivity.

3.1.2 Optimisation of RB4 Dye Concentration

The effect on the shape of the dip was studied with a range of RB4 dye concentrations. Initially using the optimum conditions from the previously described experiments, 2.0% chitosan solution was spin coated onto the glass substrate at a spin speed of 3,000 rpm. These were then stained with RB4 at concentrations ranging from 1.5 µM to 10 µM, as outlined in section 2.3.1. An unstained chitosan coated film was also examined for comparison. The reflectivity plots are shown in fig.3.2b. For the unstained waveguide (fig.3.2a), no dip in reflectivity was observed. For the dye-stained waveguides, a dip in reflectivity was observed for all concentrations tested. Indeed, the higher the dye concentration, the deeper the dip. In fig.3.3, the 'depth' of the dip is plotted against dye concentration, showing a linear relationship. Based on these finding, the high concentration of RB4 would be best to use for studying binding events in the waveguide which are based on shifts in the dip angle.

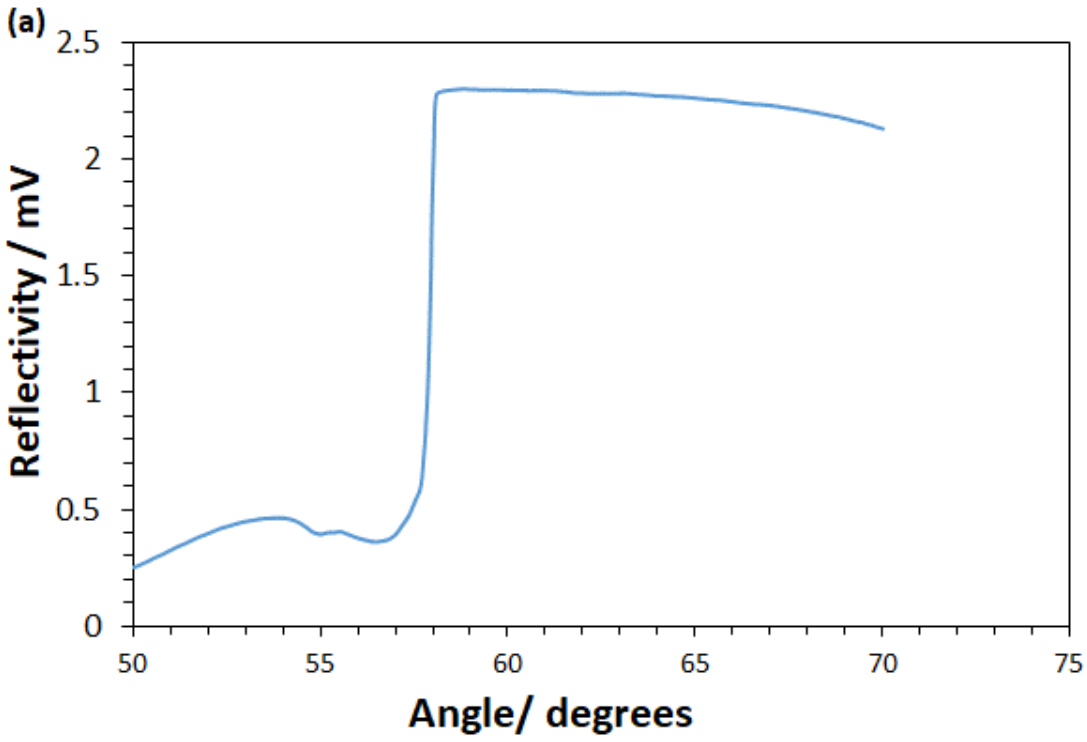

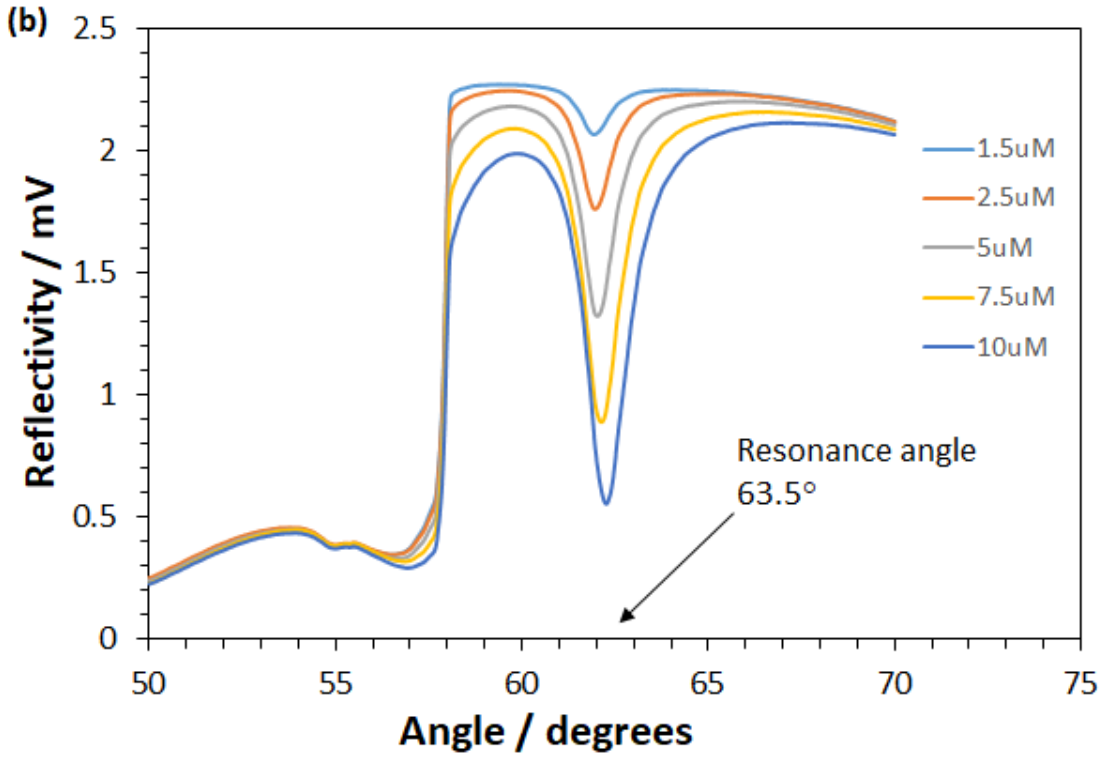

Figure 3.2 : Reflectivity curves for 2.0 w/v% of chitosan waveguide layer with spin speed, 3000 rpm in (a) water and (b) reactive blue 4 dye by using different concentrations ranging from 1.5 µM-10 µM.

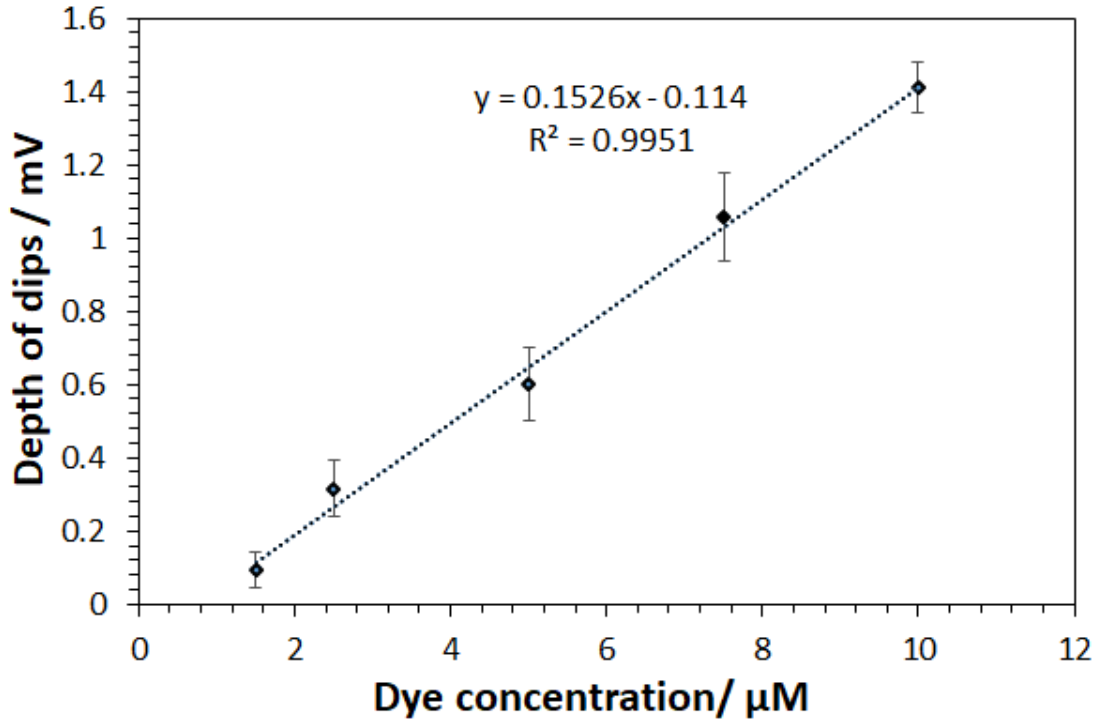

Figure 3.3: The linear relationship between absorbance and concentration using 2.0 w/v% chitosan layer with spin speed 3,000 rpm for different concentrations of the reactive blue 4 dye 1.5-10 µM at wavelength 650 nm and r^2=0.9951.

3.1.3 Study effect of different pH

Following optimisation of chitosan concentration (2.0%), spin speed (3,000 rpm) and RB4 concentration (10 μM), the effect of buffer pH on the waveguide performance was investigated. Phosphate buffer solutions with different pH values ranging from 4.0 to 10 were prepared as outlined in section 2.3.2. These were injected into the flow cell following staining with RB4 dye. The obtained reflectivity curves are shown in fig.3.4. As can be seen, both the depth of the dip as well as the resonance angle are affected by changes in buffer pH.

The lower the pH, the higher the resonance angle (fig.3.4) and also the deeper the dip (fig.3.5). At low pH values, the free amino groups in the chitosan layer are protonated ($-NH_3^+$) and thus positively charged. The electrostatic repulsion between these groups leads to swelling of the chitosan gel film. This effect is not present in basic media where the amino groups exist as neutral $–NH_2$ groups. The resonance angle is directly proportional to the optical thickness of the waveguide, which is a product of the geometrical thickness and refractive index. As a result, the resonance increases when the waveguide swells at lower pH. As the thickness of the waveguide increases, its ability to "trap" light improves i.e. the number of times light bounces backwards and forwards before it exists the waveguide increases. As light interacts with the dye in the waveguide increases, the depth of the dip increases at low pH. Therefore, this will change the thickness of chitosan layer resulting in shifting in the resonance angle, whereas the depth of the dip also increased because different pH solutions were prepared with RB4 dye.

For most biological binding assays, a pH of 7 – 8 is used. This means that can apply to any real sample.

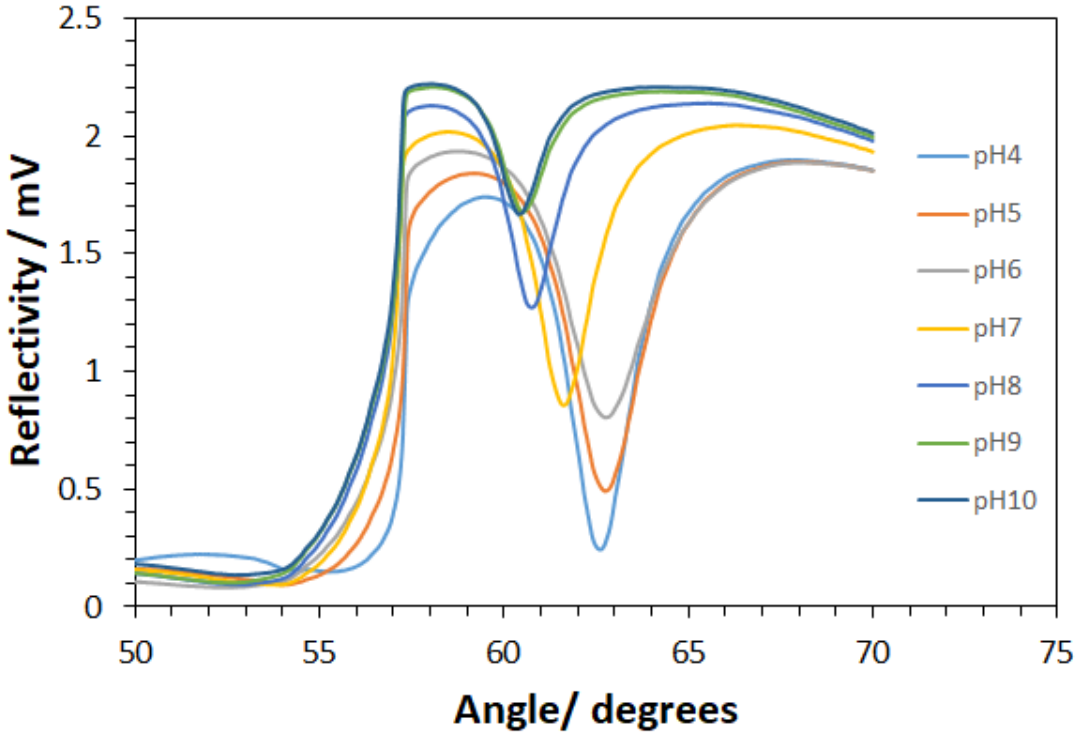

Figure 3.4: The reflectivity spectrum of the waveguide layer for 2% chitosan and 10 µM reactive blue 4 dye with spin speed 3000 rpm using different pH in the phosphate buffer (pH 4-10 (n=3).

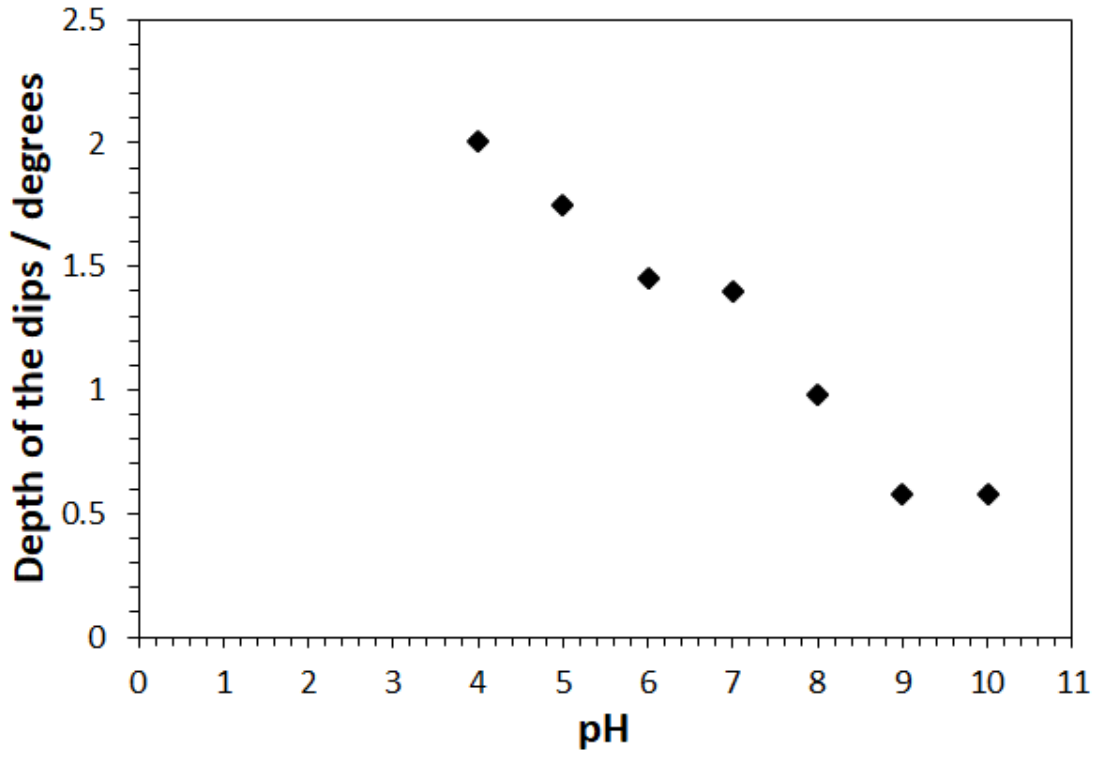

Figure 3.5: The relationship between the depth of the dips and the pH using different solutions of phosphate buffer range between 4 and 10.

3.2 Estimation of Available Amino Groups in Film

The chitosan film was characterised by determining (i) the number of moles of amino groups (n) via absorption measurements and (ii) by measuring the thickness of the film using white light interferometry (WLI). These feed into equations 2.1 and 2.2 as described is section 2.4 to estimate the number of available amino groups within the chitosan film.

3.2.1 Determination of bound dye concentration in film

The aim of this series of experiments was to measure the number of moles of amine groups (n) in the chitosan waveguide layer that bonded to the dye molecules. This was done with two different setups, (1) a conventional UV-visible spectrophotometer and (2) the waveguide setup as described in the experimental chapter (2.4.1).

Absorbance measurements of RB4 solutions in water as obtained with the UV/vis spectrophotometer are shown in fig.3.6a. A linear relationship with R^2 = 0.997 was obtained with absorbance values close to 1 for the 100 µM concentration. Absorbance measurements as obtained through the custom-built optical setup with laser light source and photodiode detection are shown in fig.3.6b. Again, a linear relationship (R^2 = 0.996) was obtained with a similar range of absorbance values from zero to about 1, indicating that both setups are equally suitable for absorbance measurements of the dye in the micromolar range.

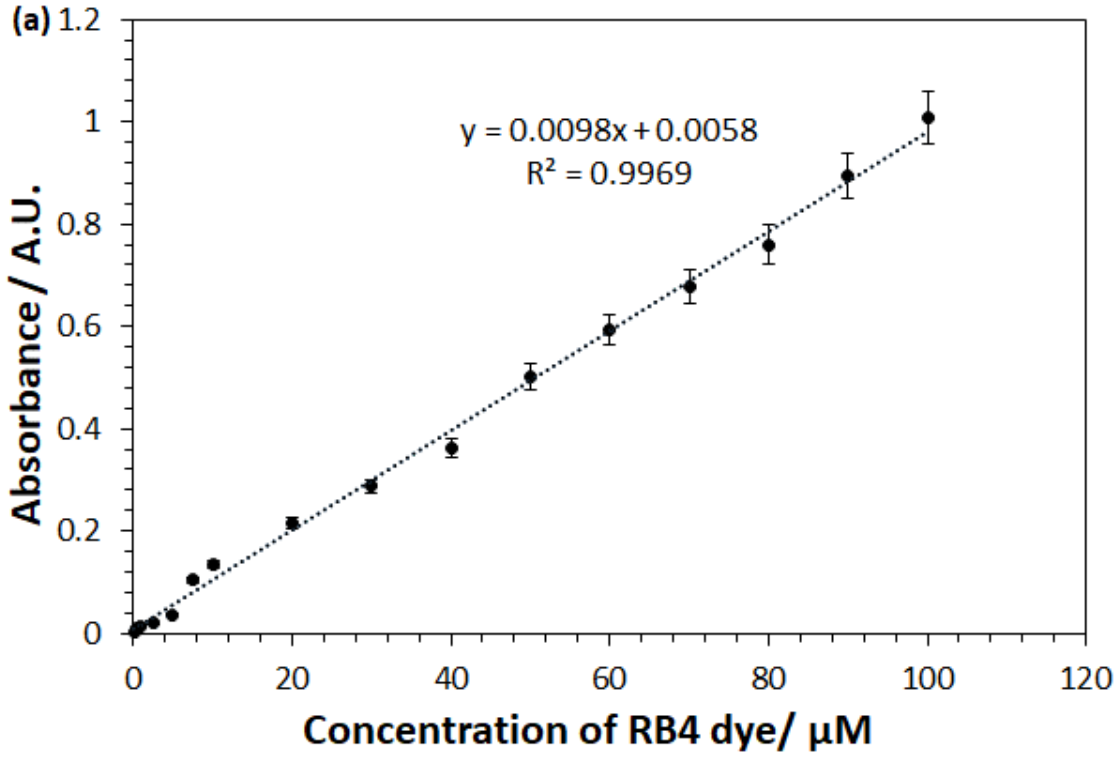

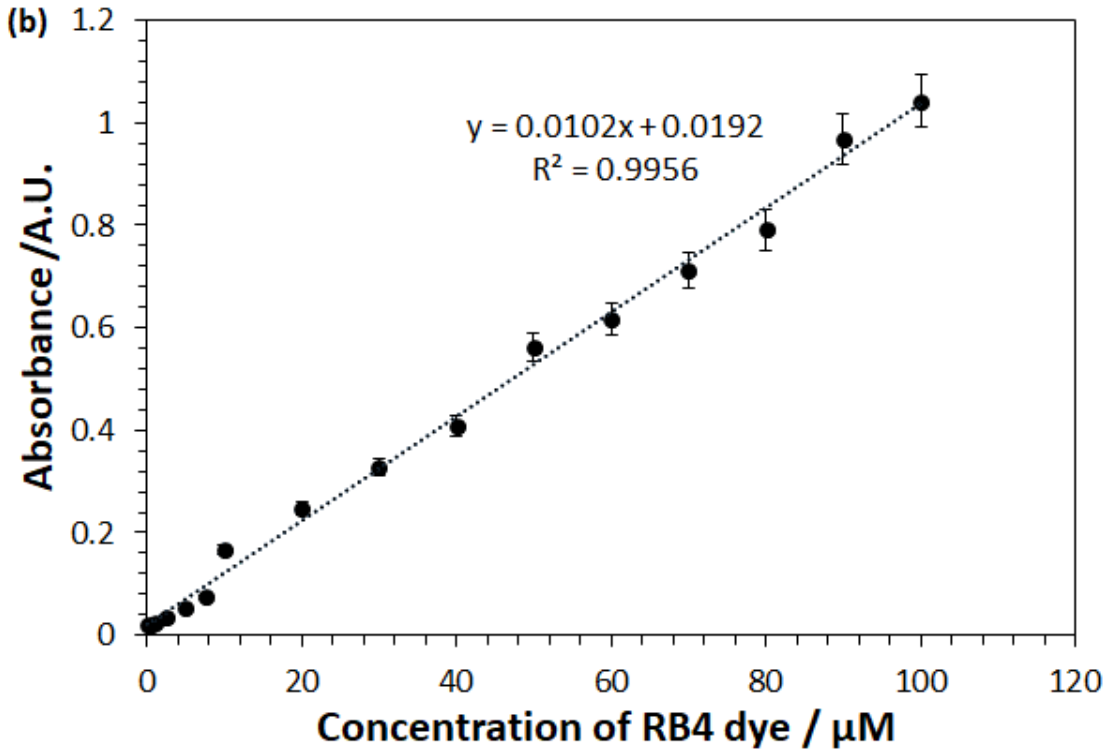

Figure 3.6: Absorbance measurements of RB4 solution at 650 nm for RB4 concentrations ranging from 0.1 µM to 100 µM (n = 3) measured via (a) conventional UV/vis spectrometer and (b) via custom-built optical setup with laser light source and photodiode detector.

The absorbance of the chitosan films as a function of staining time (10 min to 280 min) is plotted in fig.3.7a and b, measured both on the conventional UV/vis spectrophotometer and the custom-built optical system respectively. The absorbance values of the saturated chitosan films were found to be between 0.1 a.u. and 0.5 a.u., quite high given the fact that the optical path length in the chitosan film is only about 500 nm, i.e. 20 times lower than the 1 cm path length of the cuvette. The readings for the absorbance on the custom-built optical system are lower, but show the same trend, the more chitosan, the larger an amount of RB4 can be bound into the waveguide film.

The plots confirm that the 1.0% chitosan waveguide layer was saturated with RB4 after about 60 min, corresponding to a total bound concentration of RB4 dye at around 5 µM, based on the readings from the calibration curve graph from fig.3.6. The same readings when measured on the custom-built optical system showed an absorbance corresponding to 10 µM. For the 1.5% chitosan gel layer, saturation with RB4 was reached at around 100 min or more are needed to get full saturation with the dye where the total concentration was bound around 10 µM based on the UV/vis spectrometer readings and 30 µM for the optical waveguide system. For the 2% chitosan solution, saturation was achieved after about 180 min at absorbance levels corresponding to a concentration of 20

µM based on the UV/vis spectrometer readings and 50 µM from the optical waveguide setup.

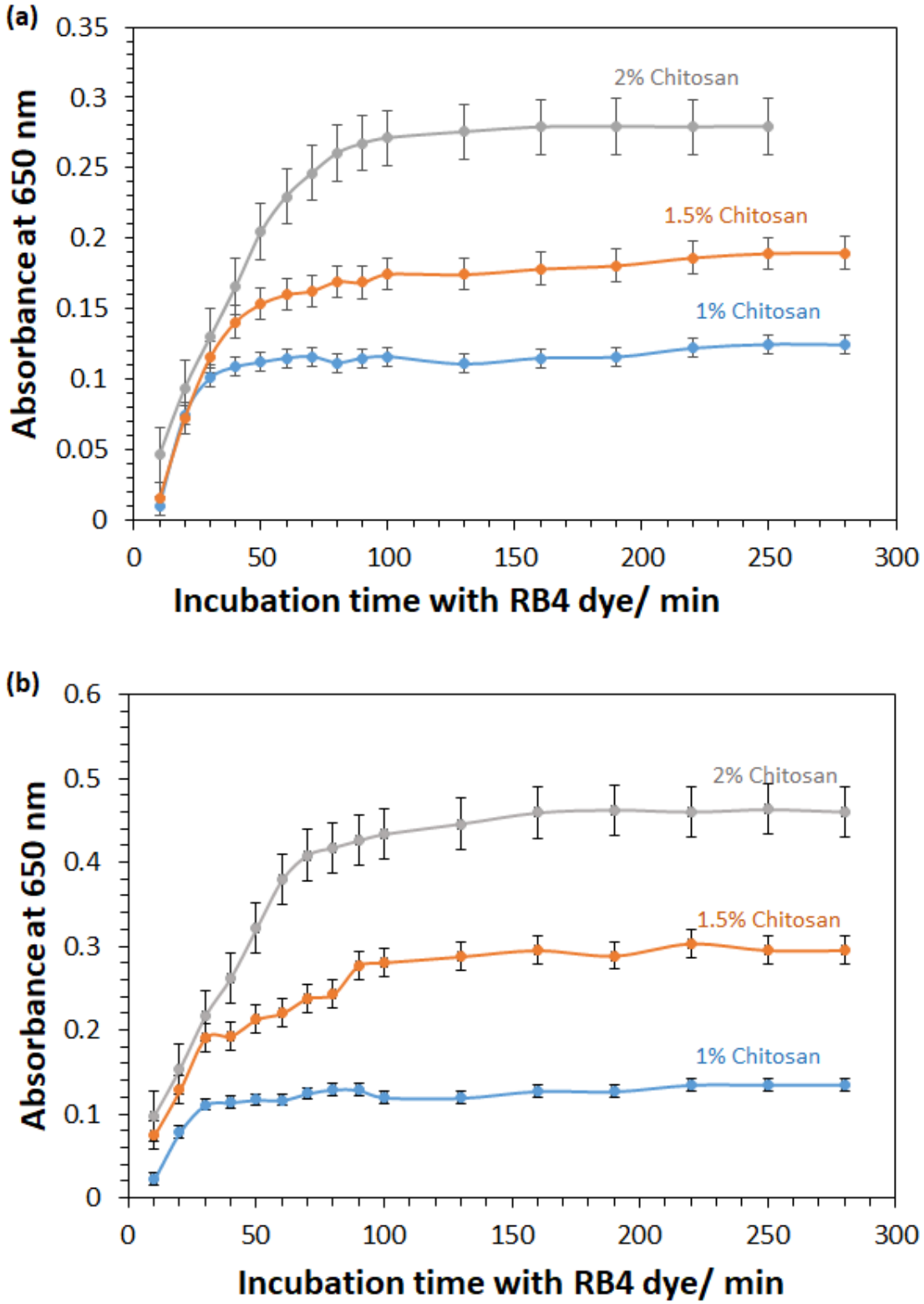

Figure 3.7: Absorbance measurements on chitosan films stained with 100 µM RB4 dye as a function of incubation time, from 10 min to 280 min measured in 10 min interval (n=3). (a) Absorbance measured on conventional UV/vis spectrophotometer, (b) absorbance measured on custom-built optical system.

3.2.2 Measurement of waveguide layer thickness

Measurement of the thickness (l) of the waveguide layer is required to estimate the volume (V) of chitosan film probed during the absorbance measurements (equation 2.1). This experiment was performed using the White Light Interferometer (WLI) as described in section 2.4.2.

Fig.3.8, shows images obtained from the WLI measurements taken from dry chitosan films, the region where the tape had been applied and the higher spin-coated chitosan layer are clearly distinguishable. The chitosan film thickens was measured in about 10 locations on the wafer. The dried film gave thicknesses of 87 nm for the 1.0% chitosan, 116 nm for the 1.5% chitosan and 137 nm for the 2.0% chitosan solution. Measurements were then also taken of wet films, three glass substrates were measured for each chitosan concentrations and height was determined in three locations. The results of these wet film measurements are plotted in fig.3.9. As expected, the wet films are thicker due to swelling and uptake of water and found to follow the same trend of increasing thickness from 505 nm for the 1.0% chitosan to 1291 nm for the 2.0% chitosan.

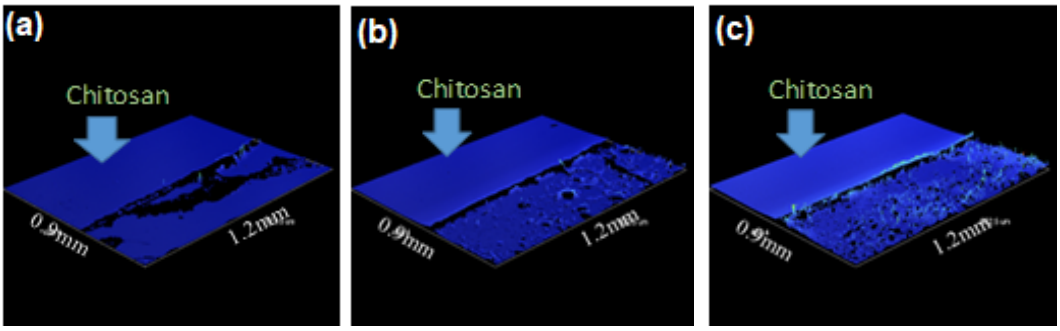

Figure 3.8: WLI images of the dry substrate surfaces clearly showing the two regions, namely the spin coated chitosan layer and the region where the tape had been applied. (a) Film from the 1.0% chitosan solution, (b) from the 1.5% chitosan solution and (c) from the 2.0 % chitosan solution.

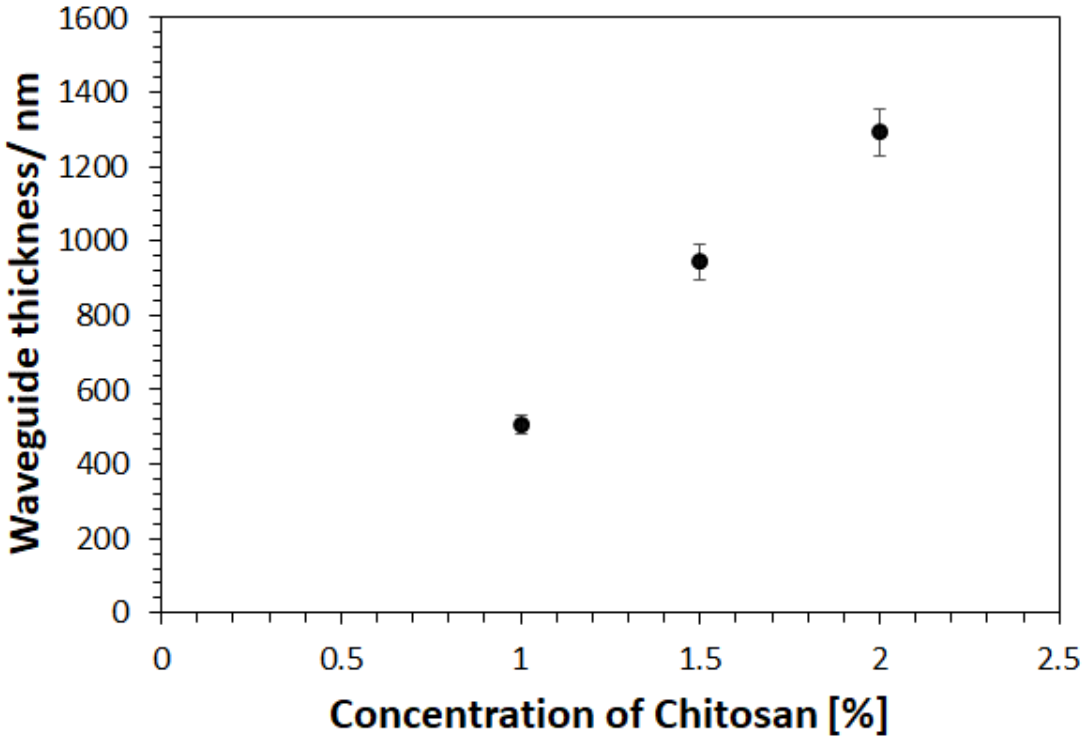

Figure 3.9: Thickness of a waveguide layer using different concentrations of chitosan (1.0%, 1.5% and 2.0%) spin coated on glass slides at 3000 rpm as measured by WLI (n=3).

3.2.3 Calculation of number of moles

The number of moles of available amino groups can be determined by equation 2.2 from the concentration (c) of RB4 in the film and from the volume (V) of probed film, which is the product of the thickness of the film (l) and the area (A_{il}) of incident light for the absorbance measurements. The area (A_{il}) was estimated at about 1.2 x 10^{-5} m^2 by measurement the laser spot size on a piece of paper held into the light path. In table 3.1, the number of moles using RB4 concentrations obtained through the UV/vis spectrophotometer are listed. They range from 18 to 183 femtomoles. As the RB4 concentration values obtained from the custom-built optical setup were higher, the number of moles of amino groups is also lower, as shown in table 3.2, values range from 36 to 456 fmol. These data can only be taken as a fairly rough estimate. From this data it is nonetheless possible to extrapolate to the total number of amino groups available in the flow channel (5 mm wide and 8 mm long) to guide choice of concentrations for the bioassays described in chapter 2. By comparison data for each setup a slightly higher concentration of Reactive blue 4 dye is shown at custom-built setup with the same chitosan chip with different concentrations 1, 1.5, and 2% of chitosan film respectively. That's due to when increasing the concentration of chitosan will increase the number of

moles of amines groups into the volume of the waveguide layer and lead to bounding more amount of the reactive blue 4 dye into the waveguide film.

Table 3-1: Summary of thickness and RB4 concentration from chitosan waveguide layers

Chitosan concentration	Chitosan film thickness / nm	Probed volume of chitosan / m^3	concentration (c) of RB4 in waveguide film (conv. UV/vis) /µM	number of moles of amino groups (n) / fmol
1.0%	505 ± 18	3.576×10^{-12}	5 µM	18
1.5%	943 ± 21	6.67×10^{-12}	10 µM	67
2.0%	1291 ± 19	9.13×10^{-12}	20 µM	183

Table 3-2: Summary of thickness and RB4 concentration from chitosan waveguide layers

Chitosan concentration	Chitosan film thickness / nm	Probed volume of chitosan / m^3	concentration (c) of RB4 in waveguide film (custom-built setup) / µM	number of moles of amino groups (n) / fmol
1.0%	505 ± 18	3.576×10^{-12}	10 µM	36
1.5%	943 ± 21	6.67×10^{-12}	30 µM	200
2.0%	1291 ± 19	9.13×10^{-12}	50 µM	456

3.3 Refractive index sensitivity of the chitosan waveguide

In order to estimate the sensitivity of the chitosan waveguide layer to changes in refractive index, different concentrations of glycerol in water were prepared ranging from 0.1% (v/v) to 10% as described in the experimental chapter, section 2.5. Glycerol was chosen because it is relatively cheap and should not adsorb physically to the chitosan layer. The refractive index for these solutions as measured on the refractometer is shown in fig.3.10. As can be seen from the figure, at concentrations of 0.1%, 0.5% and 1.0%, the refractive index change is not detectable on the refractometer. At higher concentrations, there is an increase in refractive index with increasing glycerol concentration. At 650 nm, pure glycerol has a reported refractive index of RI = 1.47 [131] water has a refractive index of

RI= 1.332, therefore the observed RI range from 1.333 to 1.348 lies within the expected range.

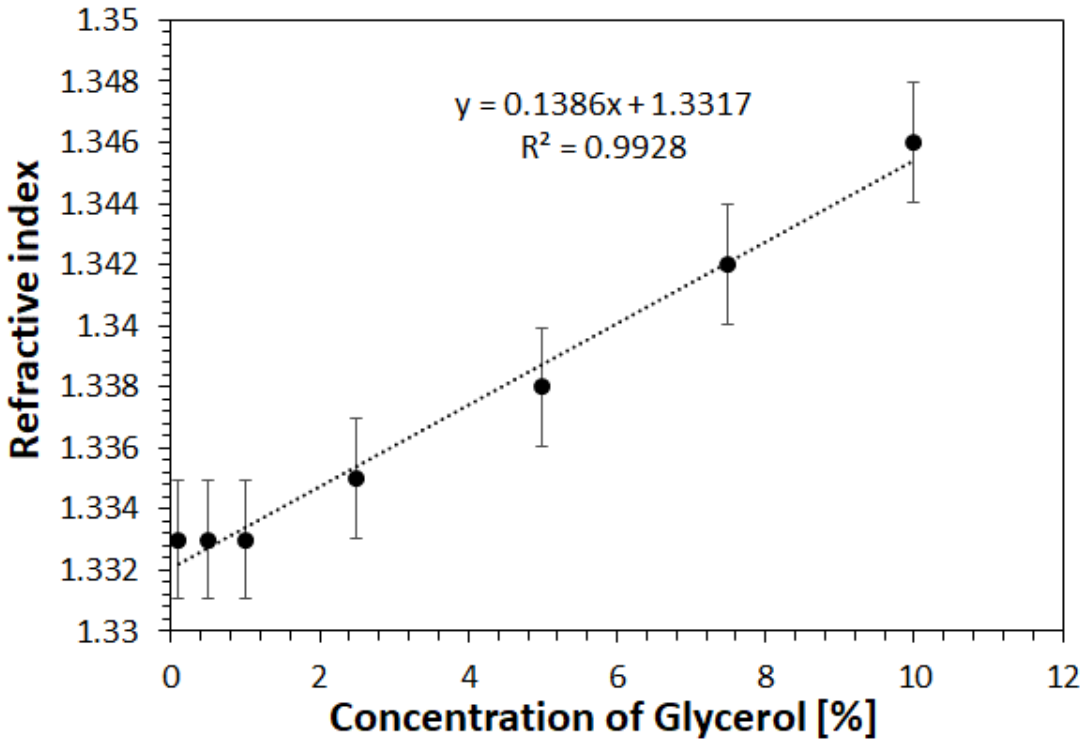

Figure 3.10: Plot of refractive index using different concentrations of 10 % (v: v %) glycerol solution (0.1%, 0.5%, 1%, 2.5%, 5%, 7.5% and 10%) prepared in de-ionised water.

For chitosan film preparation, a 2% of chitosan solution was spin coated onto the glass substrates as before. As it is the RB4 dye that absorbs light and creates the dip in reflectivity, the refractive index study was carried out by staining the chitosan film with 10 µM solution for a range of incubation times, namely, 10 min, 30 min, 60 min and 130 min. The aim was to investigate how the sensitivity to changes in refractive index may increase with increasing amounts of dye molecules immobilised in the chitosan film.

The chitosan films were interfaced to a flow cell and mounted onto the waveguide setup featuring a red LED as light source and CMOS camera for detection, as described in section 2.2.5. The angle of incident light and the angle of the detector with respect to the normal of the base was set near the resonance angle at 65°. The dip in reflectivity is presented as a dark line on the image. This dark line shifts when the refractive index of the waveguide layer changes, which is monitored through a custom-written software as described in section 2.4. In fig.3.11, examples of CMOS images of the dip are shown for film stained with RB4 for the different incubation times. These images were taken before any glycerol solutions were pumped through the device. It can be seen that as the amount

of dye molecules immobilised in the waveguide layer increase, more light is absorbed in the chitosan layer that's due to the amount of the dye molecules. It's clear that the dip becomes broader by increasing the amount of the dye into the chitosan film.

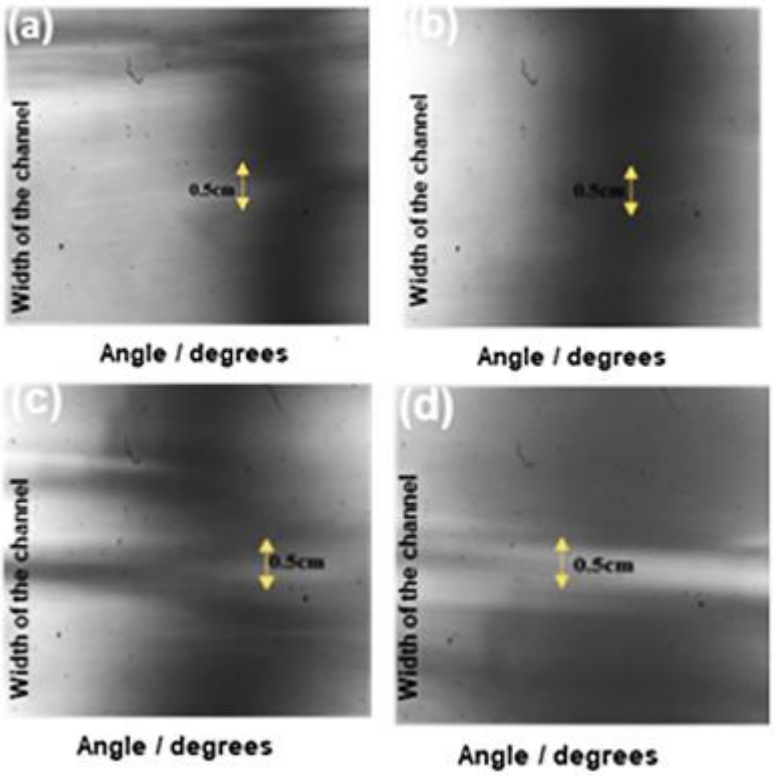

Figure 3.11: Pictures captured by the CMOS camera of glass slides incubated with RB4 dye (1 mM) for (a) 10 min, (b) 30 min, (c) 60 min and (d) 130 min.

Following staining and washing with water, glycerol solutions with increasing concentration were pumped consecutively through the flow cell as described in section 2.5. The shift in dip as a function of time is plotted in fig.3.12. As can be seen, the higher concentrations of glycerol featuring higher refractive indices caused an increasing shift in dip, as expected. Fig.3.13, shows the same plot for a waveguide layer incubated with the dye for 30 min and similarly, the plots for a dye incubation time of 60 min and 130 min are shown in figs.3.14 and 3.15, respectively. However, the data for the 130 min incubation time has been discarded, the high number of dye molecules in the waveguide meant that the light was not confined and the dip in reflectivity could not be visualised (see fig.3.11d).

As can already be appreciated from these plots, the shift of the resonance angle as the different glycerol solutions are pumped over the waveguide layer is lower for the waveguides with longer dye incubation times. This is further demonstrated by plotting refractive index of the glycerol solutions against the obtained shift in dip for the 10 min, 30 min and 60 min incubation times (fig.3.16). For all three incubation times, it was observed that the larger the refractive index, the larger the shift in dip. The 10 min incubation time showed the steepest slope, 99.8, compared to 81.4 obtained for 30 min incubation time and 75.4 for 60 min. This is because more amount of the dye into the waveguide film will result in more losing of light due to the high absorbance.

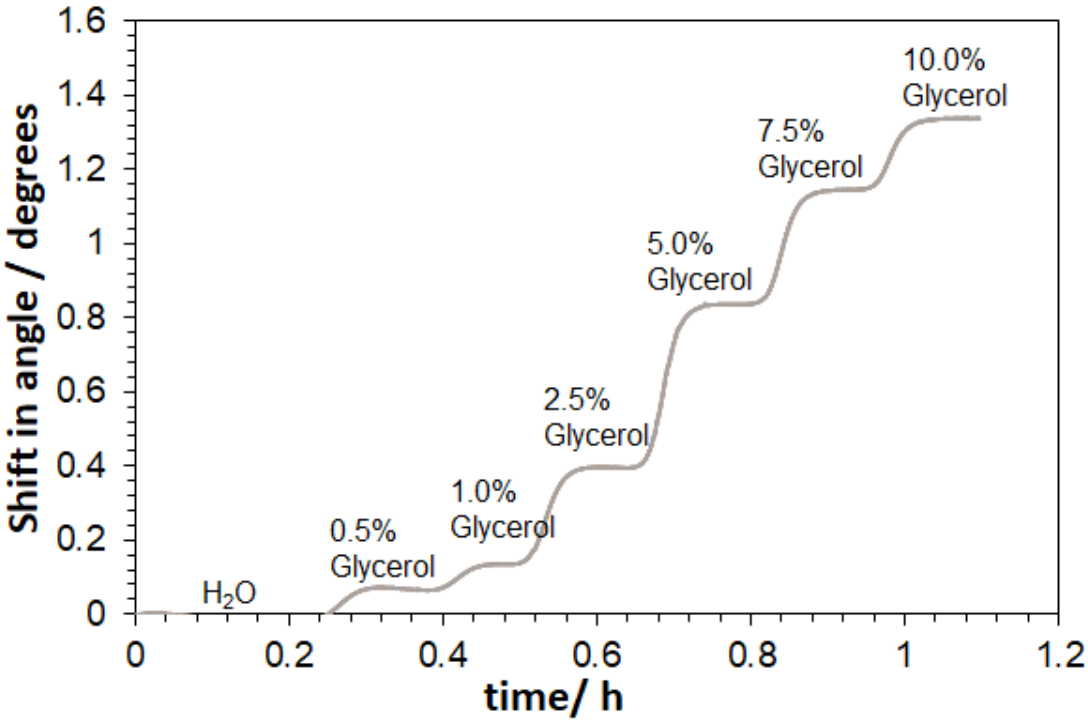

Figure 3.12: Change in the reflectivity dip angle as a function of time for a waveguide layer made from 2% chitosan incubated in RB4 dye (1 mM) for 10 min. Glycerol solutions of 0.5%, 1%, 2.5%, 5%, 7.5% and 10% were pumped consecutively over the waveguide (n=3 mean three boxes).

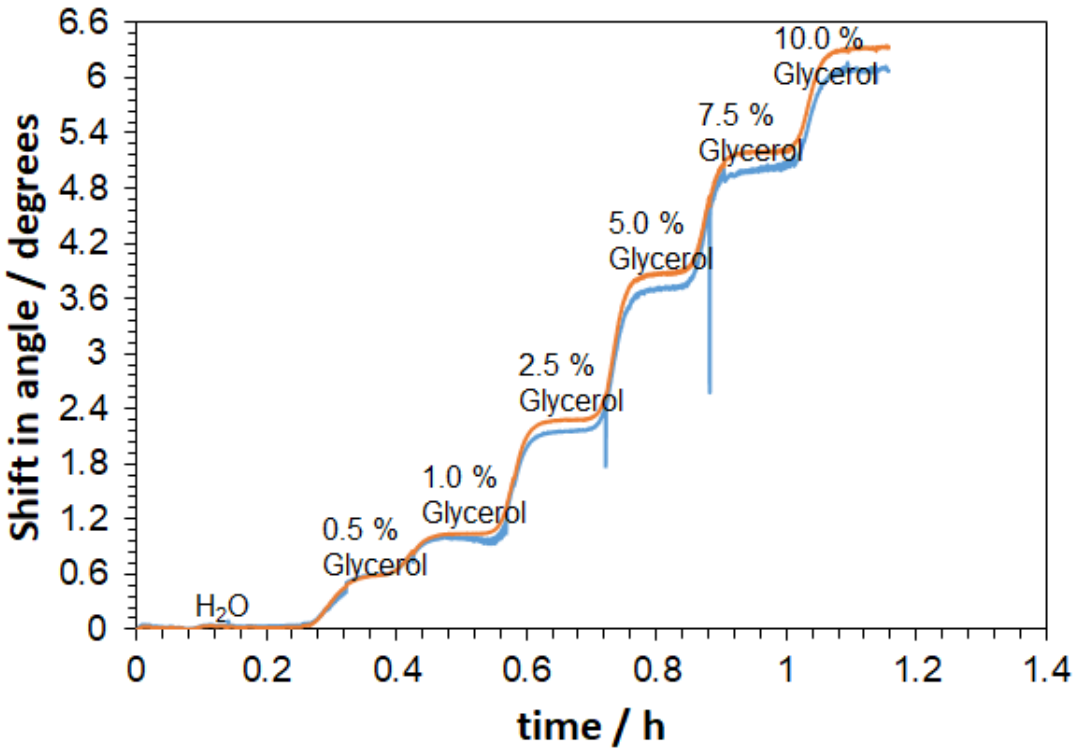

Figure 3.13: Change in the reflectivity dip angle as a function of time for a waveguide layer made from 2% chitosan incubated in RB4 dye (1 mM) for 30 min. Glycerol solutions of 0.5%, 1%, 2.5%, 5%, 7.5% and 10% were pumped consecutively over the waveguide (n = 3 mean three boxes).

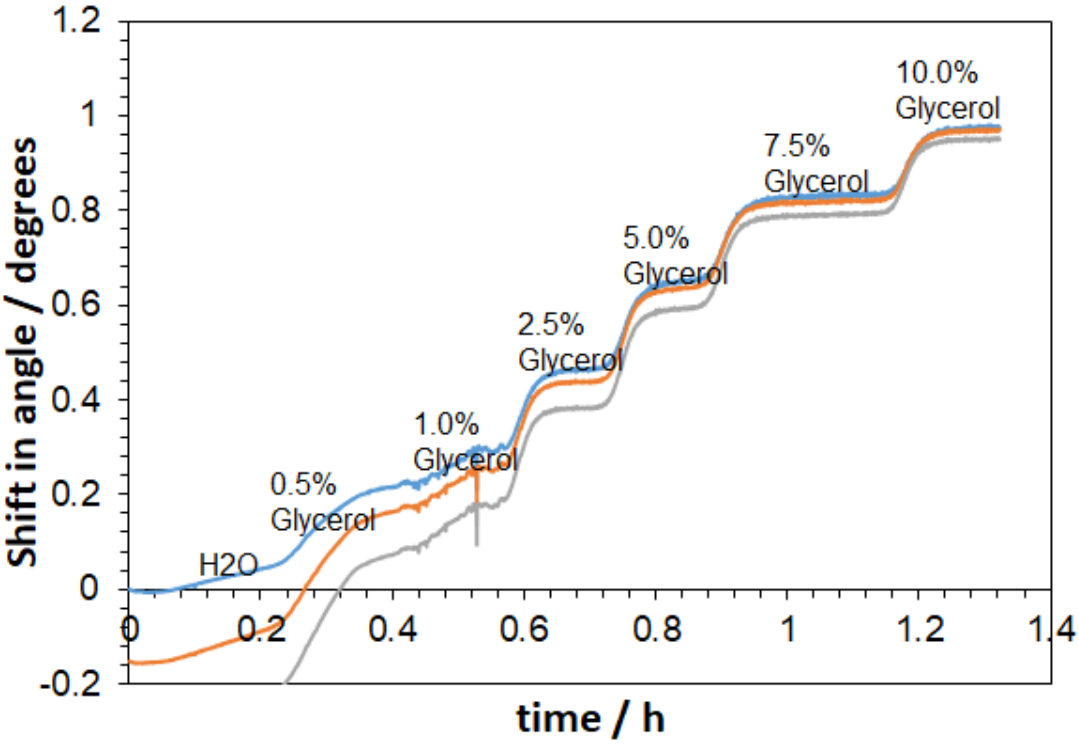

Figure 3.14:Change in the reflectivity dip angle as a function of time for a waveguide layer made from 2% chitosan incubated in RB4 dye (1 mM) for 60 min. Glycerol solutions of 0.5%, 1%, 2.5%, 5%, 7.5% and 10% were pumped consecutively over the waveguide (n = 3).

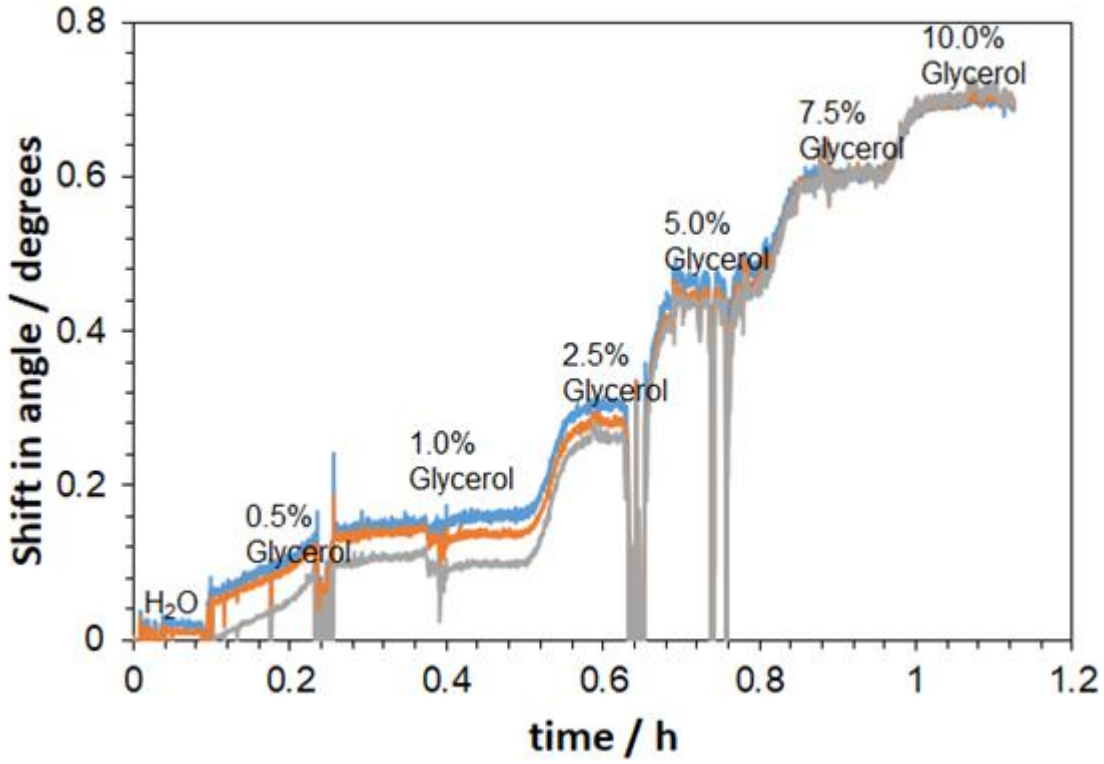

Figure 3.15: Change in the reflectivity dip angle as a function of time for a waveguide layer made from 2% chitosan incubated in RB4 dye (1 mM) for 130 min. Glycerol solutions of 0.5%, 1%, 2.5%, 5%, 7.5% and 10% were pumped consecutively over the waveguide (n = 3).

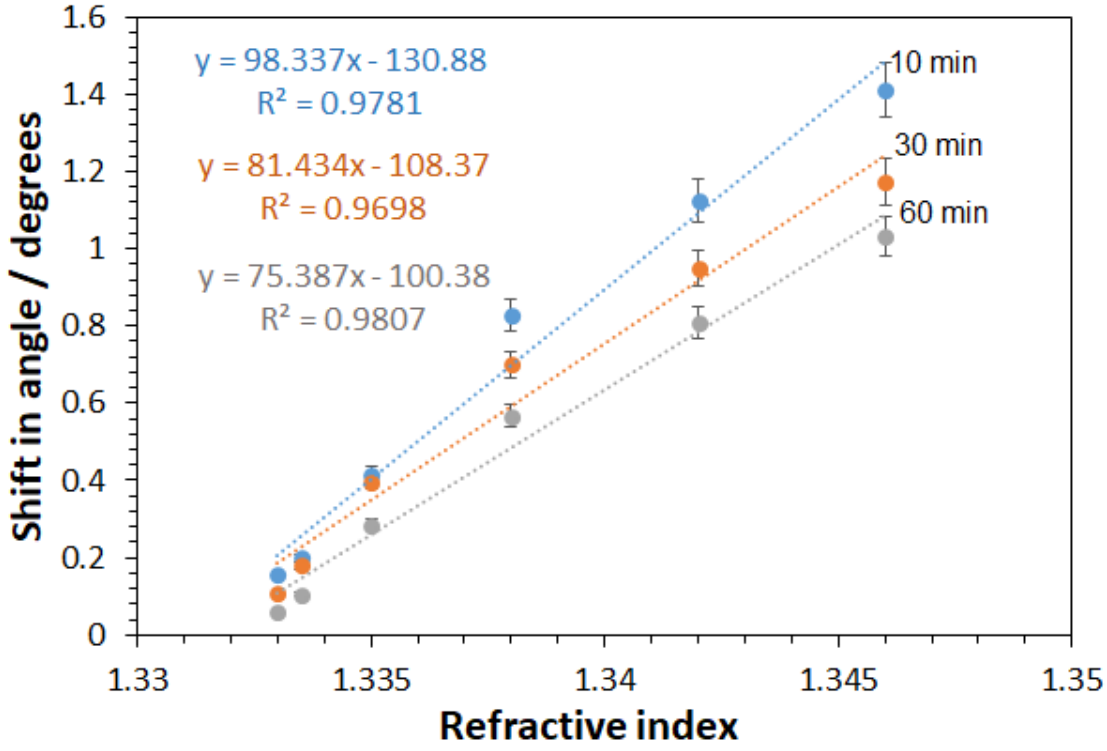

Figure 3.16: Sensitivity for the waveguide layers to changes in refractive index for 2 % (w/v %) chitosan films incubated with 1 mM RB4 dye for different times (10, 30 and 60 min).

As a result of these measurements, the incubation time of 10 min for RB4 dye was chosen for further investigation, namely to study the effect of glycerol in different buffers. Bioassays and immobilisation of biorecognition species are generally performed with buffers at pH 7.4. Two different buffer systems were compared, namely PBS (phosphate buffered saline) and HEPES (4-(2-hydroxyethyl)-1-piperazineethanesulfonic acid) buffer.

The measured refractive indices of glycerol solutions in water, PBS and HEPES buffer are plotted in fig.3.17. Each solution of glycerol has a specific value of refractive index that leads to shift in the dip position by changing the solutions. The degree of shifting is depended on the value of refractive index and on the amount of the dye that presents into the chitosan film.

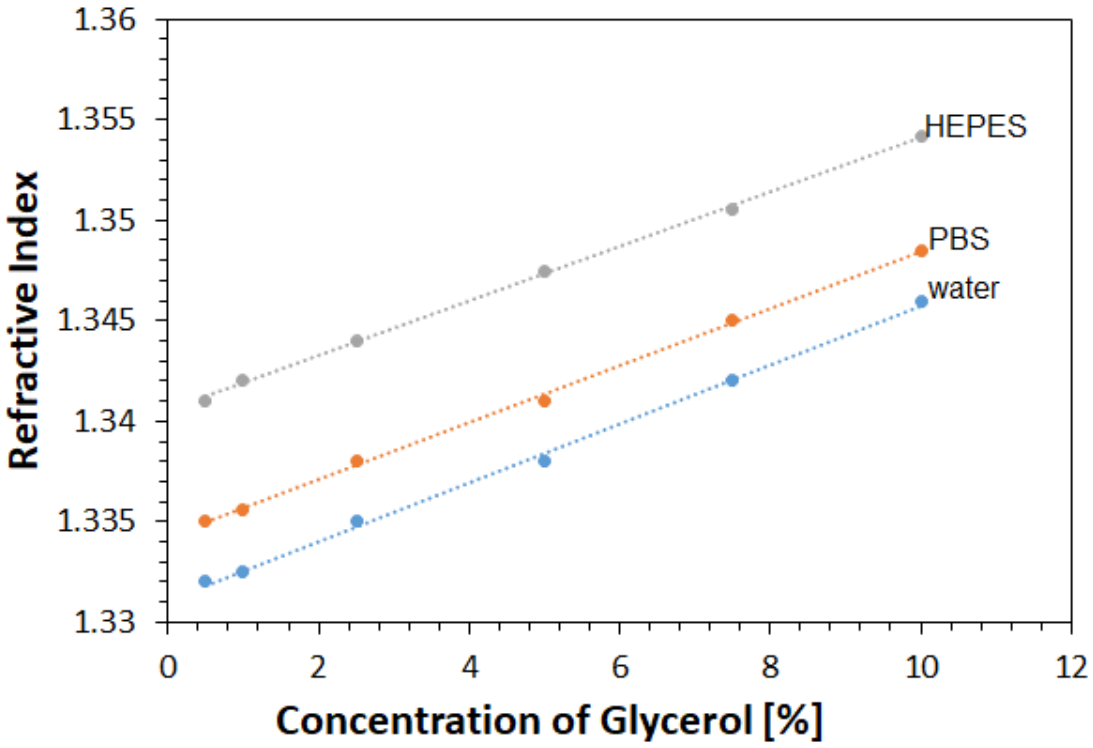

Figure 3.17: Refractive index for glycerol solutions prepared in de-ionised water, PBS and HEPES buffer.

Chitosan layers (2%) were prepared as before and stained with RB4 dye for 10 min. The plots illustrating the shift in dip as the different glycerol solutions are pumped over the waveguide are shown in fig.3.18 for water, fig.3.19 for PBS buffer in fig.3.20 for HEPES buffer. All these experiments were performed on the same chitosan-coated glass substrate. Finally, fig.3.21, Summarises the extent of shift in dip as a function of refractive index for the three types of glycerol solutions. As can be seen, water gives the largest sensitivity, PBS gives the lowest sensitivity.

Buffers with multivalent anions have been reported to crosslink chitosan, reducing the pore size and hence the sensitivity.

Discuss what this mean, the positive ammonium groups of the protonated chitosan were directly bound to negatively charged sulphate groups of PBS. This is indicative of an interaction between the amine groups on the chitosan and the phosphate ions in PBS solution. This suggested that a crosslink and/or crosslink network between the two might be set up [132].

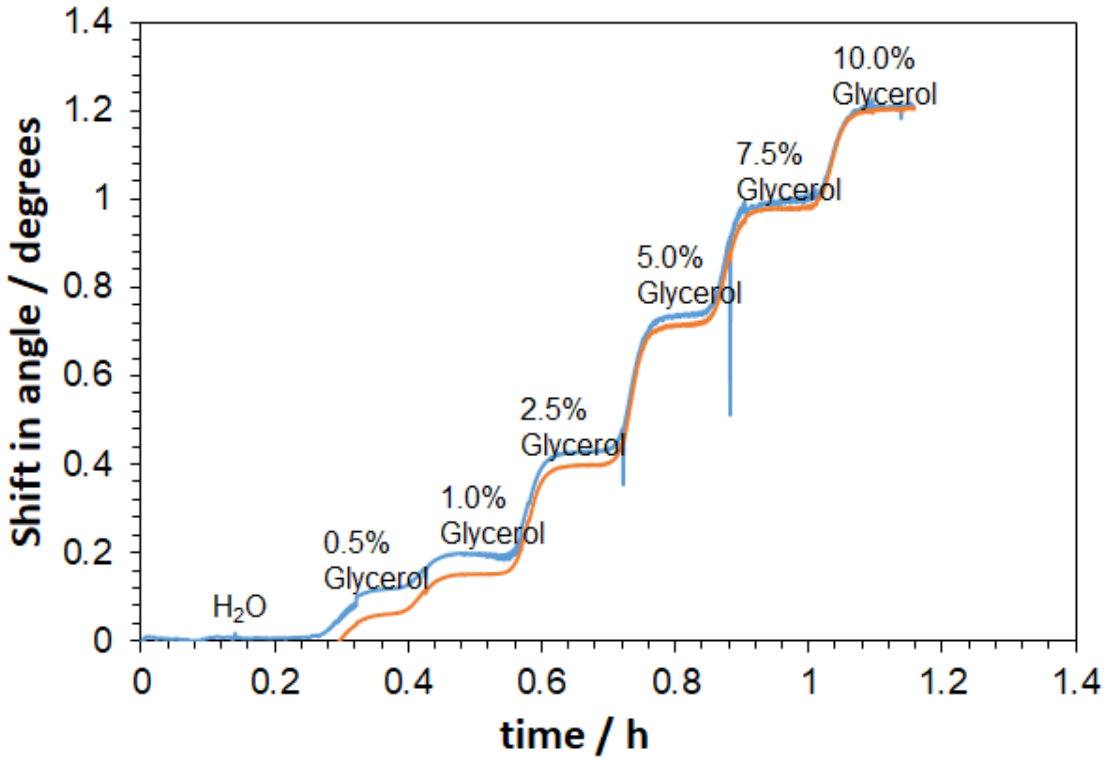

Figure 3.18: Dip shifting under different concentrations of glycerol (v:v %) solutions prepared in de-ionised water using a two channel flow cell, the surface initially incubated with dye for 30 min.

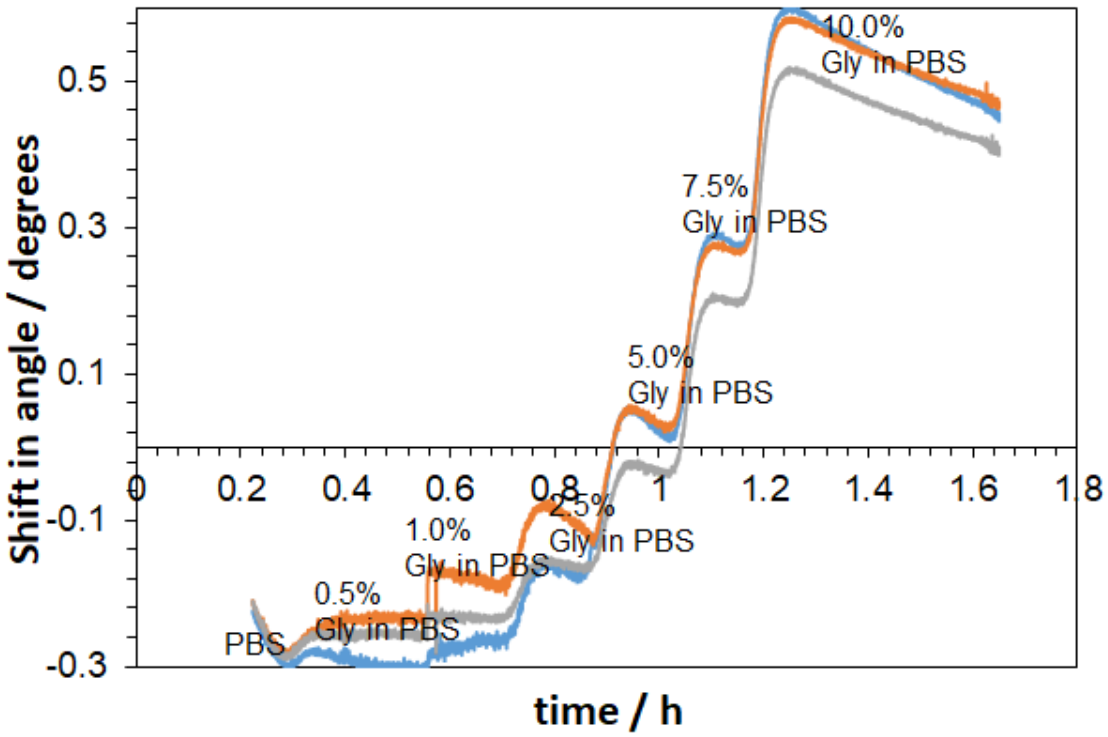

Figure 3.19: Dip shifting under different concentrations of glycerol solutions (v/v %) prepared in a PBS buffer at pH 7.4, the surface initially incubated with the dye for 30 min.

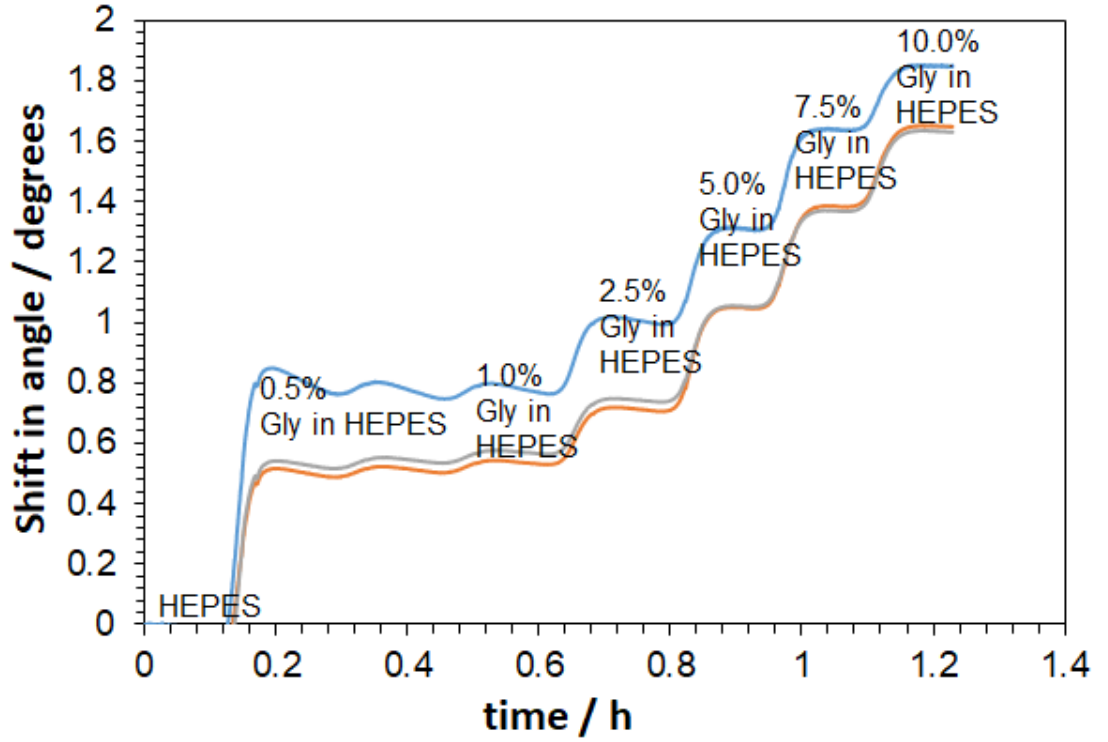

Figure 3.20: Dip shifting under different concentration of glycerol solutions (v/v %) prepared in HEPES buffer at pH 7.4, the surface initially incubated with the reactive blue 4 dye for 30 min.

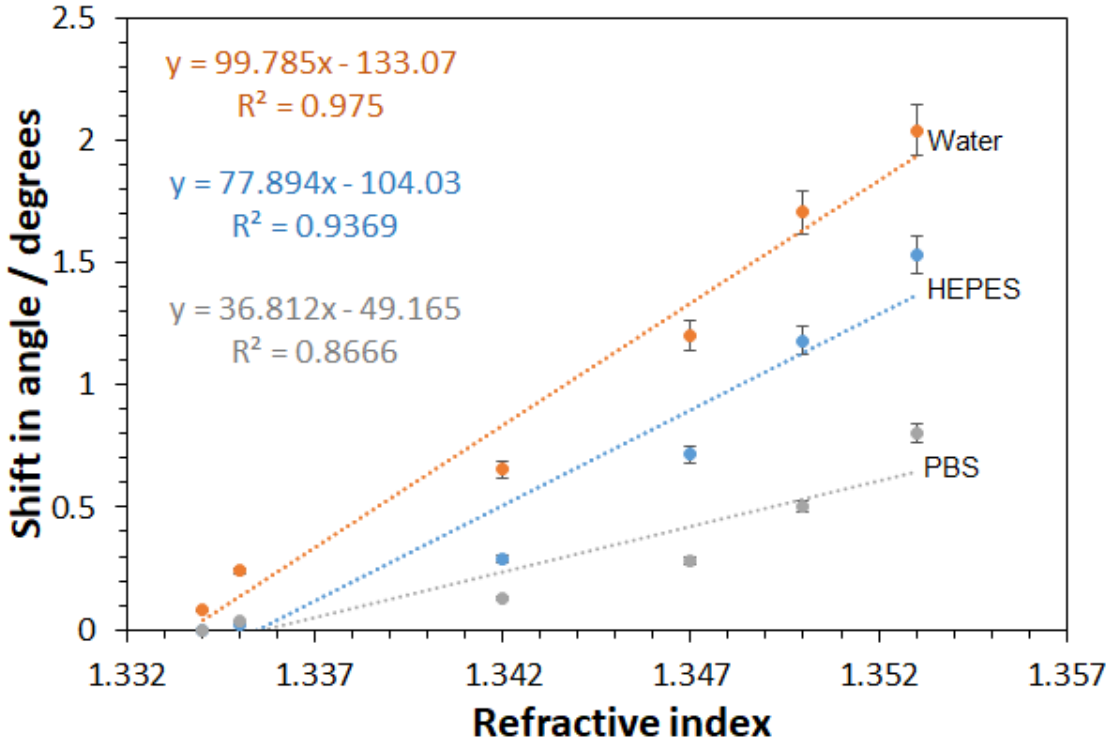

Figure 3.21: Shift in angle on chitosan waveguide layer against refractive index value. Three series of glycerol solutions were prepared in de-ionised water, PBS and HEPES, the surface initially incubated for 30 min.

3.4 Investigation of the Porosity of the Waveguide Film

3.4.1 Porosity Study with Glycerol, BSA and PEG/PEO using Optical Waveguide System

The porosity of the waveguide layer is important: it determines the available surface area for the binding of antibodies as biorecognition elements; the pore size needs to be sufficiently large to allow the antibodies as well as the relevant sample components to penetrate into the film and thus give a fast response time; the three-dimensional network structure of the film should also be fairly stable to avoid excessive swelling or components of the film layer being carried away with the flow.

In an initial set of experiments, solutions of glycerol (92 Da) and BSA (66 kDa) in PBS buffer were investigated. They were prepared as outlined in section 2.6. BSA and glycerol solutions were prepared in PBS such that they have the same refractive index value.

The curve showing the shift in dip over the progress time of the experiment is shown in fig.3.22. Initially PBS was flushed for 10 min, this was followed by the glycerol solutions from low to high concentration for 10 min each. Then the device was flushed with PBS

and the BSA solutions with increasing concentrations were pumped through consecutively for 10 min each with buffer washes in-between. Comparing the two, it can be seen that glycerol shifts the resonance angle by about 1.4°, whereas BSA only shifts the resonance angle by 0.4°. In both cases, the resonance angle returned to its original position when flushing with PBS. The lower shift in dip for the BSA with its high molecular weight is because it cannot penetrate the pores as effectively as the low MW glycerol. It can be concluded that none of BSA concentrations can be defused inside the 2% of chitosan waveguide due to the highly small pore size.

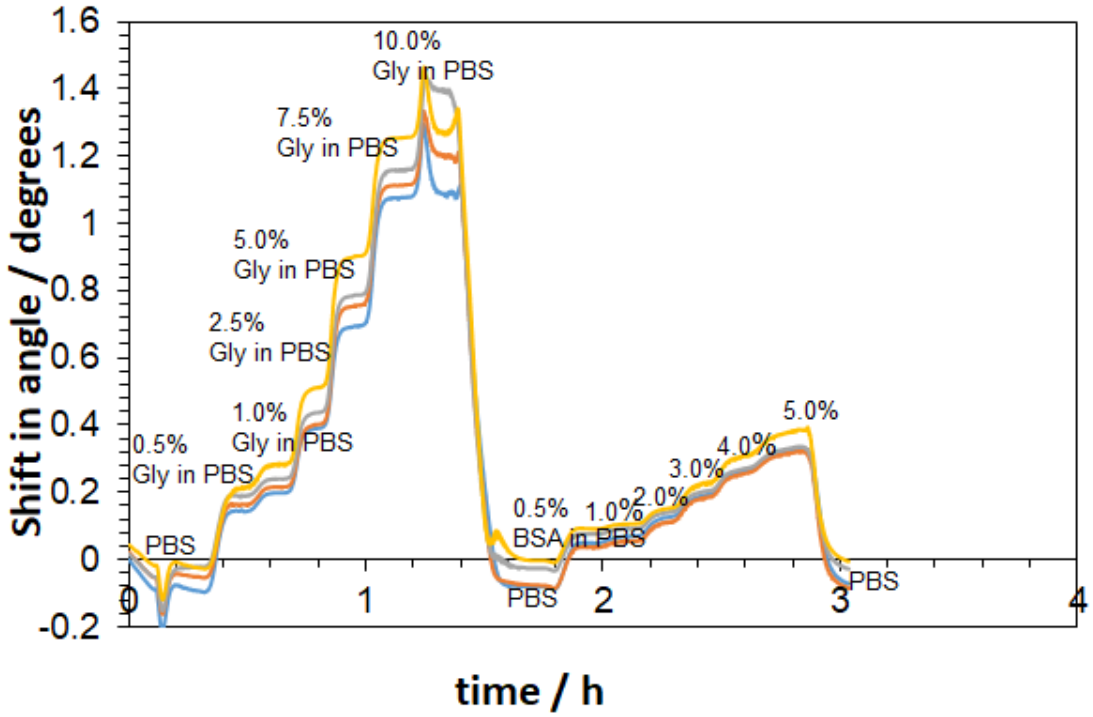

Figure 3.22: Change in the reflectivity dip angle against time using two different compounds (glycerol and BSA) featuring different molecular weights but the same refractive index. The chitosan waveguide was prepared by 2% chitosan solution and stained with 100 µM RB4 dye for 10 min.

Next, the PEG and PEO polymer solutions of higher molecular weight were investigated. 40 kDa PEG and PEO of 100 kDa, 200 kDa and 400 kDa were employed. The solutions were prepared and the experiment run as described in section 2.6.1. Fig.3.23, shows the shift in dip as the various 1% polymer solutions were pumped through the flow cell consecutively. As can be seen, the resonance angle increases with glycerol as observed before and then returns to below its original position upon PBS flushing. The polymer solutions on the other hand resulted in a reduction in resonance angle, and thus in a negative shift in dip. The PBS flushing at the end did not restore the dip to its original

position, and the shift in angle degree it can be seen with different concentrations of BSA. This can be related to the pore size is highly small size into the sensing region of chitosan waveguide as not like the glycerol. The molecular weight of BSA is 66 kDa which is totally not comparable to glycerol solution with molecular weight of 92.09 $g.moL^{-1}$.

Used flow cell 2, only one channel, not compensated for shift in temperature, that's due to the speed of light in a substance is slower than in a vacuum since the light is being absorbed and reemitted by the sample into the waveguide layer. Since the density of a liquid (sample) usually decreases with temperature, it is not surprising that the speed of light in a liquid will normally increase as the temperature increases. Thus, the index of refraction for the waveguide layer will normally decreases as the temperature increases for a liquid into the waveguide layer, might explain overall downward trend. For many organic liquids the index of refraction decreases by approximately 0.0005 for every 1 °C increase in temperature [133].

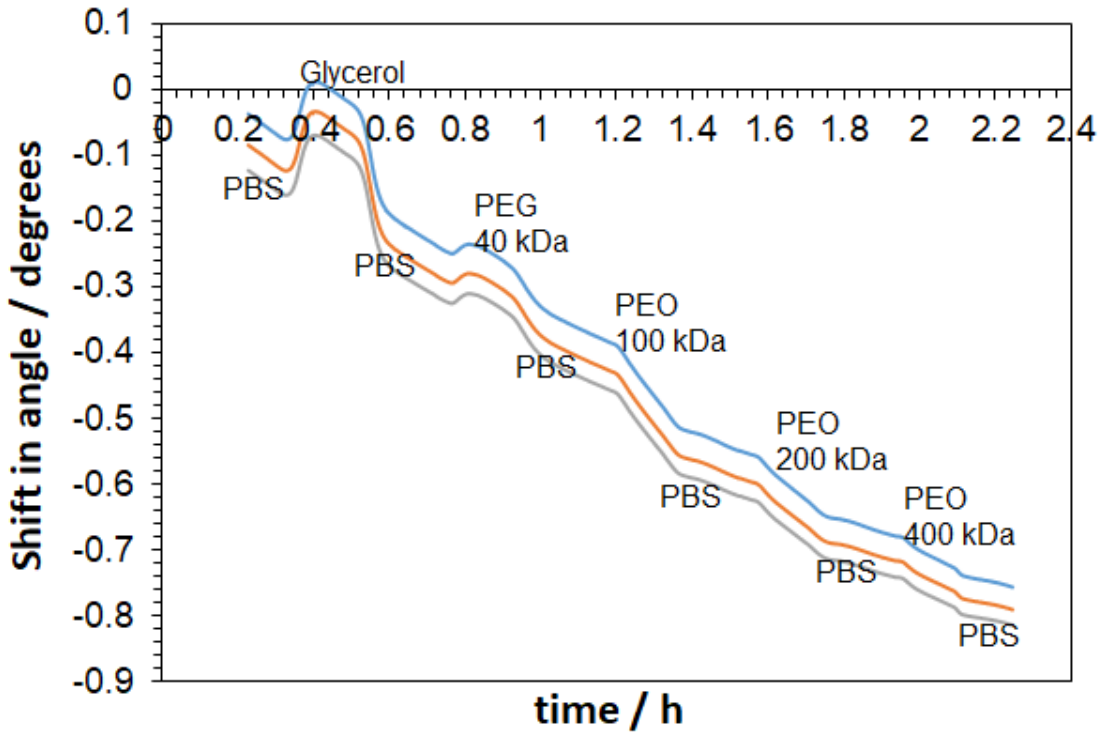

Figure 3.23: Dip shifting for different molecular weights of polymers prepared in the same buffer PBS (pH 7.4) using another solution (glycerol prepared in PBS), the glass slide initially incubated with the reactive blue 4 dye (100 µM) for 10 min. All these polymers and the glycerol solution have the same refractive index (1.3355); the refractive index for PBS was 1.3345.

3.4.2 By Fluorimeter

The aim of this experiment was to investigate the porosity of the waveguide film by studying the diffusion of fluorescently labelled BSA into the chitosan hydrogel layer using fluorescence spectrometry. As described in the experimental chapter (section 2.6.2), chitosan hydrogel was poured into cuvettes and left to dry. Solutions of FITC-labelled BSA and of FITC were added to different cuvettes and the fluorescence intensity of the gels in the cuvettes was measured. The gels were then washed with PBS. Photographs from the experiments are shown in fig.3.24. The obtained fluorescence intensities are plotted in fig.3.25.

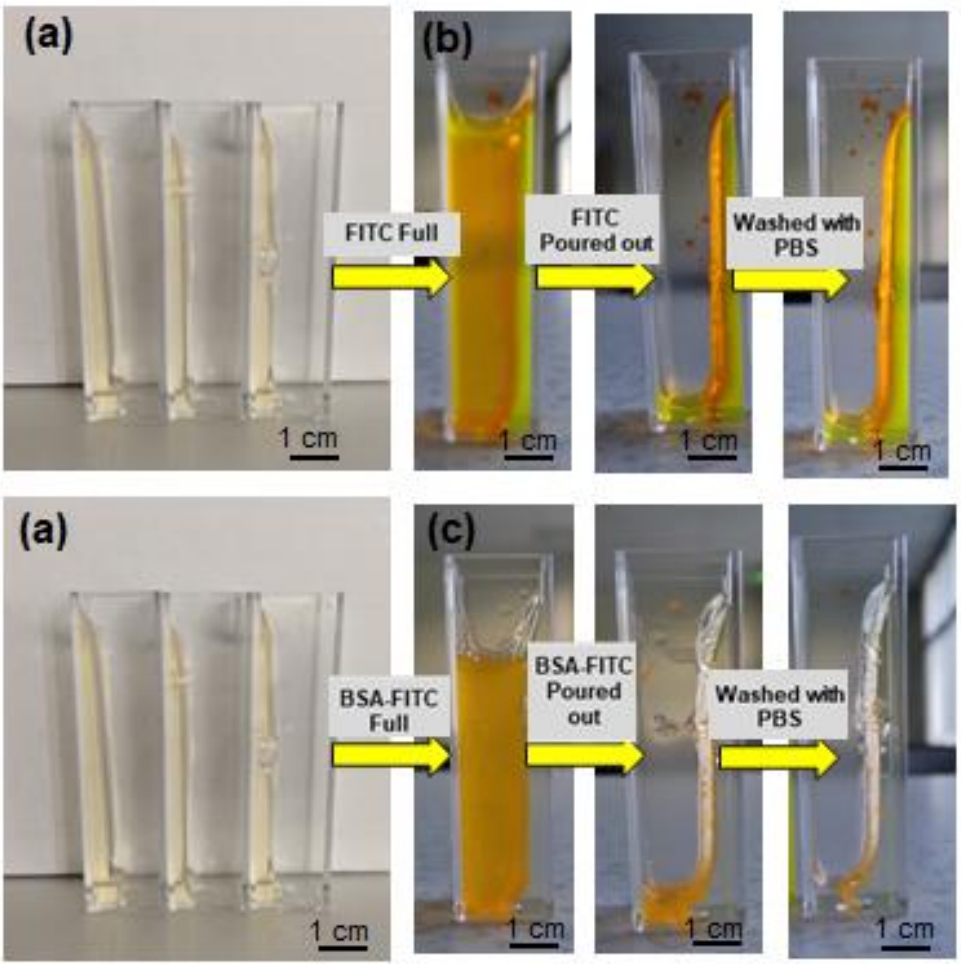

Figure 3.24: Photographs of (a) cuvettes with 1 mL of 2% of chitosan gel following drying at room temperature for 2 h. (b) FITC solution in cuvette and following washing and (c) BSA-FITC.

It can have be seen that the fluorescence intensity of the FITC stained chitosan gels (fig. 3.24b) is higher than the fluorescence intensity of the BSA-FITC stained chitosan gels (fig.3.24c). From these experiments it can be concluded that the FITC can diffuse freely into the chitosan gel and remained absorbed even following washing. On the other hand, the BSA-FITC appears to be adsorbed physically on the outside of the chitosan gel and just a small amount diffuses inside gel. This is in agreement with measurements on the DDLW setup described in the previous section. This would indicate that the pore size of the chitosan is small in comparison to the size of the relatively high molecular weight BSA molecules. Therefore, the porosity of the chitosan film would need to be increased in order to conduct meaningful binding assay on the waveguide.

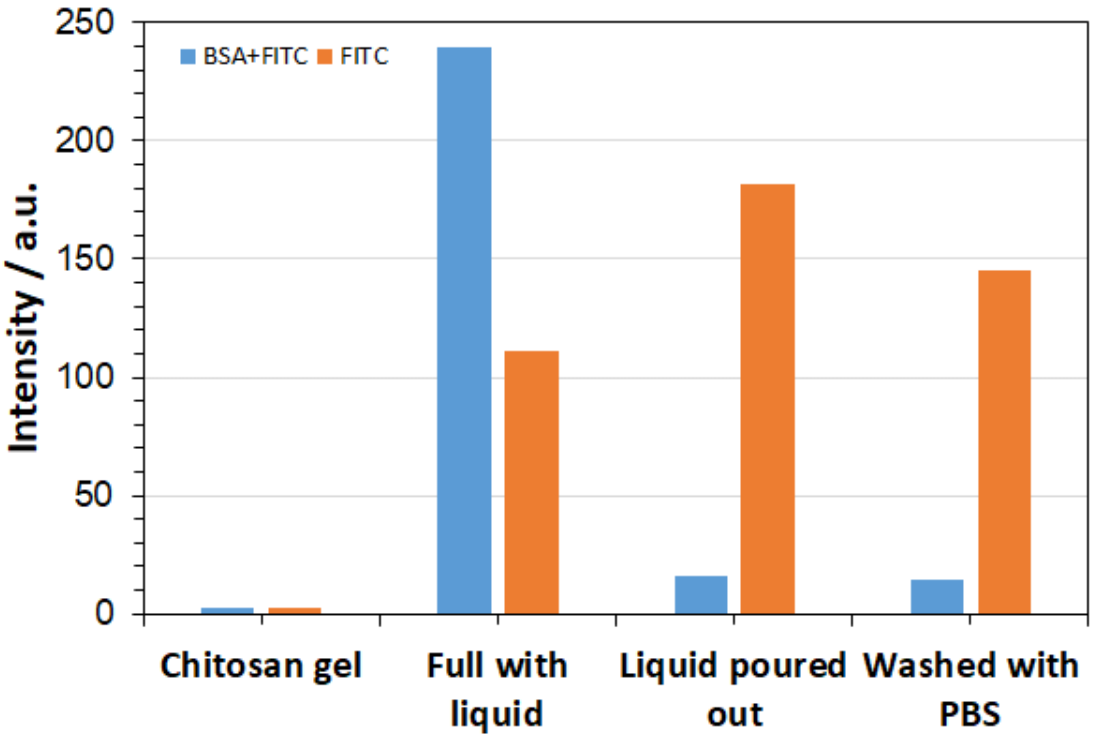

Figure 3.25: Obtained fluorescence intensity for chitosan films stained with FITC and FITC-labelled BSA.

3.5 Conclusion – waveguide characterisation and porosity

In this chapter, the conditions for spin coating the chitosan film on the glass substrate were optimised, a 2% of chitosan solution with glutaraldehyde, spin coated at 3,000 rpm for 30 s gave best results to confine the light for the waveguide effect.

To characterise the waveguide layer, the number of moles of amino groups that may ultimately be available for antibody binding in the entire volume of the chitosan was estimated with by saturating the film with blue RB4 dye and taking absorbance measurements. It was found that the film 2% of chitosan film has the number of availability of amino groups higher than 1% and 1.5% of chitosan film.

Additional experiments was carried out to investigate the sensitivity of the waveguide layer to changes in refractive index. It was found that incubation of the chitosan films with RB4 dye for 10 min resulted in a sharp dip in reflectivity and the highest sensitivity compared to longer incubation times. The sensitivity when using deionised water as solvent was found to be >90 degrees shift per 1 RIU (refractive index unit). This means the sensitivity of detection method that is based on the change of refractive index into the waveguide layer is highly depended on the amount of the dye and the porosity of the waveguide film. The sensitivity of the chitosan waveguide to the value of the refractive index when using buffers relevant to biological assays was found to be lower, for HEPES <90 degrees per RIU and for PBS also <90 degrees per RIU.

In addition the porosity of the waveguide film was investigated by studying the extend of diffusion of BSA (66 kDa) and PEG/PEO polymers (10 – 400 kDa) into the chitosan waveguide using the optical waveguide setup and fluorescence spectrophotometry. These experiments let to the conclusion that the pore size of the chitosan film is too small to allow the biomolecules to enter the film and therefore, attempts needed to be made to increase the pore size, as described in the following chapter.

The pore size of the waveguide film was investigated by using BSA and different molecular weights of PEG and PEO solutions.

Up on monitoring the shifting in the dip position, it can be concluded that none of the solutions can be diffused into the 2% of chitosan film due to the highly small pore size.

CHAPTER 4

Optimising the Porosity of the Leaky Waveguide Layer

The porosity of the waveguide film is of key importance for the detection of antibody-antigen binding in the film. The pore sizes need to be sufficiently large to allow penetration of the biorecognition elements that are to be immobilised within the film as well as penetration of the sample components of interest so that they can bind to the biorecognition elements in the film. If the porosity is too high however the film is likely to swell and loose its consistency during an experimental run. Furthermore, pore sizes on the 100s nm scale will lead to light scattering thereby compromising the function of the optical waveguide. Initial experiments described in chapter 3 indicated that pore size of the spin-coated 2.0% chitosan film with added glutaraldehyde was too small, not allowing BSA (66 kDa) and PEG/PEO (10 kDa – 400 kDa) to enter. In this chapter, investigations are described that were aimed at increasing the pore size of the chitosan gel layer, namely using silica nanoparticles as porogens that are embedded and later dissolved. Another approach studied involved varying the amount of cross-linker and drying time of the spin-coated chitosan layers.

4.1 Silica nanoparticles as Porogens

4.1.1 Investigation of solubility of silica NPs in NaOH

Silica nanoparticles (NPs) were envisaged as porogens. The idea was to incorporate them during the waveguide film deposition and to then dissolve them with sodium hydroxide (NaOH) in order to obtain pores of the size of the silica particles. Initially, commercially available silica nanoparticles (100 nm) were studied. Silica particles were mixed with a range of NaOH solutions (5%, 10% and 15%) for reaction times between 2 h and 17 h has laid out in section 2.7.1. The results are summarised in tables 4.1, 4.2 and 4.3. As can be seen, only for the highest concentrations of NaOH (7% and 10% in reaction vessel) and longest reaction time (17 h) were the silica particles found to dissolve.

Table 4-1: Solubility of silica NPs; 20 uL of a 1% silica particle suspension were mixed with different volumes (5, 10, 20, 30, 40 µL) of 5% NaOH for reaction times of 2, 4, 6 and 17 h.

Volume of 5% NaOH / µL	**Reaction time / h**			
	2 h	4 h	6 h	17 h
5	not dissolved	not dissolved	not dissolved	not dissolved
10	not dissolved	not dissolved	not dissolved	not dissolved
20	not dissolved	not dissolved	not dissolved	not dissolved
30	not dissolved	not dissolved	not dissolved	not dissolved
40	not dissolved	not dissolved	not dissolved	not dissolved

Table 4-2: Solubility of silica NPs; 20 uL of a 1% silica particle suspension were mixed with different volumes (5, 10, 20, 30, 40 µL) of 10% NaOH for reaction times of 2, 4, 6 and 17 h.

Volume of 10% NaOH / µL	Reaction time / h			
	2 h	4 h	6 h	17 h
5	not dissolved	not dissolved	not dissolved	not dissolved
10	not dissolved	not dissolved	not dissolved	not dissolved
20	not dissolved	not dissolved	not dissolved	not dissolved
30	not dissolved	not dissolved	not dissolved	not dissolved
40	not dissolved	not dissolved	not dissolved	dissolved

Table 4-3: Solubility of silica NPs; 20 uL of a 1% silica particle suspension were mixed with different volumes (5, 10, 20, 30, 40 µL) of 15% NaOH for reaction times of 2, 4, 6 and 17 h.

Volume of 15% NaOH / µL	Reaction time / h			
	2 h	4 h	6 h	17 h
5	not dissolved	not dissolved	not dissolved	not dissolved
10	not dissolved	not dissolved	not dissolved	not dissolved
20	not dissolved	not dissolved	not dissolved	not dissolved
30	not dissolved	not dissolved	not dissolved	not dissolved
40	not dissolved	not dissolved	not dissolved	dissolved

4.1.2 Incorporate of silica NPs into chitosan and dissolution

As a next step, the dissolution of the commercially available 100 nm silica particles in NaOH was investigated in the chitosan gel. Silica particle suspensions and chitosan solutions were mixed as described in section 2.7.1 and left to gel for 24 h. Then sodium hydroxide was added and the mixtures were left to incubate on the hotplate at 80 °C for time intervals ranging from 10 min to 100 min. Following this, the gel was incubated with BSA-FITC for 2 h and washed with PBS. Photographs of the gels following NaOH treatment and BSA-FITC staining are shown in fig.4.1. It was found that a strong and flexible chitosan gel was obtained that did not show any signs of shrinkage upon drying. Fluorescence measurements of the gels are plotted in fig.4.2. For these measurements it can be seen that the fluorescence intensity increased with increasing incubation time up to a saturation point (50 min) and then decreased. This indicates that the pores in the chitosan gel were completely filled with the BSA-FITC after 50 min of incubation time and therefore, this adsorption period is sufficient to reach adsorption equilibrium.

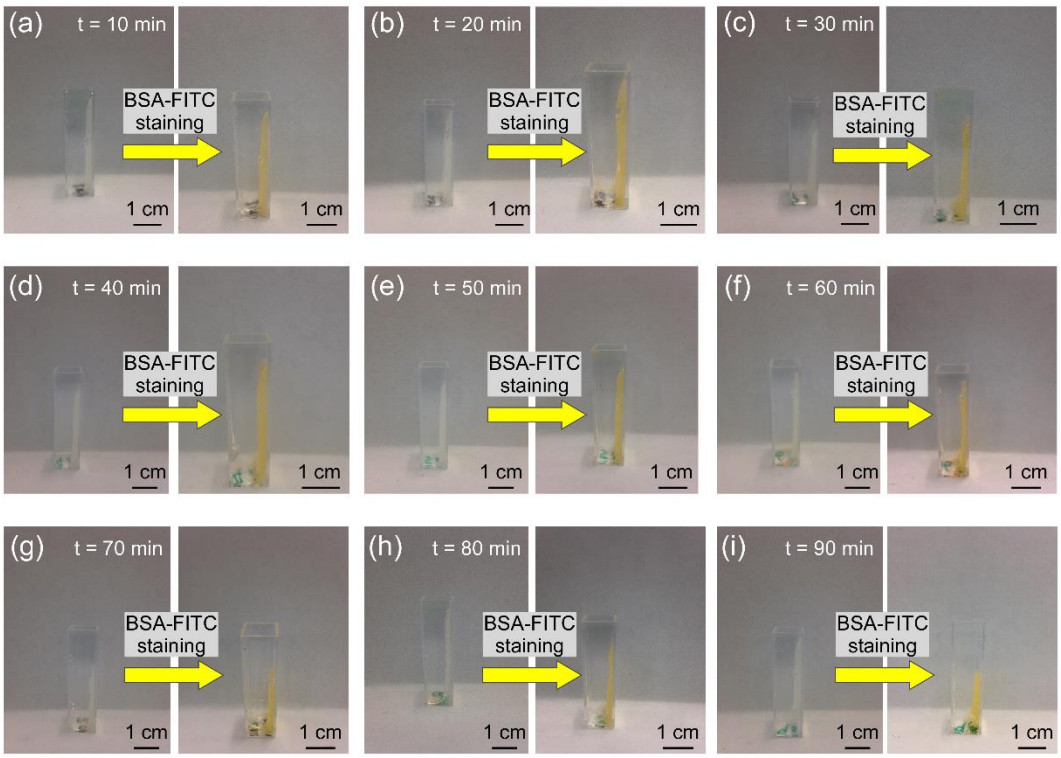

Figure 4.1: Chitosan gel with embedded silica nanoparticles prepared in cuvettes. The gels were incubated with NaOH for (a) 10 min, (b) 20 min, (c) 30 min, (d) 40 min, (e) 50 min, (f) 60 min, (g) 70 min, (h) 80 min and (i) 90 min. For each incubation time a photograph before and after staining with BSA-FITC was taken.

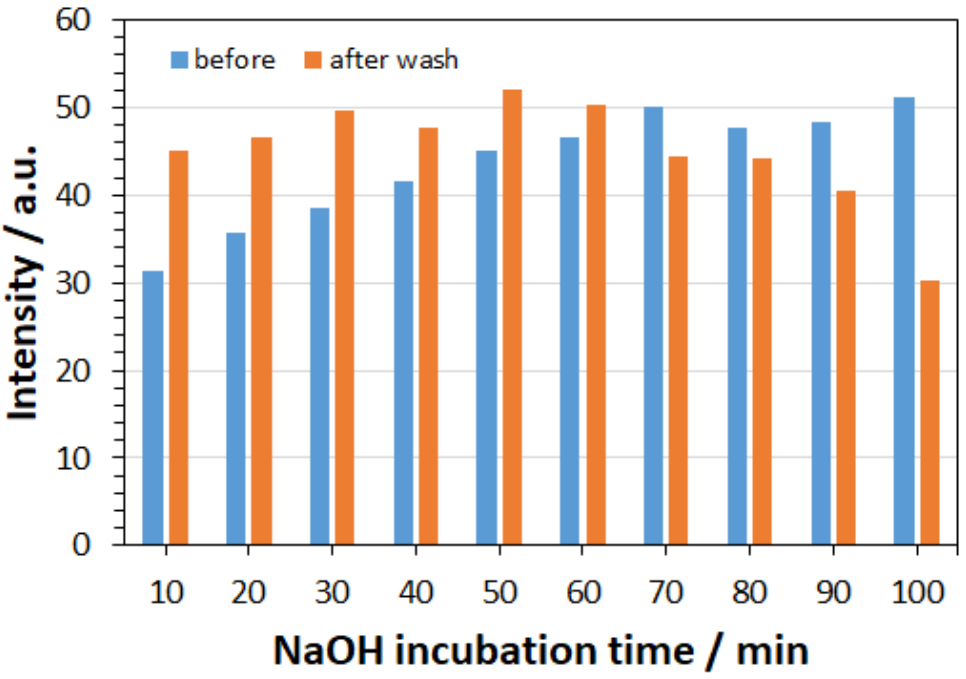

Figure 4.2: Fluorescence intensity of chitosan with embedded silica nanoparticles, following incubation with NaOH for 10 to 100 min to dissolve the particles and staining with BSA-FITC (blue bars) as well as following washing with phosphate buffer (red bars).

To further investigate the porosity with silica nanoparticles as porogens, different chitosan/particle ratios were tested. The chitosan solution and particle suspensions were prepared as before and mixed at ratios of 2:1, 1:1, 1:2 and 1:3. They were stirred for 1 h and then poured into cuvettes and left for 24 h at room temperature to form a gel. The silica particles were then dissolved with NaOH solution for 17 h has described before and washed with deionised water to remove the NaOH. The cuvettes were then again incubated with BSA-FITC for 2 h and washed with PBS. Photographs of these gels are shown in fig.4.3.

Fig.4.4, shows results from measurements of the fluorescence intensity of the native gel, the gel when immersed in BSA-FITC solution, the gel following decanting of the BSA-FITC and the gel after washing with PBS.

As can be seen in the figures, all the gels retained some fluorescence indicating that BSA-FITC has been bound into the gel. The gels with higher chitosan ratio retained more BSA-FITC. It was found that the ratio to 1:2 of silica to chitosan lead to a smooth mixture. These ratios of gel to porogen were also reported to sustain higher flow rates and mechanical stability in continuous flow processes [139] . The key conclusion of this experiment was Diffusion silica beads into the chitosan layer has shown a remarkable results where BSA molecules can be easily diffused inside the chitosan hydrogel.

As these commercially available silica nanoparticles are relatively expensive it was decided to synthesis of silica nanoparticles in-house using the Stöber method [128, 134].

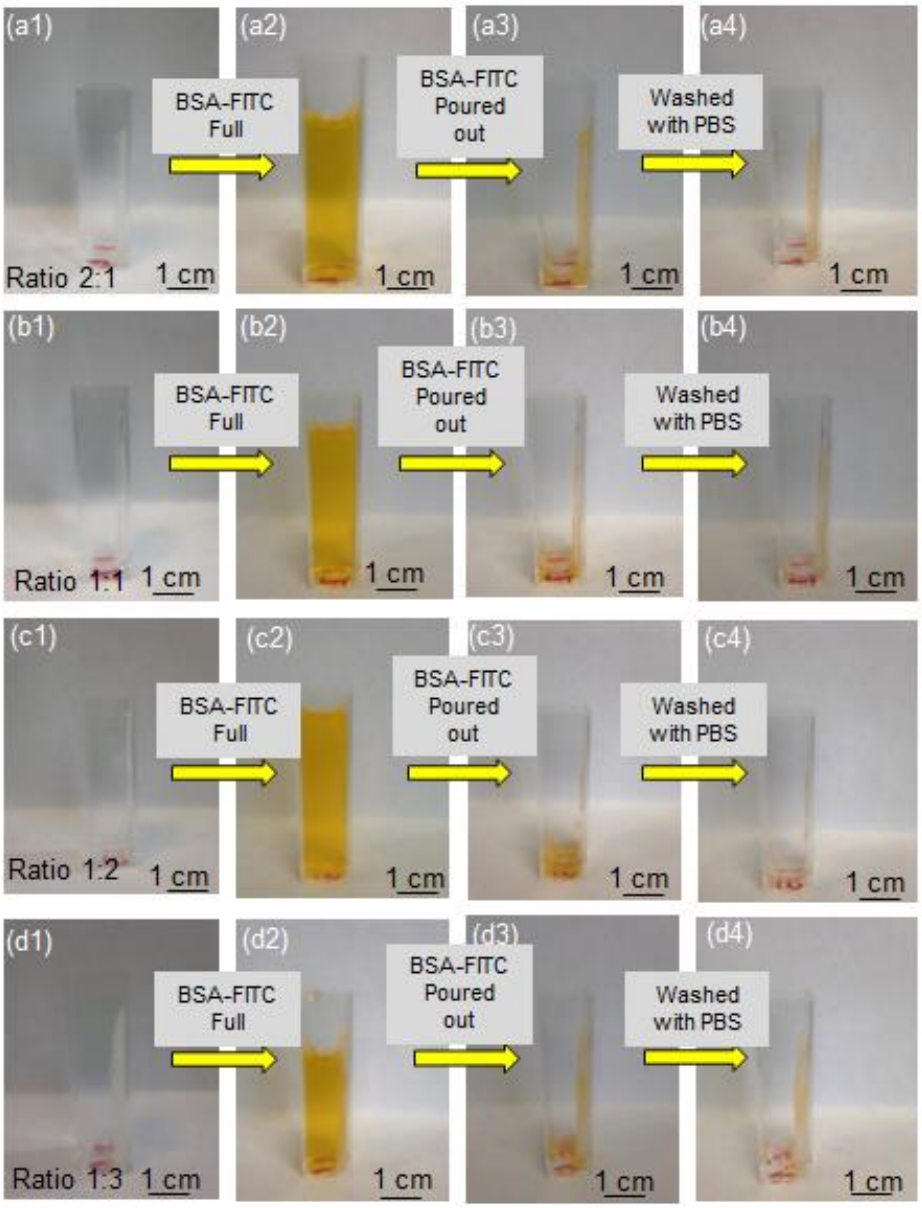

Figure 4.3: Chitosan gel prepared by mixing different ratios of a 2.5% chitosan solution with a suspension of 1% silica particles, leaving the gel to form for 24 h and then dissolving the silica particles with NaOH. (a) Ratio 2:1, (b) ratio 1:1, (c) ratio 1:2 and (d) ration 1:3. The photos show (1) the prepared gel, (2) the cuvette with the gel after addition of 2 mL BSA-FITC for 2 h, (3) the cuvette with gel after the BSA-FITC supernatant had been poured out and (4) the cuvette with the gel after washing with PBS.

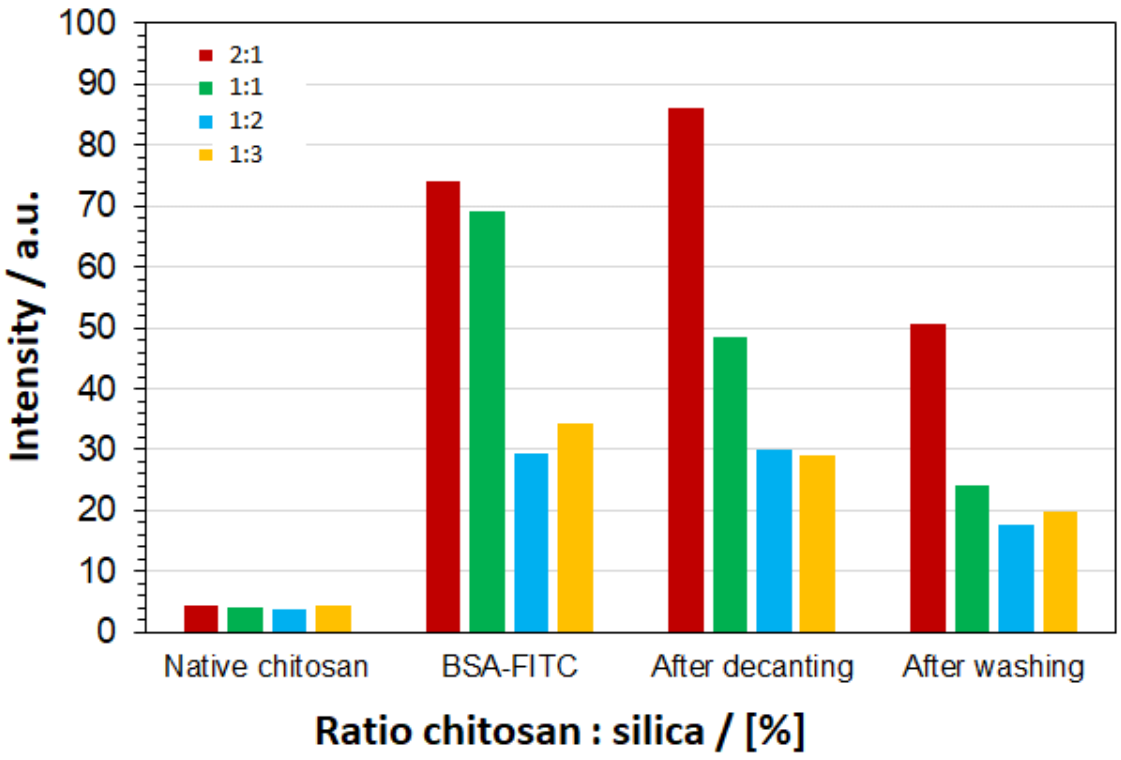

Figure 4.4: Fluorescence intensity for chitosan with silica beads prepared at ratios of 2:1, 1:1, 1:2 and 1:2 measured in the cuvette before addition of fluorescently labelled BSA, after incubation with 2 mL of fluorescently labelled BSA for 2 h, after pouring out of excess solution and finally following washing with PBS.

4.1.3 Synthesis of silica nanoparticles via Stöber Method

Silica nanoparticles were synthesised via the Stöber Method based on hydrolysis of tetra-ethyl ortho-silicate (TEOS) in ethanol using a range of ammonium hydroxide concentrations [134], as explained in section 2.7.2. Particle size was measured using a zeta sizer. An example of such a plot is shown in fig.4.5a, showing preparation of silica nanoparticles by sequential addition method (Stöber Method). The average sizes of the particles prepared in the different ammonium hydroxide solutions are summarised in fig.4.5b. The size of the silica particles as obtained by zeta sizer measurement ranged between around 300 nm and 380 nm for the lower ammonium hydroxide concentrations (0.86 M – 1.15 M). Using the higher ammonium hydroxide concentrations of 1.30 M and 1.44 M resulted in particles of about 130 – 140 nm in diameter. The obtained particle sizes are significantly larger than the 55 nm – 130 nm diameters obtained from TEM measurements reported in ref. (134). If silica particles much larger than 100 nm are used, the resulting pore sizes in the waveguide film would cause light scattering and diminish the performance of the sensor. Therefore, an alternative procedure was followed to obtain smaller silica nanoparticles.

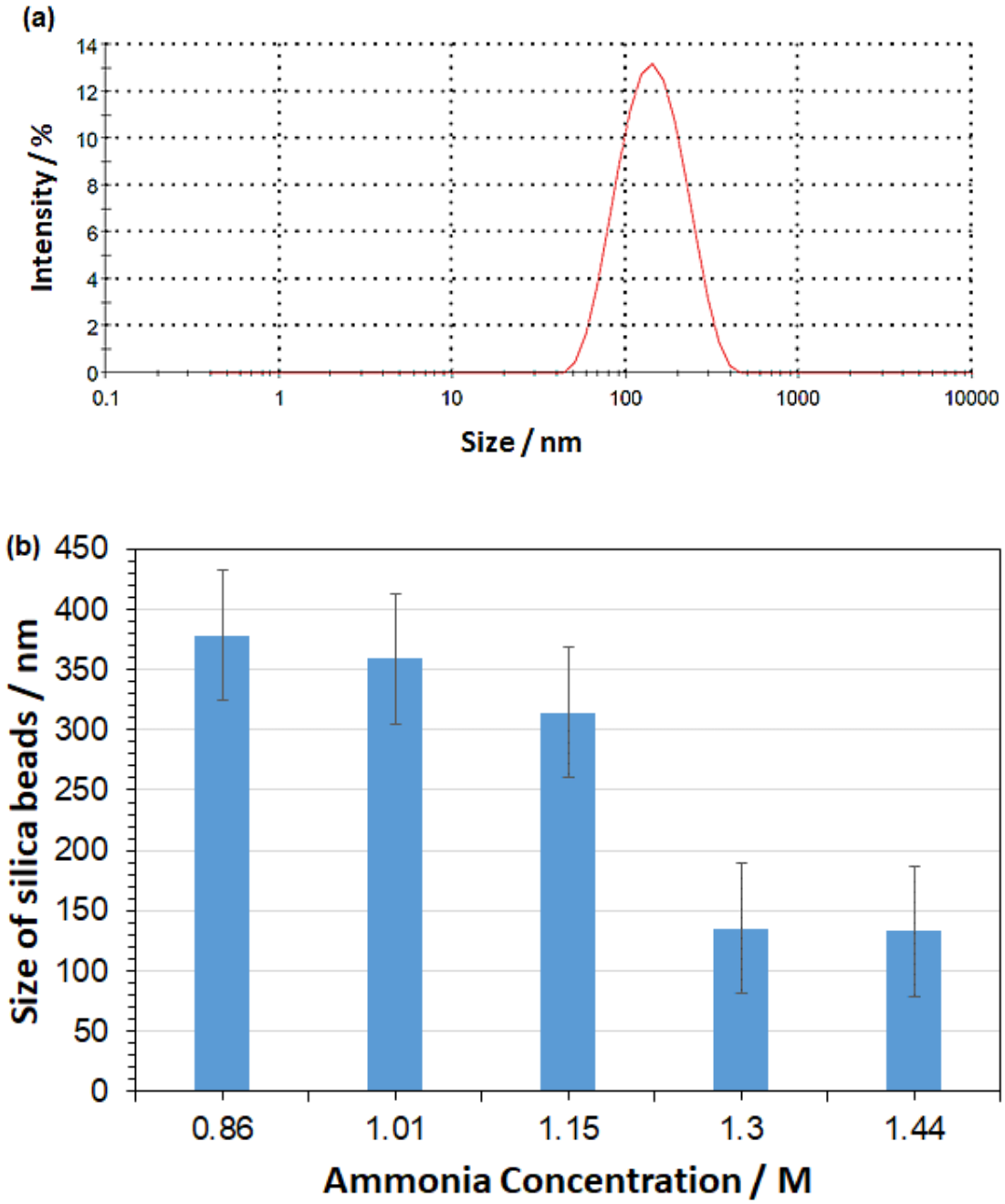

Figure 4.5: (a) Example of a size measurement as obtained from 0.86 M – 1.15 M (b) Average size of silica particles measured by zeta sizer obtained from different concentrations of ammonium hydroxide with a TEOS concentration of 0.045 M in 4 M aqueous ethanol.

A variation of the Stöber Method [128] was investigated which has been reported to produce smaller particles. The particles were prepared as outlined in section 2.7.2 and the average size was measured with zeta sizer. Fig.4.6a and b, shows the results of particle size measurements. As can be seen from the figure, particle size decreased with increasing ethanol concentration over a range from 200 nm to 50 nm. Whilst the particle size distribution was larger than those reported in ref. (128), the particles were sufficiently

small and thus functional for study of their ability to act as porogens for the chitosan hydrogels.

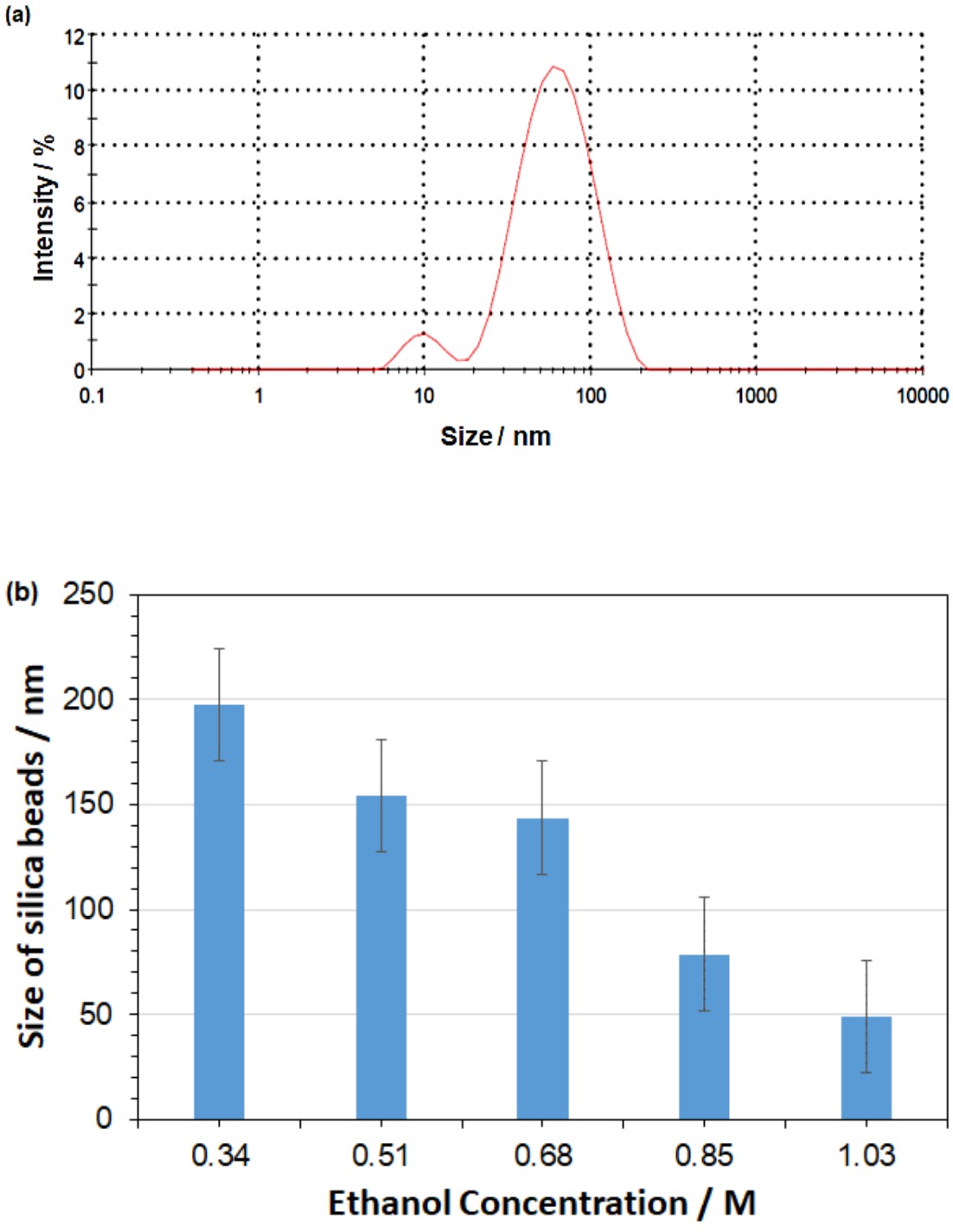

Figure 4.6: (a) Example of zeta sizer measurement. (b) Average size of silica particles obtained in an aqueous solution containing 0.4 M TEOS, 0.2 M NH_3 and ethanol concentrations ranging from 0.34 M to 1.03 M.

4.1.4 Porosity studied by fluorimeter following BSA-FITC incubation

The porosity of the chitosan gel with 50 nm diameter silica nanoparticles was investigated similar to the experiments described in section 4.1. The small particles were chosen because they should ensure increased porosity whilst not leading to excessive light scattering in the waveguide. Gels from 2.5% (w/v%) chitosan with glutaraldehyde were prepared as before and mixed with suspensions of 1%, 2% and 3% of the 48 nm ± 25 nm silica nanoparticles. Then different ratios of chitosan solution to silica beads were investigated (2:1, 1:1, 1:2 and 1:3). Once the gel was formed, the silica NPs were dissolved with NaOH to yield a porous gel material, which was stable and not found to shrink visibly. The ability of these materials to take up BSA-FITC (66 kDa) was studied as before. Photographs of the cuvettes showing the gel after the silica NP dissolution, the cuvette with BSA-FITC solution, the gel in the cuvette following BSA-FITC decanting and finally, the cuvette with gel following washing with PBS buffer as shown in fig.4.7. Fluorescence measurements of these gels are summarised in fig.4.8.

As can be seen fluorescence intensities are low and, as found before with the commercially available 100 nm silica nanoparticles (see fig.4.7), the gel prepared from the 2:1 ratio of chitosan to silica particles retained the largest amount of BSA.

Also, a 1:2 ratio of silica to chitosan leads to an approximately symmetric waveguide layer as indicated in this figure.

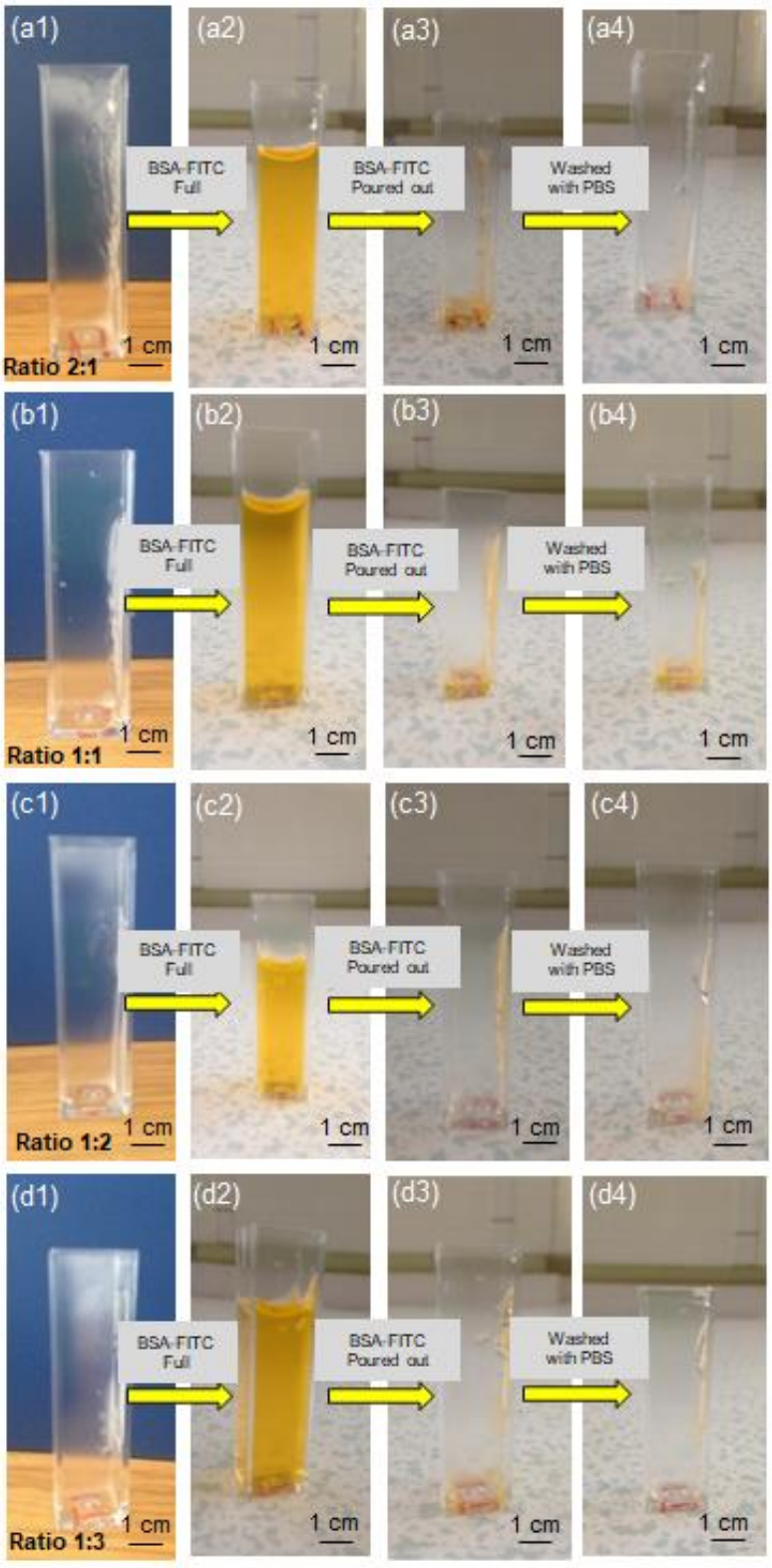

Figure 4.7: Photographs of gels incubated with BSA-FITC to investigate gel porosity. The gels were prepared from 2.5% chitosan and a 10% suspension of silica nanoparticles of 48 nm ± 25 nm at ratios of (a) 2:1, (b) 1:1, (c) 1:2 and (d) 1:3. The silica NP were dissolved with NaOH to render a porous gel material. The photographs show (1) the gel after NaOH treatment, (2) the cuvette filled with BSA-FITC solution, (3) the cuvette after decanting of excess BSA-FITC solution and finally (4) after washing with PBS.

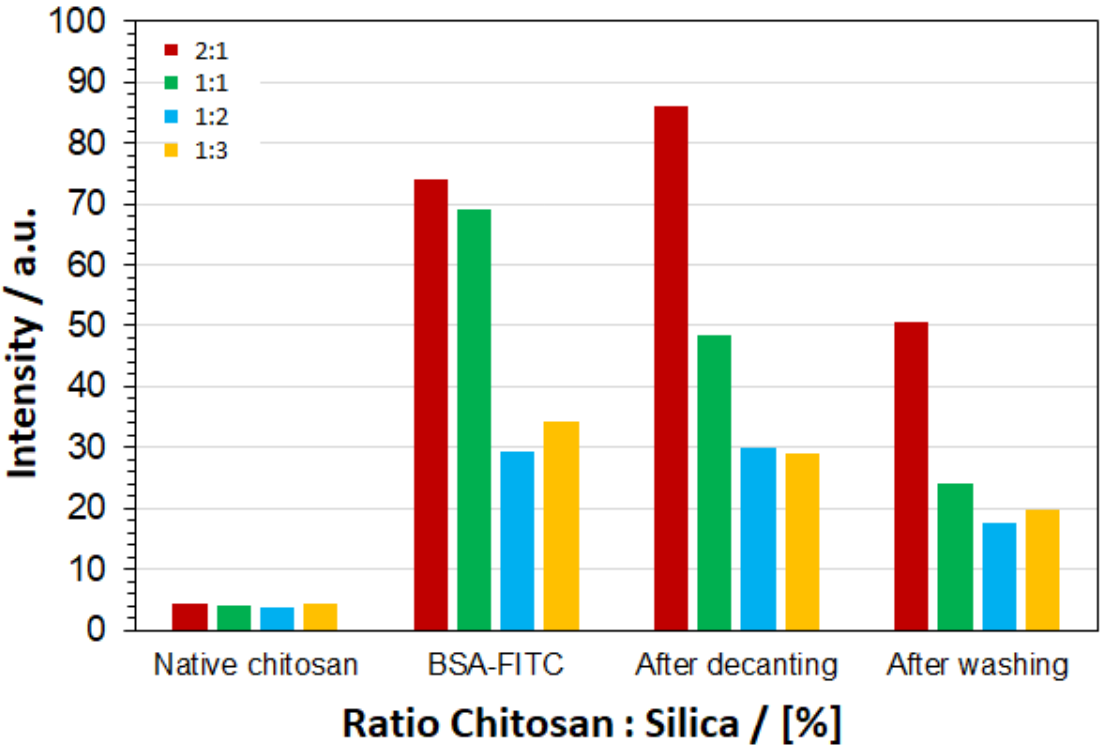

Figure 4.8: Fluorescence intensity for chitosan with 50 nm silica nanoparticles prepared at ratios of 2:1, 1:1, 1:2 and 1:2 measured in the cuvette before addition of fluorescently labelled BSA, after incubation with 2 mL of fluorescently labelled BSA for 2 h, after pouring out of excess solution and finally following washing with PBS.

4.1.5 Performance of chitosan film as optical waveguide with following porogen treatment

The porosity of the chitosan hydrogel gel following treatment with commercial (100 nm) and synthesised (50 nm) silica nanoparticles was investigated by studying the shift in dip upon incubation with various molecular weight polymers. The porous chitosan gels were prepared as described in 2.7.4, based on a 2.0% chitosan solution mixed initially with glutaraldehyde and then with a 1% suspension of silica nanoparticles in a ratio of 2:1. The mixture was spin-coated onto glass substrates and then incubated with 10% NaOH to dissolve the silica. The slides were washed with water. At this point, the chitosan film was observed to detach from the glass substrate. Nonetheless, the glass substrate was immersed in RB4 (10 µM) for 10 min to stain any chitosan that might be remaining. This was then interfaced with the flow cell (design 2) and placed on the optical setup with the laser and CMOS camera positioned at 65º with respect to the base of the prism. In fig.4.9, an image obtained from the CMOS camera of the film with 100 nm silica particles as porogens is shown following RB4 incubation. As expected, there is no clearly apparent

dip on the glass slide, only a few dark areas, as the chitosan layer was washed away. Whilst the sodium hydroxide seemed effective in dissolving the silica, the chitosan gel itself became detached from the glass substrate.

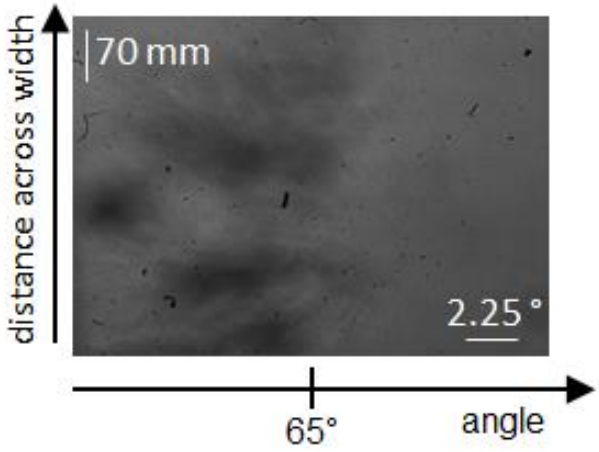

Figure 4.9: CMOS image obtained from dye doped chitosan film with 100 nm silica nanoparticles as a porogen following incubation with RB4 (10 µM).

Nonetheless, boxes for tracking of the dark area were drawn on the computer software and the shifting of these was tracked when the various solutions, *i.e.* 0.5% glycerol and different molecular weight polymers (PEG and PEO) ranging from 10 kDa t0 200 kDa (as detailed in section 2.7.4) as shown in fig.4.10.

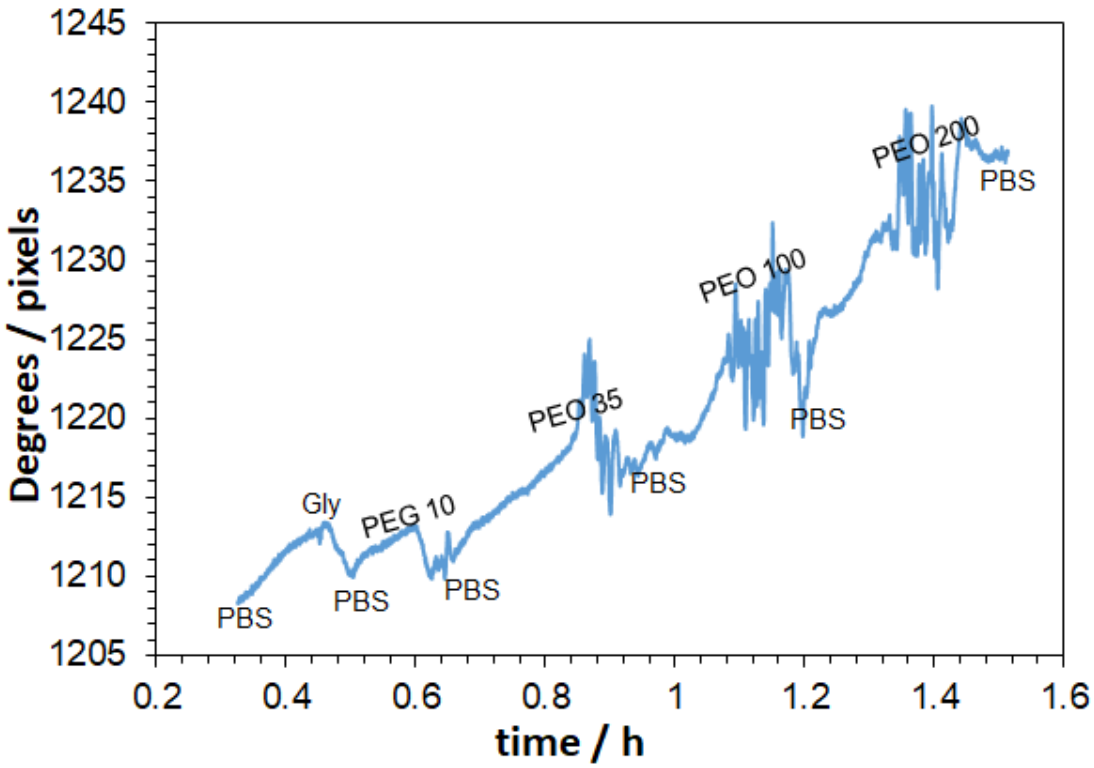

Figure 4.10: Dip shifting for different molecular weights of polymers prepared in the same buffer, PBS (PH=7.4), using another solvent (water) ; surface of the glass slide initially incubated with 10% (0.1 M) of sodium hydroxide for 17 h at room temperature and for 10 min at 80ºC. All of these polymers and glycerol solutions have the same refractive index 1.3355. The refractive index for PBS was 1.3345.

Next, the 100 nm commercially available silica NP were investigated. Fig.4.11, shows a gel composed of a 2:1 ratio (chitosan to silica NPs) incubated with sodium hydroxide for 2 h at room temperature. A sharp dip is clearly and encouragingly visible in this image. Fig.4.12, shows a plot of tracking the position of the dip for this waveguide following flushing with glycerol and polymer solutions. It can be seen that the glycerol caused a significant shift in dip, indicating it could penetrate into the waveguide. The polymer solutions however did not yield in any significant dip in position, indicating that they could not penetrate into the waveguide layer. The overall downward drift maybe a result of external fluctuation (room temperature, and humidity), since flow cell design does not have a reference channel to account for these.

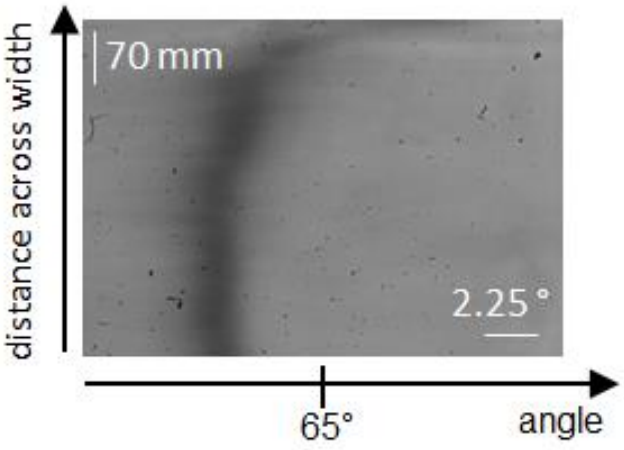

Figure 4.11: CMOS image from waveguide coated onto glass substrate with 2:1 ratio chitosan to commercial silica particles (100 nm), dissolved with 10% NaOH for 2 h following RB4 staining (1 mM) for 10 min.

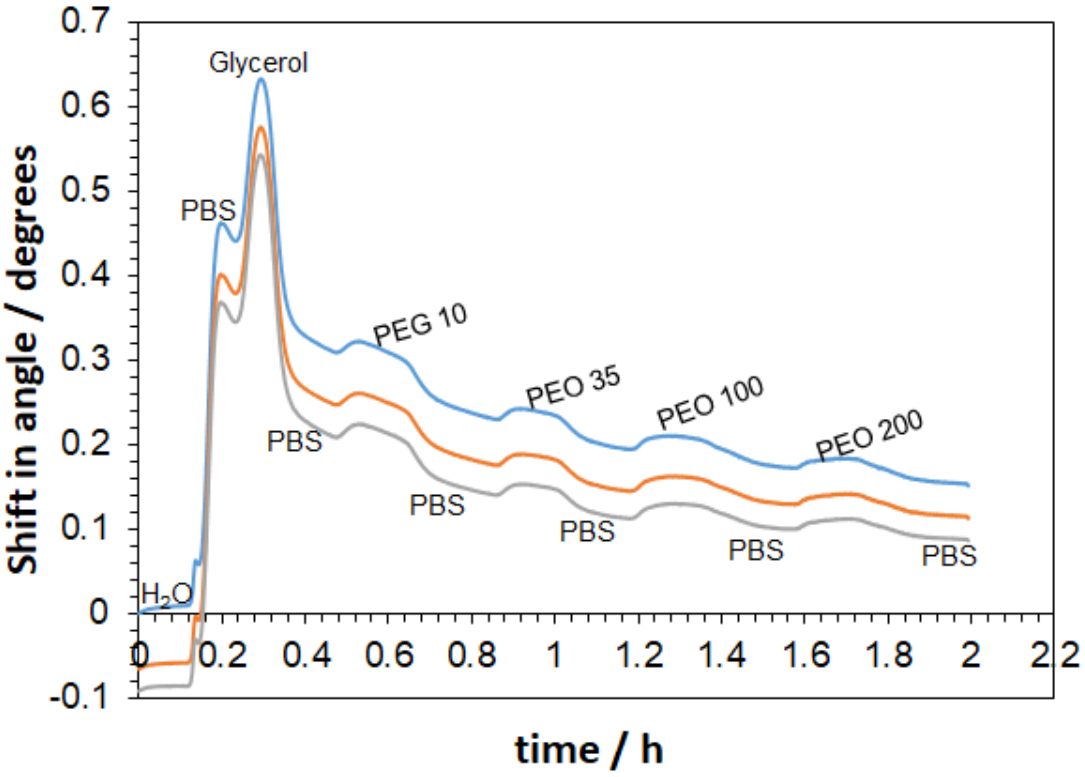

Figure 4.12: Dip shifting for different molecular weights of polymers PEG and PEO prepared in PBS 2:1 ratio chitosan to commercial 100 nm silica beads. The surface of glass slide initially incubated with 10% of 0.1 M sodium hydroxide for 2 hrs, then washed with distilled water; after that incubated with the reactive blue 4 dye (10 µM) for 10 min and washed with water. All these polymers and glycerol solution have the same refractive index, 1.3355, and the refractive index for PBS was 1.3345.

This experiment was repeated with synthesized silica nanoparticles (around 50 nm) Figure 4.13, shows the image from the CMOS detector clearly showing a dip in reflectivity.

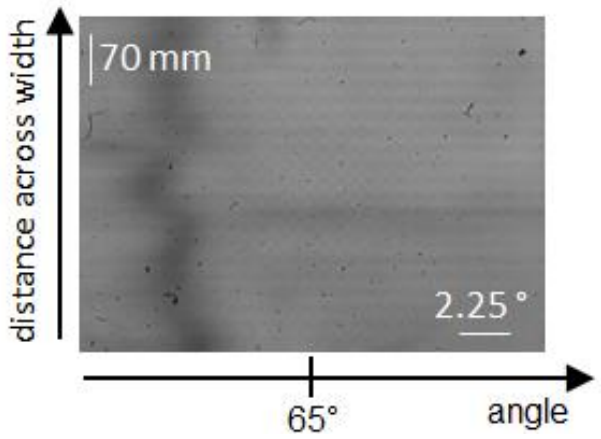

Figure 4.13: CMOS image of waveguide prepared from a 2:1 ratio chitosan to silica NPs (ca. 50 nm) that were then dissolved with NaOH to yield a porous film.

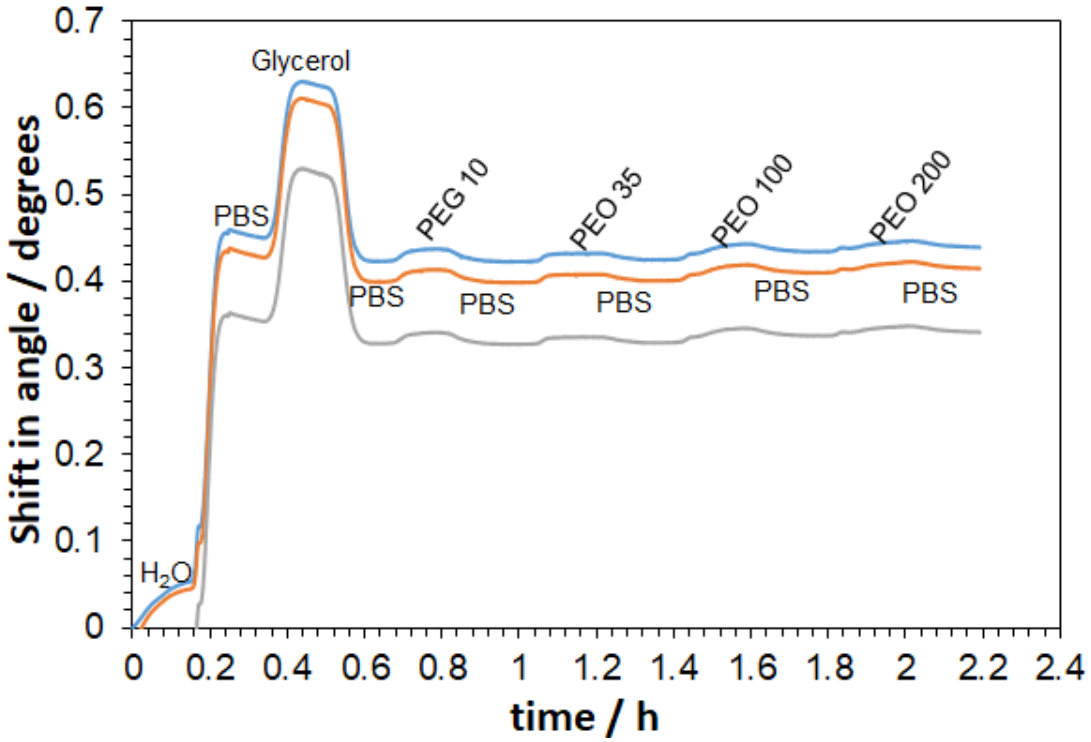

Figure 4.14: Dip shifting for different molecular weights of polymers, 2:1 ratio chitosan to synthesised silica beads (48 nm), and the surface of glass slide initially incubated with 10% of sodium hydroxide for 2 hrs. All of these polymers and glycerol solution have the same refractive index 1.3355, and the refractive index for PBS was 1.3345.

To conclude, the pore size of the leaky waveguide layer with commercial and synthesized silica beads has been investigated by diffusion of a glycerol solution and polymer solutions. Glycerol has a low molecular weight and can easily diffuse into the waveguide layer. PEG and PEO solutions with different molecular weights but almost no shift in dip was observed, fig.4.14, indicates that none of these solutions can diffuse inside the film i.e. that at the pore size is still too small. In many cases it was found that the chitosan film

lifted from the substrate when dissolving the porogens with NaOH treatment. Therefore, different methodologies were used to enhance and control the porosity of a chitosan layer.

4.2 Controlling Porosity by Drying Time of Chitosan Layer

It has been reported in the literature [78] that wet chitosan is porous and highly permeable to ions. A highly porous material would also not support the waveguide mode to a large scattering of light from the surface. In contrast, a fully dried chitosan film produced by a spin coater or hydrogel that is cast on a cuvette without modification has not provided any enhancement to the porosity as was shown in section 2.7.5. It was hypothesised that by controlling the drying time following spin-coating of the chitosan solution a waveguide layer of suitable porosity may be obtained.

The experimental procedure was carried out as described in section 2.7.5 by using different concentrations of chitosan (0.5%, 1.0% and 2.0%), different spin speeds (900-1500 rpm) and different drying times (1 min to 10 min). The obtained films were dyed with RB4. Reflectivity curves were obtained as laid out in section 2.7.5

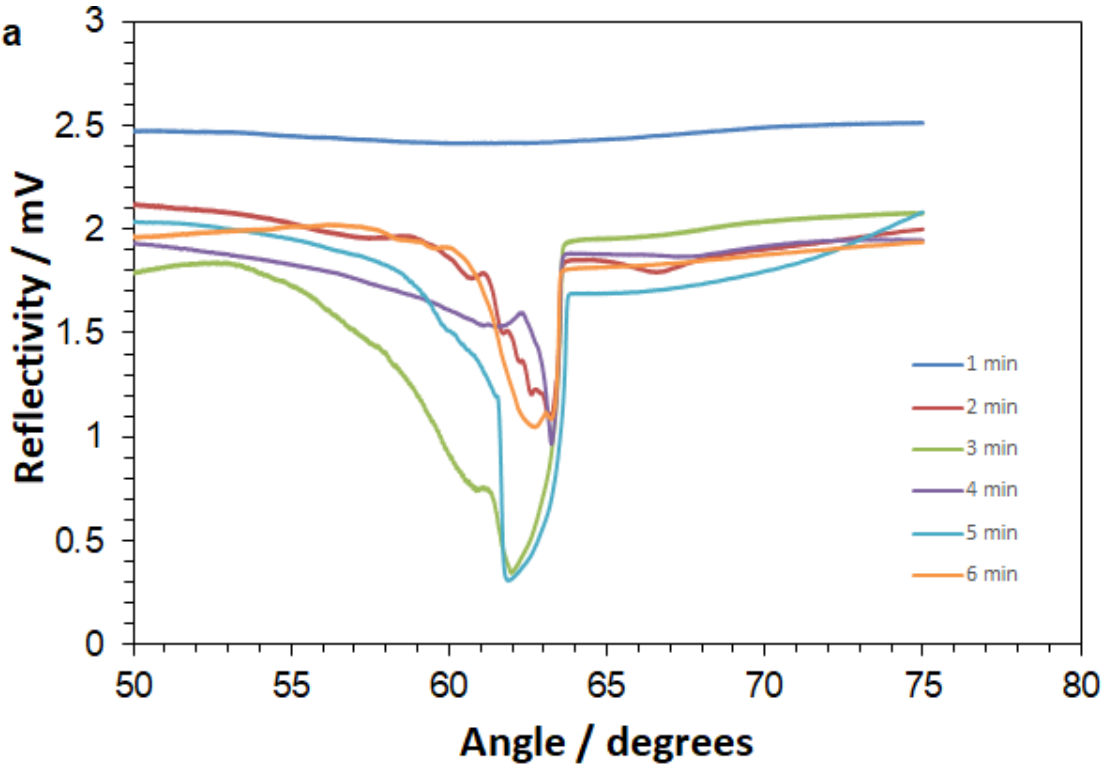

Figure 4.15: The reflectivity curve of the waveguide layer from 0.5% chitosan using different drying times (1, 2, 3, 4, 5 and 10 min) at spin speed 900 rpm.

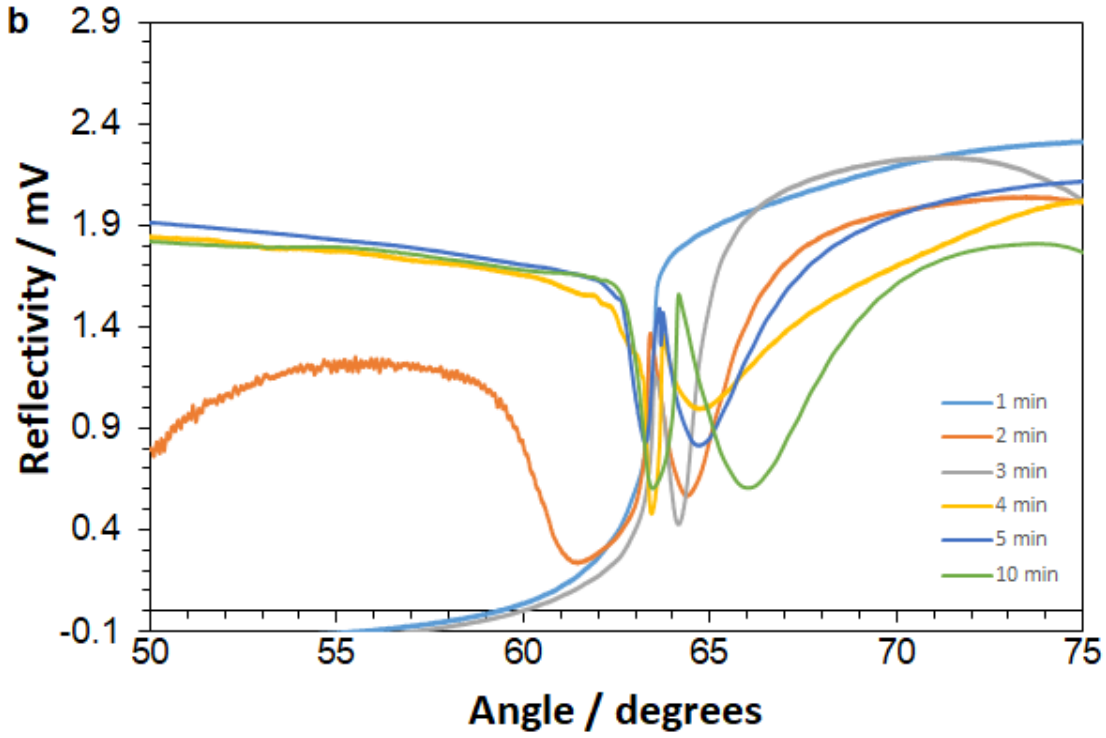

Figure 4.16: The reflectivity curves of the waveguide layer prepared from 1.0% chitosan using different drying times (1, 2, 3, 4, 5 and 10 min) at spin speed 900 rpm.

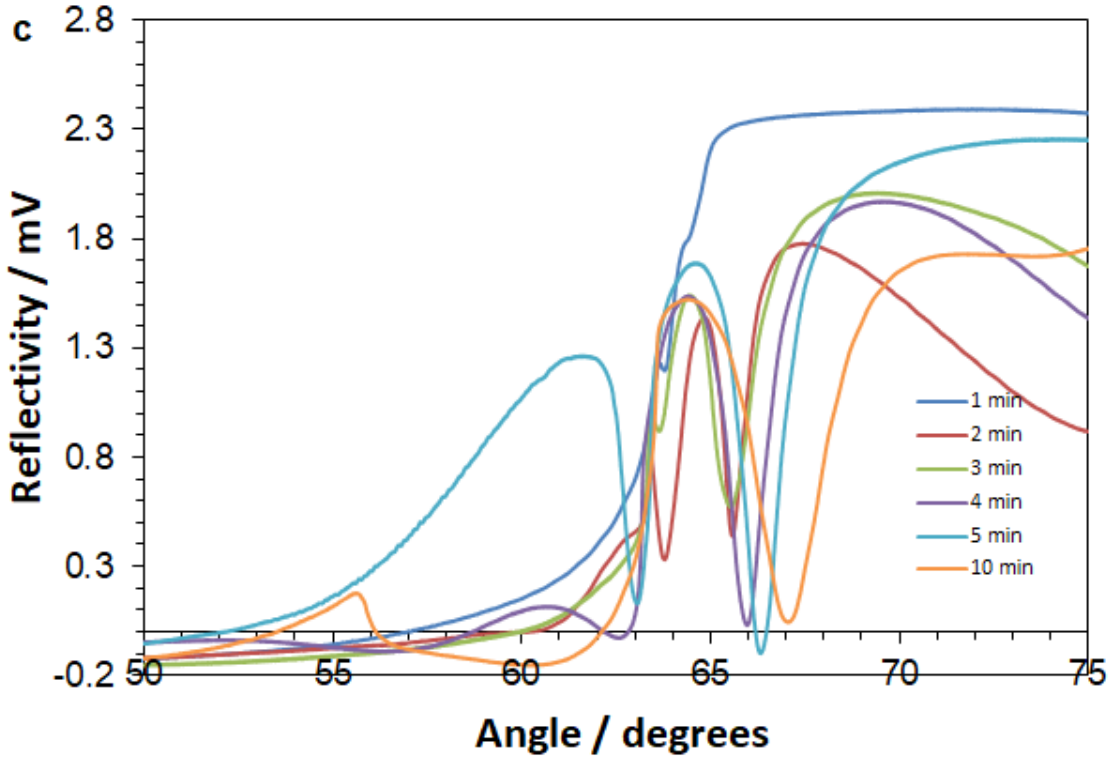

Figure 4.17: Reflectivity curves of waveguide layer prepared from 1.5% chitosan using different drying times (1, 2, 3, 4, 5 and 10 min) at a spin speed 900 rpm.

Fig.4.18 (a, b, and c), indicates different single dips obtained at different drying times from 3 min to 10 min. However, the sharpest dip was seen at 3 min where by increasing the time of drying, a broader dip was observed. This could be due to water molecules being evaporated from the chitosan surface which leads to irreversible shrinking of the thickness of the surface and consequently decrease in the pore size. This would increase the density of the chitosan, a result that corresponds to a longer time of light confinement inside the waveguide before coupling out. Therefore, more light will be absorbed by the dye molecules during that time and hence a broader dip is observed. There is no dip at 2 min drying time and this can be related to the larger pore size present, which cannot support a waveguide mode. The sharpest dip responds to the value of the refractive index with the highest sensitivity, thus this condition was chosen for further investigation. Therefore, the optimal condition for a waveguide mode under different drying times was seen as 1% (w/v) of chitosan concentration coated at 900 rpm and then left to dry for 3 min.

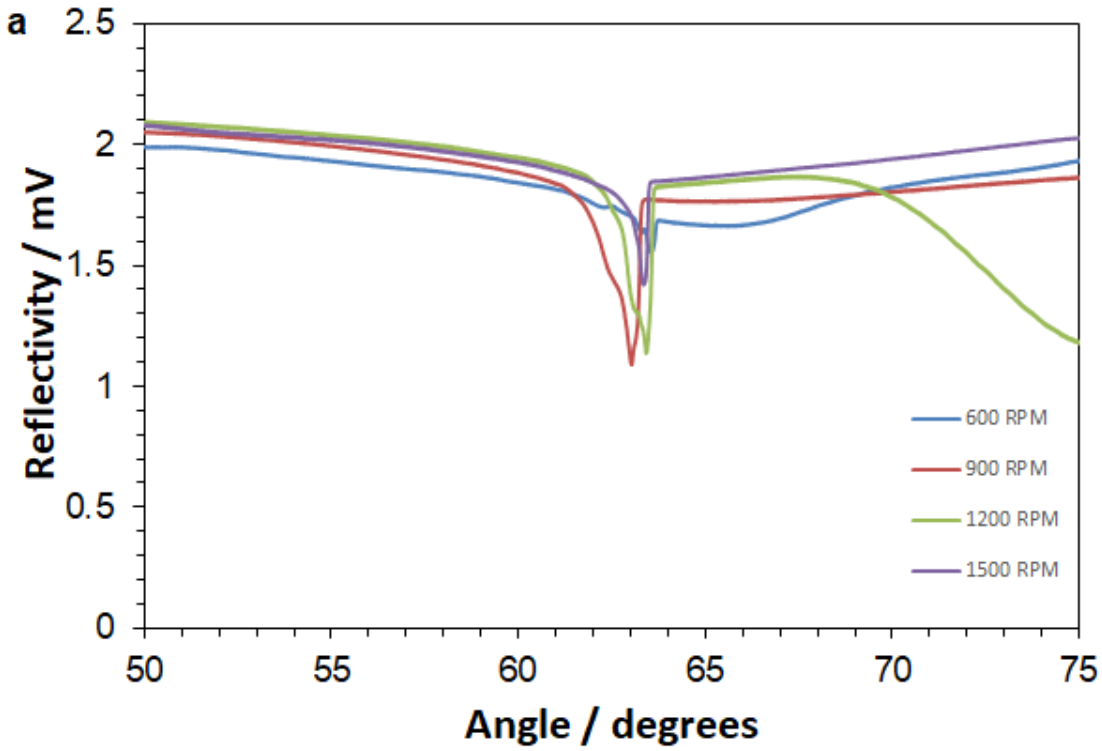

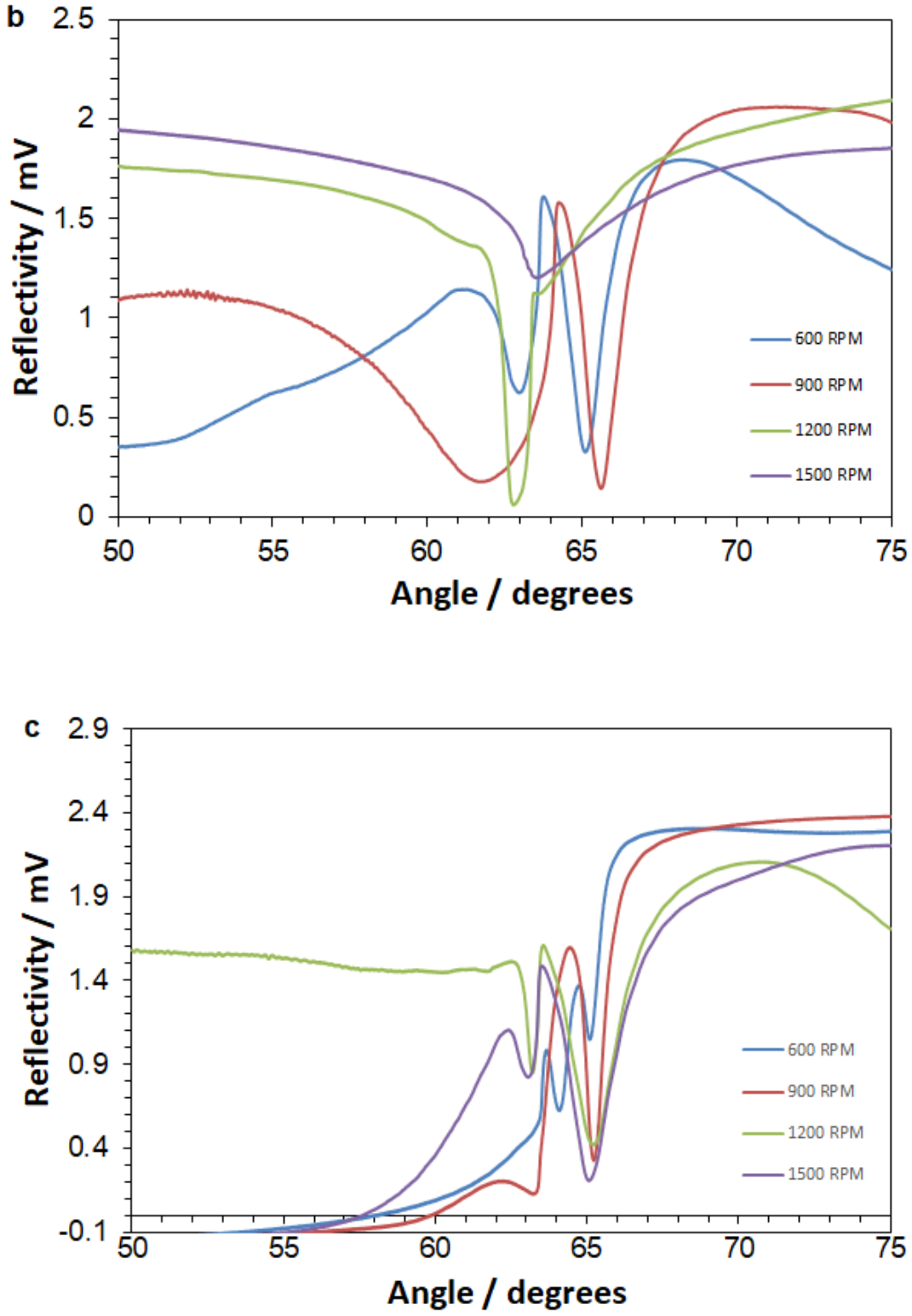

Figure 4.18: The reflectivity curve of the waveguide layer with the dye using different spin speeds (600, 900, 1200 and 1500 rpm), 3 min dry time; concentration of chitosan was a: 0.5%; b: 1%; c: 1.5%. The optimum drying time 3 min was further examined under different concentrations of chitosan at different spin speeds. It's clear from concentrations of chitosan at different spin speeds.

4.3 Characterization of Film Porosity

4.3.1 Diffuse Different Molecular Weights of Polymers PEG and PEO

Different solutions of glycerol, PEG and PEO were injected through a peristaltic pump at a flow rate of 0.25 mL min^{-1}, all these solutions have the same refractive index. As indicated in fig.4.19, the degree of shift in angle with all PEG and PEO solutions averaged 0.071 which is identical to what has been observed with glycerol solution 0.09. This indicates significant enhancement in the pore size of the chitosan, which we suggest is large enough to sense even with the highest molecular weight of PEO (400 kDa).

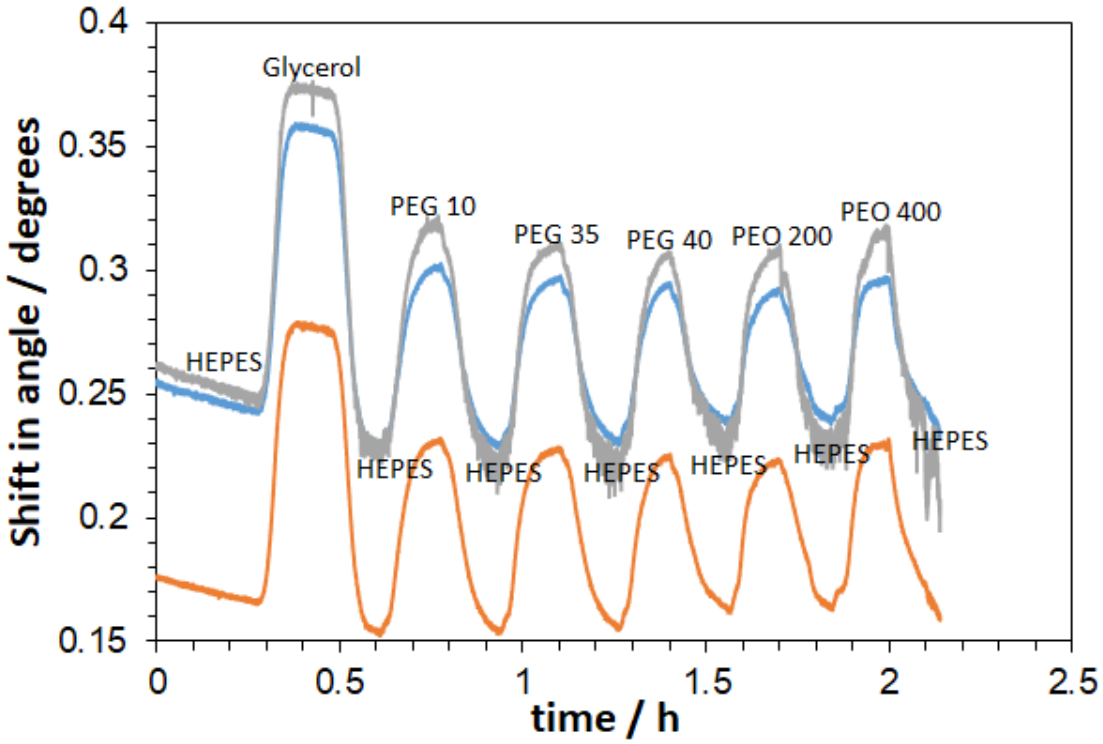

Figure 4.19: The reflectivity curve of the waveguide layer using 1% concentration of chitosan at spin speed 900 rpm with the different molecular weights of glycerol and polymers PEG and PEO solutions, which all have the same refractive index (1.3365).

Thus, the degree of shift varied slightly at different regions suggesting that some pore sizes were somewhat smaller than in the other regions of the dip. All the solutions were made up with the same refractive index (1.3365).

4.3.2 Diffuse Different concentrations of BSA protein

The pore size of the leaky waveguide layer was investigated with different concentrations of bovine serum albumin (BSA, 66 kDa) and glycerol (92.1 g mol^{-1}) as described in section 2.6.2. A plot of the shift in the dip is shown in fig.4.20.There was an increase in the shift of angle with an increase in the concentration of BSA solutions from 0.35 to 1.65, which did not return to the starting position of 0.35 with HEPES buffer. Moreover, higher concentrations of BSA show a shift in angle as can be seen with 0.5, 1 and 2% of BSA. This can be related to the pore size of the chitosan film which is clearly too large to diffuse the BSA molecules into the sensing region of the chitosan film, like the glycerol.

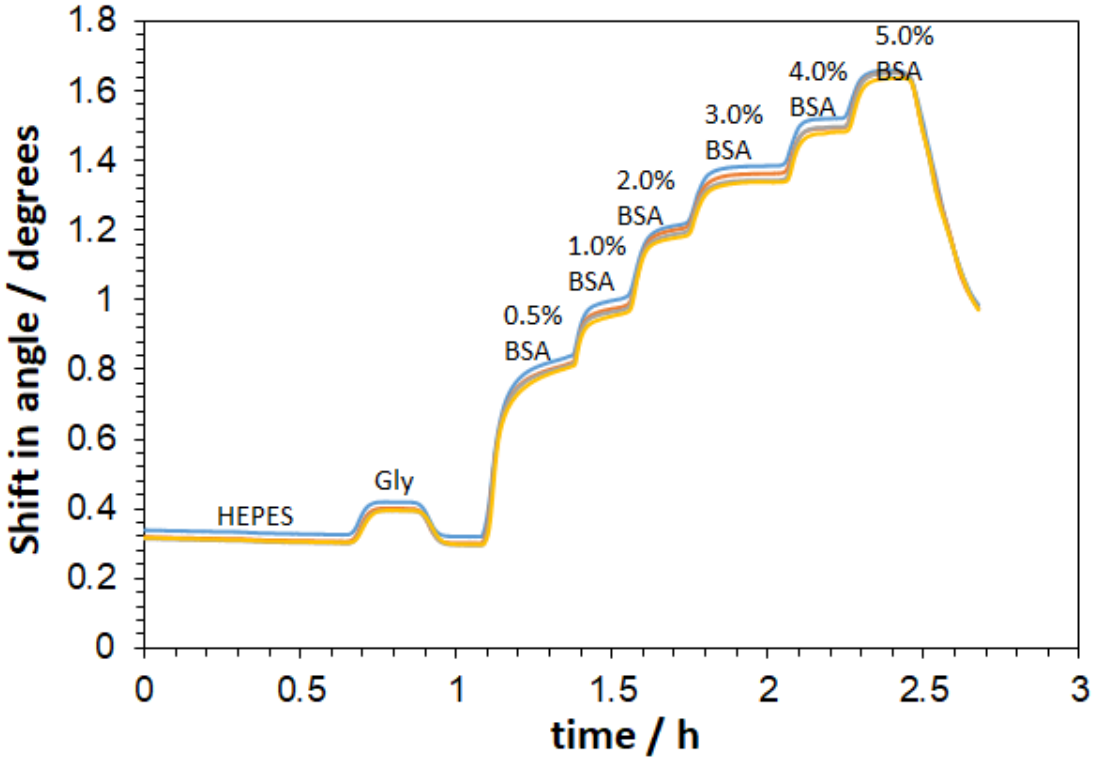

Figure 4.20: Changing in the reflectivity dip angle versus time using two different solutions (glycerol and BSA). The surface initially incubated with reactive blue4 dye (100 mM) for 5 min.

4.3.3 Study Effect of pH

The pH value can play a significant role on the surface of chitosan layer leading to a swelling or shrinking of the waveguide film by protonation and de-protonation of the amino group. The condition of the chitosan waveguide layer which has significant pore size was further investigated in terms study the effect of pH. Fig.4.21, shows the effect of pH value on the degree of shift in which it decreased from approximately 0.3 to 0.15 when the buffer was switched from pH 7.4 to 8.4, giving an average shift of 0.15 degrees. At higher pH a deprotonation process occurs, which leads to a reduced positive charge and thus decreases the repulsion between the amine groups. Therefore a shrinking of the chitosan waveguide would be expected. The dip position did not return to the normal position even when pH 7.4 buffer was flushed through the channel. At pH 6.4 and 5.4 there was an increase in the degree of shift which can be easily returned to the baseline by flushing with pH 7.4. At lower pH more protonation of amino groups takes place and to some extent, the chitosan will be dissolved. This was observed at pH 4.4 in which the dip totally disappeared due to chitosan, dissolving as shown in fig.4.22.

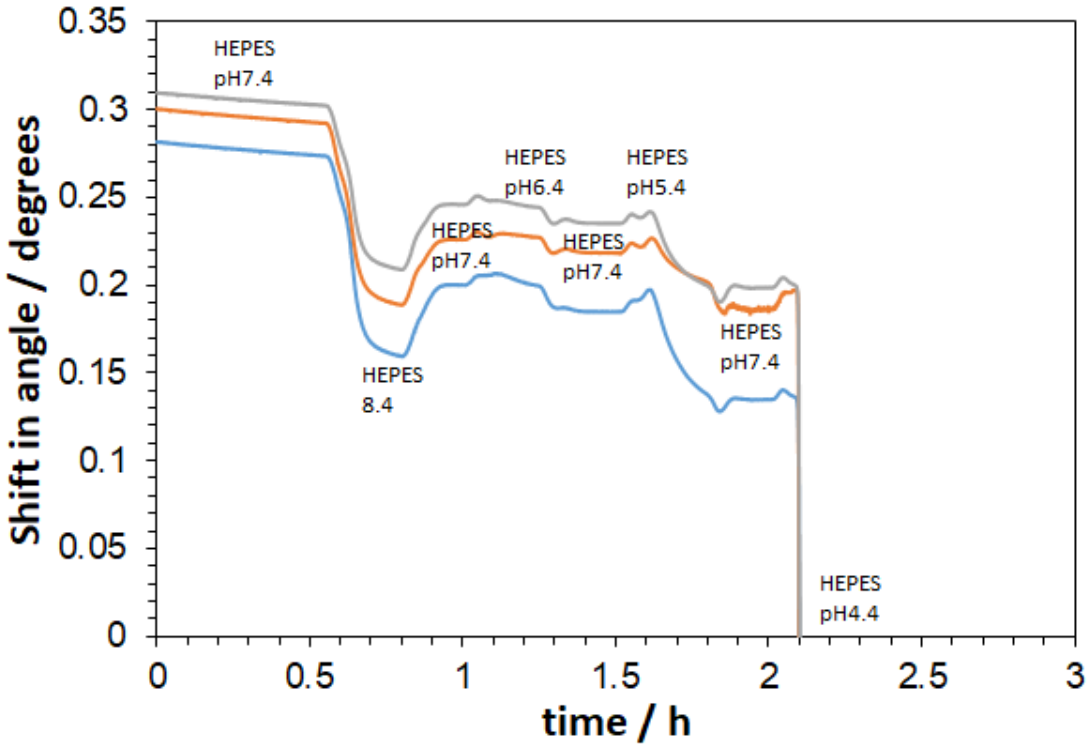

Figure 4.21: Changes in the reflectivity dip angle versus time using different pH solutions of HEPES buffer (8.4, 7.4, 6.4, 5.4 and 4.4). The surface initially incubated with the RB4 dye (100 µM) for 5 min.

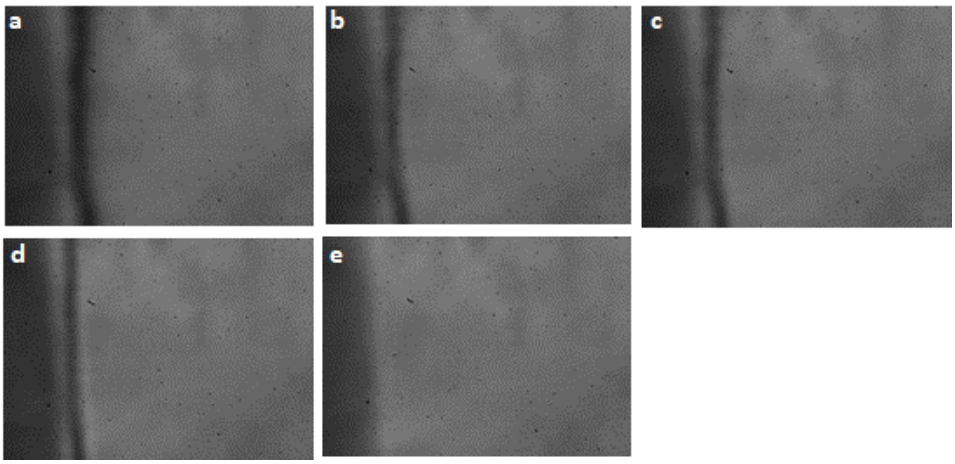

Figure 4.22: profile pictures captured by the camera of glass slide injected with different pH solutions: a: HEPES pH 7.4 buffer; b: HEPES pH 8.4 buffer; c: HEPES pH 6.4 buffer; d: HEPES pH 5.4 buffer; and e: HEPES pH 4.4 buffer.

4.3.4 Effect of Cross-linker

The effect of crosslinking the chitosan waveguide was studied with *N* hydroxysuccinimide-polyethylene glycol-*N* hydroxysuccinimide (NHS-PEG-NHS) of with different lengths as described in section 2.9. The most common way of crosslinking the amine group in the chitosan layer involves reacting an amine group of chitosan with the NHS of a linker. NHS-PEG-NHS is a popular amine-specific functional group. When incorporated into the chitosan layer this can give a level of control over the pore size via formation of amide bonds as shown in fig.4.23.

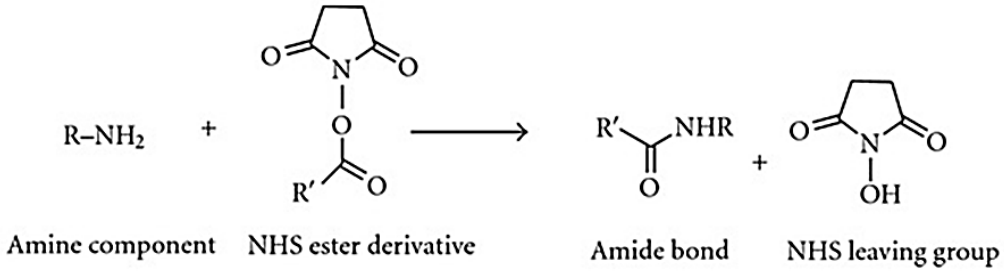

Figure 4.23: Reaction of amine group of chitosan layer with a linker NHS-PEG-NHS.

The experimental procedure was the same as in the previous experiment, except that 1 mM of NHS-PEG-NHS was prepared in 100 mM of HEPES buffer with lengths of 500 Da, 2 kDa and 3 kDa was added after the drying process to the coated chips for 5 min followed by washing with HEPES and incubation with the dye.

Fig.4.24, Shows a run performed with 500 Da crosslinker. The shift in degrees varied from solutions where glycerol still exhibits the highest value of shift which gradually decreases with an increase in the molecular weight of polymers.

In fig.4.25. On the other hand, exhibits the average of the three runs performed by using the 2 kDa NHS-PEG-NHS crosslinker. The shift with PEG and PEO solutions were clearly lower than with glycerol. However, the difference in the shift degree of the polymer solutions was not very high particularly between PEG 35, PEO 40, PEO 200 and PEO 400.

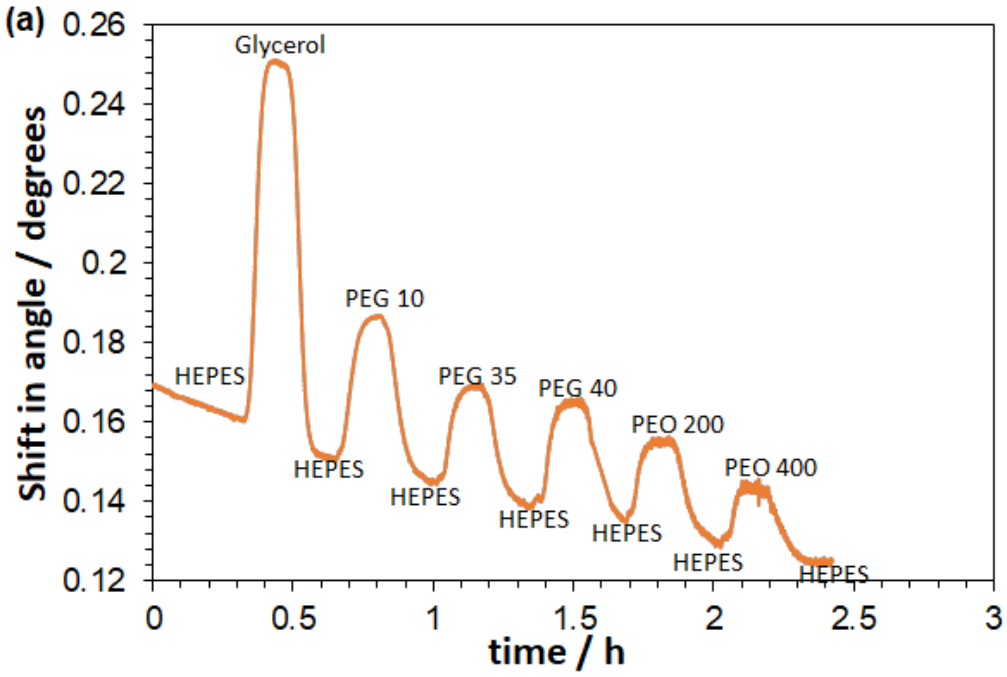

Figure 4.24: Reflectivity curve of waveguide layer with different molecular weights of cross linker (NHS-PEG-NHS) using 1% concentration of chitosan at a spin speed 900 rpm with 500 Da.

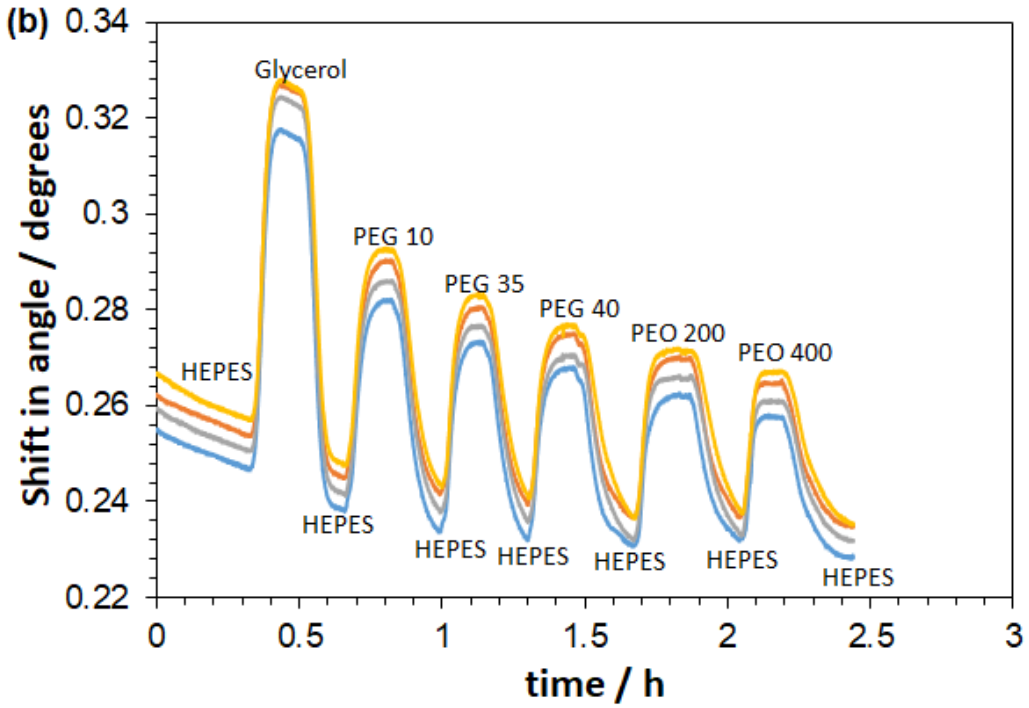

Figure 4.25: Reflectivity curve of waveguide layer with different molecular weights of cross linker (NHS-PEG-NHS) using 1% concentration of chitosan at a spin speed 900 rpm with 2 kDa (for 4 boxes).

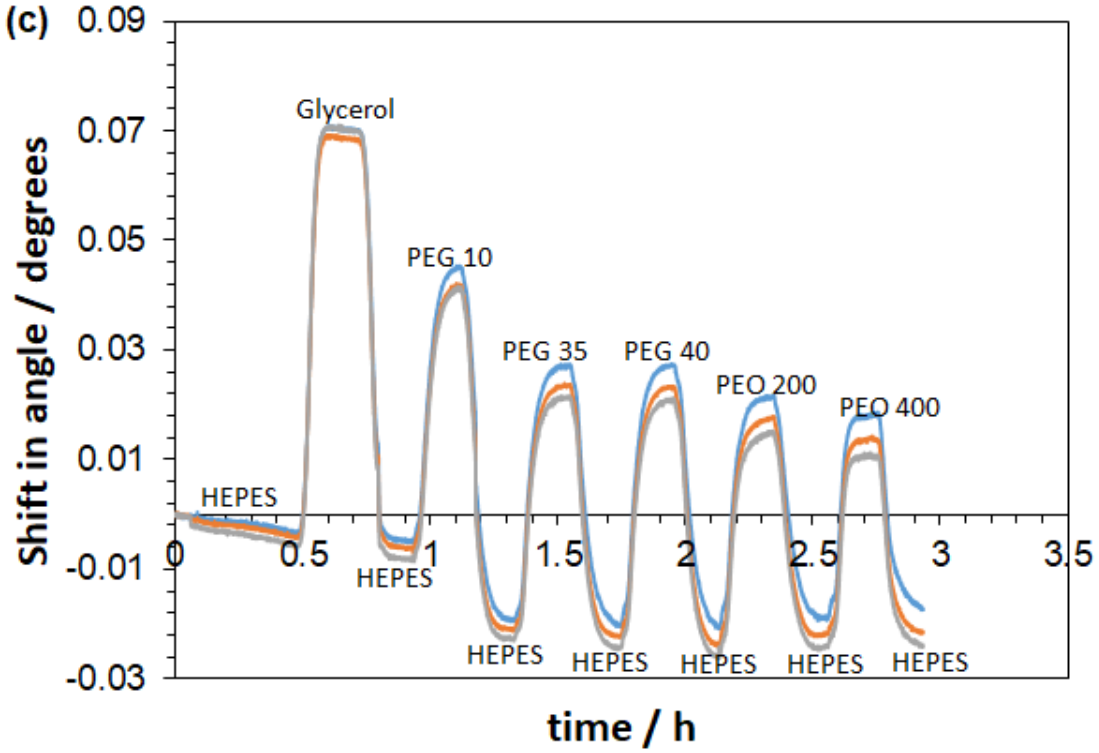

Figure 4.26: Reflectivity curve of waveguide layer with different molecular weights of cross linker (NHS-PEG-NHS) using 1% concentration of chitosan at a spin speed 900 rpm with 3 kDa (for 3 boxes).

A significant enhancement in the pore size of chitosan was also observed with a surface that was initially crosslinked with 3 kDa of NHS-PEG-NHS. As illustrated in fig.4.26, the movement of the dip position on applying different solutions having the same refractive index value is highly similar for each solution. This indicates the superior improvement in the chitosan's pore size. The porosity on the surface somewhat varies in size as shown in the figure, with different shifting between lines. Non-crosslinked surfaces (fig.4.19, have shown the highest shift in angle among all conditions that were used. Therefore, the variation in the pore size of the chitosan waveguide was clearly observed. This would be related to the fluctuations in humidity and temperature that can have an impact on the porosity of the waveguide film.

4.3.5 Effect of different pH

The experiment to study the effect of different pH values on the waveguide film was performed with the optimum condition of chitosan waveguide using a crosslinker (3 kDa) of NHS-PEG-NHS, as shown in Fig.4.27, crosslinking the chitosan molecules by a covalent bond with an amino group would help to prevent the dissolving of chitosan at lower pH.

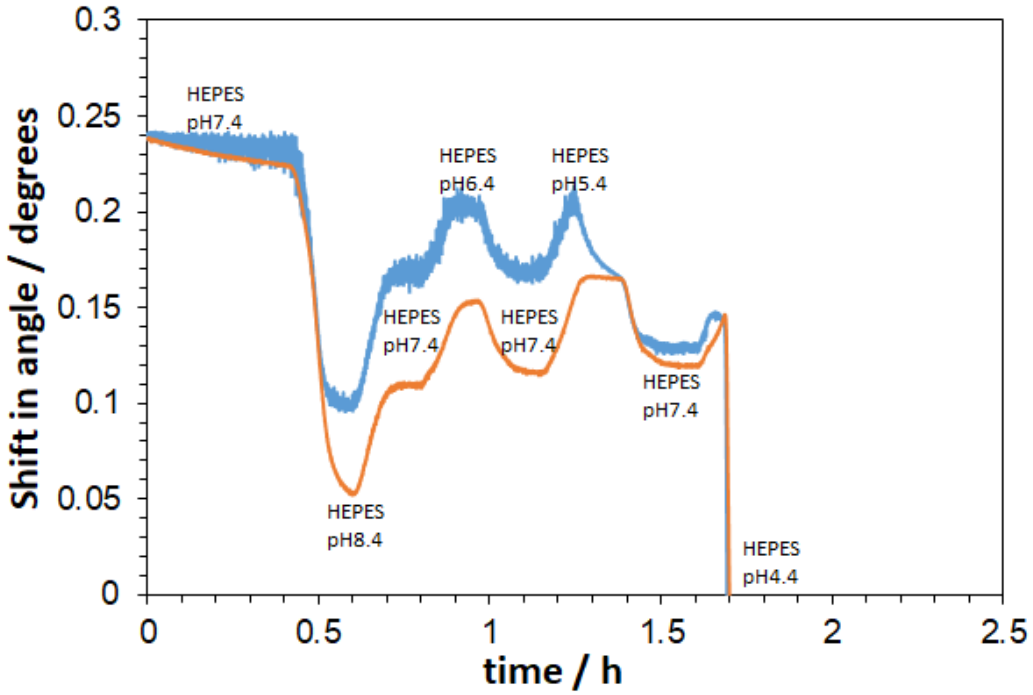

Figure 4.27: Changes in the reflectivity dip angle over time using different pH solutions of HEPES buffer (8.4, 7.4, 6.4, 5.4 and 4.4). The surface was initially incubated with the cross linker (Mwt 3000 Da) and the RB4 dye (100 mM) for 5 min (for 2 bobex).

The degree of shift under different pH of HEPES buffer between pH 7.4 and 8.4 was close to that obtained with the previous experiment without cross-linker (see fig.4.21). Unfortunately, the chitosan waveguide dissolved at lower pH as indicated in fig.4.28.

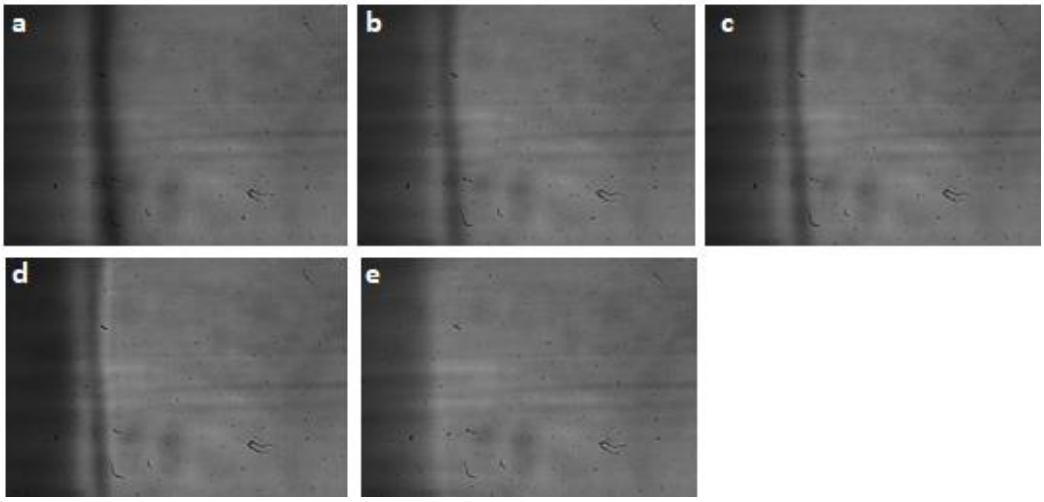

Figure 4.28: profile pictures captured by the camera of glass slide injected with different pH solutions. a: HEPES pH 7.4 buffer; b: HEPES pH 8.4 buffer; c: HEPES pH 6.4 buffer; d: HEPES pH 5.4 buffer and e: HEPES pH 4.4 buffer.

This would suggest that the amino groups of the chitosan layer are not bound with the cross-linker into the chitosan layer. That is because the optimum pH for the reaction between the amino groups and NHS was recommended in the literature to be higher (between 8 and 8.5). This can be related to the fact that at higher pH, more covalent bonds occur. That is due to the more deprotonation of the amino groups existing in the waveguide film. This experiment has proved that the variations in the porosity of the waveguide layer can be controlled by the drying time of the chitosan layer, and they are not related to the length of the cross-linker.

4.4 Conclusion

In the previous chapter, we have seen by monitoring the shifting in the dip position it can be concluded that none of the solutions can be diffused inside the 2% of chitosan waveguide due to the extremely small pore size.

Therefore, different methodologies were used to enhance the porosity of the chitosan film. Diffusion of silica beads into the chitosan layer has shown remarkable results where BSA molecules can easily diffuse inside the chitosan hydrogel. However, the chitosan film cannot be stable under NaOH treatment. Controlling the drying time of chitosan that can provide a waveguide mode with an enhancement, to some extent, in the porosity of the waveguide layer that has achieved fascinating results where the pore size was large enough for all molecules. Moreover, crosslinking of the chitosan waveguide with cross-linkers (NHS-PEG-NHS) of different lengths has been used in drying time experiments for enhancement of the pore size of the waveguide film at 3 min drying time. Therefore, this experiment has indicated that the variations in the porosity of the 1% chitosan layer coated at 900 rpm can be controlled by drying time. This was considered the optimum condition, and it is not related to the length of a cross-linker.

CHAPTER 5

Surface Characterisation of

Waveguide layer

This chapter describes techniques used to characterise the thin hydrogel waveguide film. The function at its best, the waveguide layer should be smooth, of good optical quality and sufficiently large high pore size to allow penetration and immobilisation of the binding antibody and sample components of interest. The surface flatness and thickness of the spin-coated chitosan layer were profiled by means of white light interferometry and a Dektak surface profiler. The porosity of the waveguide layer was studied with confocal microscopy. As will be discussed in the following section. In this chapter, the techniques relevant to my research are described.

5.1 Surface Characterisation of a Leaky Waveguide Film

5.1.1 White Light Interferometer (WLI)

White light interferometry is a versatile measurement technology for examining surface thickness with very high precision. The basic principle of this interferometer depends on the wave superposition principle to combine waves in a way that will cause the results of their combination to extract information from these simultaneous wavefronts. It is an optical device that will split a beam of light coming from a broadband white light source into two beams, the reference and measurement beams and then recombines them to create bright and dark bands called fringes (similar to lines on a topographic map). The reference beam is reflected by the reference mirror, whereas the measurement beam is reflected or scattered from the sample surface[134]. The returning beams are retransmitted to the CCD image sensor by the beam splitter, and the interference pattern of the sample surface topography is spatially sampled by the individual CCD pixels [134] as indicated in fig.5.1.

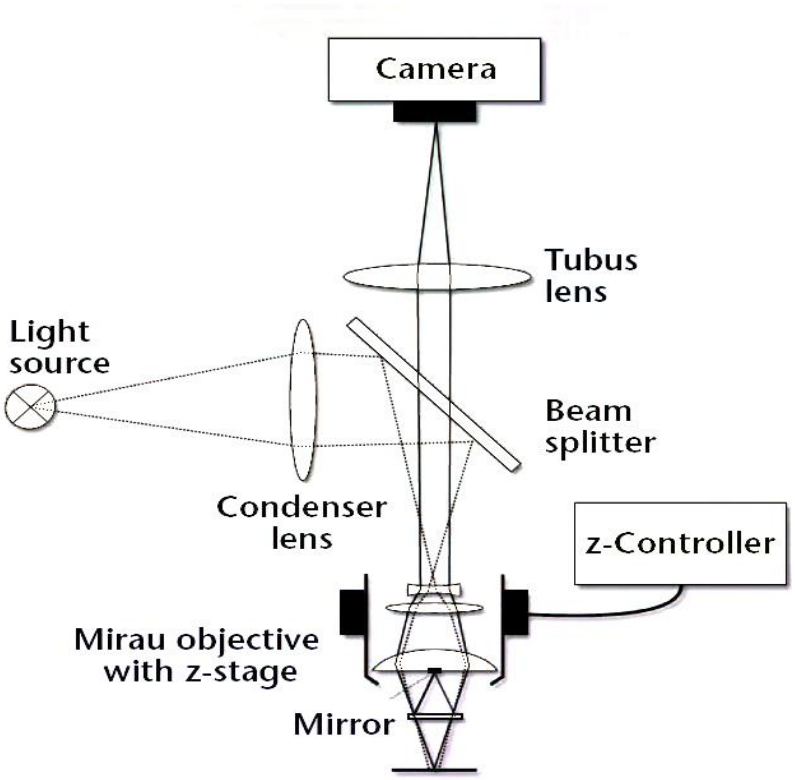

Figure 5.1: Schematic layout of white light interferometer microscope [135].

The thickness of a thin chitosan film can be obtained from further measurement by analysing the interference fringes of the film obtained from a White light interferometer (WLI). Different concentrations of chitosan (0.5, 1, and 1.5%) were prepared in 10 mL of 0.1 M of acetic acid stirred till totally dissolved as described in section 2.8: see Figure 5.2. As can be seen in table 5.1, increasing the chitosan concentration lead to an increase in the viscosity of the solution. The thickness of a waveguide film is easily changed by changing the viscosity of chitosan solution.

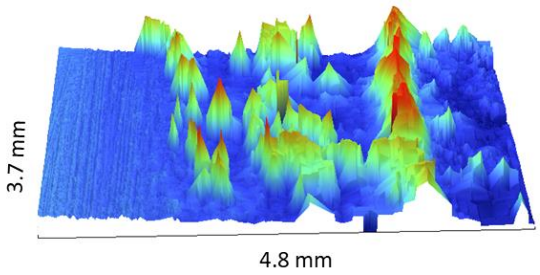

Figure 5.2: Waveguide chitosan film thickness as measured by a White light interferometer (WLI) for 1% of chitosan.

Table 5.1: Thickness of different concentrations (0.5%, 1% and 1.5%) of chitosan thin film using White Light Interferometer (WLI) (n=3).

Concentration / %	Thickness / nm
0.5	119.7
1	663.9
1.5	1046.8

5.1.2 Dektak Profilometer

The Bruker Dektak XT profilometer can measure film thickness by sensing the deviation of a flexible stylus which scans over features fluctuating in height between 1 mm and 5 nm. Thus, the surface roughness of the chitosan waveguide film can be measured on both flat and curved surfaces. Accurate profile measurement required scanning across a significant portion of the substrate centre (typically 70% or higher), and scans before and after the deposition of chitosan should be represented the same portion of the substrate [136].

The sensing mechanism depends on the moving of a diamond-tipped stylus across the substrate surface according to user-programmed scan length, style force and speed (fig.5.3). The stylus is connected to a linear variable differential transformer (LVDT) that generates and processes electrical signals which correspond to the surface variations of the sample. These surface variations are stored after being converted to a digital format for display and analysis.

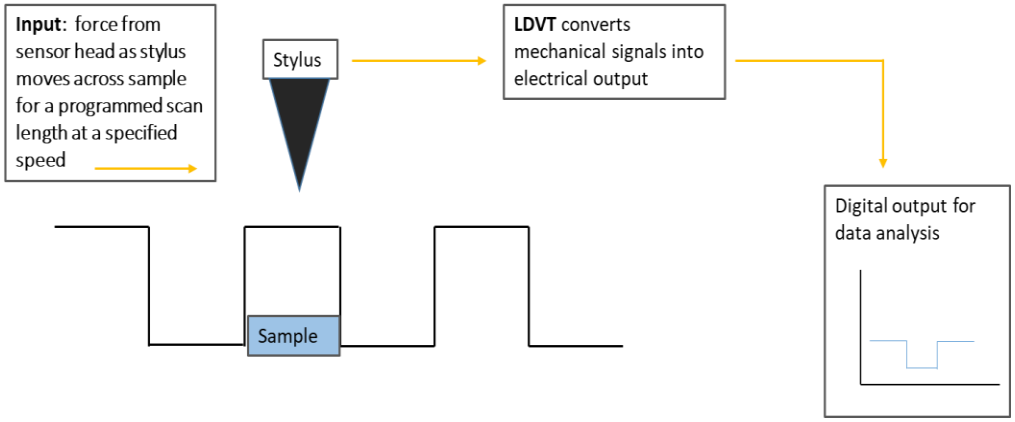

Figure 5.3: overview of the sensing mechanism during data measurement by Dektak XT Bruker profilometer [137]

Data was provided by the Dektak XT of the flatness of different concentrations of the chitosan film spin-coated onto glass substrate at different spin speeds in an experiment performed as described in section 2.8. The surface characterization of 1% chitosan thin film using this contact measurement technique is illustrated in fig.5.4.

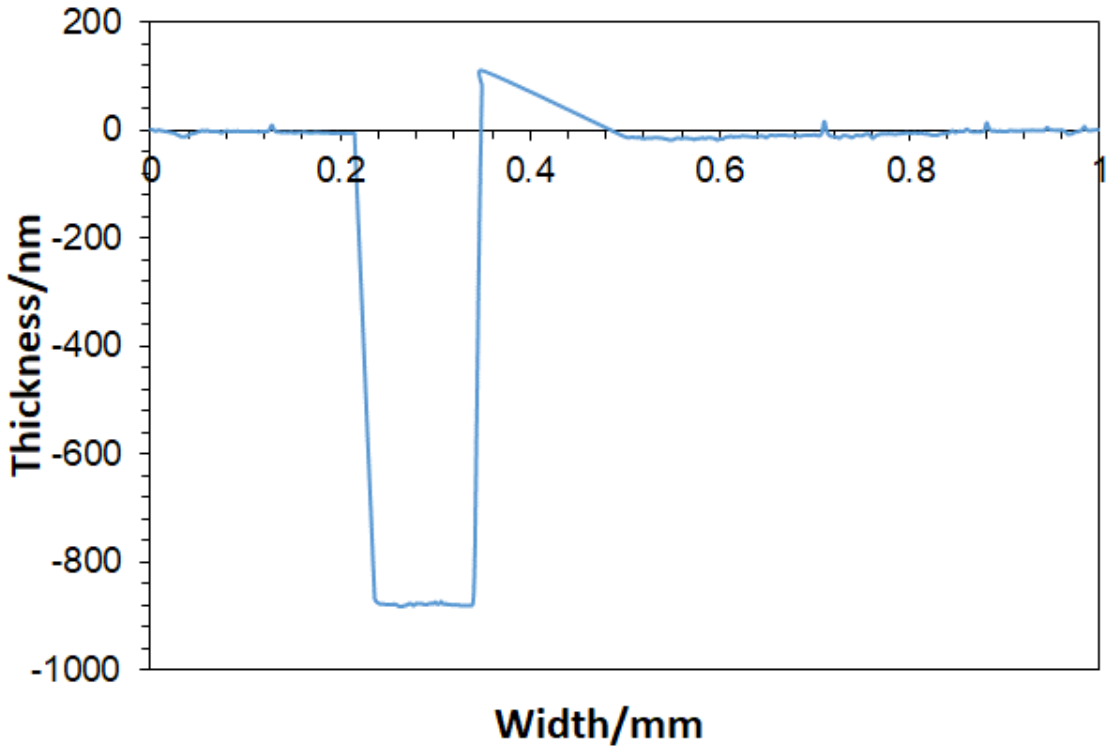

Figure 5.4: Surface characterization of 1% chitosan thin film spin coated onto a glass slide at spin speed 200 rpm, using Dektak XT Bruker profilometer.

Different concentrations of chitosan were coated onto the glass surface, and three slides were prepared for each concentration to allow for reproducibility at different spin coating speeds as indicated in table 5.2. to measure the flatness of the waveguide film for each slide.

Table 5.2: Average measurements for different concentrations of chitosan thin film at different spin coating speeds (n=3).

Concentration / (%)	Spin Coat / RPM	Thickness / nm	Thickness average / nm
1	200	920, 876, 864	886.66
	500	665, 531, 560	585.33
	900	101, 105, 97	101
1.5	300	554, 597, 611	587.33
	700	346, 341, 396	361
	900	263, 232, 267	254
2	2800	210, 207, 207	208
	3000	175, 168, 164	169
	3500	152, 149, 154	151.66

The measurements in the above table are of the thickness of the film for each concentration. Each measurement has been repeated three times, with different thicknesses that are approximately close to each other.

5.1.3 ImageJ Surface Characterization

The whole surface of glass slides of the chitosan thin film waveguide was scanned for different concentrations of chitosan (1%, 1.5% and 2%). A thin film spin-coated at different spin speeds, as indicated in fig.5.5, before waveguide run in terms of analysis these data by using ImageJ software (figs.5.6, and 5.7).

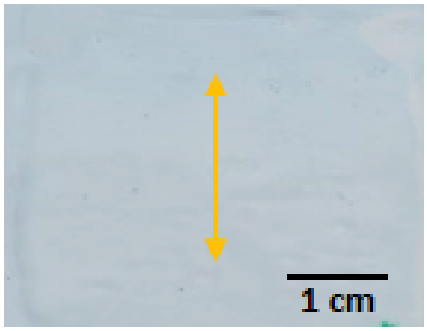

Figure 5.5: 1% chitosan thin film spin-coated onto a glass slide (before waveguide run), with the yellow arrow indicating profiled region.

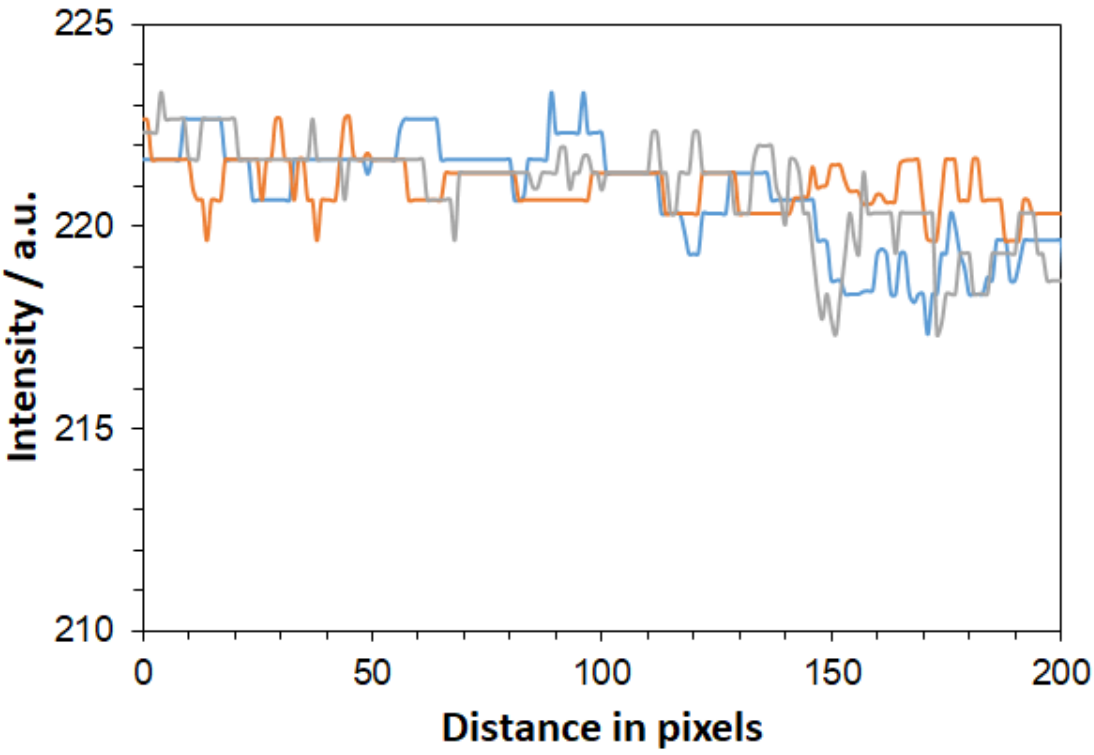

Figure 5.6: Image J surface characterization of 1% chitosan thin film spin coated onto a glass slide (before waveguide run).

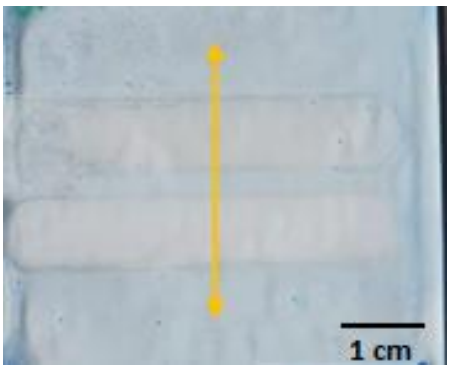

Figure 5.7: 1% chitosan thin film spin coated onto a glass slide (after waveguide run). Imprints on slide indicate flow cell regions, with a yellow arrow indicating characterized region.

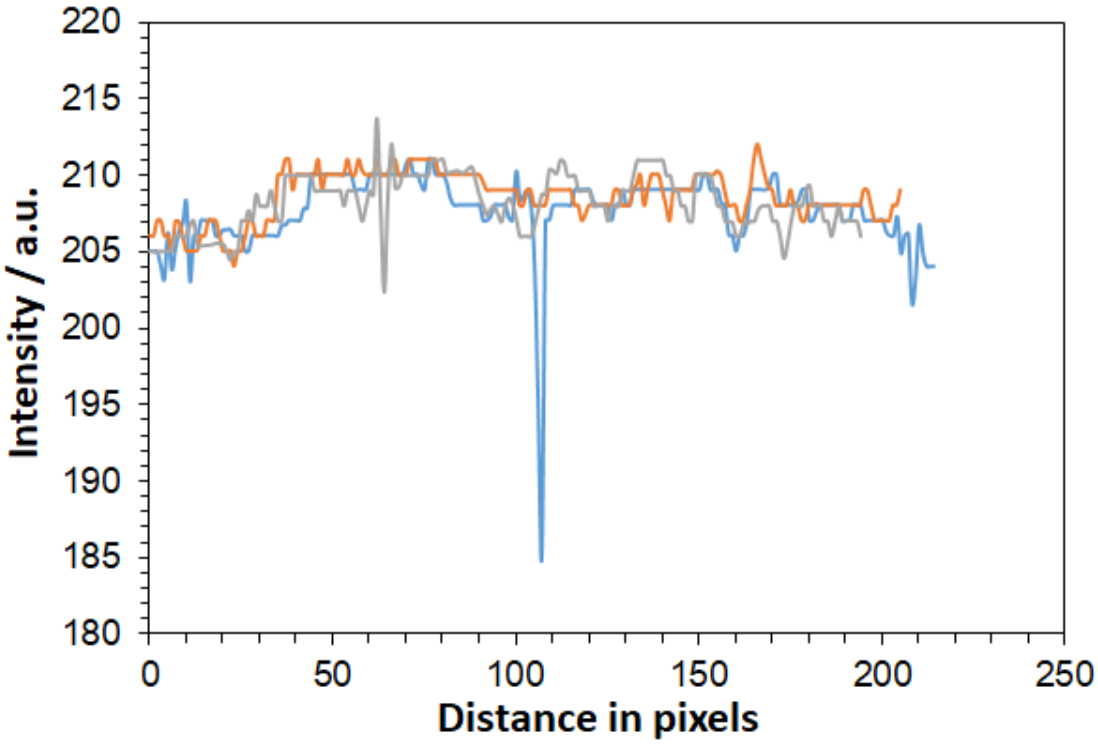

Figure 5.8: Image J surface profiling of 1% chitosan thin film spin coated onto a glass slide (after waveguide run).

A comparison was made of 1% waveguide chitosan thin film before and after waveguide run. The surface characterization includes flow cell regions which come into close contact with the chitosan thin film. Here, the values obtained through the blue channel are compared to show the before and after differences of 1% chitosan film incubated in 100 mM of reactive blue 4 dye solution.

Here, figs.5.6 and 5.8 indicate a significant difference in intensity of blue channel values within the flow cell regions. This also indicates removal of reactive blue 4 dye and the

instability of the waveguide thin film during a waveguide run see figs.5.9 and 5.10 for 1.5% and 2% of chitosan thin film.

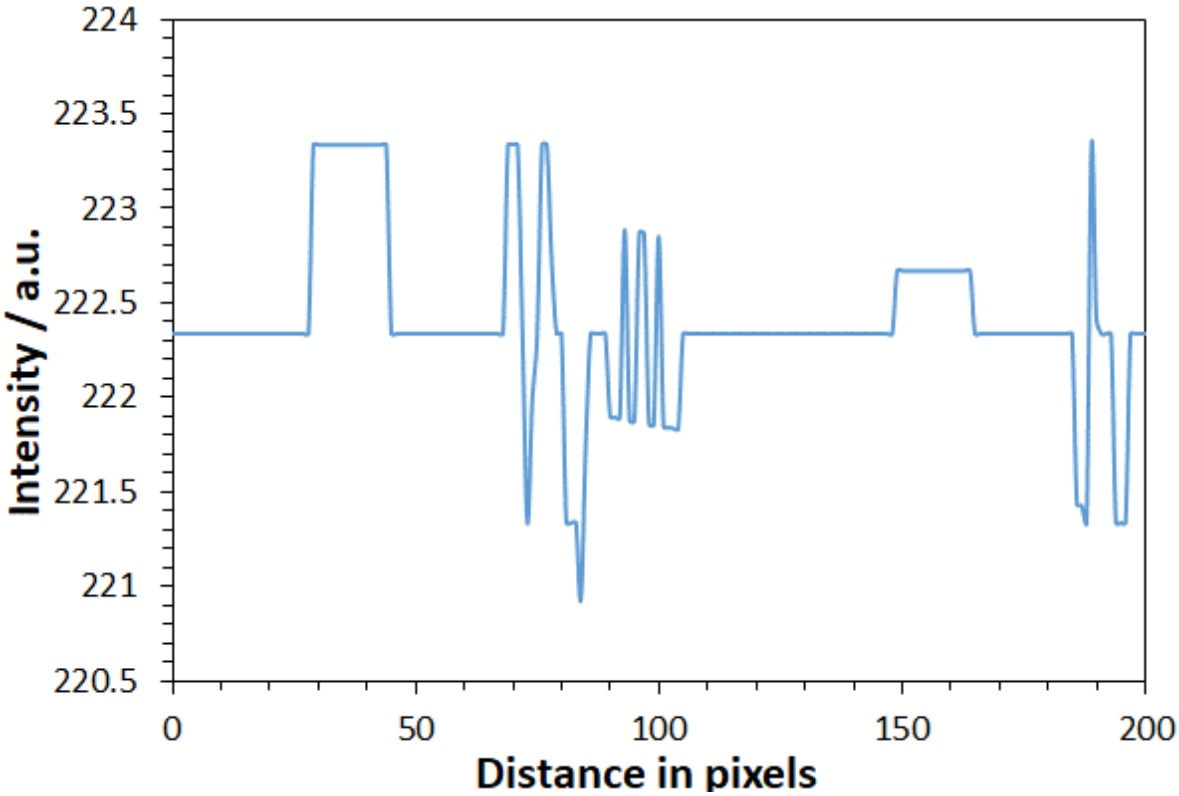

Figure 5.9: Image J surface characterization of 1.5% chitosan thin film spin-coated onto a glass slide, spin speed 500 rpm.

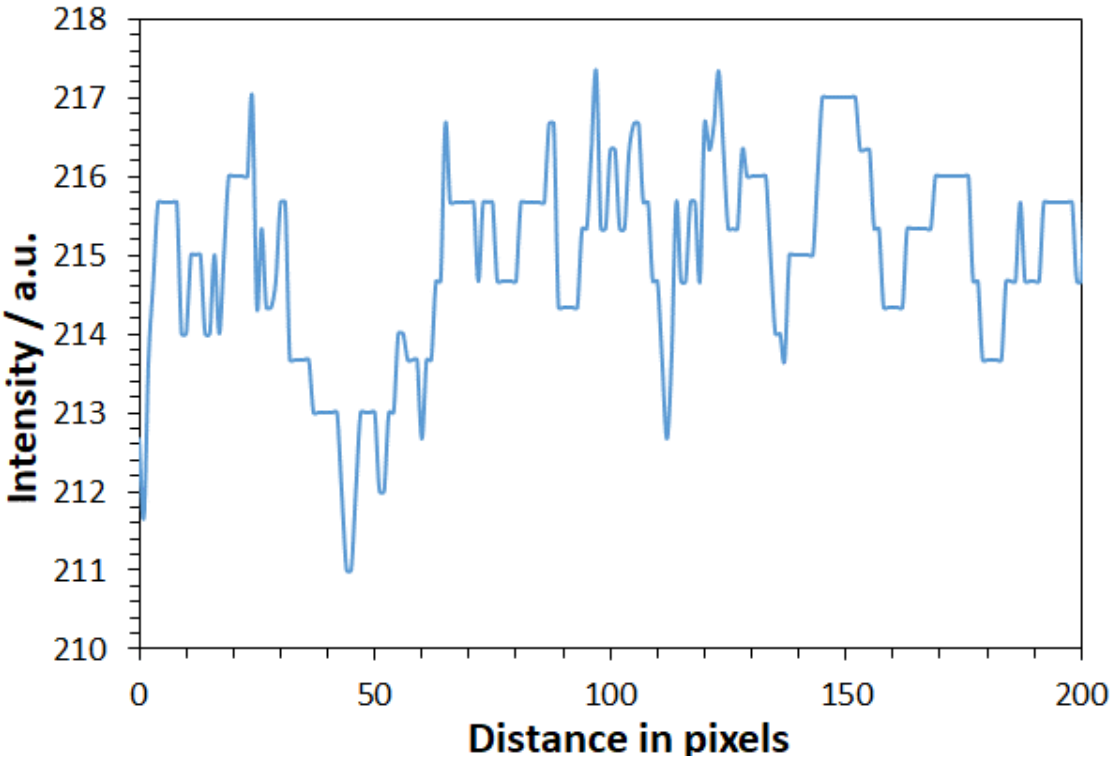

Figure 5.10: Image J surface characterization of 2% chitosan thin film spin-coated onto a glass slide, spin speed 2800 rpm.

5.1.4 Confocal Scanning Microscope

Measurement of the porosity of the waveguide thin film is a great benefit in the step of immobilising biorecognition elements, in this research, anti-rabbit IgG as a model of the antibody. Therefore, the confocal microscope was used: its key feature is that it is capable of producing blur-free images of thick films at different depths. The excitation wavelength for the fluorescence imaging was 488 nm, and emitted light was collected above 500 nm [138].

Waveguide films were incubated in Fluorescein Isothiocyanate (FITC) for 15 min followed by fluorescence and reflectance imaging. Images of the Chitosan film were taken point-by-point and recomposed with a computer rather than observed through an eyepiece [139] as indicated in Figure 5.11.

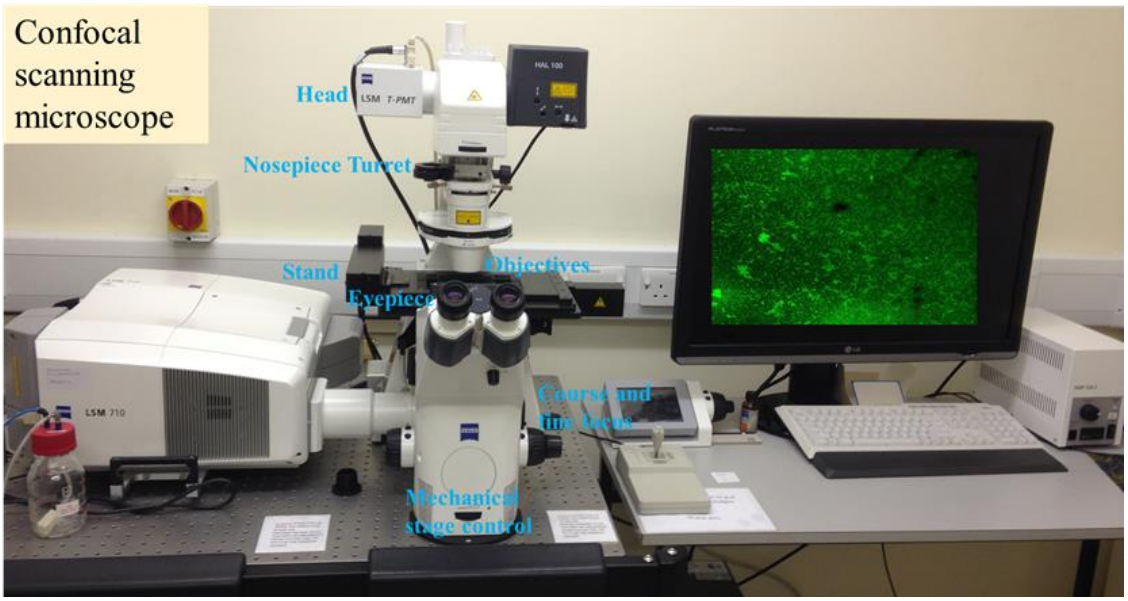

Figure 5.11: Confocal scanning microscope

Under the confocal scanning microscope, the porosity and uniformity of chitosan waveguide films were evaluated, and 1 % of chitosan waveguides prepared with different drying times (1, 2, 3, 4 and 5 min), were compared with this and measured.

Porosity measurements indicated that the chitosan solution dispensed on the substrate (glass slides) was thicker round the edges when they were coated at a spin speed of 900 rpm (range=2-50 µm) than in the centre of the substrate (range=2-10 µm).The reflected light confocal images showed a non-uniform structure in all the corner chitosan films

examined as illustrated in fig.5.12. This is similar to the images in biofilms that had been measured by WLI and Dektak profilometer previously.

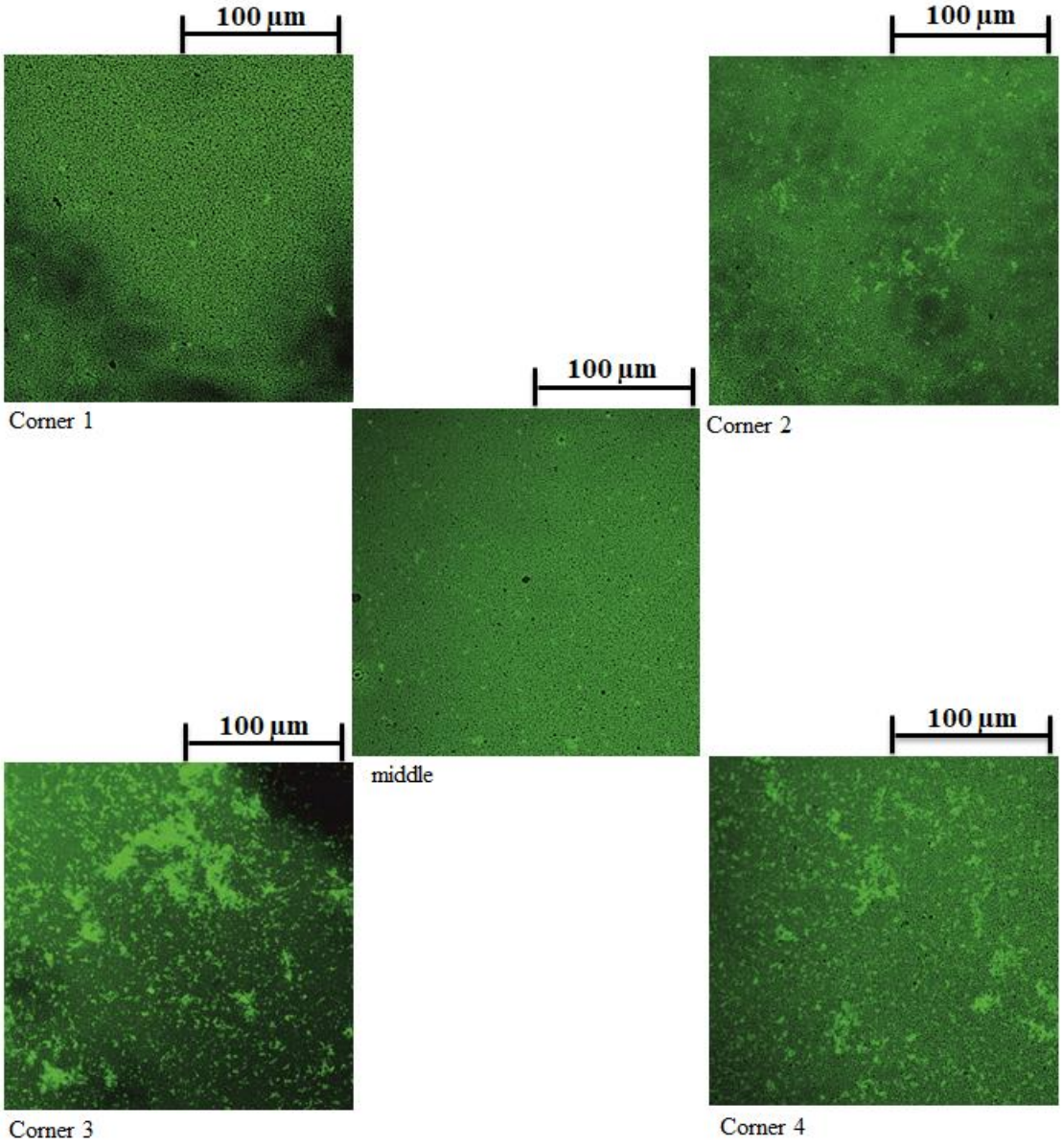

Figure 5.12: Confocal laser microscopic images of 1% chitosan films with different drying times (1, 2, 3, 4 and 5 min) spin-coated at 900 rpm of various corners of the substrate. (a): corner 1; (b): corner 2; (c): corner 3; (d): corner 4; and (e): middle. Chitosan films were incubated with Fluorescein Isothiocyanate (FITC).

5.2 Conclusion

All the techniques that have been used in this chapter to characterize the waveguide thin film obtain high optical quality for different concentrations of chitosan thin film spin-coated at different spin speeds to be available for the immobilization step. A white light interferometer was used for examining the surface thickness of the spin-coated chitosan layer. That indicated that increasing the chitosan concentration in the thin film led to an increase in the viscosity of the solution. The thickness of the waveguide films is easily changed by changing the viscosity of the chitosan solution. The thicknesses were measured as indicated in table 5.1.

The Bruker Dektak XT profilometer 3D was also utilized to measure the thickness and uniformity of the thin film by scanning over features fluctuating in height between 1 mm to 5 nm. In seconds, the surface roughness of the chitosan waveguide film had been measured on both flat and curved surfaces. Accurate profile measurement needs scans across a more significant portion of the substrate centre (typically 70% or higher), and the deposition of chitosan before and after should be represented the same portion of the substrate. The measurement data was represented thickness for different concentrations (0.5, 1, and 2%) of chitosan has been repeated three times these different values of thickness. These experiments indicated removal of reactive blue 4 dye and the instability of the waveguide thin film during a waveguide run.

Moreover, the waveguide chitosan thin film has been scanned to a whole surface of glass slides for different concentrations of chitosan (1%, 1.5% and 2%) before and after waveguide run. The values obtained through the blue channel are compared to show before and after differences of 0.5, 1 and 2% of chitosan film incubated in 100 mM of reactive blue 4 dye solution. This also indicates removal of reactive blue 4 dye and the instability of the waveguide thin film during a waveguide run.

The Confocal Scanning Microscope has been of great benefit in the measurement of the porosity of the chitosan waveguide film. Porosity measurements indicated that the chitosan solution dispensed on the substrate (glass slides) was thicker round the edges at spin coated 900 rpm (range=2-50 μm) than in the centre of the substrate (range=2-10 μm). This means there is a difference in the porosity with different dry time and different spotted for the same substrate.

CHAPTER 6

Immobilisation of antibody

(Anti-rabbit IgG)

This chapter reports how the dye-doped leaky waveguide sensor was applied for measuring small concentrations of the antibody anti-rabbit IgG into the porous layers (chitosan thin film)[80]. This project includes creation of responsive hydrogel thin films dyed by reactive blue 4 dye to visualise the confinement, and which causes a dip in the reflectivity curve at a resonance angle, as well as measuring this film by an optical waveguide. Different forms of immobilization chemistry will be used in this section in order to modify the chitosan layer with biomolecules such as antibodies (anti-IgG) through its entire volume to allow specific binding for immunoassays. The binding of rabbit IgG to anti-rabbit IgG will be investigated as an initial example application. Such binding events cause a change in refractive index within the waveguide layer and thus a shift in the resonance angle (dip). This is used for quantification of the binding events occurring in the waveguide layer.

6.1 Immobilization of anti-rabbit IgG

A range of immobilisation chemistries were tried to immobilise the antibody in the waveguide thin film, such as covalent binding, site-specific binding, biotin-streptavidin interactions, intermediate proteins, and affinity tags.

6.1.1 Using EDC-Sulpho-NHS chemistry

Antibodies are specific proteins produced in the body to resist pathogenic invaders called antigens, also referred to as immunoglobulins. Similar to all proteins, antibodies include carboxylic acid and amino groups. They can divided into two main classes, IgG and IgM each has different roles and resists different pathogens.

The most prominent strategies are based on the covalent binding of antibodies, as this is rapid, highly stable antibody-binding, leach-proof with high immobilisation density. The heterobifunctional is used most widely of the covalent binding strategies for crosslinking the carboxyl groups on the antibody to the free amino groups in the waveguide thin film using EDC ((1-Ethyl-3-(3-dimethylaminopropyl), which is a carbodiimide along with Sulpho-NHS to form an O-acylisourea ester [140]. Subsequently amide bonds are formed with the amino groups present in the chitosan film as indicated in Figure 6.1. Sulpho-NHS is used to stabilize the intermediate in the crosslinking reaction.

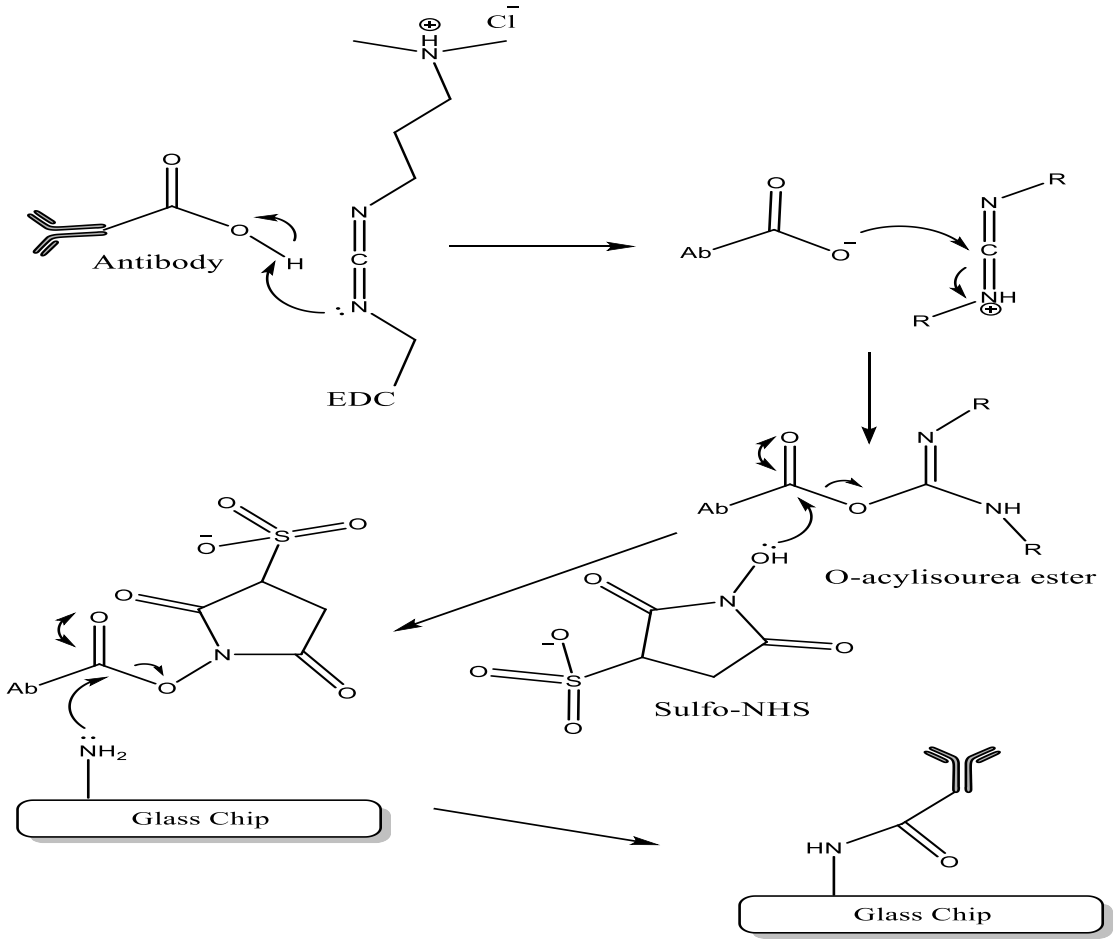

Figure 6.1: Schematic diagram indicating the mechanism to immobilize the antibody onto the amine groups of the chitosan film on the glass surface by using EDC-Sulpho NHS strategy.

Immobilisation of polyclonal anti-rabbit IgG antibody using different ratios of EDC-Sulpho-NHS based crosslinking method [141]. Figure 6.2, shows the results of the first experiment to investigate the binding of polyclonal anti-IgG onto the amine groups of the waveguide layer as described in section 2.9.1

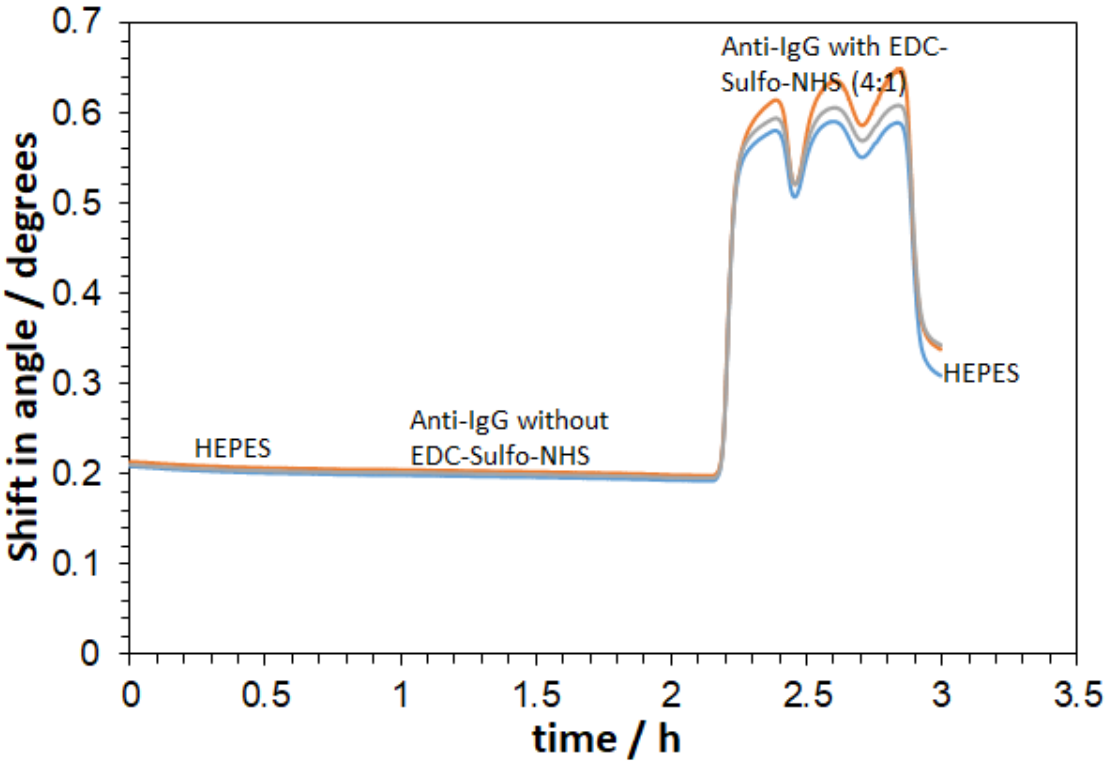

Figure 6.2: Changes in the reflectivity dip angle over time using two different solutions (HEPES buffer and anti-IgG without EDC-Sulpho-NHS) 0.01 µM for one hour, then anti-IgG with EDC-Sulpho-NHS was pumped also for one hour). The surface initially incubated with cross linker (3000 Dalton) and RB4 dye for 5 min.

NHS-PEG-NHS is a cross linker which is used to stabilize the waveguide thin film and compare the results of the immobilization as shown in Figure 6.3 and Figure 6.4.

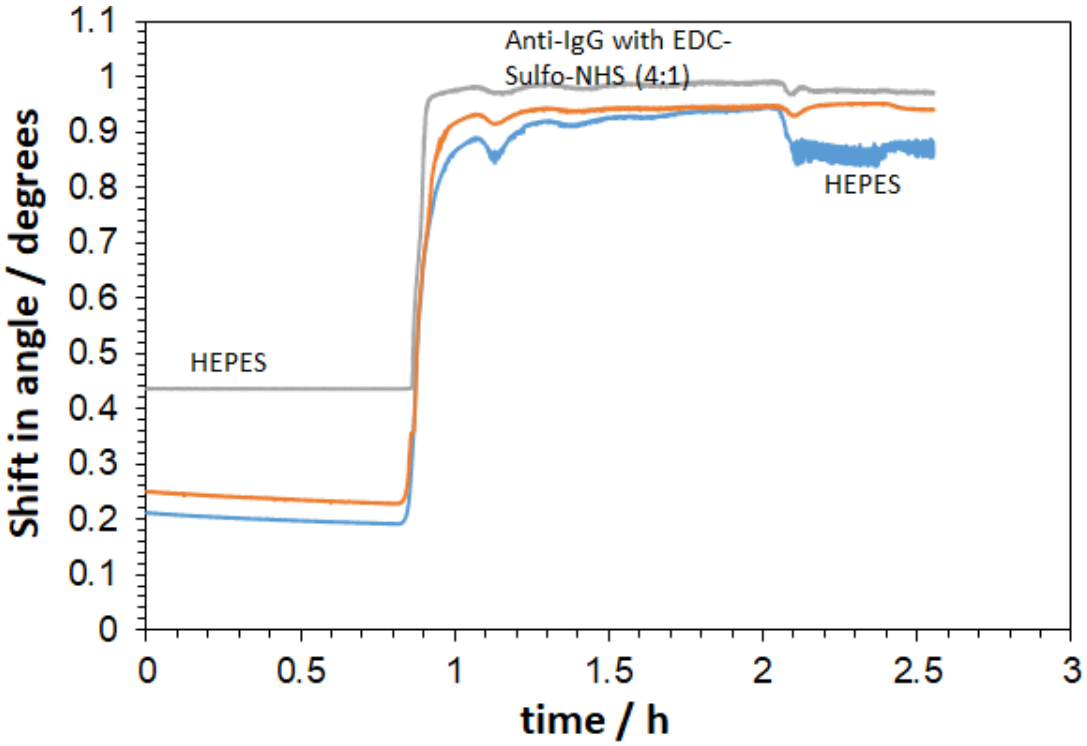

Figure 6.3: Changes in the reflectivity dip angle over time using two different solutions (HEPES buffer and Anti-rabbit IgG 0.01 µM for one hour). The surface initially incubated with dye for 5 min, without cross linker for thee boxes.

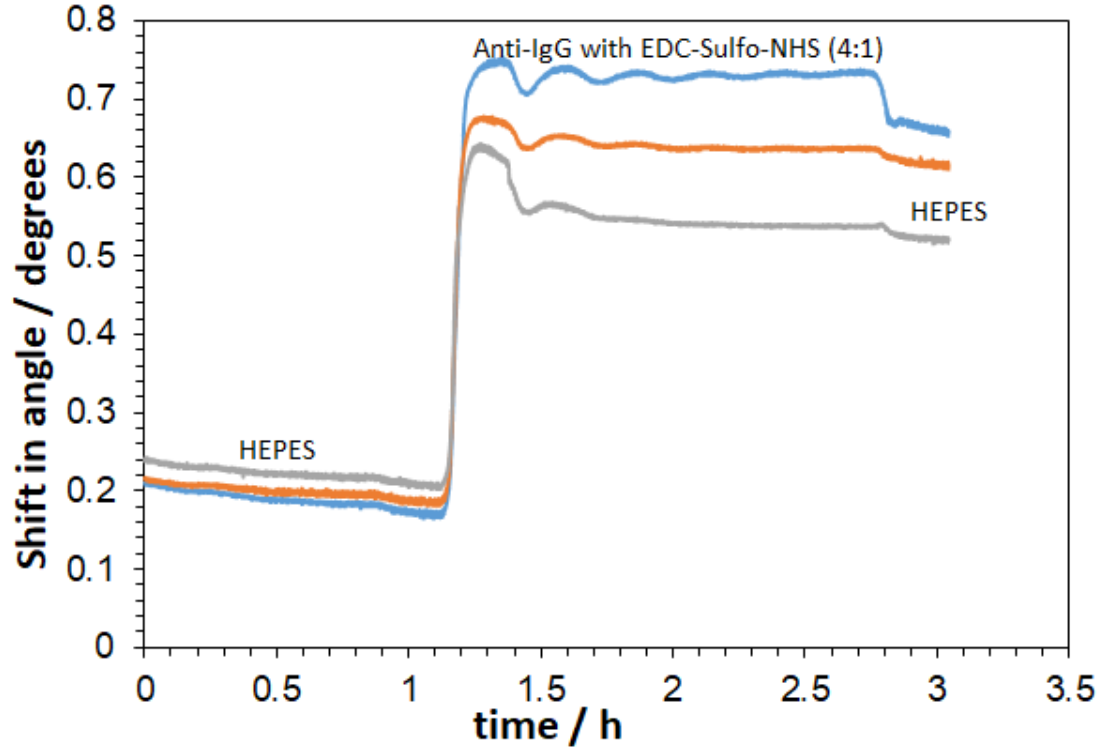

Figure 6.4: Changes in the reflectivity dip angle over time using two different solutions (0.01 µM HEPES buffer and Anti-rabbit IgG) for half an hour with EDC and Sulpho-NHS and without it). The surface initially incubated with cross linker (3000 Dalton) and RB 4 dye for 5 min for 3 boxes.

It is clear that there was a shift in the angle degree once Anti-Rabbit IgG solution ($2.5*10^{-9}$ M) with EDC-Sulpho-NHS was injected into the sensing area of the waveguide thin film for one hour. The dip position did not return to a straight line with HEPES buffer pH7.4, indicating the binding of the antibody into the chitosan waveguide film. Fig.6.2 indicates when injection of the antibody without EDC-Sulpho-NHS there is still not showing any binding for the antibody with the waveguide film there is no shift observed still straight line.0.5% of BSA was used as blocking molecules for nonspecific binding after immobilizing the polyclonal anti-IgG 10^{-9} M. Then detection rabbit polyclonal IgG (10^{-7} M) was injected in order to ensure that the antibody was successfully immobilised into the chitosan waveguide film (see fig.6.5).

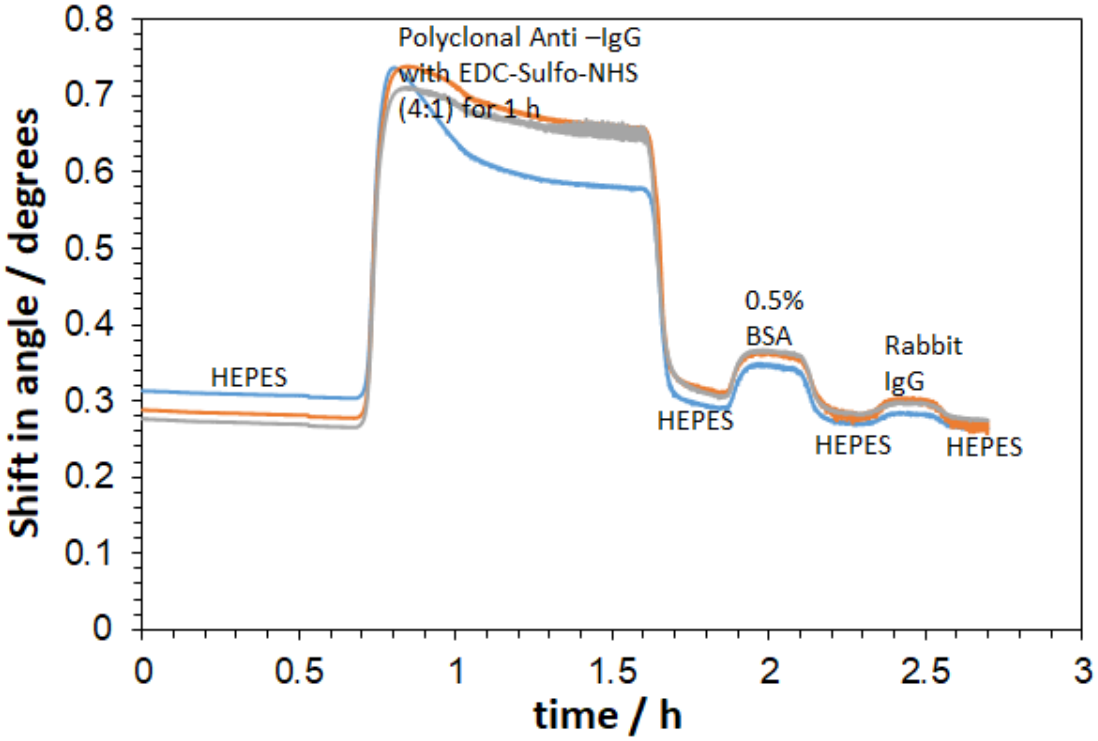

Figure 6.5: Changes in the reflectivity dip angle over time using different solutions (HEPES buffer (pH 7.4) and polyclonal Anti-rabbit IgG (0.01 µM) for one hour interacting with detection antigen 0.1 µM), the surface initially incubated with dye for 5min for 3 boxes.

A complementary binding of the antibody (Anti-rabbit IgG) with the detection antigen (Rabbit IgG) was prepared in HEPES buffer as described in section 2.9.1 which indicates the immobilization process where the high shift was obtained with Anti-Rabbit IgG ($2.5*10^{-9}$ M) followed by flushing with HEPES buffer pH7.4 to remove any unbounded anti-IgG. Bovine serum albumin (BSA) 0.5% followed Anti-IgG as a blocking molecule for nonspecific binding, then Rabbit IgG (10^{-7} M) was flushed to react with the antibody as a complementary binding [142].

According to Figure 6.5 it can be said that the antibody (Anti-IgG) was immobilized into the chitosan waveguide film via reaction between the amine groups of the chitosan layer and the carboxylic acid of the antibody, but there is no reaction between the polyclonal antibody and antigen. That is very clear when the preparation was flushed with HEPES buffer, after which the reflectivity dip angle goes down to a straight line. It was hypothesized that is may be related to the antibody because it would be polyclonal (non-specific) binding. Therefore, the next experiment t tested the use of monoclonal antibody.

6.1.1.1 Using ratio 1:4 of EDC-Sulpho-NHS [143]

The amine groups in the chitosan waveguide layer can bind with the carboxyl group through an activation process by using of EDC-Sulpho-NHS in the ratio 1:4. Figure 6.6 represents the immobilization of the anti-Rabbit IgG conjugated with the carboxyl group activated with EDC-Sulpho-NHS before being injected into the sensing area into the waveguide layer.

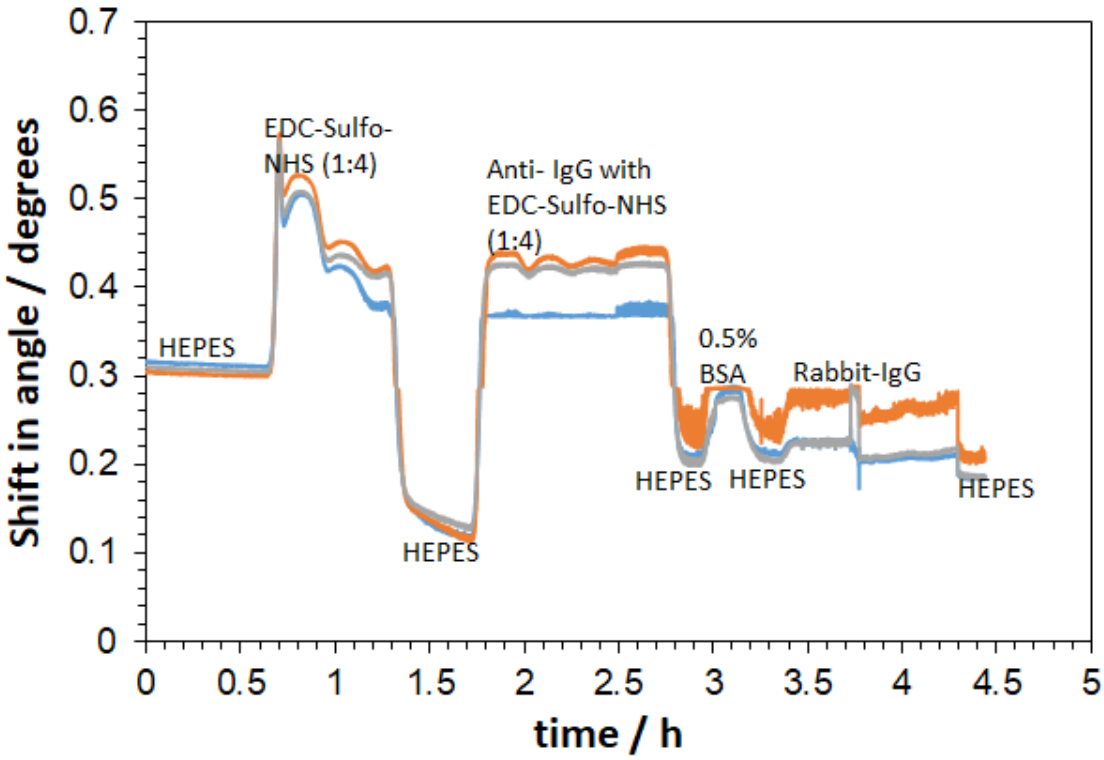

Figure 6.6: Changes in the reflectivity dip angle over time using different solutions (HEPES buffer pH 7.4, EDC-Sulpho NHS (1:4) and Anti-Rabbit monoclonal IgG (10^{-7} M) for 2 hrs with EDC-Sulpho NHS (1:4), 0.5% BSA as a blocking molecule and monoclonal rabbit IgG (10^{-7} M); the surface initially incubated with the RB4 dye (100 µM) for 5 min.

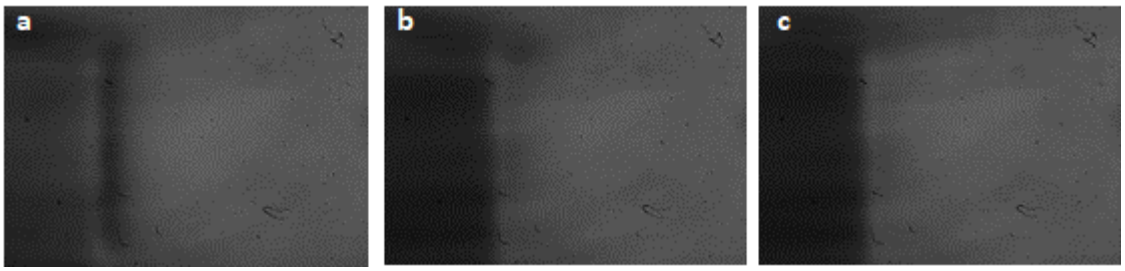

Figure 6.7: profile pictures captured by the camera of glass slide immobilised with EDC-ph (1:4), then with the monoclonal Anti-rabbit IgG (0.01 µM) for 2 hrs at pH7.4 a: with HEPES buffer pH7.4; b: with EDC-Sulpho-NHS (1:4), and c: with Anti-rabbit IgG activated by EDC and Sulpho-NHS (1:4).

From fig.6.7, there is a clear shift with the EDC-Sulpho-NHS solution to a high degree in angle and the dip was fully washed away when HEPES buffer was pumped fig 6.7c. Therefore, different ratio of EDC-Sulpho-NHS were tried.

6.1.1.2 Using ratio 1:1 of EDC-Sulpho NHS [144]

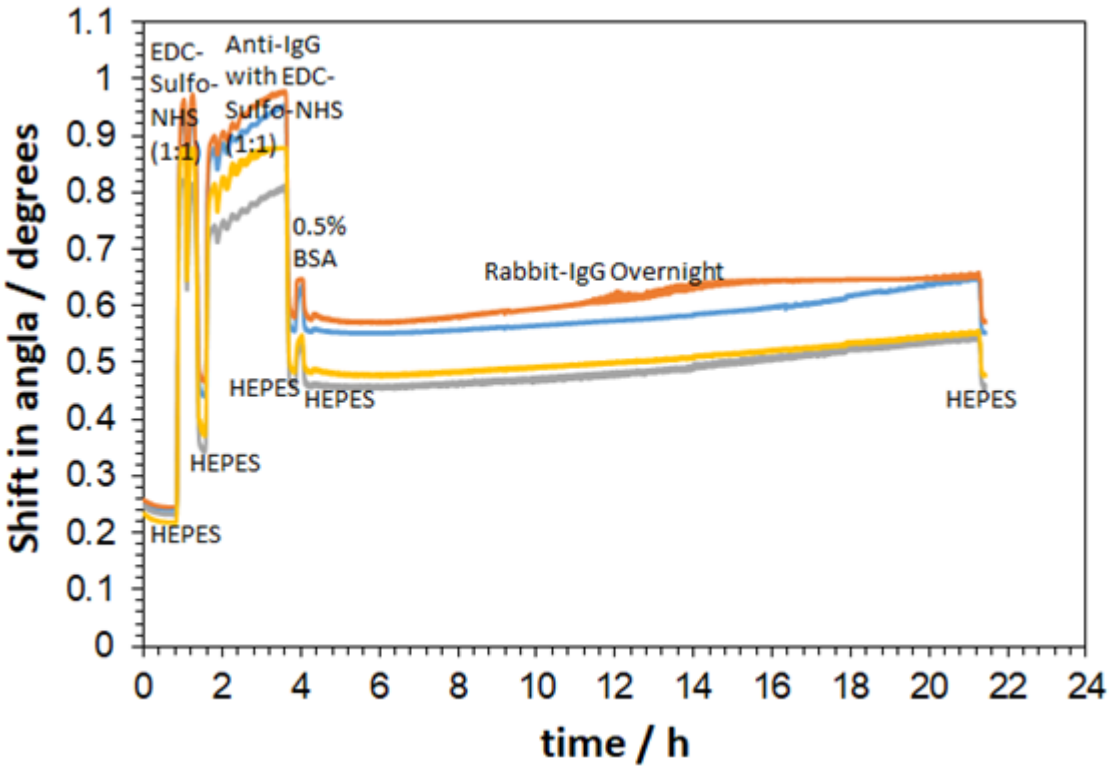

Figure 6.8: Changes in the reflectivity dip angle over time using different solutions (HEPES buffer pH 7.4, EDC-Sulpho-NHS (1:1) and Anti-Rabbit monoclonal IgG (0.01 µM) for 2 hrs with EDC-Sulpho-NHS (1:1), 0.5% BSA as blocking molecule and monoclonal rabbit IgG (0.1 µM); the surface initially incubated with RB4 dye (100 µM) for 5 min.

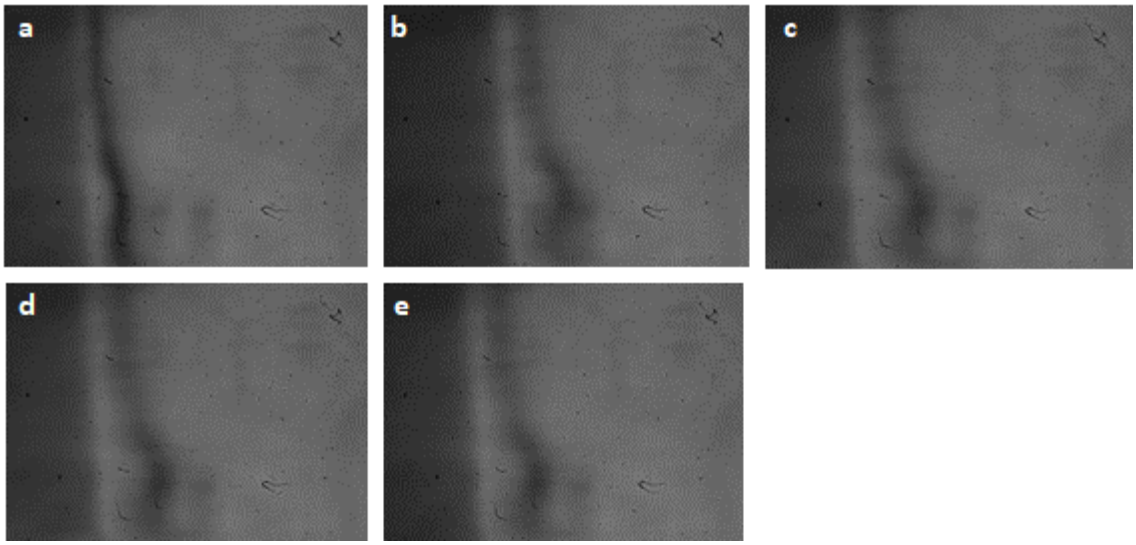

Figure 6.9: profile pictures captured by the camera of glass slide immobilised with EDC-Sulpho-NHS (1:1), then with the monoclonal Anti-rabbit IgG (0.01 µM) for 2 hrs at pH7.4 a: with HEPES buffer pH7.4; b: with EDC-Sulpho-NHS (1:1), c: with Anti-rabbit IgG activated by EDC-Sulpho-NHS (1:1), d: with 0.5% BSA, and e: with monoclonal rabbit IgG (0.1 µM).

Fig. 6.8, indicates the immobilization process of the antibody by using EDC-Sulpho-NHS (1:1), there is a clear shifting in the degree of the antibody was very little and although the dip is not washed away but became lighter see fig.6.9, and the sensitivity of the reaction between the antibody and the antigen was very low, therefore, this reaction will be enhanced by using different ratio of EDC-Sulpho-NHS.

6.1.1.3 Using ratio 4:1 of EDC-Sulpho NHS [145]

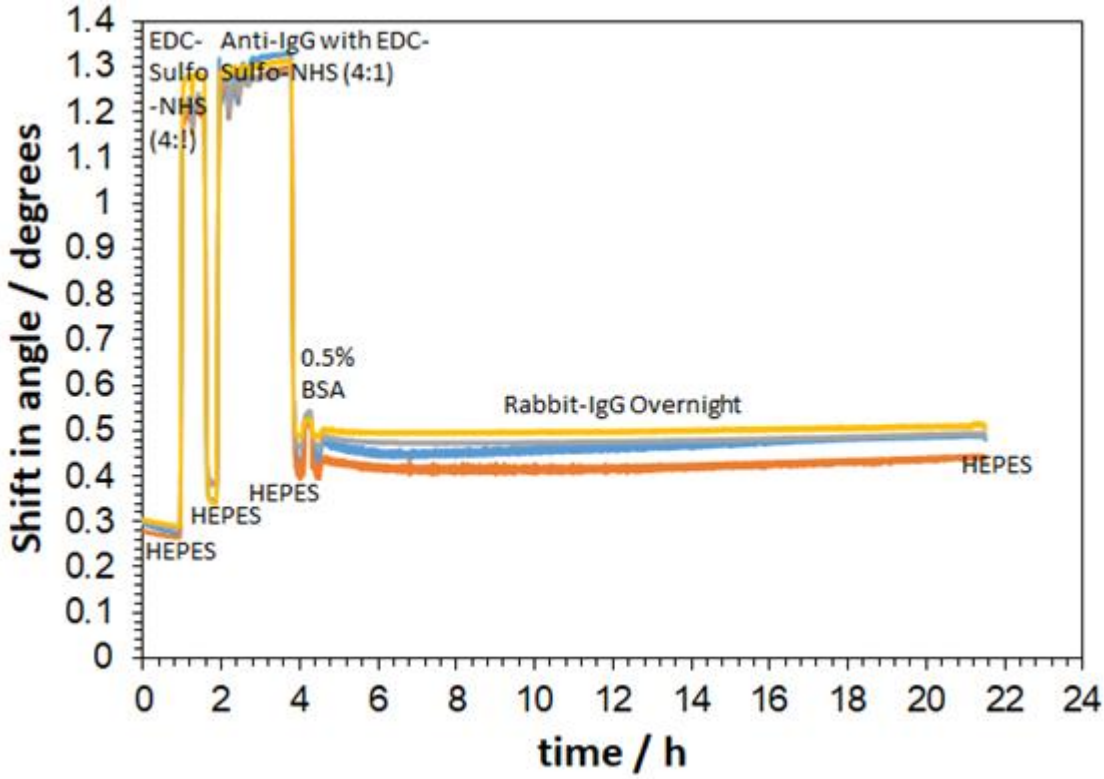

Figure 6.10: Changes in the reflectivity dip angle over time using different solutions (HEPES buffer pH 7.4, EDC-Sulpho-NHS (4:1) and Anti-Rabbit monoclonal IgG (0.01 µM) for 2 hrs with EDC-Sulpho-NHS (4:1), 0.5% BSA as blocking molecule and monoclonal rabbit IgG (0.1 µM). The surface was initially incubated with the RB 4 dye (100 µM) for 5 min.

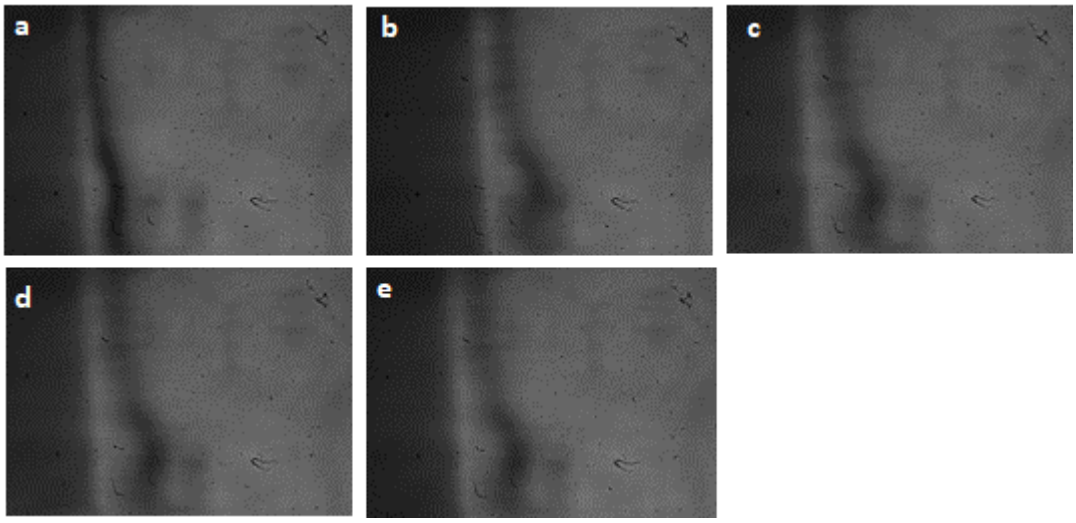

Figure 6.11: profile pictures captured by the camera of glass slide immobilised with EDC-Sulpho-NHS (4:1), then with the monoclonal Anti-rabbit IgG (0.01 µM) for 2hrs at pH7.4 a: with HEPES buffer pH7.4; b: with EDC-Sulpho-NHS (4:1); c: with Anti-rabbit IgG activated by EDC- Sulpho-NHS (4:1); d: with 0.5% BSA; and e: with the monoclonal rabbit IgG (0.1 µM).

The binding of the antibody (Anti-Rabbit IgG) into the waveguide chitosan film was enhanced. Fig.6.10, indicates that the shift in degree with the antibody activated by EDC-Sulpho-NHS (4:1) can be clearly observed fig.6.11, and the sensitivity of the reaction of the antibody with the antigen was better than when EDC-Sulpho-NHS used in ratios of 1:4 and 1:1. However, the next experiment focused on the optimisation of antibody immobilization and enhancing of the sensitivity for the reaction between the antibody and the antigen (Anti-Rabbit IgG and Rabbit-IgG).

6.1.2 Optimization of antibody immobilization

6.1.2.1 Cross linker

Cross linking is the important factor influencing antibody immobilization. This is related to the stability of the antibody, loading amount, and the sensitivity reaction of the antibody with the antigen in the waveguide chitosan layer[146]. 1 mM of N-hydroxysuccinimide-polyethylene-glycol-N-hydroxysuccinimide prepared in 100 mM of HEPES buffer, length 3000 Dalton, was used with 3 min of drying time.

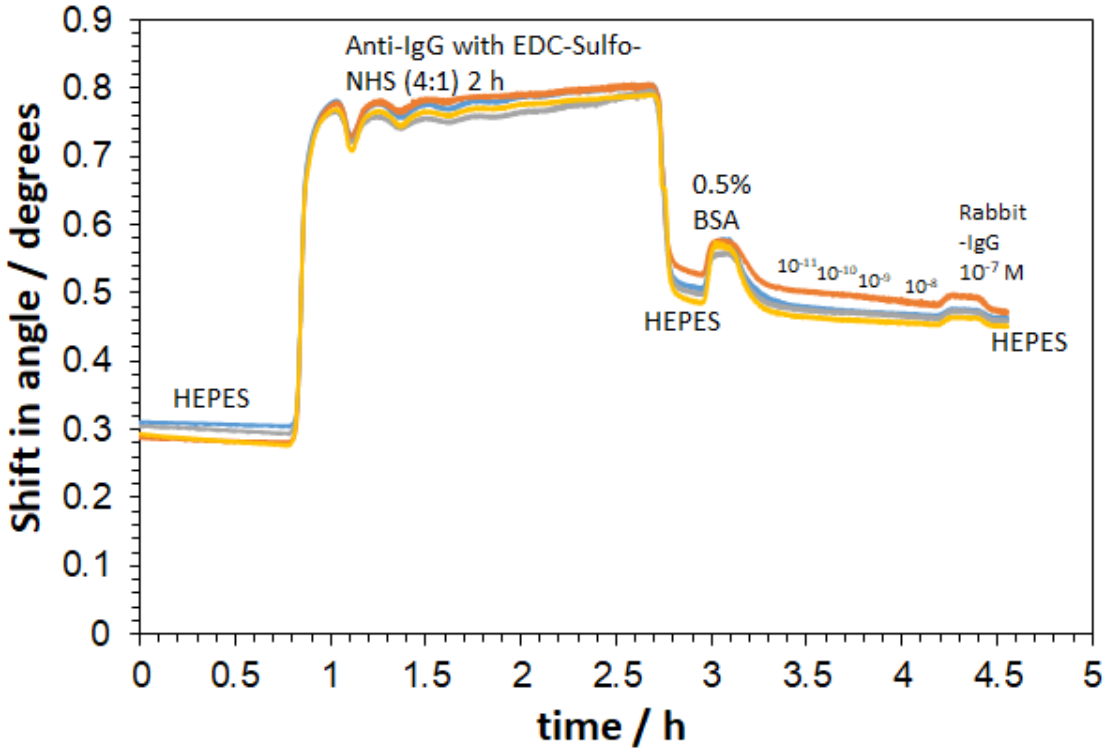

Figure 6.12: Changes in the reflectivity dip angle over time using two different solutions (HEPES buffer and Anti-Rabbit monoclonal IgG (0.01 µM) for 2 hrs with EDC-Sulpho-NHS 4:1), 0.5% BSA as blocking molecule and monoclonal rabbit IgG (0.1 µM). The surface was initially incubated with a cross linker (3000 Dalton) and (100 µM) RB 4 dye for 5 min.

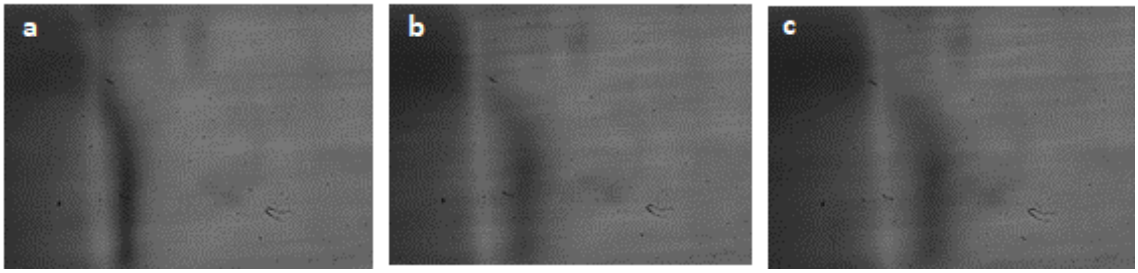

Figure 6.13 profile pictures captured by the camera of glass slide immobilised with monoclonal Anti-rabbit IgG (0.01 µM) for 2 hrs. a:HEPES buffer; b: Anti-rabbit IgG activated by EDC-Sulpho-NHS (4:1); and c: Rabbit -IgG.

As shown in Figs.6.12 and 6.13, when the antibody was immobilized into the waveguide chitosan film by using a cross linker, the degree of shift from the baseline was about 0.3º,and the sensitivity of the reaction with anti-Rabbit IgG when the detection antibody (rabbit-IgG) is pumped still does not show a high shift. Once HEPES buffer is flushed through the sensing area into chitosan film, the shift in angle goes down to a straight line.

6.1.2.2 Without a cross linker

The experiment was repeated with the same procedure but without a cross linker in order to study the effect of a cross linker on the antibody immobilization.

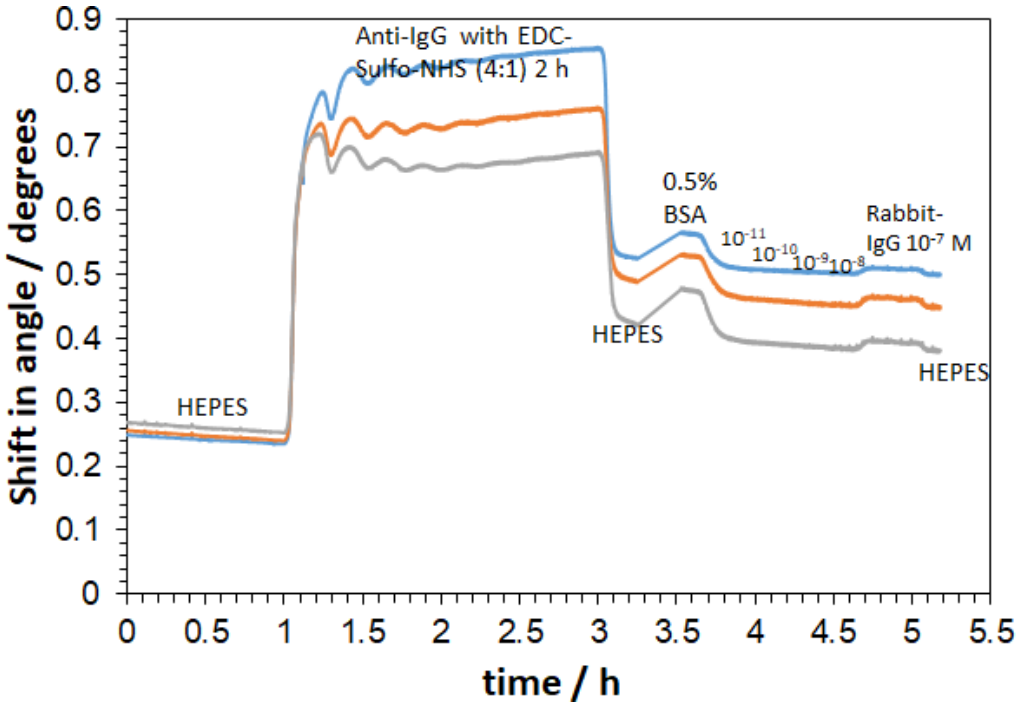

Figure 6.14: Changes in the reflectivity dip angle over time using two different solutions (HEPES buffer and Anti-Rabbit monoclonal IgG (0.01 µM) for 2 hrs with EDC-Sulpho-NHS 4:1), 0.5% BSA as blocking molecule and monoclonal rabbit IgG (0.1 µM). The surface was initially incubated with RB4 dye (100 µM) for 5 min.

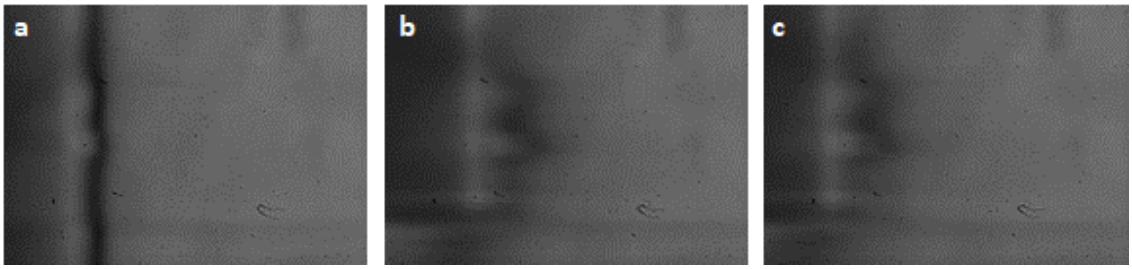

Figure 6.15: profile pictures captured by the camera of glass slide immobilised with monoclonal Anti-rabbit IgG and EDC-Sulpho-NHS (4:1) (0.01 µM) for 2 hrs. a: with HEPES buffer; b: with monoclonal Anti-Rabbit IgG activated by EDC-Sulpho-NHS (4:1) and c: Monoclonal Rabbit IgG.

Fig.6.14, shows the antibody immobilization process without using a cross linker. Comparison with Figure 6.12, which represents the antibody immobilization with a cross linker (NHS-PEG-NHS) shows that there is no difference between the two experiments in the angle, which was approximately 0.3º, and the sensitivity of the reaction Anti-IgG and detection IgG still does not show any difference. When the sensing area was flushed with HEPES buffer after the injection of detection IgG into the chitosan film, as described in section 2.10.1, the shift in the degree of angle returned fully to the straight line. This means there is no difference in antibody immobilization with a cross linker and without a cross linker. Also, there is no difference in the results of the two experiments for the binding between Anti-IgG and detection IgG.

6.1.2.3 Effect of pH

pH is an important parameter that has a significant role in the swelling and shrinking of the waveguide chitosan film by the protonation and de-protonation of the amine groups as explained in section 2.12.2. It has an effect also on the activity of EDC-Sulpho-NHS because the activation reaction of EDC-Sulpho-NHS is most efficient at pH4.5-6.5. This is because NHS esters have a half-life of more than 5 hrs, forming a more stable Sulpho-NHS intermediate that reacts slowly with amines to form a stable amide bond with the amino groups of the chitosan film [147]. This decreases as indicated in fig.6.16, when the buffer was flushed for only 10 min at pH8.5.

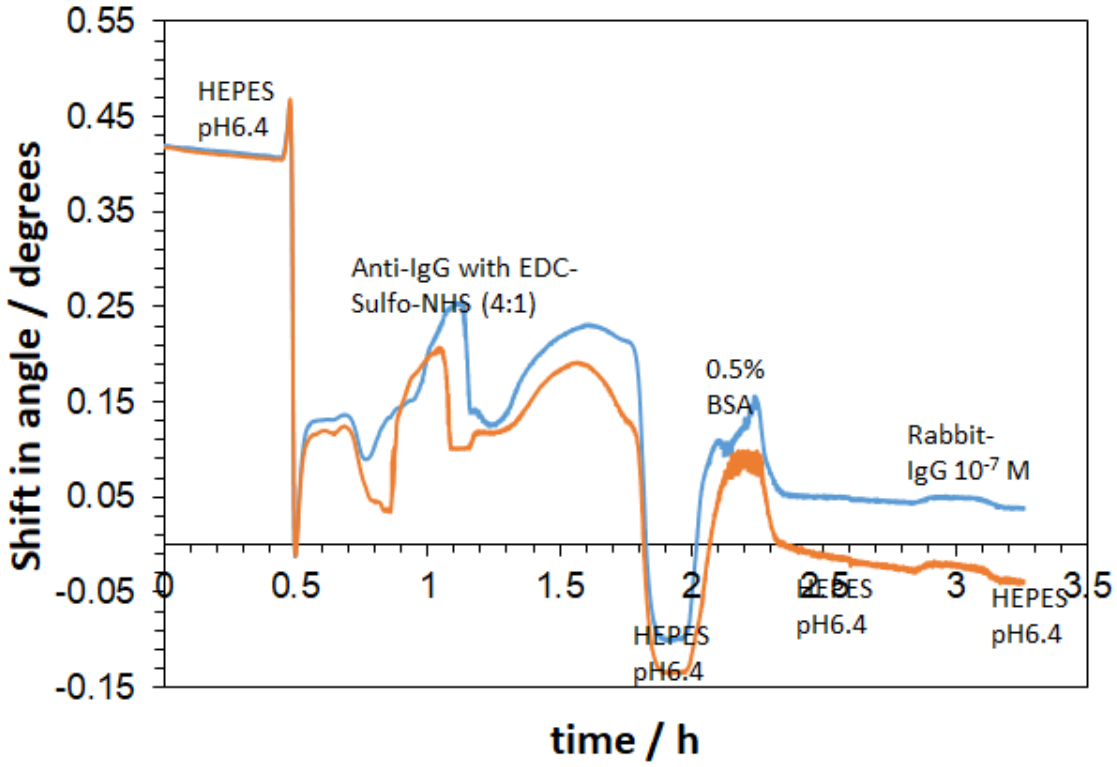

Figure 6.16: Changes in the reflectivity dip angle over time using two different solutions (HEPES buffer pH 6.4 and Anti-Rabbit monoclonal IgG (0.01 µM) for 2 hrs with EDC-Sulpho-NHS 4:1), 0.5% BSA as blocking molecule and monoclonal rabbit IgG (0.1 µM). The surface was initially incubated with RB4 dye (100 µM) for 5 min.

Figure 6.17: profile pictures captured by the camera of glass slide immobilised with monoclonal Anti-rabbit IgG (0.01 µM) and EDC-Sulpho-NHS (4:1) for 2 hrs at pH6.4. a: with HEPES buffer pH6.4; b: with monoclonal Anti-rabbit IgG activated by EDC and Sulpho-NHS (4:1); and c: Monoclonal Rabbit-IgG.

As indicated in fig.6.17, the dip is mostly dissolved at pH6.4 and the degree of shift decreases when flushed with the antibody (see fig.6.16). That's due to the fact that at lower pH (6.4) protonation of amino groups is taking place and to some extent, therefore, the chitosan film will be dissolved, which affects the antibody immobilization and the activity of EDC-Sulpho-NHS. That means the optimum pH value for the antibody immobilization process using EDC-Sulpho-NHS (4:1) is 7.4.

6.1.2.4 Optimise the concentration of detection IgG

This experiment was performed in order to detect the reaction of the antibody with detection IgG and its complementary reaction[148]. Different concentrations of monoclonal Rabbit-IgG (10^{-11}, 10^{-10}, 10^{-9}, 10^{-8} and 10^{-7} M) were prepared in HEPES buffer (pH7.4) and injected using a peristaltic pump, to show the binding between Anti-IgG and detection IgG.

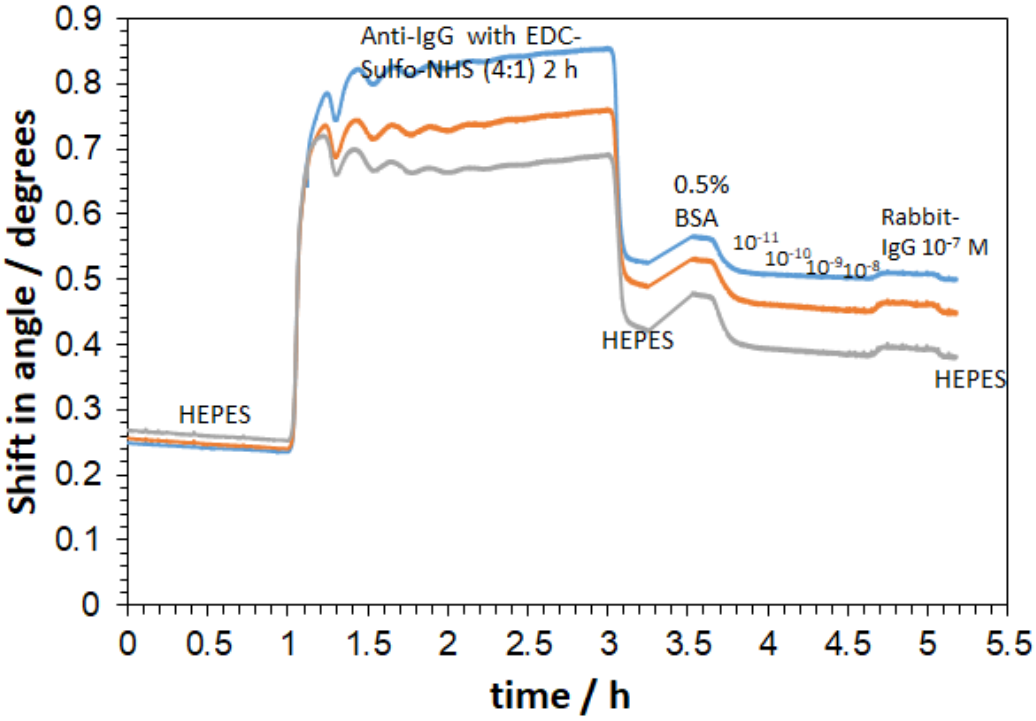

Figure 6.18: Changes in the reflectivity dip angle over time using two different solutions (HEPES buffer and Anti-Rabbit monoclonal IgG (10^{-8} M) for 2 hrs with (4:1) EDC-Sulpho-NHS), 0.5% BSA as blocking molecule and different concentrations of monoclonal rabbit IgG (10^{-11}, 10^{-10}, 10^{-9}, 10^{-8} and 10^{-7} M). The surface was initially incubated with RB4 dye (100 µM) for 5 min.

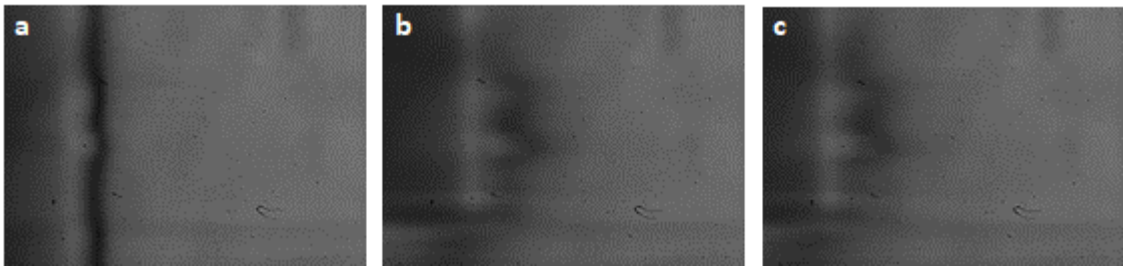

Figure 6.19: profile pictures captured by the camera of glass slide immobilised with monoclonal Anti-rabbit IgG (0.01 µM) for 2 hrs. a: with HEPES buffer; b: with Anti-rabbit IgG activated by (4:1) EDC-Sulpho-NHS; and c: with Monoclonal Rabbit-IgG.

Fig.6.18 and fig.6.19, are illustrate the antibody immobilization process where Anti-IgG was prepared in HEPES buffer at pH7.4, was pumped to the sensing area in the waveguide chitosan film for 2 hrs until a straight line was obtained. The shift is clearly observable with Anti-IgG, followed by HEPES buffer pH7.4 that shifted the dip position to a few degrees lower. To detect the binding of the antibody with the antigen different concentrations of detection IgG were flushed until only 10^{-7} M was detected as lower concentration.

6.1.3 Enhancement of the interaction sensitivity

6.1.3.1 Increasing interaction time for anti-IgG with detection IgG

The binding of Anti-Rabbit IgG into the waveguide chitosan layer to enhance the interaction sensitivity of Anti-IgG with detection-IgG can be improved by increasing the time of incubation between the antibody and the amino groups of the chitosan film.

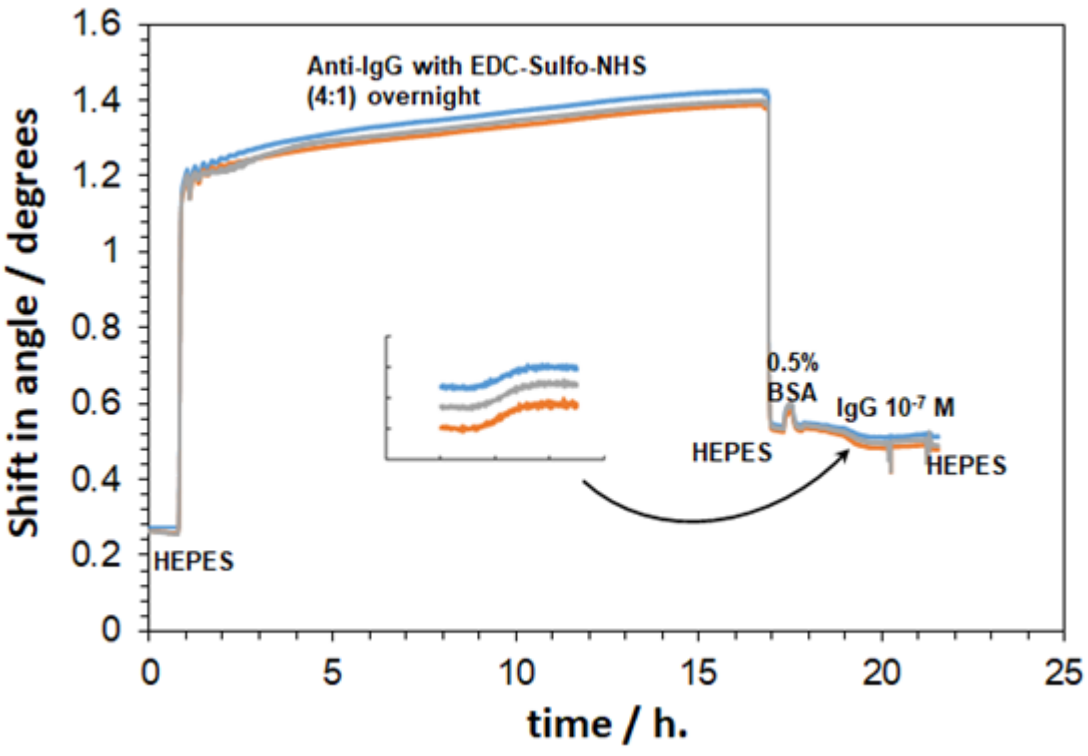

Figure 6.20: Changes in the reflectivity dip angle over time using different solutions (HEPES buffer pH 7.4, monoclonal Anti-Rabbit IgG (0.01 µM) overnight with EDC-Sulpho-NHS (4:1), 0.5% BSA as blocking molecule and monoclonal Rabbit-IgG (0.1 µM) for 4 hrs. The surface was initially incubated with RB4 dye (100 µM) for 5 min.

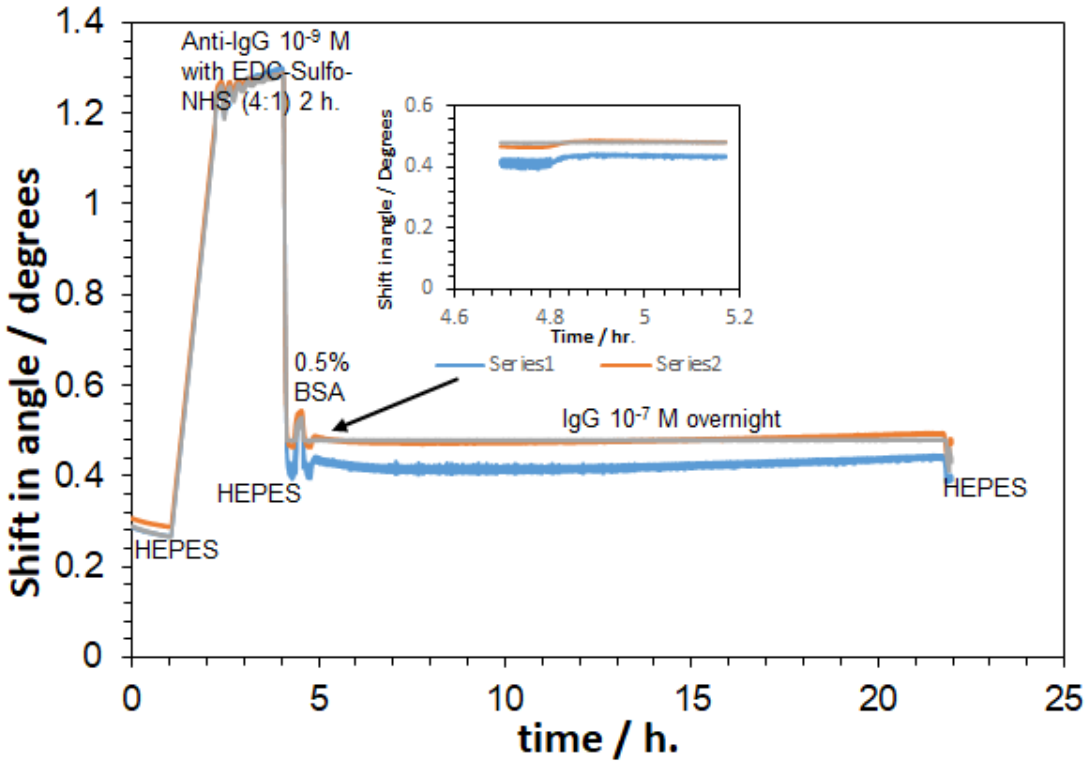

Figure 6.21: Changes in the reflectivity dip angle over time using different solutions (HEPES buffer pH 7.4and monoclonal Anti-Rabbit IgG (0.01 µM) with EDC-Sulpho-NHS (4:1) for 2 hrs 0.5% BSA as blocking molecule and monoclonal rabbit IgG (0.1 µM) overnight. The surface was initially incubated with RB4 dye (100 µM) for 5 min.

Figs.6.20, and 6.21, were shown the reflectivity curves of the incubation of the waveguide chitosan film with Anti-IgG for a longer time (overnight). They demonstrate the stability and amount of the antibody into the chitosan film to enhance the interaction sensitivity for Anti-IgG with detection IgG. The shift can clearly be observed: the degree of shift around 0.3º for the immobilization of Anti-IgG into the waveguide layer, followed by HEPES buffer which did not fully return to the straight line. However, in the previous experiment, the shift of degree for immobilization of the Antibody was about 0.2º for 2 hrs, while nothing changed for the interaction sensitivity between Anti-IgG and detection IgG. The shift in the dip position is due to a different refractive index for detection IgG. On the other hand, as also shown in Figure 6.21, when detection IgG was incubated with the antibody overnight to increase the reaction for the antibody with the antigen the same results were achieved.

6.1.3.2 Increasing incubation time of blocking molecules

Anti-IgG (0.01 µM) was immobilized overnight and BSA (0.5%) was used as blocking molecule for nonspecific binding longer time for 2 hrs until a baseline was obtained for the binding of the antibody with the antigen[149]. This was followed by detection IgG (0.1 µM) being pumped through the sensing area for 2 hrs., again until a base line was obtained.

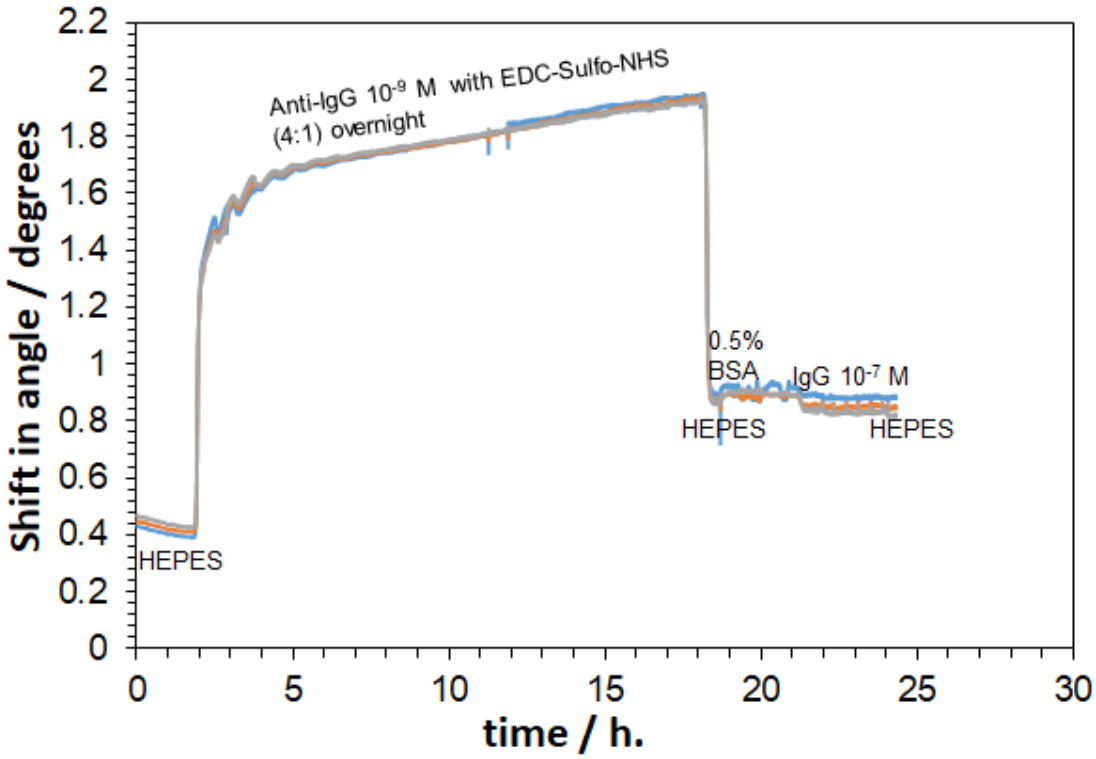

Figure 6.22: Changes in the reflectivity dip angle over time using different solutions (HEPES buffer pH 7.4, EDC-Sulpho-NHS (4:1) and Anti-Rabbit monoclonal IgG (0.01 µM) overnight with EDC-Sulpho-NHS (4:1), blocking with 0.5% BSA for 2 hrs and monoclonal rabbit IgG (0.1 µM) for 2 hrs. The surface was initially incubated with RB4 dye (100 µM) for 5 min.

The purpose of this experiment was to incubate Anti-IgG with blocking molecules for a longer time see fig.6.22, to enhance the interaction of Anti-IgG with detection IgG. The antibody was pumped overnight (about 16 h.). Followed by HEPES buffer, and then BSA was injected for 2 hrs. This clearly occurred, there is no reaction between the antibody and the antigen.

6.1.3.3 Reducing the flow-rate

The stability of antibody immobilization depends on the density of the antibody in the waveguide layer. This will improve the interaction of the antibody with the detection antibody. That requires immobilizing of the antibody to remain attached to the waveguide chitosan film for much longer. Therefore, in this experiment the flow-rate of the solution pumping was reduced to 0.118 mL $min^{-1.}$

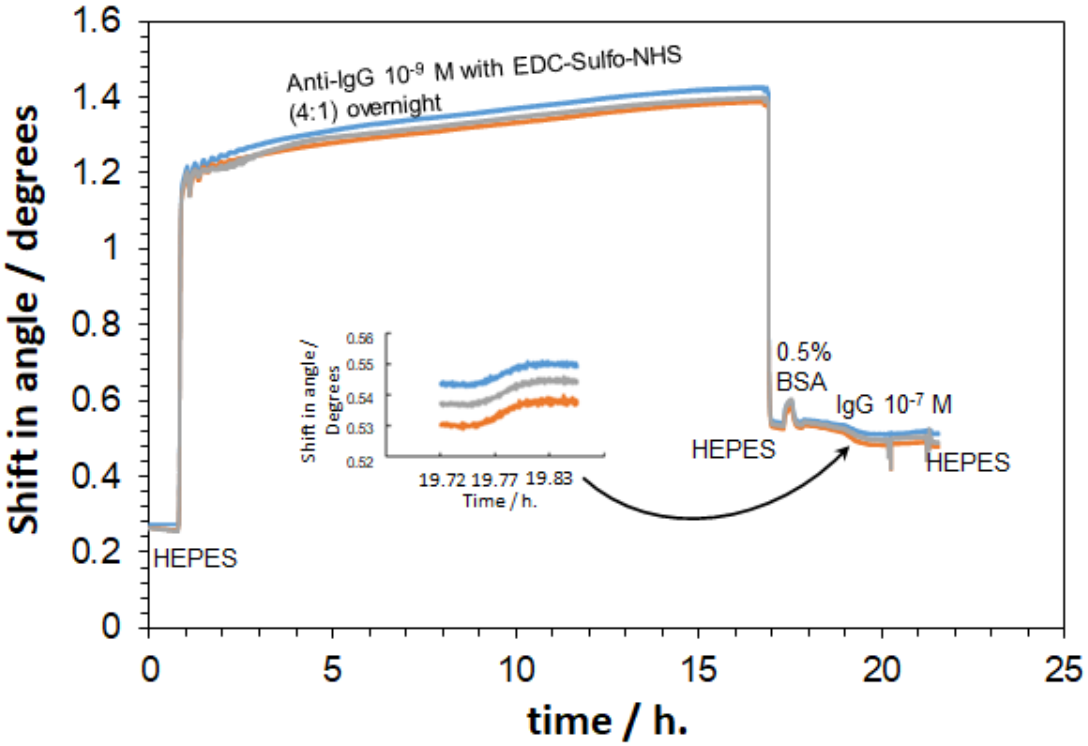

Figure 6.23: Changing in the reflectivity dip angle versus time using different solutions (HEPES buffer pH 7.4, EDC-Sulpho NHS (4:1) and Anti-Rabbit monoclonal IgG (0.01 µM) for 3 hrs with EDC-Sulpho-NHS (4:1), 0.5% BSA as a block molecule and monoclonal rabbit IgG (0.1 µM) overnight. The surface was initially incubated with RB4 dye (100 µM) for 5 min.

That's a clear shift from Anti-IgG to the higher degree in angle around 0.2˚which was incubated with the amino groups of the waveguide film overnight as indicated in fig.6.23. However, as in the previous experiments, there is no reaction when is flushed detection IgG and the shift in angle goes down to the straight line.

6.1.3.4 Flowing effect

Antibody flow has a significant effect on the immobilization of Anti-IgG in the waveguide chitosan film. This experiment incubated the antibody with the amino groups of chitosan film for longer. The aim was to track the shift in the angle degree when pumping the antibody, then when the pump was stopped, in order to study the effect of flowing on the antibody immobilization.

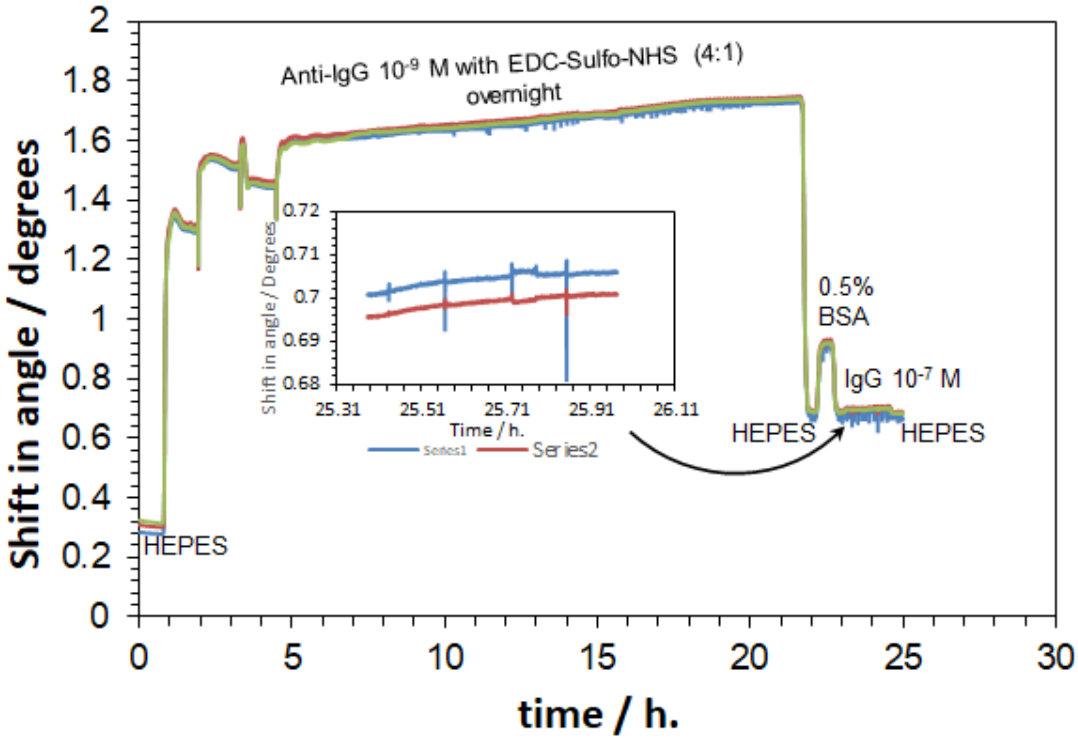

Figure 6.24: Changes in the reflectivity dip angle over time using different solutions (HEPES buffer (pH 7.4), EDC-Sulpho-NHS (4:1) and Anti-Rabbit monoclonal IgG (0.01 µM) injected for (10 min) then paused for one hour, repeated three times, after which the antibody was left overnight. The preparation was activated with EDC-Sulpho-NHS (4:1), blocking with 0.5% BSA for 2 hrs. Monoclonal rabbit IgG (0.1 µM) was flushed for 2hrs. The surface was initially incubated with RB4 dye (100 µM) for 5 min.

Immobilisation Anti-Rabbit IgG (0.01 µM) was injected for 10 min, paused for one hour, then injected for 10 min and paused again for one hour. This was repeated three times, then the Anti-IgG was left overnight. After that BSA (0.5%) was injected as blocking molecules for 2 hrs., then Rabbit IgG (0.1 µM) was reacted and left for 2 hrs. till the baseline was achieved. It can be clearly observed that the shift in the angle degree was enhanced approximately 0.7˚ for the immobilization of Anti-IgG, but nothing changed for the interaction between Anti-IgG and detection IgG as shown in fig.6.24.

6.1.3.5 Ionic strength of HEPES buffer

HEPES (4-(2-hydroxyethyl)-1-piperazineethanesulfonic acid) is a common buffering chemical and is classified as a "Good's buffer". The purpose of the addition of NaCl 100 mM, 150 mM, 200 mM and 250 mM into 0.1M HEPES buffer pH 7.4 is to neutralize the acidic and basic group that already in the chemical structure of HEPES buffer because HEPES buffer is zwitterionic organic chemical buffering agent (molecules has two or more function groups one acidic and other basic) to pH 7.4. This is to investigate if the sensitivity of the reactions can be increased.

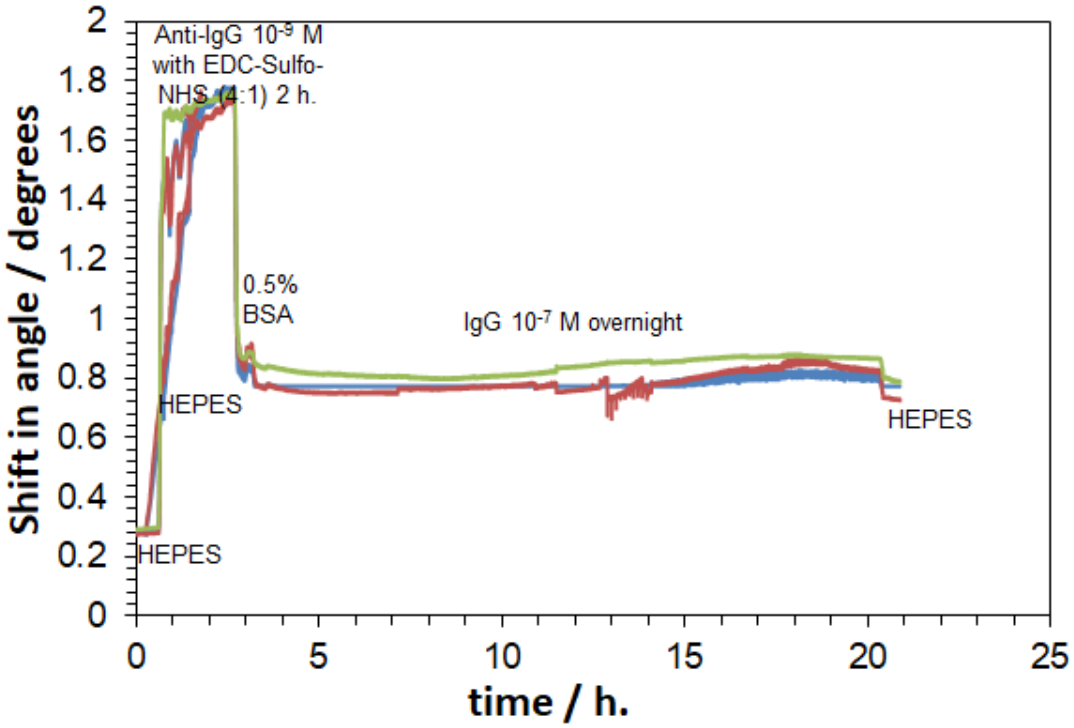

Figure 6.25: Changes in the reflectivity dip angle over time using different solutions (HEPES buffer pH 7.4, EDC-Sulpho-NHS (4:1)/salt NaCl (100 mM) and Anti-Rabbit monoclonal IgG (0.01 µM) for 3 hrs activated with EDC-Sulpho-NHS (4:1), blocked by 0.5% BSA molecules and monoclonal rabbit IgG (0.1 µM) was flushed overnight. The surface was initially incubated with RB4 dye (100 µM) for 5 min.

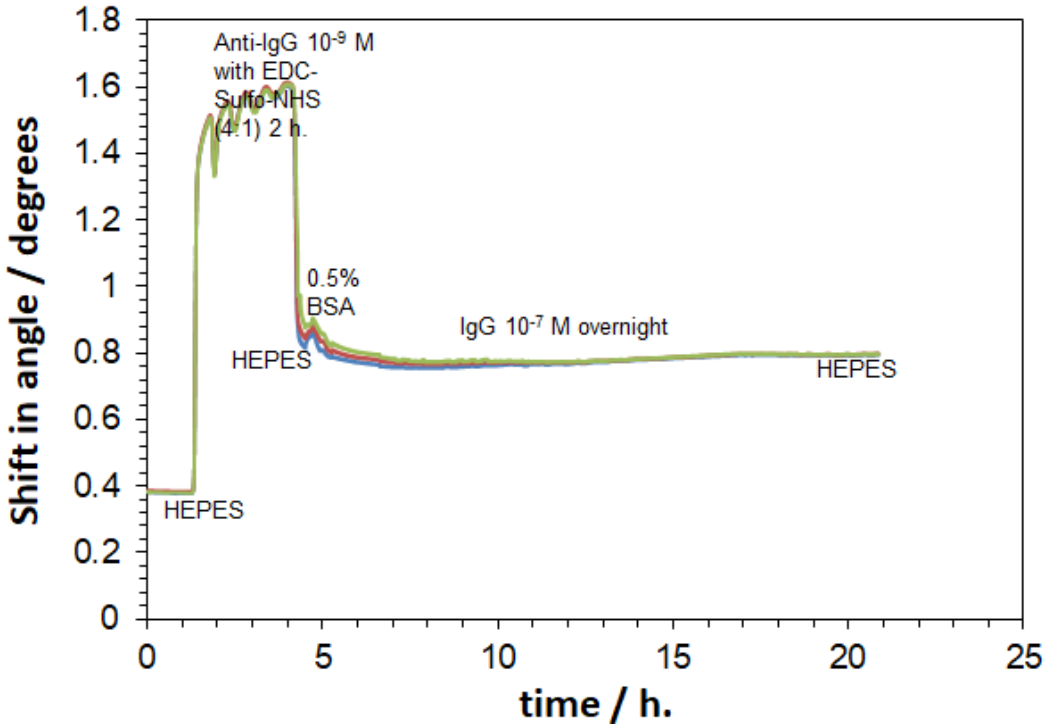

Figure 6.26: Changes in the reflectivity dip angle over time using different solutions (HEPES buffer pH 7.4, EDC-Sulpho NHS (4:1)/salt NaCl (150 mM) and Anti-Rabbit monoclonal IgG (0.01 µM) for 3 hrs activated with EDC-Sulpho-NHS (4:1), blocked by 0.5% BSA molecules and monoclonal rabbit IgG (0.1 µM) was flushed overnight. The surface was initially incubated with RB4 dye (100 µM) for 5 min.

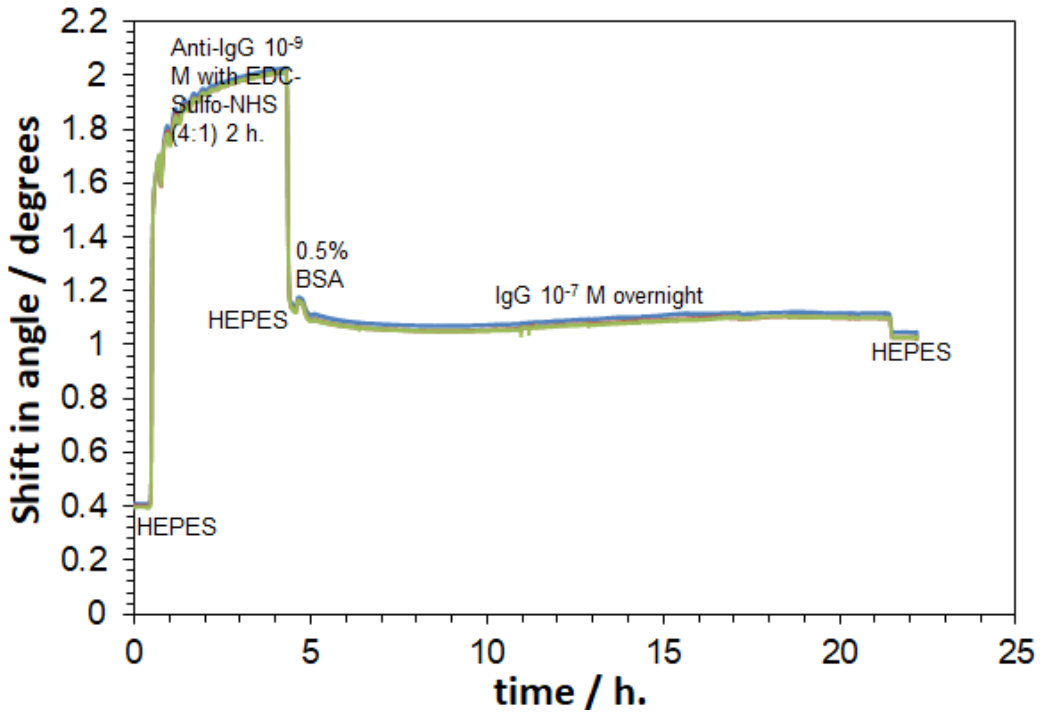

Figure 6.27: Changes in the reflectivity dip angle over time using different solutions (HEPES buffer pH 7.4, EDC-Sulpho-NHS (4:1)/ NaCl salt (200 mM) and Anti-Rabbit monoclonal IgG (0.01 µM) for 3 hrs activated with EDC-Sulpho-NHS (4:1), blocked by 0.5% BSA molecules and monoclonal rabbit IgG (0.1 µM) was flushed overnight. The surface was initially incubated with RB4 dye (100 µM) for 5 min.

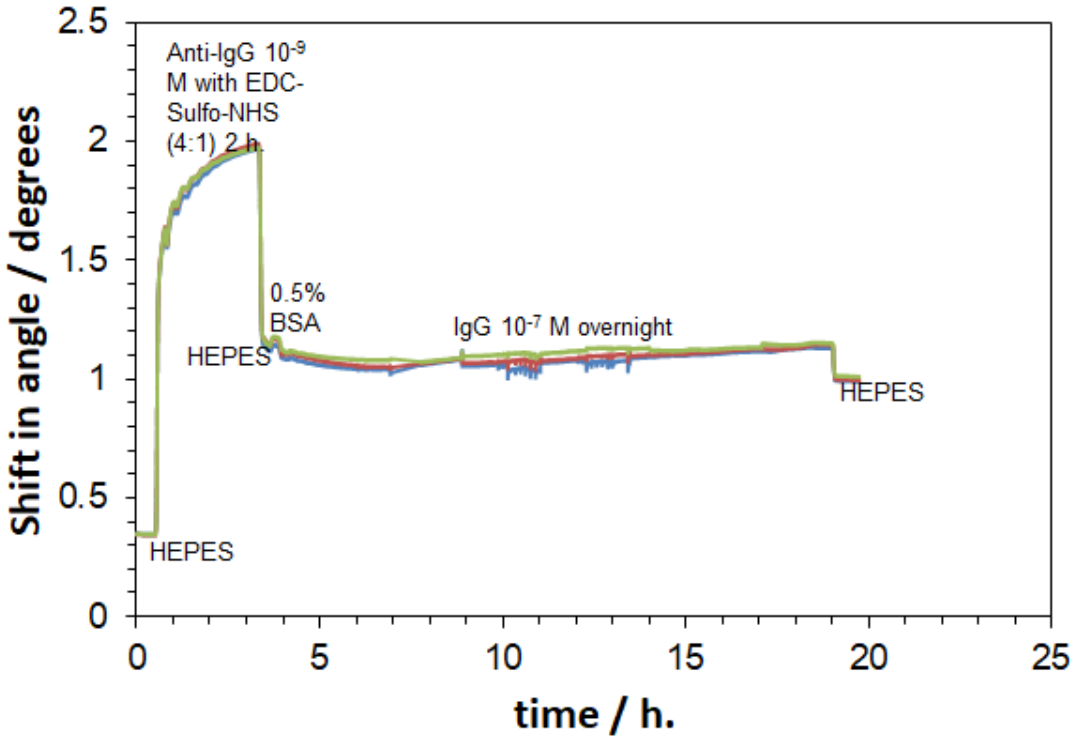

Figure 6.28: Changes in the reflectivity dip angle over time using different solutions (HEPES buffer pH 7.4, EDC-Sulpho-NHS (4:1)/ NaCl salt 100 mM and Anti-Rabbit monoclonal IgG (0.01 µM) for 3 hrs activated with EDC-Sulpho-NHS (4:1), blocked by 0.5% BSA molecules and monoclonal rabbit IgG (0.1 µM) was flushed overnight. The surface was initially incubated with RB4 dye (100 µM) for 5 min.

Figs.6.25, 6.26, 6.27, and fig.6.28, indicate that the immobilization of antibody has a high degree of shift s and the immobilized antibody is not washed away. The dip is also stable and is not washed away. The addition of NaCl solution to neutralize 0.1 M HEPES buffer low increasing in the shifting of the antibody solution when passed through the peristaltic pump[150]. However, the antibody and antigen interaction has low sensitivity and limited interaction, which can be observed from the low shift during the antibody and antigen interaction. Here, the result obtained indicates no change from the previous experiments.

6.1.4 Investigation of the antibody immobilization

A wide range of detection methods were used to characterize and quantify bio-recognition elements for a biomolecular process, such as Fluorescence microscopy, Confocal Microscope, etc.

6.1.4.1 Fluorescence Microscopy

The fluorescence detection method was chosen to detect Rabbit-IgG. That is preferred for the detection of biorecognition elements because of its high safety, sensitivity and relative ease of use and for an increasingly large selection (in biocompatibility, physiochemical/structural properties) of labelling agents involving green fluorescence protein, fluorophores, metal cages, photochromic proteins, semiconductor quantum dots, and others. The experiment has been carried out as explained in section 2.12.1.

6.1.4.1.1 Fluorescence Microscopy at a flow-rate of 0.25 mL min^{-1}

A. without HEPES buffer

The antibody immobilization process has been carried out` using a leaky waveguide sensor to detect the binding of Anti-IgG into the waveguide chitosan layer which was flushed at a flow-rate of 0.25 $mL.min^{-1}$ with HEPES buffer pH 7.4 until a straight line was achieved to study the effect of flow-rate and HEPES buffer on the antibody immobilization.

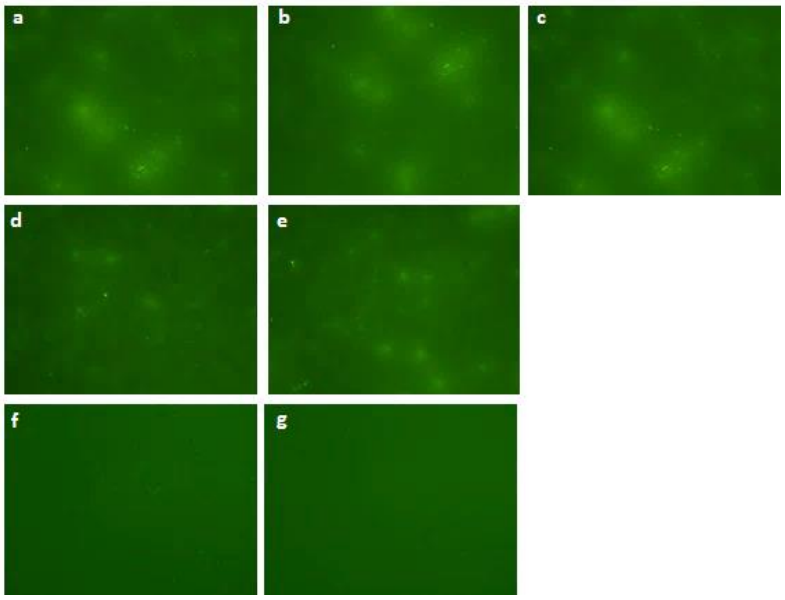

Figure 6.29: Fluorescence Microscopy of (a, b, c, d and e) immobilisation Anti-Rabbit IgG-FITC into the chitosan layer at a flow rate of 0.25 mL min^{-1} using purpose-built apparatus, and (f, g) chitosan layer tag FITC-labelled goat anti-rabbit IgG as a control.

B. with HEPES buffer

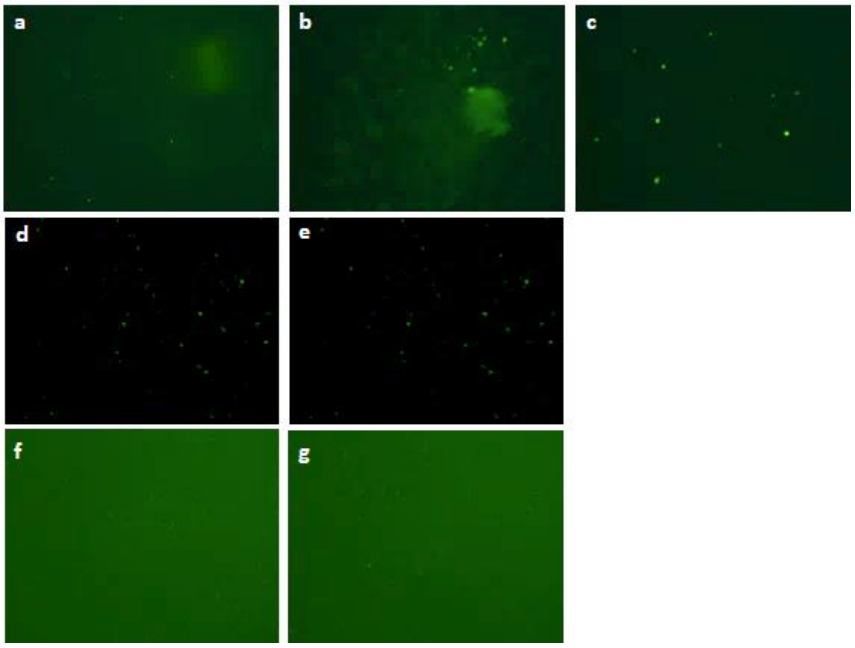

Figure 6.30: The images show Fluorescence Microscopy using purpose-built apparatus of (a, b, c, d and e) immobilisation of Anti-Rabbit IgG-FITC into the chitosan layer at a flow rate of 250 µL.min^{-1}, then washed with HEPES buffer; (f and g) chitosan layer tag FITC-labelled goat anti-rabbit IgG as a control.

The fluorescence microscopy images in fig.6.29 and fig.6.30, show the results of the immobilisation of Anti-Rabbit IgG overnight at a flow rate of 0.25 mL min^{-1} using purpose-built apparatus. The chitosan layer was, in a first run of the experiment, not washed with HEPES buffer, and in the second, washed with HEPES buffer, demonstrating the effect of HEPES buffer on immobilisation into the waveguide layer.

6.1.4.1.2 Fluorescence Microscopy at flow-rate 0.118 mL min^{-1}

A. without HEPES buffer

The binding of the antibody to the amino groups of the waveguide layer was performed, reducing the flow-rate of the peristaltic pump that was used in the immobilization of Anti-IgG into the waveguide chitosan layer to 0.118 mL min^{-1}. Detection of the antibody immobilization was fluorescence microscope.

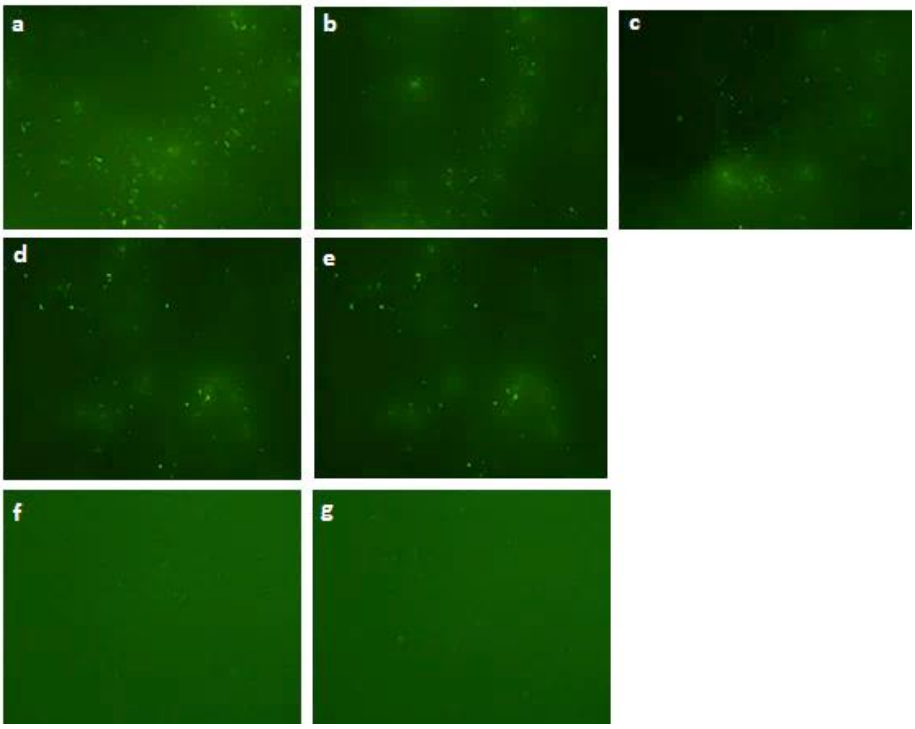

Figure 6.31: Fluorescence Microscopy of (a, b, c, d and e) immobilisation Anti-Rabbit IgG-FITC into the chitosan layer at a flow rate of 0.118 mL min^{-1} using purpose-built apparatus, and (f and g) chitosan layer tag FITC-labelled goat anti-rabbit IgG as a control.

B. with HEPES buffer

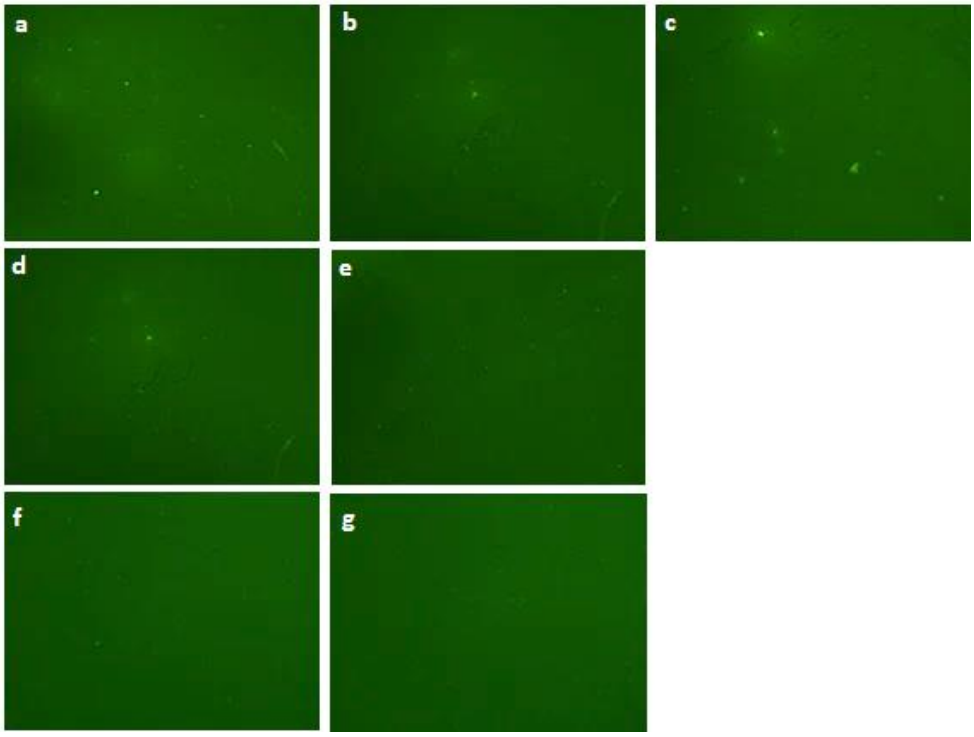

Figure 6.32: Fluorescence Microscopy of (a, b, c, d and e) immobilisation Anti-Rabbit IgG-FITC into the chitosan layer at a flow rate of 0.118 mL min^{-1} then washed with HEPES buffer by using purpose-built apparatus, (f and g) chitosan layer tag FITC-labelled goat anti-rabbit IgG as control.

As indicated in the fluorescence microscopy images figs.6.31, and fig.6.32 show the results of the immobilisation of Anti-IgG overnight at a flow rate of 0.118 mL min^{-1} using purpose-built apparatus, first when it was not washed with HEPES buffer, and then with HEPES buffer, demonstrating the effect of HEPES buffer on immobilisation into the waveguide layer at different flow rates.

6.1.4.2 Confocal Microscope

An investigation of the immobilization of Anti-Rabbit IgG was carried out using a Confocal Microscope see fig.6.33. Three coverslips were spin coated with 1% chitosan film at 900 rpm, with 3 min drying time, and incubated overnight with HEPES buffer pH7.4, after that incubated with Anti-IgG-FITC overnight and left in the fridge overnight (more than 12 hr.).

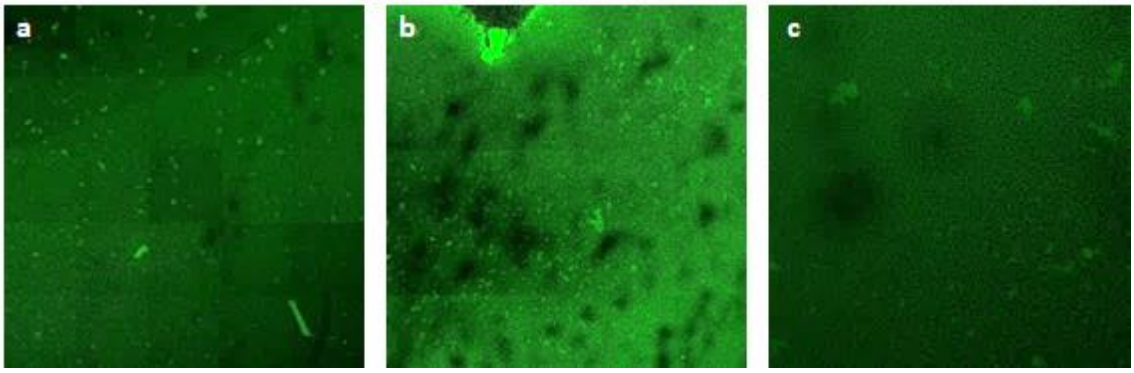

Figure 6.33: Confocal Microscope of (a): immobilisation Anti-Rabbit IgG-FITC into the chitosan layer left it in the fridge overnight, not washed with HEPES buffer; (b): immobilisation Anti-Rabbit IgG-FITC into the chitosan layer, left in the fridge overnight, and washed with HEPES buffer; and (c) Chitosan layer tag FITC as a control.

The immobilization of Anti-IgG into the chitosan film was carried out without injecting the antibody by using a leaky waveguide sensor to investigate the binding of the antibody, study the effect of pumping on the immobilization process and the temperature. Therefore, the coverslips of 1% chitosan were left in the fridge overnight. In the green spots indicate the binding of Anti-IgG into the waveguide chitosan layer, and the coverslip was not washed with HEPES buffer; while b shows the chitosan film washed with HEPES buffer. That shows the effect of the pumping on the antibody immobilization into the waveguide chitosan layer.

6.1.4.3 Dye-doped leaky waveguide sensor (DDLW)

Immobilisation Anti-Rabbit IgG (0.01 µM) was carried out using a flow cell. Two channels were injected with the same solution .Anti-Rabbit IgG was injected through one channel to compare the immobilisation of the antibody on the same slide. Then it was left overnight, injected with BSA (0.5%) as blocking molecule for longer than 2 hrs. Then it was reacted with 0.1 µM Rabbit IgG and left for 2 hrs until it achieved the baseline.

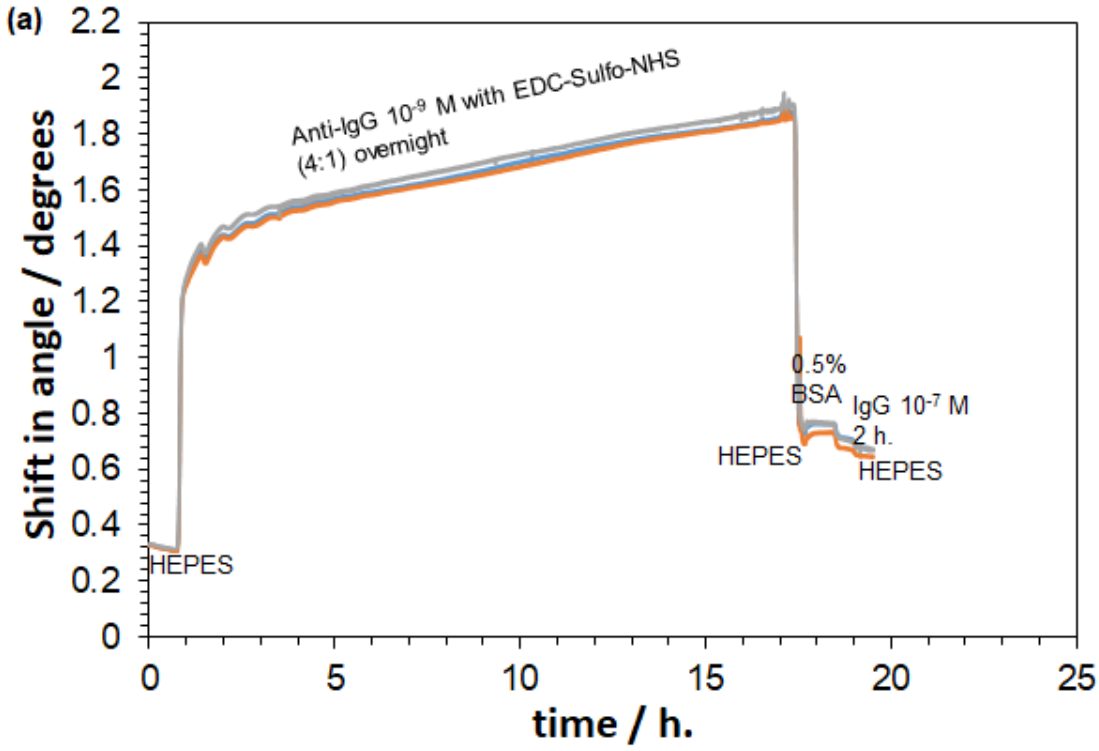

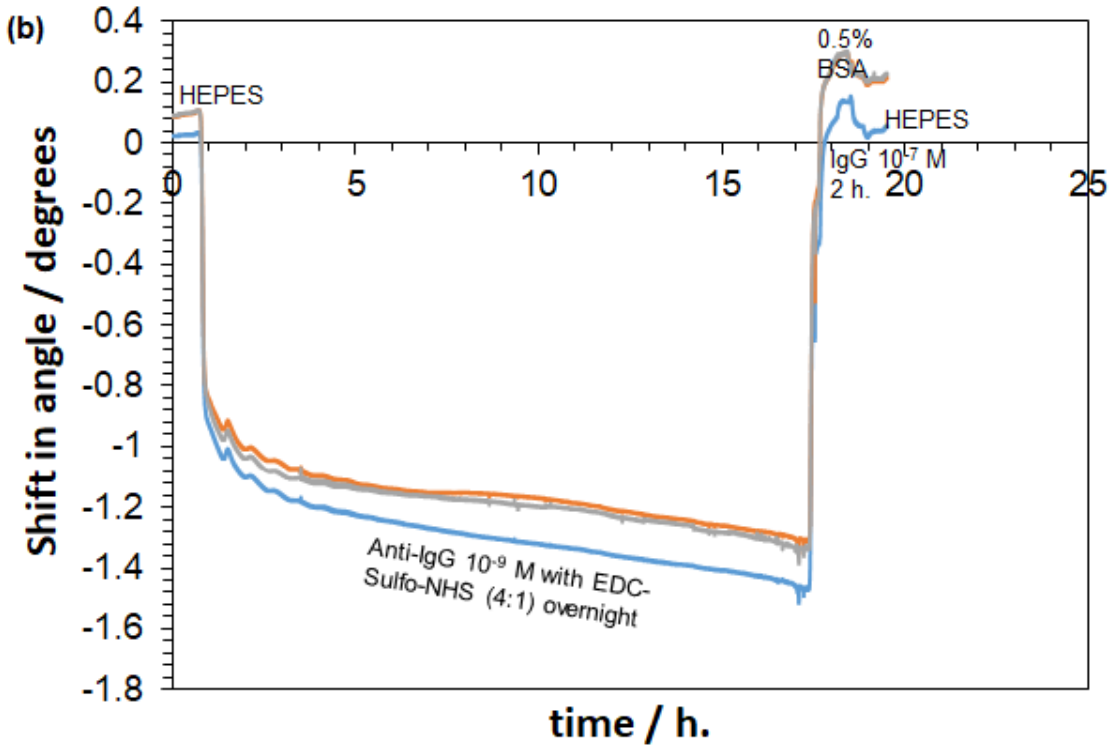

Figure 6.34: a- Changes in the reflectivity dip angle over time using different solutions in one channel (HEPES buffer pH 7.4, Anti-Rabbit monoclonal IgG (0.01 µM) injected overnight activated with EDC-Sulpho-NHS (4:1), blocked by 0.5% BSA molecule for 2 hrs and monoclonal rabbit IgG (0.1 µM) was flushed for 2 hrs until the baseline wasreached);.While the second channel was flushed all solutions that were pumped in the first channel instead of Anti-rabbit monoclonal IgG. The surface was initially incubated with RB4 dye (100 µM) for 5 min; b: Inverse of graph a.

Shows the binding of Anti-IgG into the chitosan layer by leaky waveguide sensor, carried out by injection into the first channel of different solutions: HEPES buffer, Anti-IgG activated with EDC-Sulpho-NHS, 0.5%BSA, then reacted with IgG; while in the second channel whole solutions that were flushed in the first channel instead of the antibody (Anti-IgG) to investigate the binding of the antibody into the waveguide chitosan layer. Fig.6.34 b, indicates reverse of fig.6.34a after elimination from the first channel of data from the second channel. That clearly shows that there is no binding of the antibody with the amino groups of chitosan film.

6.1.5 Immobilization of the Antibody by a Crosslinker (Glutaraldehyde)

The crosslinking of the antibody with the amino groups of the waveguide layer should start by selecting a crosslinker for optimal reaction with the proteins. There are different features should be taken into account when choosing a crosslinker, like membrane permeability, solubility, and reversibility. Also, maintenance of the original structure of the protein should be capable of being conducted under natural conditions of temperature and pH. Some homobifunctional reagents, such as DMA, DMS, phenols, DTBP and glutaraldehyde, work very well with chitosan's amines to make them more chemically resistant and physically harder.

Covalent glutaraldehyde crosslinking has been used in many circumstances for the reaction of amino groups of chitosan with glutaraldehyde to detect their presence in the solution (organic or inorganic compound, complex or simple). To explain this behaviour, three recognizable structures are proposed: (a) one aldehyde group of glutaraldehyde reacts to form only one Schiff base, while other aldehyde groups remain free for a subsequent reaction; (b) Two chitosan units will react with one aldehyde group to form two Schiff bases including both aldehyde groups of the glutaraldehyde molecule; (c) amino groups will crosslink with more than one glutaraldehyde molecule and form a greater crosslinking chain through polymerization of glutaraldehyde[151].

In general, the best method to improve attaching the antibody to chitosan's amines is covalent bonding using glutaraldehyde crosslinking. The glutaraldehyde molecule has aldehyde groups on both sides which bind covalently to chitosan's amines; an imine bond is formed immediately as shown in fig.6.35. The resonance of the adjacent ethylenic double bond will be stabilized by the imine bond. Thus, a strong link will be established between the waveguide chitosan film and the antibody.

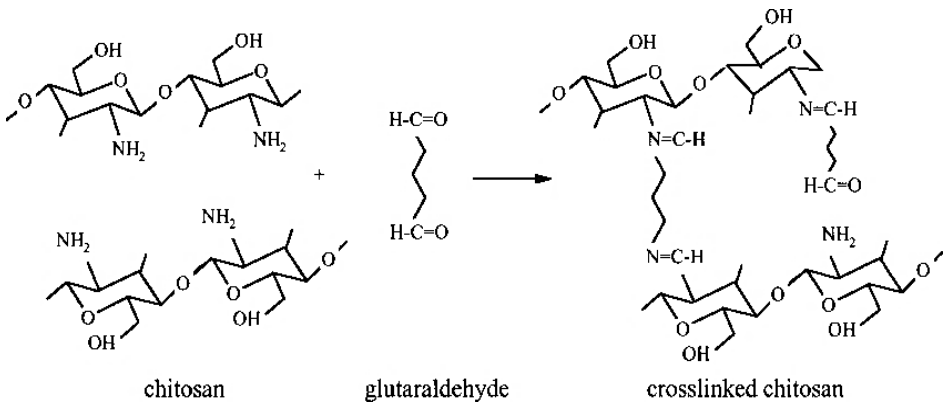

Figure 6.35: The mechanism of reaction crosslinking of chitosan with glutaraldehyde[152]

The waveguide chitosan film is modified with Anti-IgG using glutaraldehyde crosslinking, to enhance attaching chitosan's amines with the antibody by covalent bonding. The functional groups of the antibody (carboxyl group) which can be linked to chitosan's amines by using different concentrations of a linker are described in section 2.13

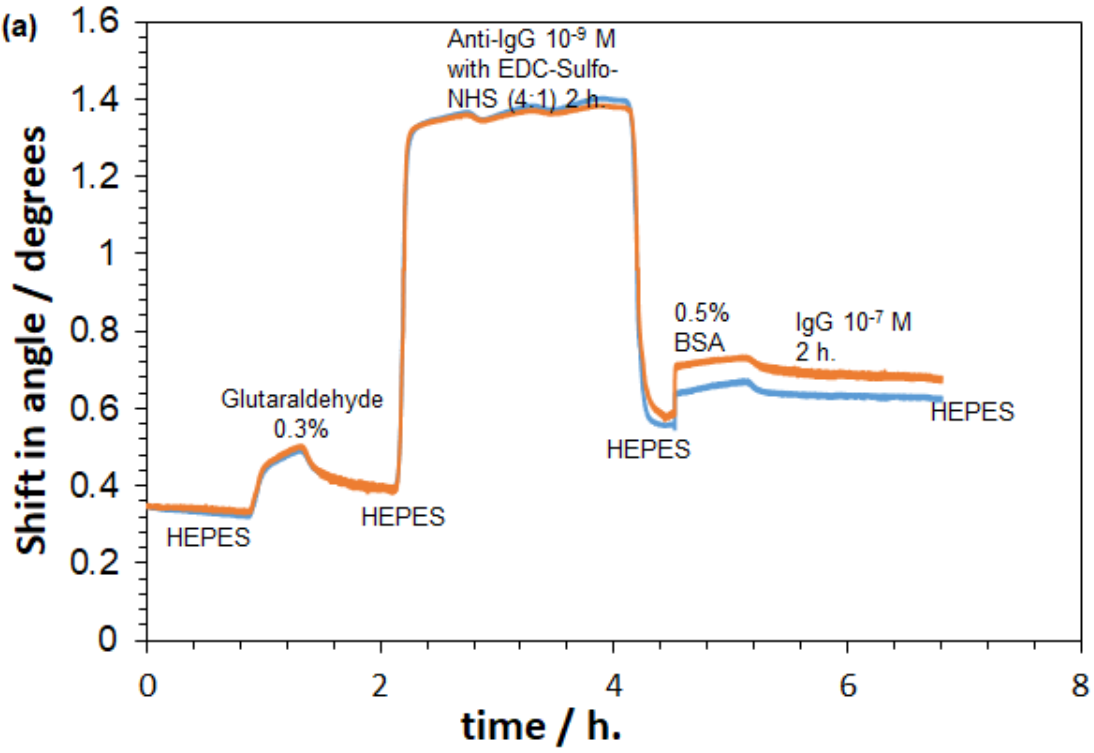

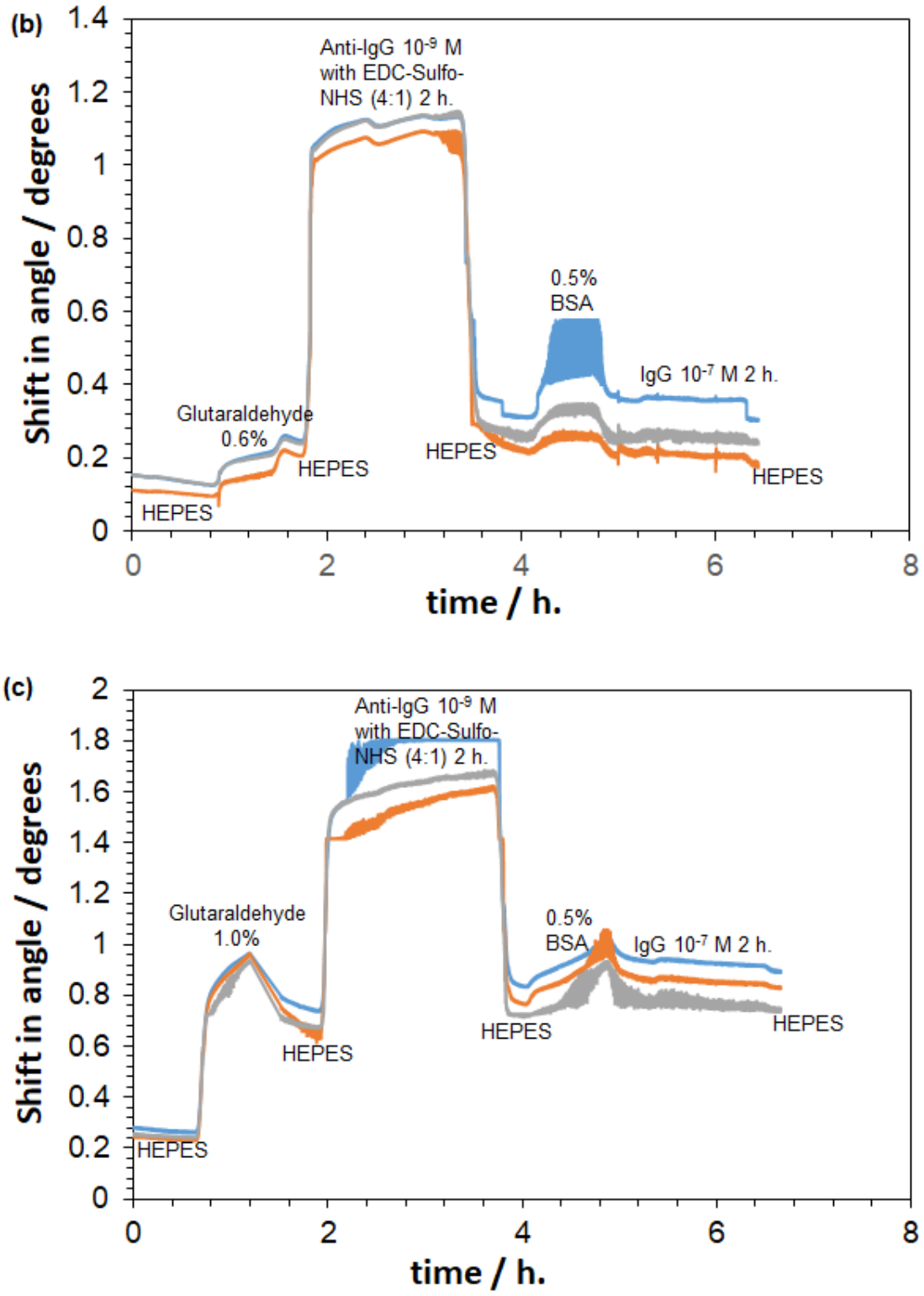

Figure 6.36: Changes in the reflectivity dip angle over time using different solutions (HEPES buffer pH 7.4, Anti-Rabbit monoclonal IgG (0.01 µM) activated with EDC-Sulpho-NHS (4:1) until the baseline was reached, blocked by 0.5% BSA molecules for 30 min,; after that reacted with monoclonal rabbit IgG 0.1 µM for 2 hrs. The surface was initially incubated with RB4 dye (100 µM) for 5 min by using glutaraldehyde as a crosslinker of chitosan's amines; (a) 0.3% of glutaraldehyde (b) 0.6% of glutaraldehyde (c) 1% of glutaraldehyde.

This experiment was carried out using different concentrations of glutaraldehyde as shown in fig.6.36a, b, and c, to produce a more chemically resistant and physically harder waveguide film, with the improved method for attaching the antibody to chitosan's amines by crosslinking. Shows a high shift in the degree for Anti-IgG when cross-linked by 0.3% of glutaraldehyde; by comparison with around 0.2º in b and c. As illustrated in the shift in degree was approximately 0.1º and 0.15º respectively. This clearly shows the difference in antibody immobilization using different concentrations of glutaraldehyde, but there is no change in the interaction sensitivity of detection IgG.

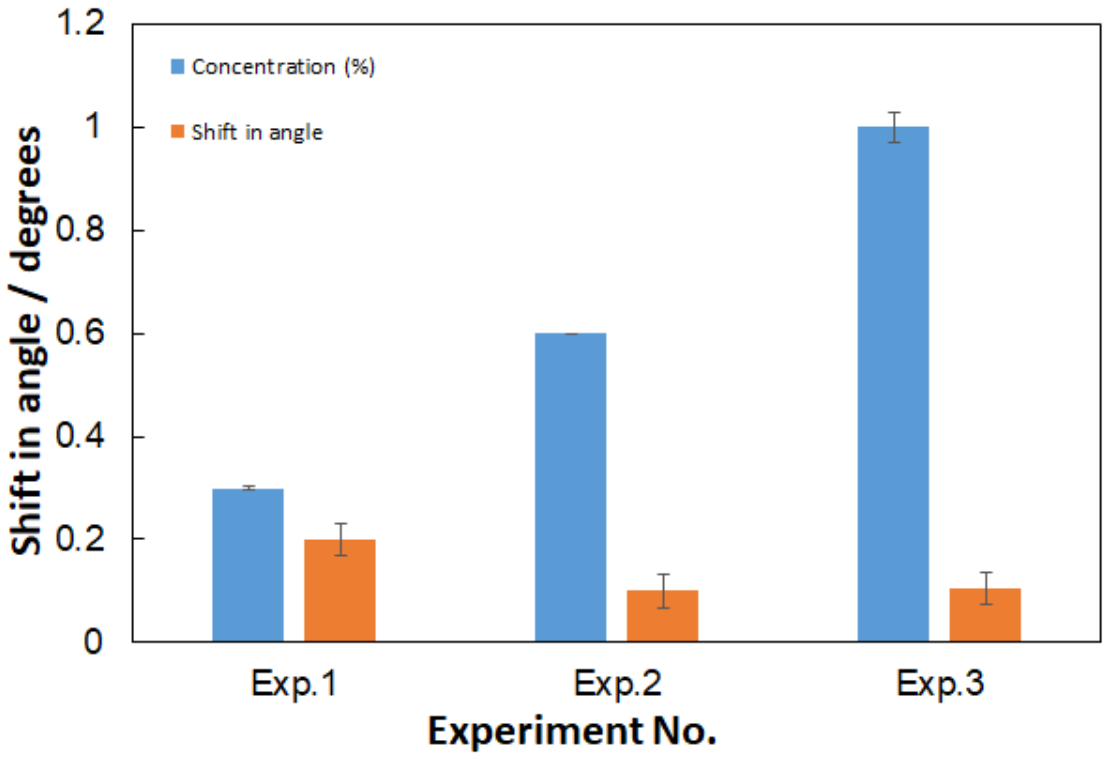

Figure 6.37: The differences between the concentrations of glutaraldehyde with the shift in the angle.

As observed in fig.6.37, there is no reaction between Anti-IgG and detection IgG. That is because in immobilization in this manner, random (non-specific) attachment of the antibody to chitosan waveguide layer can reduce antibody stability and lead to minimizing the interaction between Anti-IgG and detection IgG. Therefore, the next experiments focus on oriented (site-specific) Anti-IgG immobilization methodology.

6.1.6 Immobilization of the Antibody by the Biotin-Streptavidin System

The biotin-streptavidin system is a more specific methodology to study the attachment immobilization of Anti-IgG t with the uniform orientation of the antibody to the chitosan waveguide where the bioactive site (carboxyl group) is freely available to react with detection IgG see fig.6.38. This will increase the biological activity of the antibody and the interaction sensitivity for Anti-IgG with IgG.

On the other hand, non-covalent immobilization of the antibody includes relatively weak and reversible interactions. This will lead to leaching of the antibody from the chitosan waveguide layer when the buffer is flushed to remove unbound molecules. However, this experiment has been performed by streptavidin's reaction with the waveguide layer, with biotinylated Anti-IgG as described in section 2.14. The binding between streptavidin and biotin has long been regarded as, the strongest and most rapid noncovalent interaction known [153]. Therefore it's used in various biological applications as mentioned previously in section 1.13.

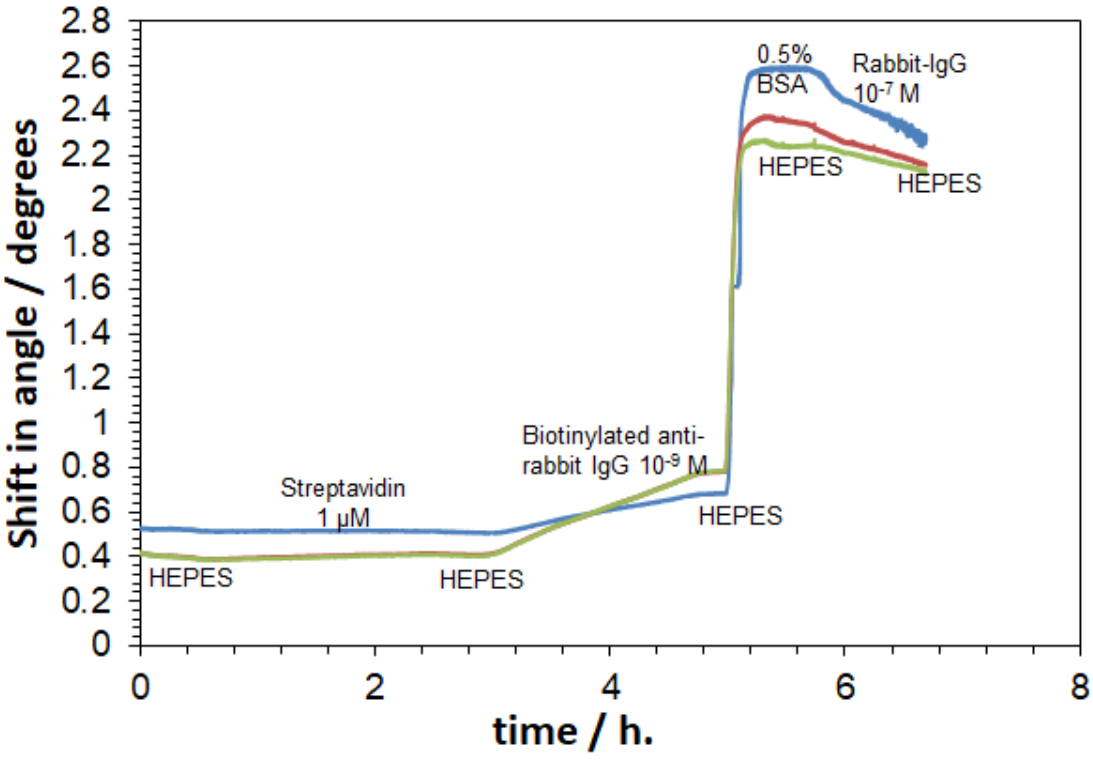

Figure 6.38: Changes in the reflectivity dip angle over time using different solutions (HEPES buffer pH 7.4, Streptavidin 1.0 µM and biotinylated Anti-Rabbit monoclonal IgG 0.01 µM) until the baseline was reached, blocked by 0.5% BSA molecules for 30 min, and then reacted with monoclonal rabbit IgG 0.1 µM for 2 hrs. The surface was initially incubated with RB4 dye 0.1 µM for 5min.

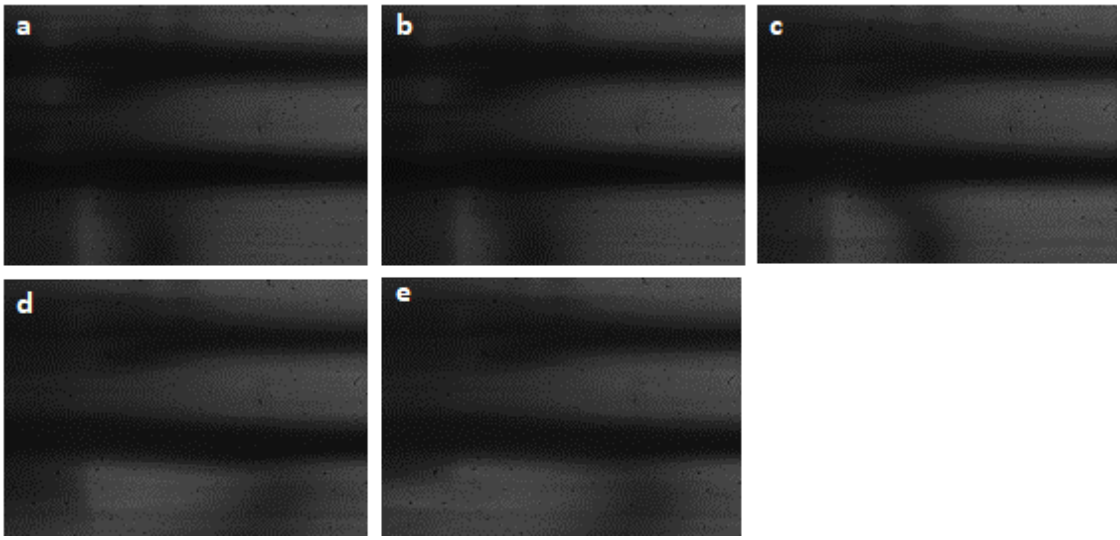

Figure 6.39: Pictures captured by the camera to a glass slide with a flow cell, one channel of which was a: HEPES buffer, b: Streptavidin (1.0 µM), c: Anti-IgG 0.001 µM, d: BSA (0.5%) and e: IgG 0.1 µM.

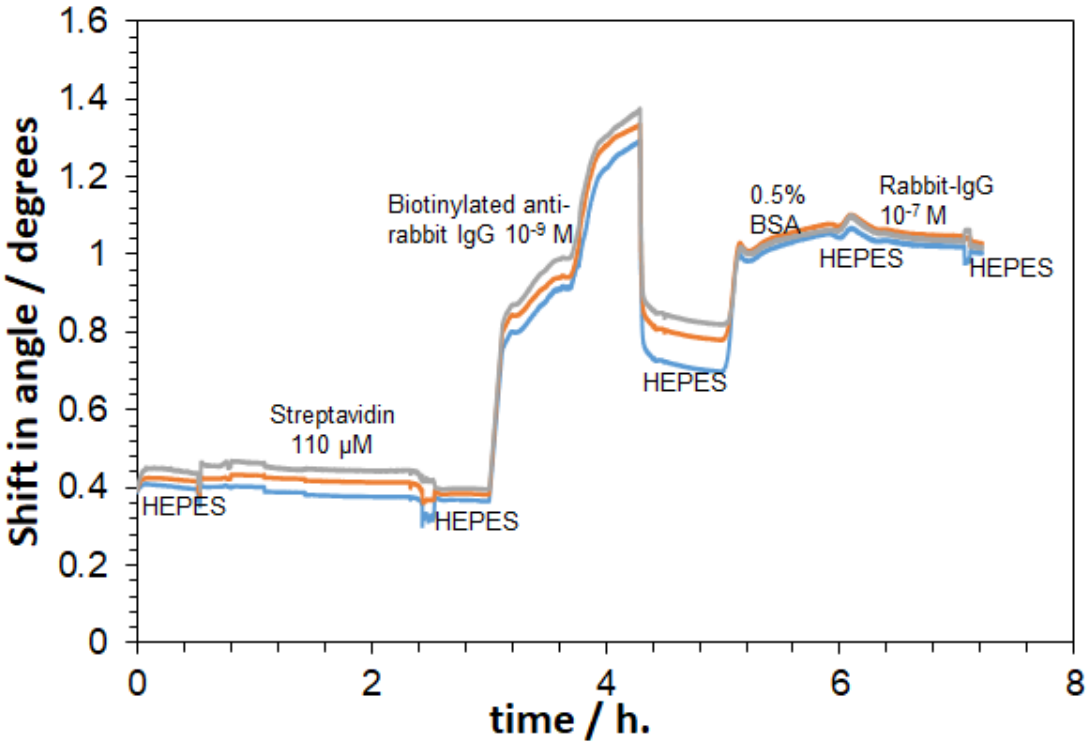

Figure 6.40: Changes in the reflectivity dip angle over time using different solutions (HEPES buffer pH 7.4, Streptavidin 1.0 µM and biotinylated Anti-Rabbit monoclonal IgG 0.001 µM) until the baseline was reached, blocked by 0.5% BSA molecules for 30 min, and then reacted with monoclonal rabbit IgG 0.1 µM for 2 hrs. The surface was initially incubated with RB4 dye 0.1 µM for 5 min.

Figs.6.39, and 6.40, indicate the immobilization of biotinylated antibody using different (low and high) concentrations of streptavidin (1 µM and 22 µM) reacted with the chitosan waveguide film to increase the specific attachment of Anti-IgG. However, it can clearly be seen that there is no reaction between streptavidin and the amine groups of the chitosan waveguide layer. Therefore, the immobilization of biotinylated Anti-IgG with streptavidin requires a linker (Glutaraldehyde) between the chitosan layer and the streptavidin indicates a high shift in the degree (0.3%) for Anti-IgG when linked by of glutaraldehyde, around 0.2º more than with 0.6% and 1% of glutaraldehyde.

The next experiment involved linking chitosan waveguide film by 0.3% of glutaraldehyde with 1% of chitosan to immobilize biotinylated Anti-IgG 0.001 µM by using different concentrations of streptavidin (1 µM and 22 µM) as described in section 2.14

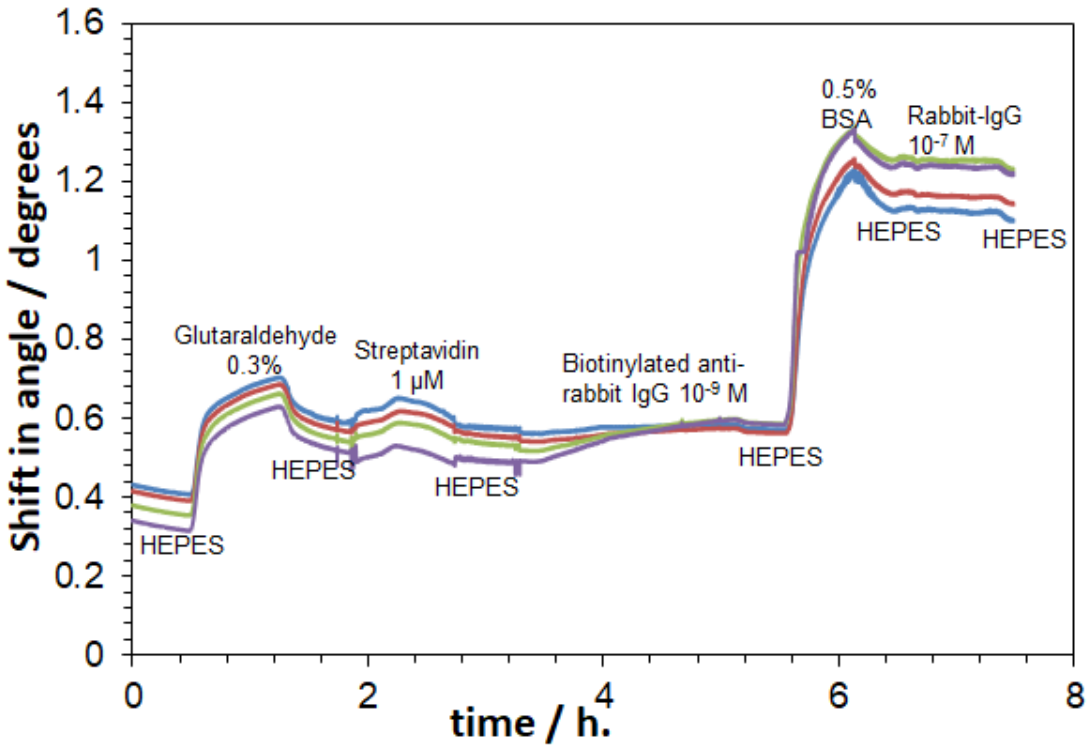

Figure 6.41: Changes in the reflectivity dip angle over time using different solutions (HEPES buffer pH 7.4, 0.3% of glutaraldehyde as linker for the waveguide layer, Streptavidin 1.0 µM, biotinylated Anti-Rabbit monoclonal IgG 0.001 µM) until the baseline was reached, 0.5% BSA as blocking molecules for 30 min, reacted with monoclonal rabbit IgG (0.1 µM) for 2 hrs. The surface was initially incubated with RB4 dye (0.1 µM) for 5 min.

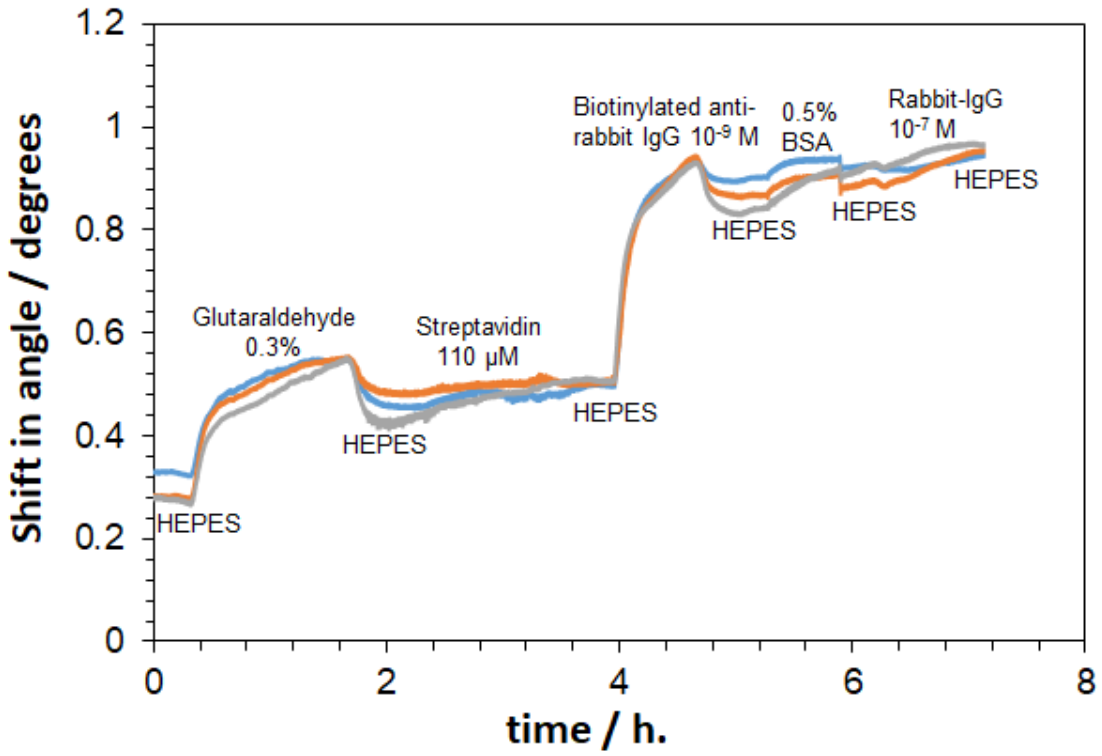

Figure 6.42: Changing in the reflectivity dip angle versus time using different solutions HEPES buffer pH 7.4, 0.3% of glutaraldehyde as a linker for the waveguide layer, Streptavidin 22 µM, biotinylated Anti-Rabbit monoclonal IgG 0.001 µM till get baseline, 0.5% BSA as blocking molecules for 30 min, reacted with monoclonal rabbit IgG (0.1 µM) for 2 hrs. The surface initially incubated with the RB4 dye (0.1 µM) for 5 min.

Immobilization of the antibody by linking the chitosan with 0.3% of glutaraldehyde has shown remarkable results. See figs.6.41, and 6.42, which illustrate immobilizing of biotinylated Anti-IgG with 22 µM of streptavidin, whereas, there was no reaction between the antibody and detection antibody (IgG), as in the previous results with EDC-Sulpho-NHS alone, glutaraldehyde and streptavidin alone. However, biotinylated Anti-IgG with 22 µM of streptavidin by linking of the waveguide layer with 0.3% of glutaraldehyde is needed to optimise the attachment time, streptavidin concentration, etc.

6.1.6.1 Optimizing attachment time

The immobilization of the antibody by the biotin-streptavidin system through crosslinking with the chitosan waveguide film has been done to orient (site-specific) Anti-IgG immobilization and increase the antibody stability, which will lead to the maximising of the interaction between Anti-IgG and detection IgG. This experiment was performed to enhance the sensitivity of detection of the interaction IgG through increasing attachment time for IgG and leaving it overnight to interact with biotinylated Anti-IgG 0.001 µM.

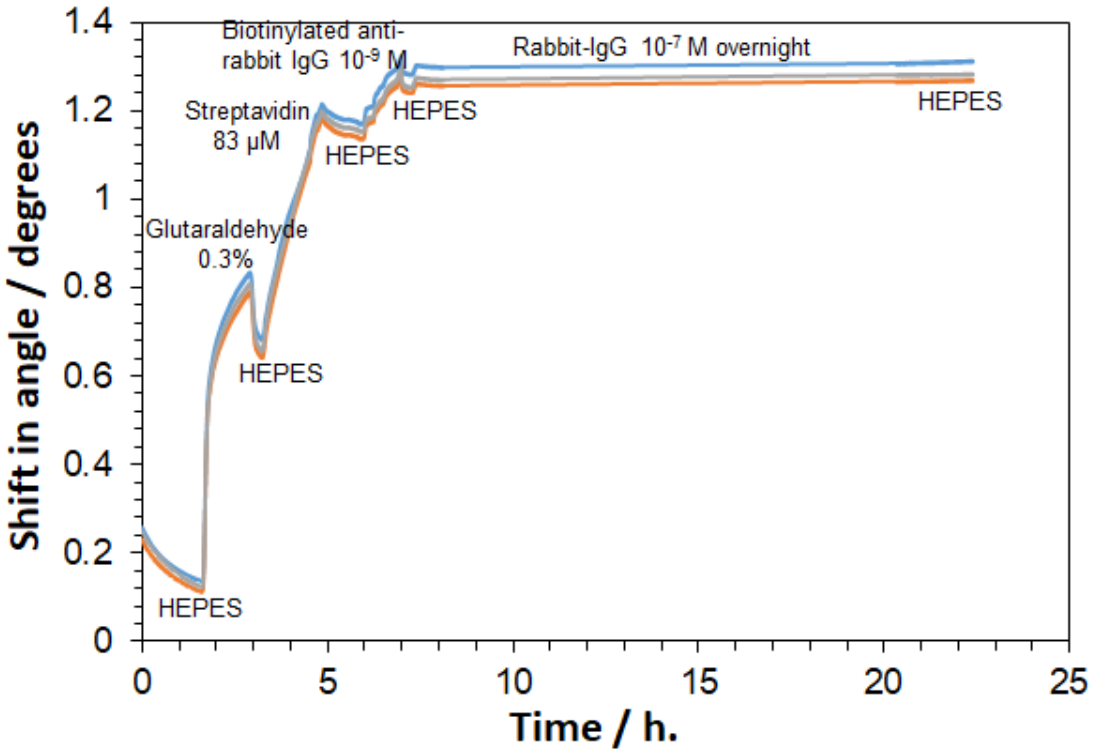

Figure 6.43: Changes in the reflectivity dip angle over time using different solutions (HEPES buffer pH 7.4, 0.3% of glutaraldehyde as linker for the waveguide layer, Streptavidin 22 µM, biotinylated Anti-Rabbit monoclonal IgG 0.001 µM) until a baseline was reached; after that reacted with monoclonal rabbit IgG 0.1 µM overnight. The surface was initially incubated with RB 4 dye (0.1 µM) for 5 min.

As shown in fig.6.43, the interaction of biotinylated Anti-IgG with detection IgG has been increased with increasing the attachment time. When HEPES buffer was pumped after detection IgG is not gone down to the straight line, that's due to the orientation and stability of the antibody into chitosan waveguide layer by using the biotin-streptavidin system and crosslinking of chitosan layer by 0.3% of glutaraldehyde.

6.1.6.2 Optimizing Streptavidin concentration

Different concentrations (1, 22, 62, and 83 µM) of streptavidin were used to investigate its reaction with biotinylated Anti-IgG, using 0.5% of bovine serum albumin (BSA) as a blocking molecule. This is a most popular agent as it binds to all the unoccupied sites in the chitosan waveguide film. This means that when biotinylated Anti-IgG is added to streptavidin in the waveguide layer there are unoccupied sites into the waveguide film to which it can attach other than to the binding sites of biotinylated Anti-IgG, thus increasing the possible interaction between Anti-IgG and detection IgG.

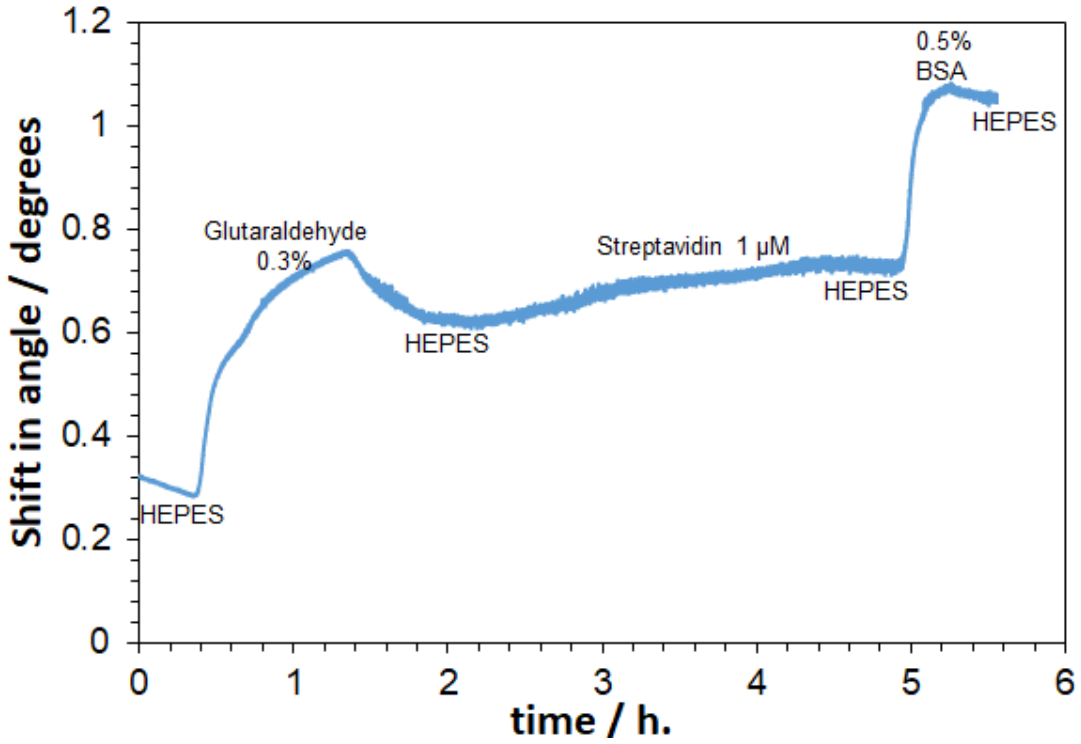

Figure 6.44: Changes in the reflectivity dip angle over time using different solutions (HEPES buffer pH 7.4, 0.3% of glutaraldehyde as linker for the waveguide layer, Streptavidin 1 µM), blocked by 0.5% of BSA. The surface was initially incubated with RB4 dye (0.1 µM) for 5 min.

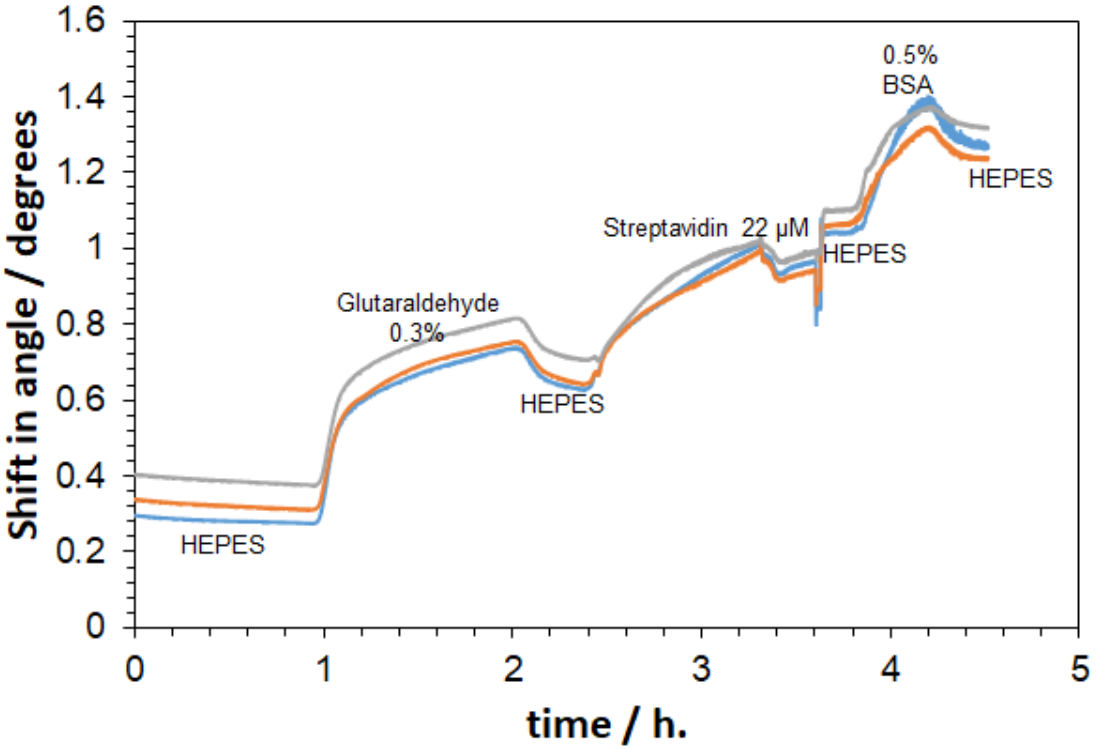

Figure 6.45: Changes in the reflectivity dip angle over time using different solutions (HEPES buffer pH 7.4, 0.3% of glutaraldehyde as linker for the waveguide layer, Streptavidin 22 µM), blocked by 0.5% of BSA. The surface was initially incubated with RB4 dye (0.1 µM) for 5 min.

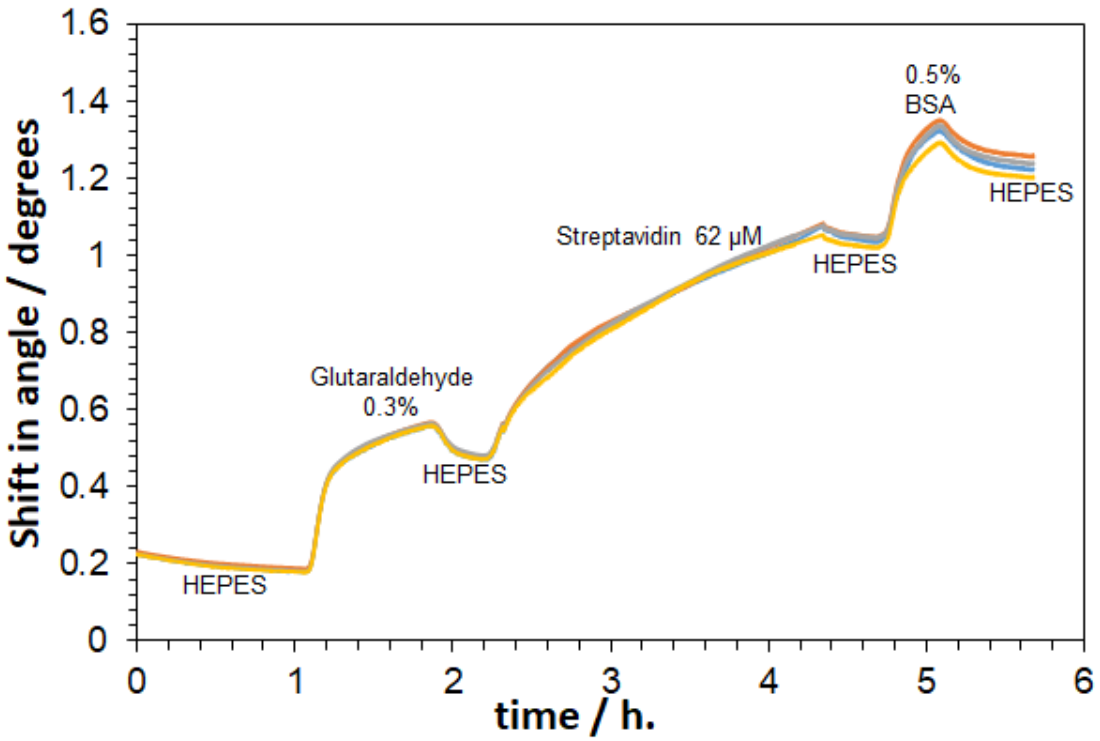

Figure 6.46: Changes in the reflectivity dip angle over time using different solutions (HEPES buffer pH 7.4, 0.3% of glutaraldehyde as linker for the waveguide layer, Streptavidin 62 µM), blocked by 0.5% of BSA. The surface was initially incubated with RB4 dye (0.1 µM) for 5 min.

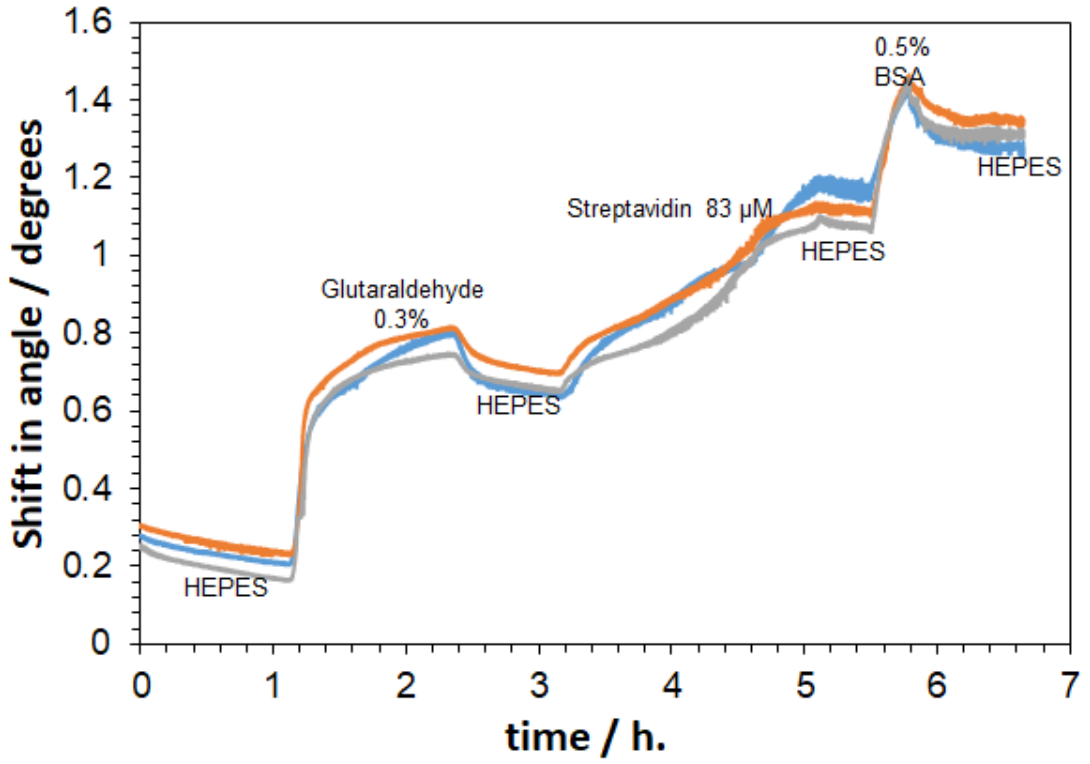

Figure 6.47: Changes in the reflectivity dip angle over time using different solutions (HEPES buffer pH 7.4, 0.3% of glutaraldehyde as linker for the waveguide layer, Streptavidin 83 µM), blocked by 0.5% of BSA. The surface was initially incubated with RB4 dye (0.1 µM) for 5 min.

Different concentrations of streptavidin were pumped into the chitosan waveguide film to investigate the interaction between glutaraldehyde and streptavidin through the injection of blocking molecules as indicated in and the shift in angle was clearly observed about 0.55º when 1 µM of streptavidin was flushed to interact with 0.3% of glutaraldehyde fig.6.44, compared with the results fig.6.45, when 22 µM of streptavidin, fig.6.46, when flushed 63 µM of streptavidin, and 83 µM of streptavidin was flushed as shown in fig.6.47. That means the shift in angle decreased when streptavidin concentrations increased, as shown in, which summarizes Figs.6.44, 45, 46, and 47 in fig.6.48, and indicates the relation between streptavidin concentrations and the shift in the angle of blocking molecules BSA.

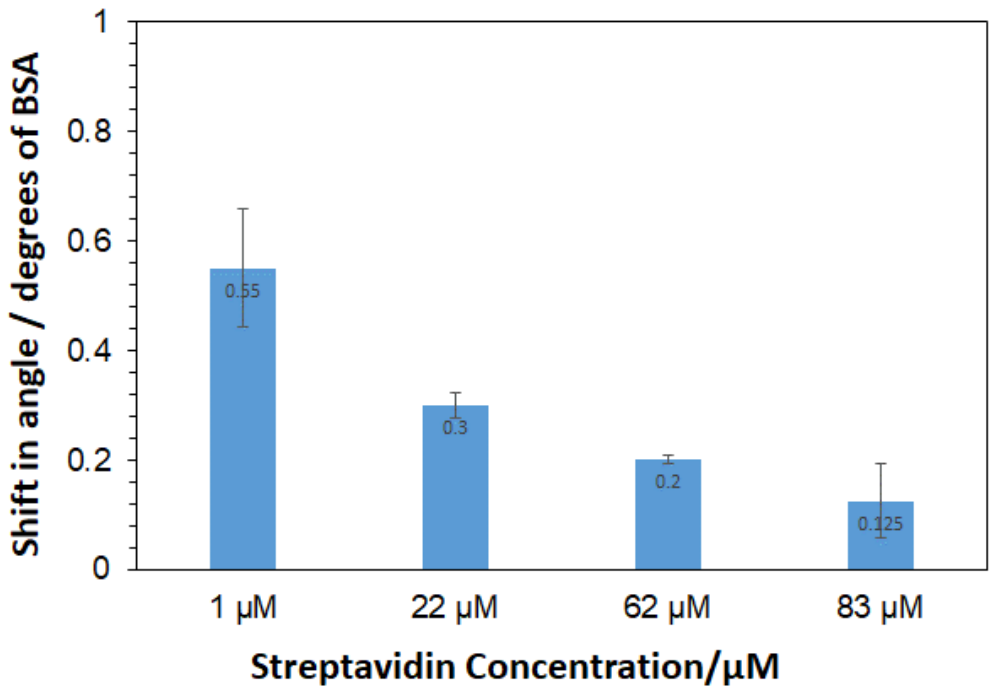

Figure 6.48: The differences between streptavidin concentrations and the shift in the angle of blocking molecules BSA.

Fig.6.49, shows the whole immobilization process carried out by using 0.3% of glutaraldehyde as a linker which interacts with streptavidin 83µM and immobilized biotinylated Anti-IgG 0.001 µM After that the chitosan waveguide film was blocked with 0.5% of BSA. At the end, detection IgG was injected to react with Anti-IgG and left overnight.

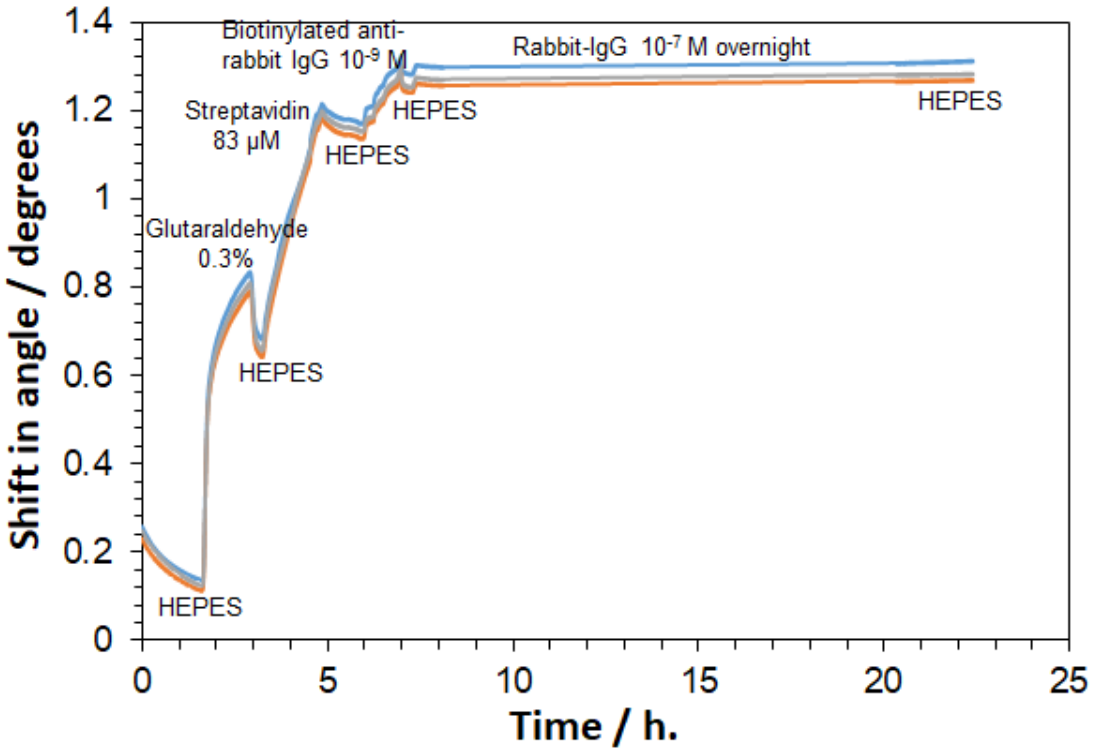

Figure 6.49: Changes in the reflectivity dip angle over time using different solutions (HEPES buffer pH 7.4, 0.3% of glutaraldehyde as a linker for the waveguide layer, Streptavidin 83 µM), blocked by 0.5% of BSA. The surface was initially incubated with RB4 dye (0.1 µM) for 5 min.

6.2 Verify the binding of streptavidin and biotin

The experiment was performed to verify the binding between streptavidin and biotin by using BSA and biotinylated BSA. BSA should not bind to the streptavidin while biotinylated BSA should do as it is conjugated with biotin. Upon obtained a shift in the dip position with 0.5% of biotinylated BSA that would indicate the reaction between streptavidin 83 µM and biotin as shown in fig.6.50.

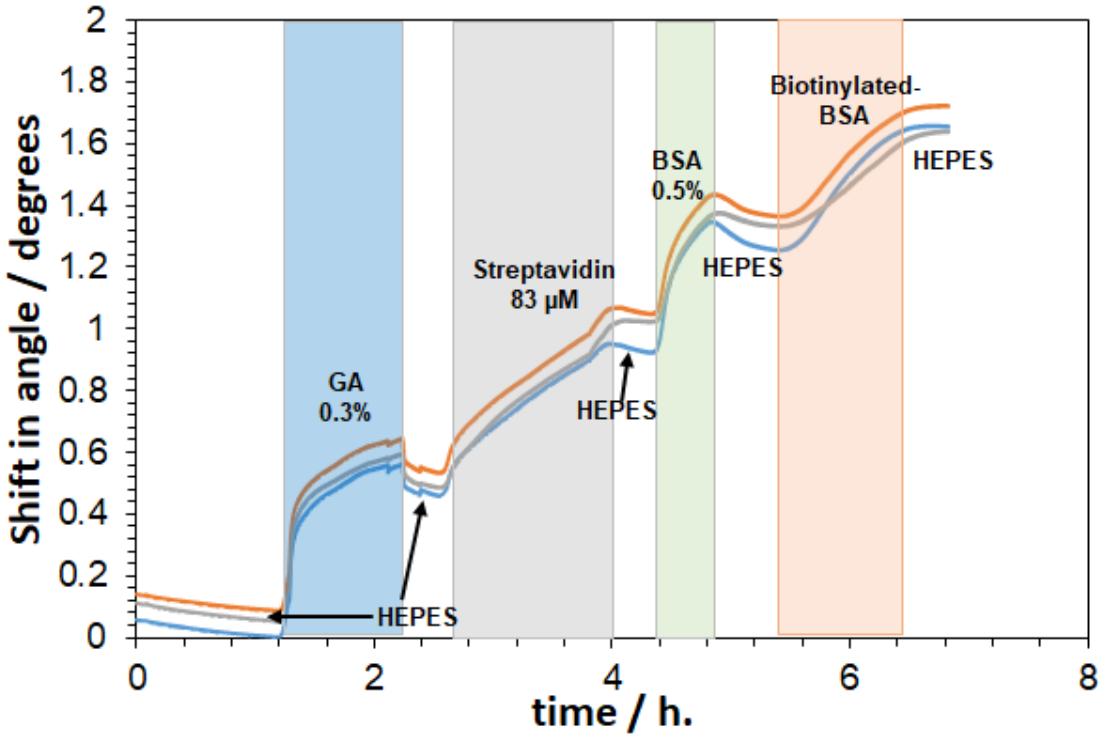

Figure 6.50: Changing in the reflectivity dip angle versus time using different solutions HEPES buffer pH 7.4, 0.3% of glutaraldehyde as a linker for the waveguide layer, Streptavidin 83 µM, blocked by 0.5% of BSA. Then Biotinylated-BSA. The surface initially incubated with the RB4 dye (0.1 µM) for 5min.

Immobilization of BSA and Biotinylated-BSA fig.6.50, indicated that the binding between streptavidin-biotin when using concentration of streptavidin 83 µM and 0.5% concentration of blocking molecules BSA.

6.3 Increase an Interaction Time of the Antibody -Antigen

This experiment is done to let the biotinylated antibody to react with streptavidin for an overnight as this would lead to more binding of antibody to the chitosan surface. As indicated in fig.6.51. When left the biotinylated antibody to react with streptavidin for an overnight as this was led to more binding of antibody to the chitosan surface.

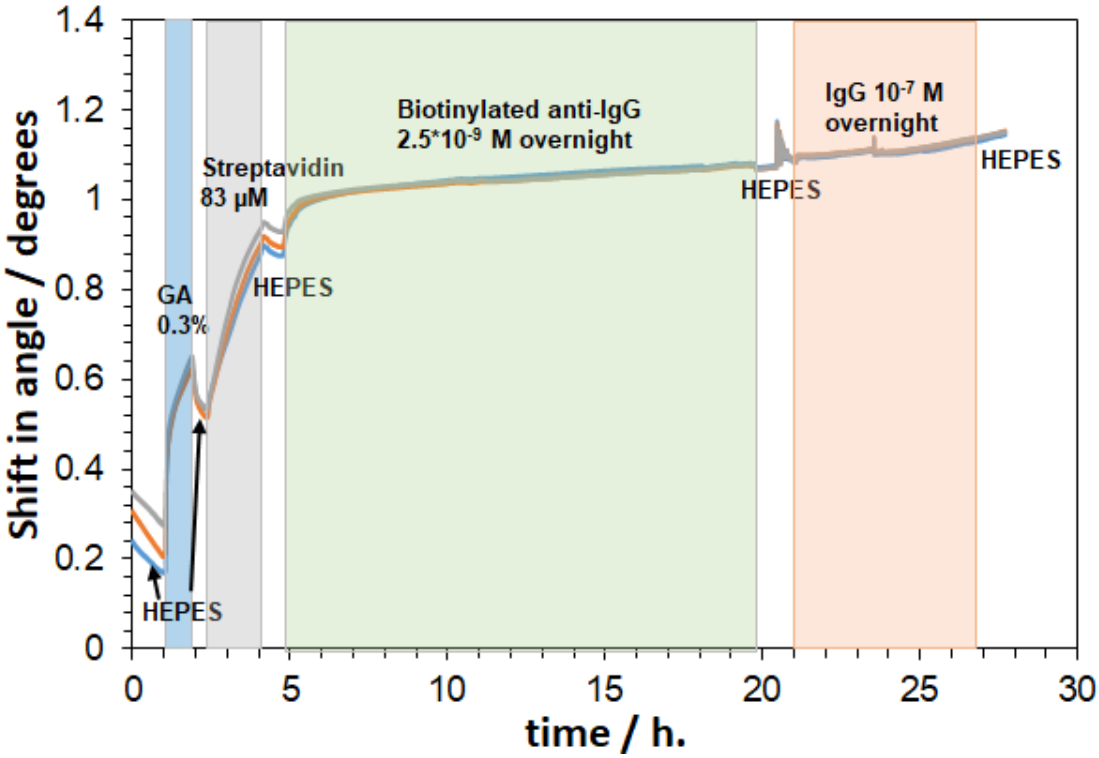

Figure 6.51: Changing in the reflectivity dip angle versus time using different solutions HEPES buffer pH 7.4, 0.3% of glutaraldehyde as a linker for the waveguide layer, Streptavidin 83 µM, blocked by 0.5% of BSA. Biotinylated anti-IgG 2.5*10^{-9} M was injected for 2 h, and IgG 10^{-7} M was injected overnight. The surface initially incubated with the RB4 dye (0.1 µM) for 5 min.

Immobilization of Biotinylated-Anti-IgG 2.5*10^{-9} M was injected overnight and IgG 10^{-7} M was injected also overnight when put HEPES buffer still goes up after overnight, this means the reaction sensitivity between antibody-antigen was increased via applying streptavidin-biotin reaction. According to the results, the binding of rabbit-IgG and the immobilised anti-rabbit IgG was studied and has been developed.

6.4 Conclusion

In this chapter the binding of rabbit IgG to anti-rabbit IgG using different immobilization methodologies has been described. Firstly, EDC-Sulpho-NHS was utilized to crosslink anti-IgG antibody into the chitosan waveguide layer at pH 7.4. The mechanism of this immobilization depends on the activation of a carboxyl group which is conjugated to the antibody by using a different ratio, 1:4, 1:1 or 4:1, of EDC-Sulpho-NHS. It was found that EDC-Sulpho-NHS based crosslinking of anti-IgG has lower attaching efficiencies, which is contrary to the literature stating[141] that the binding efficiencies were enhanced when EDC-Sulpho-NHS was used. That may be due to the molecular interactions between EDC and Sulpho-NHS, which might be interfering with the binding of EDC-Sulpho-NHS activated Anti-IgG to the amino groups of chitosan waveguide layer. Secondly, glutaraldehyde as a bifunctional cross-linker was used to cross-link anti-IgG by forming a Schiff base, and used as a linker to the amines of chitosan when an imine bond is formed immediately. Thus, a strong link between the chitosan waveguide film and the antibody will be established. But as indicated in the results, there is high reactivity of glutaraldehyde toward chitosan's amine but no interaction for Anti-IgG with detection IgG. That may be due to the orientation of the antibody, which means that the aldehyde group of glutaraldehyde reacted with the amino groups of the antibody and affected the orientation of the antibody. Lastly, the biotin-streptavidin system was used to immobilize the antibody. Streptavidin was bound to the amine groups within the chitosan layer using glutaraldehyde. Then biotinylated anti-rabbit IgG was immobilised by binding between streptavidin and biotin. Finally, the binding of rabbit-IgG and the immobilised anti-rabbit IgG was studied. Once the immobilisation chemistry has been developed, it is intended that the waveguide system should be used to study the release of tissue factor (TF) from pancreatic cells in real time, and that its results will be compared to those of the conventional microwell-based ELISA system. These label-free biosensors have potential for continuous measurement for healthcare monitoring.

CHAPTER 7

Quantification of Tissue Factor (III)

Tissue factor (TF) is well known to be a principal initiator of the external pathway of coagulation, with a concentration around 100–150 pg mL^{-1} of TF in a healthy person in the blood; it is a trans-membranous 47 kDa glycoprotein which contains 263 amino acids [1]. It is also known as full-length TF (fITF) factor (III) and CD142. The high expression of TF in primary pancreatic cells is thought to be related to one of the underlying mechanisms giving rise to the hyper-coagulable state associated with this malignancy [2]. Moreover, there is a relationship between high expression of TF with other types of malignancy such as colorectal cancer and non-small cell lung carcinoma. Researchers in these fields propose that the aggressive path of cell invasion and thrombosis is correlated with high expression of TF from pancreatic cell lines. The main purpose of the current study was to retrieve tissue factor sample (supernatant), perform ELISA to quantify its TF and compare this data with an assay performed on the waveguide layer. Two types of pancreatic cell lines, Miapaca-2 and Aspc-1 were used to measure the concentration of expression TF (III). Miapaca-2 is generated from a patient with a primary adenocarcinoma tumour, and has epithelial cell-like morphology, abundant cytoplasm, low/no TF expression; Aspc-1 is generated from pancreas ascites from an adenocarcinoma patient, low/moderate TF expression).

The chapter is divided into the following sections the expression and activity of TF in these cells was confirmed as below. The pancreatic cell lines were supplemented with a range of concentrations. The cells were analysed by ELISA and TF concentrations were determined from a standard curve prepared alongside.

7.1 Expression of Tissue factor receptor from pancreatic cell lines

To determine the concentration of tissue factor (TF), two types of pancreatic cell lines Aspc-1, and Miapaca-2 were cultured in PRMI-1640 supplemented with 10% fetal calf serum and DMEM (high glucose Dulbecco's Modified Eagle Medium (Hyclone) supplemented with 10% fetal bovine serum (FBS), penicillin and streptomycin) media respectively, as a first step. This was followed by harvesting them as described in sections 2.15.2.1, 2.15.2.2, and 2.15.2.3, respectively. The average number of viable pancreatic cells were counted within the cell suspension for various recovery periods (0, 1, 2 … and 72 h) as indicated in fig.7.1.

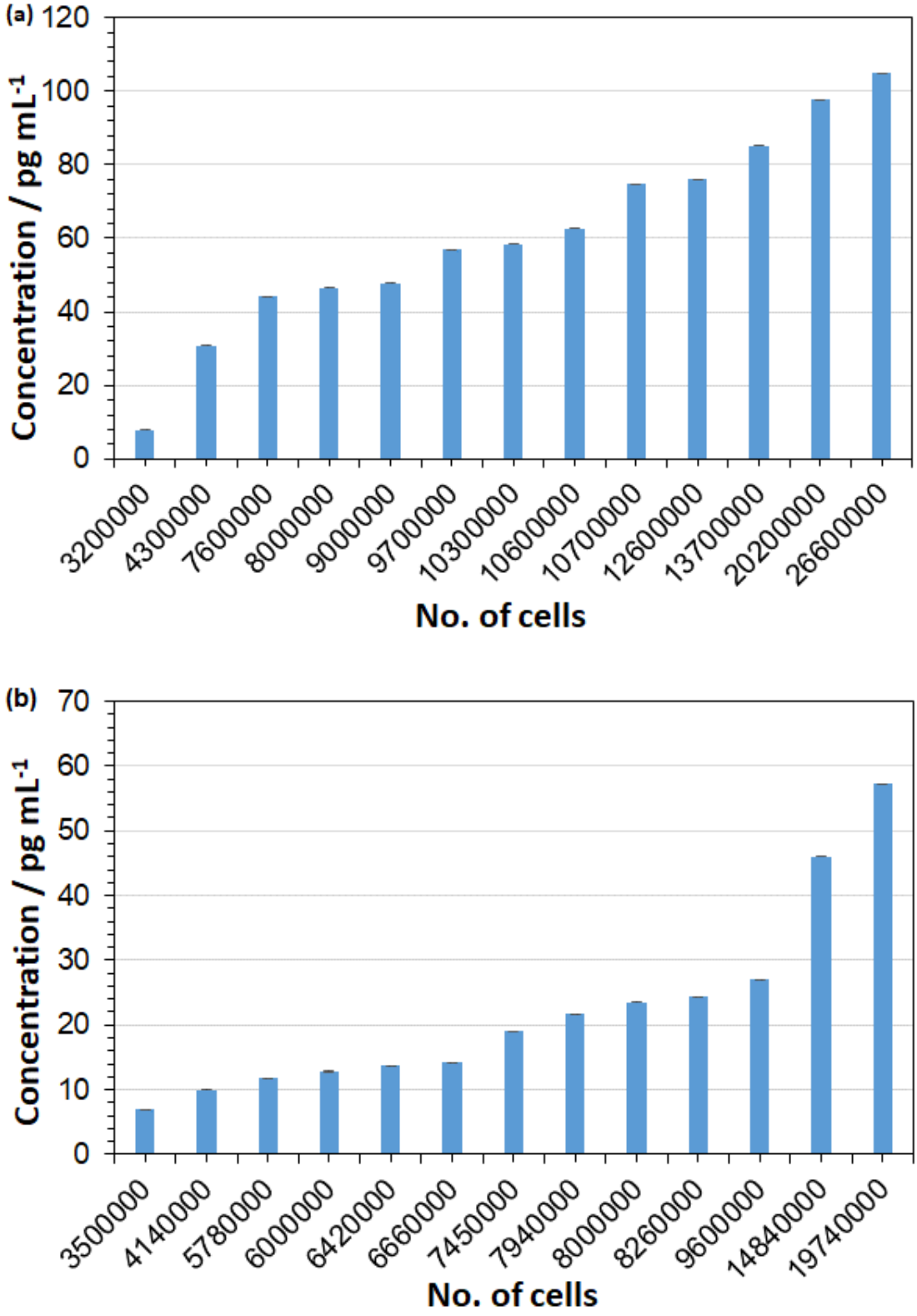

Figure 7.1: The correlation between the concentration of Tissue factor (TF) and the number of viable Aspc-1 (a) and Miapaca-2 cells (b) through various recovery periods [λ_{max} at 450 nm] and the rate of centrifugation 400 rpm (n=3).

The expression of Tissue Factor (III) concentration within pancreatic adenocarcinoma cells is directly proportional to the number of living cells through the recovery period. The highest expression of TF was noted on the Aspc-1 cell line, compared with the concentration of Tissue factor expressed within Miapaca-2 cell line. Many studies have confirmed the difference between pancreatic carcinoma cell lines in the expression of tissue factor. This variation might be due to systemic hypercoagulopathy in pancreatic cancer [154], as mentioned previously.

7.2 Tissue Factor (TF) ELISA method

A range of standard Aspc-1 and Miapaca-2 pancreatic cell lines (7.825-500 pg mL^{-1}) were used to generate a calibration curve figs.7.2, and 7.3, and This standard curve is constructed by plotting the mean absorbance for each standard on the y-axis against the concentration on the x-axis and drawing a best-fit curve through the points on the graph only for demonstration purposes. A standard curve should be generated for each set of samples assayed.

Typical data from Human Tissue Factor (III) was obtained for each type of pancreatic cell lines (Aspc-1 and Miapaca-2 cells). The mean of the triplicate readings for each standard, control, and sample were obtained and the average zero standard optical density (O.D.) were subtracted as indicated in tables 7.1, and 7.2. The data was linearized by plotting the log of the human Coagulation Factor III concentrations versus the log of the O.D., and the best-fit line was determined by regression analysis.

The absorbance of standard solutions prepared for these cells was recorded by an ELISA plate reader at 450 nm, as described in section 2.15.3.1 and 2.15.3.2. Bound (TF) protein is detected by emission of light, which is proportional to the amount of antibody/antigen complex captured from the samples. The TF concentrations of standard solutions, which are proportional to the colour intensity, were measured.

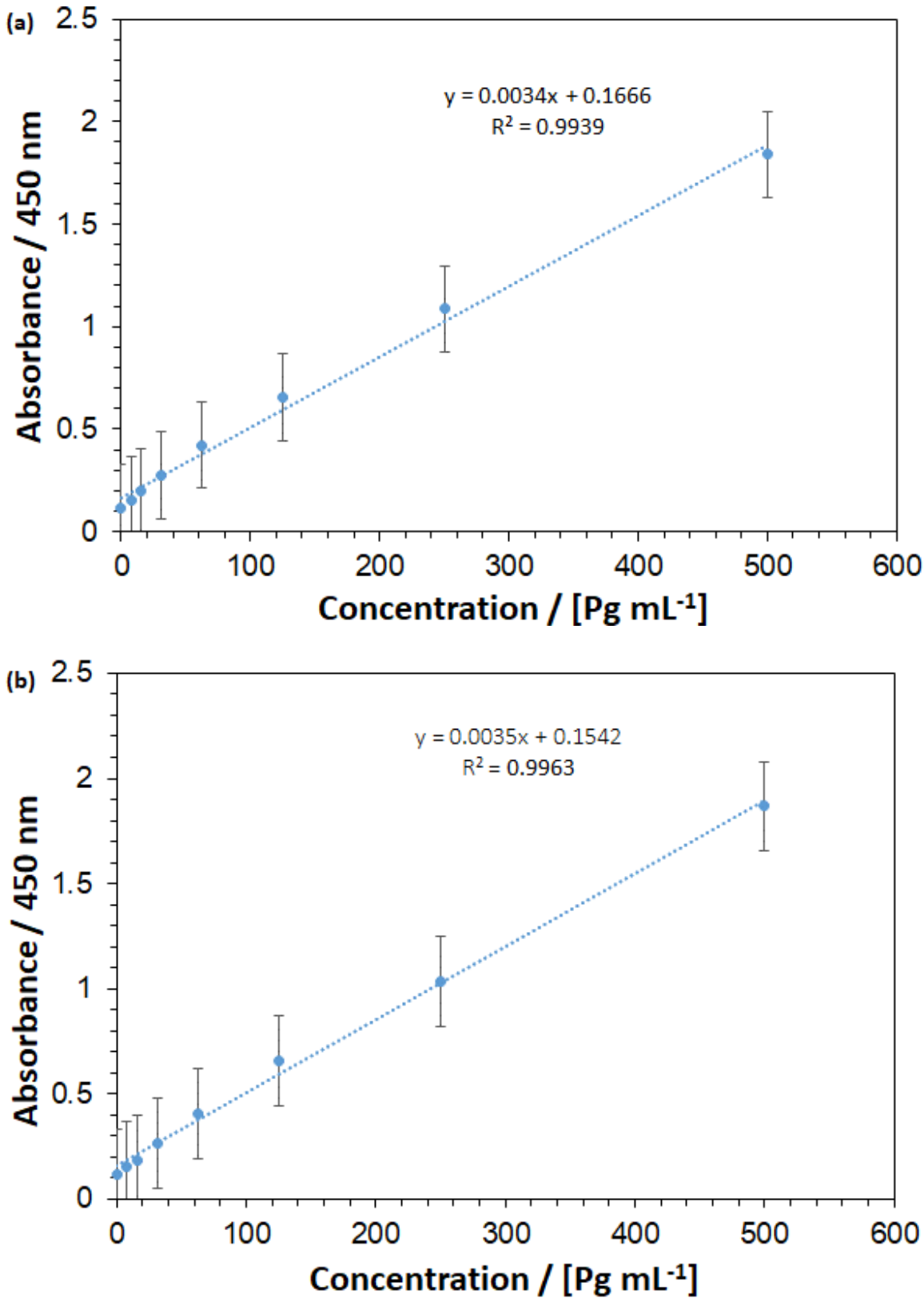

Figure 7.2: Calibration curve of Tissue Factor (TF) standards, The set of known average standard concentration was used to plot the curve, and unknown sample concentration was determined by using this equation: Y=MX+C, where Y is the absorbance of the unknown sample; M from above is the slope of the fitting line; X is the concentration of the unknown sample; and C represents the intercept (equals zero for the best fitting line). (a) Aspc-1 and (b): Miapaca-2 cells with error bar (±0.1).

This standard curve is constructed by plotting the mean absorbance for each standard on the y-axis against the concentration on the x-axis and drawing a best-fit curve through the points on the graph only for demonstration purposes. A standard curve should be generated for each set of samples assayed.

Typical data from Human Tissue Factor (III) was obtained for each type of pancreatic cell lines (Aspc-1 and Miapaca-2 cells). The mean of the triplicate readings for each standard, control, and sample were obtained and the average zero standard optical density (O.D.) were subtracted as indicated in tables 7.1, and 7.2. The data was linearized by plotting the log of the human Coagulation Factor III concentrations versus the log of the O.D., and the best-fit line was determined by regression analysis.

Table 7.1: Correlation between the Concentration of Tissue Factor (TF) standards and the absorbance. Seven standard tests were run three times, and average absorbance was calculated for Aspc-1 cell lines.

Concentration of TF standard /pg mL^{-1}	**Absorbance. 1**	**Absorbance. 2**	**Absorbance. 3**	**Mean of absorbance**	**STDEV**
7.825	0.159	0.158	0.155	0.157	±0.002
15.65	0.185	0.191	0.173	0.183	±0.001
31.1	0.255	0.277	0.256	0.262	±0.012
62.5	0.409	0.411	0.398	0.406	±0.007
125	0.665	0.66	0.647	0.657	±0.009
250	1.066	1.026	1.017	1.036	±0.026
500	1.888	1.853	1.86	1.867	±0.018

Table 7.2: Correlation between the Concentration of Tissue Factor (TF) standards and the absorbance. Seven standard tests were run three times, and mean absorbance was calculated for MiaPaca-2 cell lines.

Concentration of TF standard /pg mL^{-1}	Absorbance. 1	Absorbance. 2	Absorbance. 3	Mean of absorbance	STDEV
7.825	0.154	0.157	0.157	0.156	±0.0017
15.65	0.199	0.199	0.192	0.19667	±0.004
31.1	0.282	0.277	0.269	0.276	±0.0065
62.5	0.427	0.422	0.421	0.42333	±0.003
125	0.621	0.668	0.672	0.65367	±0.028
250	1.121	1.065	1.074	1.08667	±0.030
500	1.806	1.821	1.894	1.84033	±0.047

The concentration of Tissue Factor expressed from pancreatic cell lines can be noted as proportional over time up to 72 h (see fig.7.3). And the correlation between concentrations of TF and time is illustrated in for AsPC-1 and Miapaca-2 cells respectively. Concentrations of Tissue Factor (III) expressed on pancreatic cell lines ere 107.82 pg mL^{-1}, and 57.27 pg mL^{-1} after 72 hr. The absorbance was 0.52 nm for Aspc-1 cells, whereas it was 0.35 nm for Miapaca-2 cells, respectively after 72 h as shown in fig.7.4. The amount of human Tissue Factor captured in strips is proportional to the intensity of yellow solutions that changes after adding acidic stop solution. Further studies were found TF concentrations that expression from pancreatic cell lines in patients with pancreatic cancer to be more than in normal controls that TF secreted by activated leukocytes.

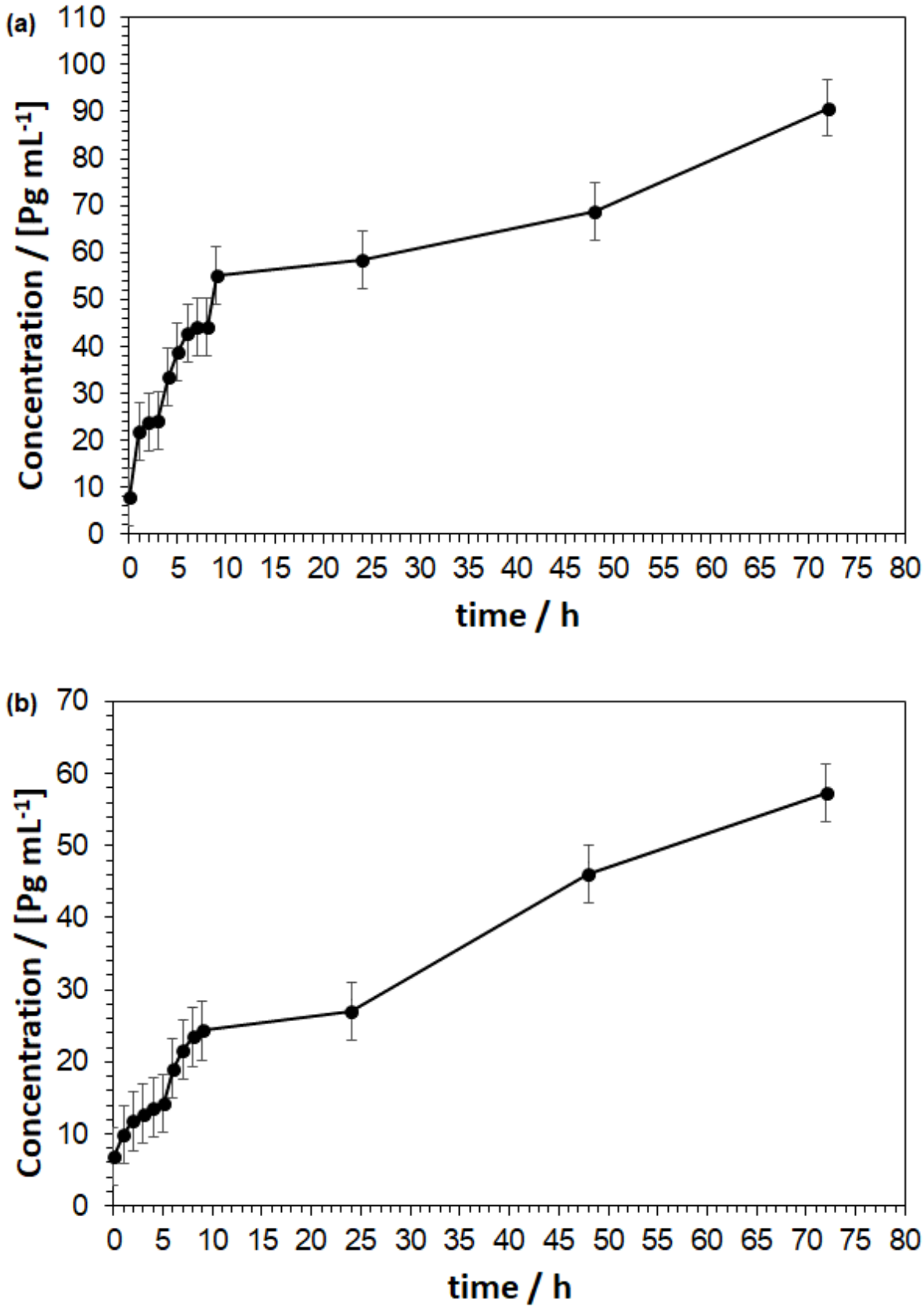

Figure 7.3: relationship between time and the concentration of Tissue Factor expressed from (a) Aspc-1 and (b) Miapaca-2 cells at λ_{max} at 450 nm, rate of centrifugation 400 rpm.

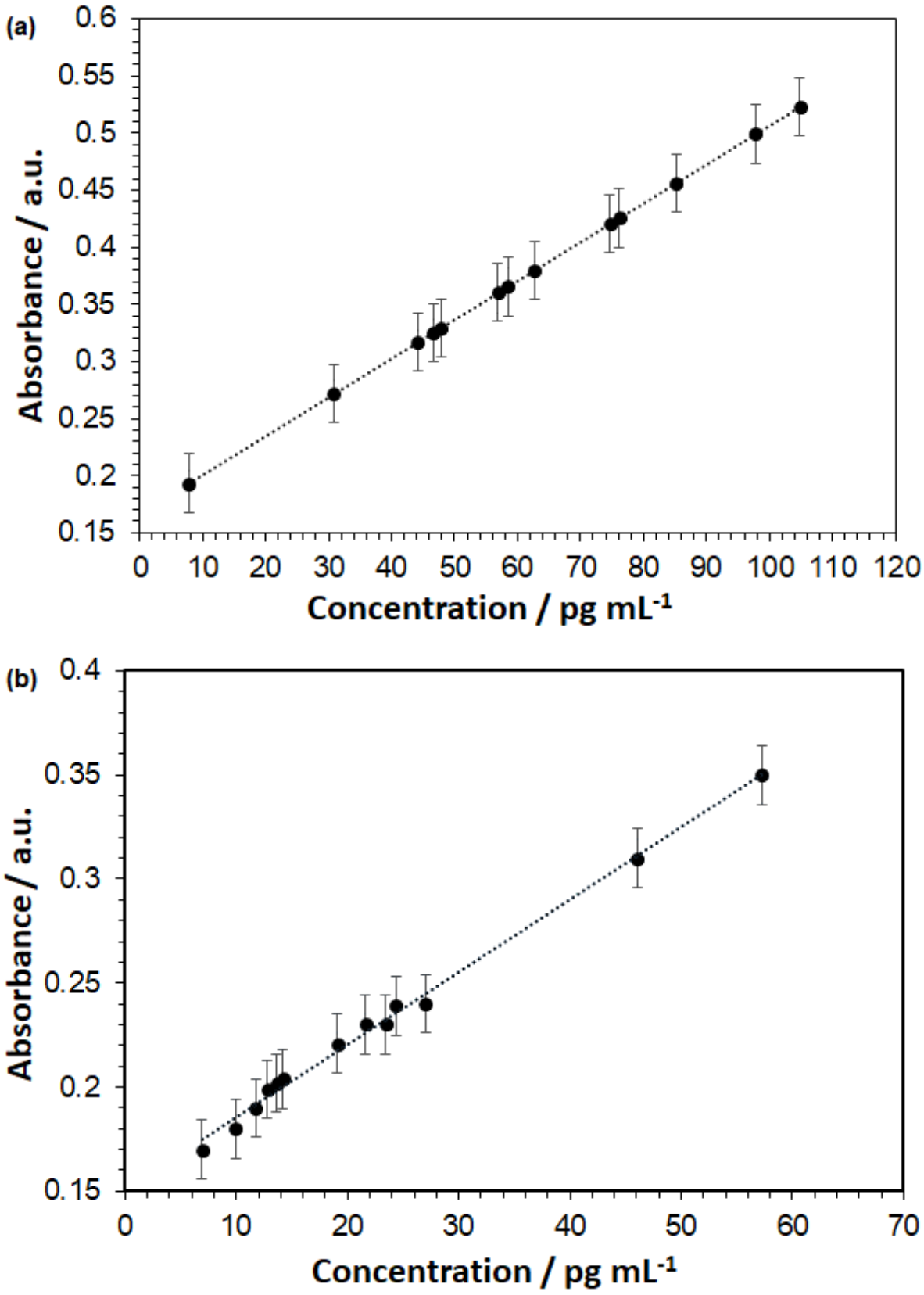

Figure 7.4: The relationship between concentration and absorbance of Tissue factor expressed from (a) Aspc-1 cells and (b) Miapaca-2 cells at different times [λ_{max} at 450nm]; rate of centrifugation 400 rpm.

From the previous results of TF that have been released from pancreatic cell lines (Aspc-1 and Miapaca-2 cells) into the cell culture media was studied over a period of 72 h and quantified via ELISA with a calibration curve in the concentration range of 7.825 to 500 pg mL^{-1}. Cell numbers were established via haemocytometer. From the ELISA data it could be estimated that, for the Aspc-1 cells, TF release raised for the first 24 h and then dropped after 72 h. For the Miapaca-2 cells, TF release rose over the first 10 h and then rained at this level.

7.3 Immobilisation of Biotinylated- anti human coagulation Factor (III) using Dye-Doped Leaky waveguide sensor

Tissue factor binding was then studied on the dye-doped leaky waveguide system. The concept and expected sensor output area with a TF concentration of 30 pg mL^{-1} is shown in fig.7.5. This experiment has been performed to investigate the binding of Biotinylated goat anti-human coagulation Factor (III) using different concentration (1, 0.1, 0.01, and 0.001 µM) with once concentration of antigen standard TF (III) 30 pg mL^{-1}.

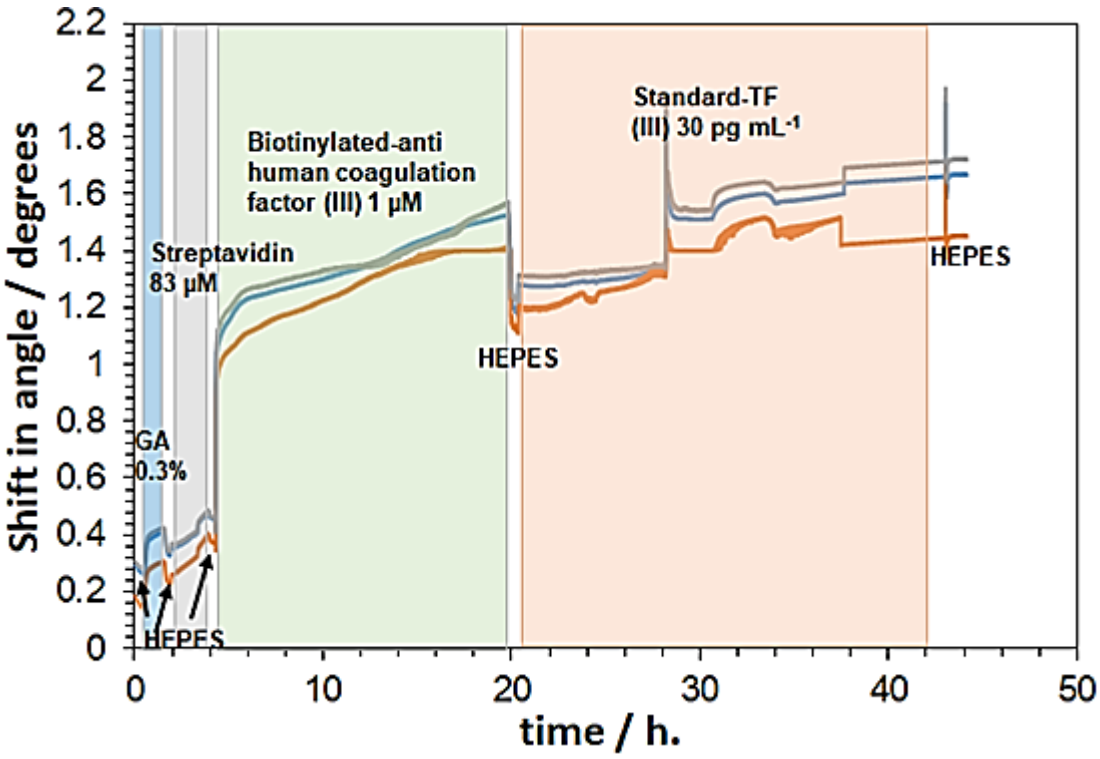

Figure 7.5: Changing in the reflectivity dip angle versus time using different solutions HEPES buffer pH 7.4, 0.3% of glutaraldehyde as a linker for the waveguide layer, Streptavidin 83 µM, Biotinylated goat anti-human coagulation Factor (III) 1 µM overnight. Then recombinant human coagulation Factor (III) 30 pg mL^{-1}overnight. The surface initially incubated with the RB4 dye (0.1 µM) for 5 min.

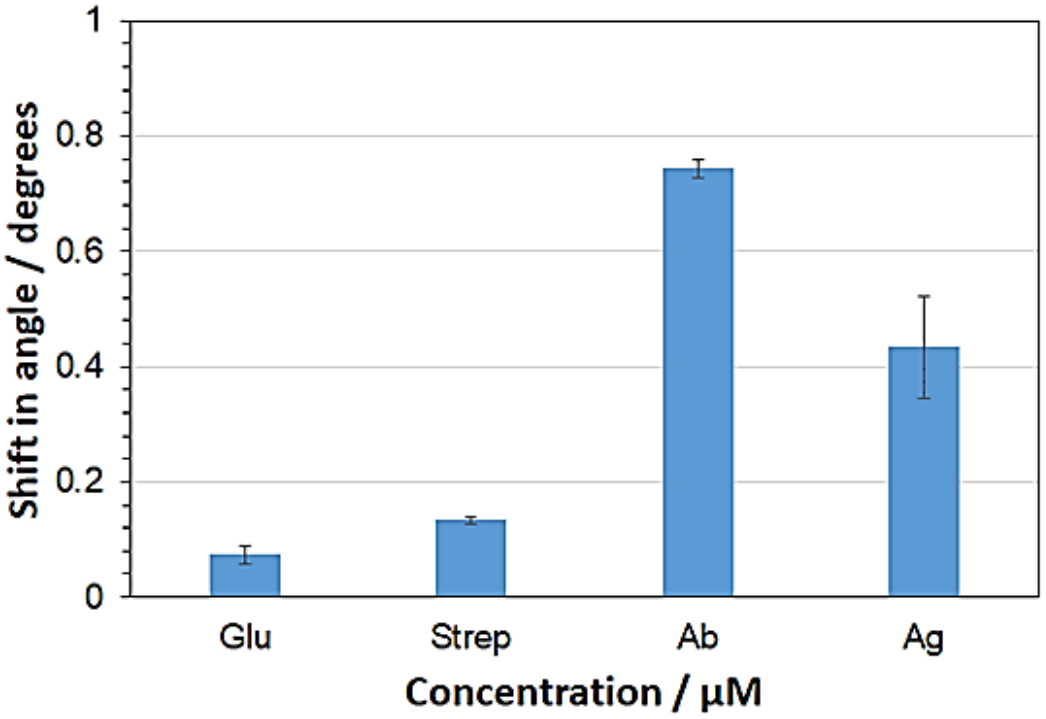

Figure 7.6: Variation of shift in angle according to change the concentration of Biotinylated anti-goat human coagulation Factor (III) 1 µM.

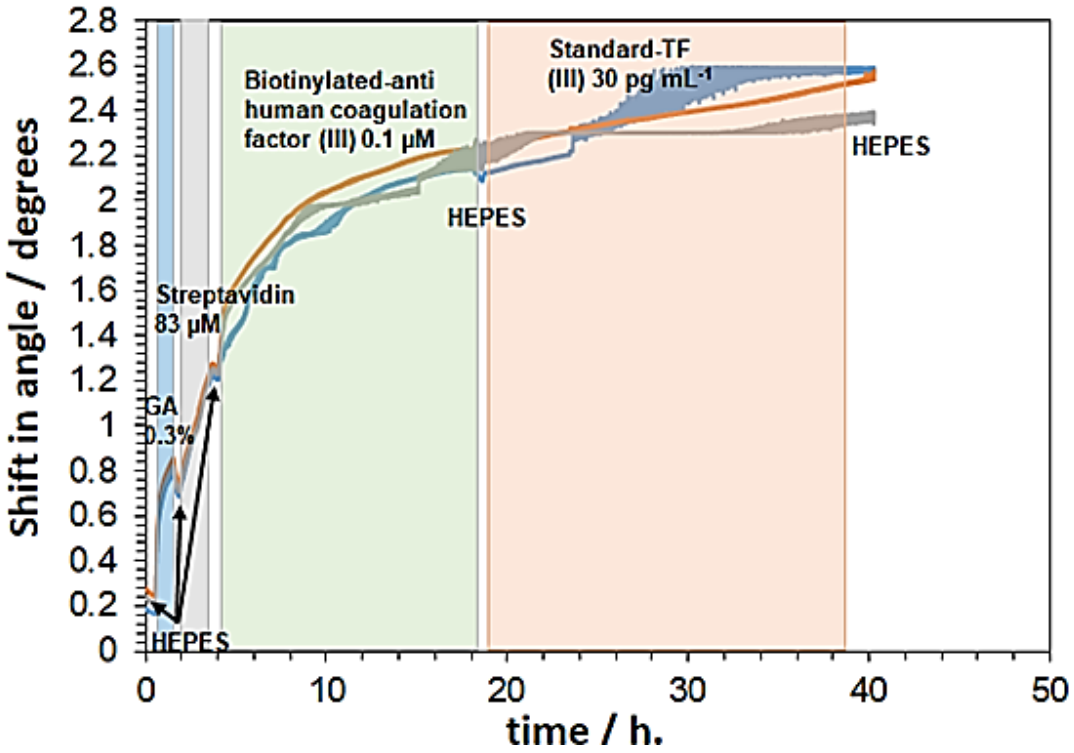

Figure 7.7: Changing in the reflectivity dip angle versus time using different solutions HEPES buffer pH 7.4, 0.3% of glutaraldehyde as a linker for the waveguide layer, Streptavidin 83 µM, Biotinylated goat anti-human coagulation Factor (III) 0.1 µM overnight. Then recombinant human coagulation Factor (III) 30 pg mL^{-1} overnight. The surface initially incubated with the RB4 dye (0.1 µM) for 5 min.

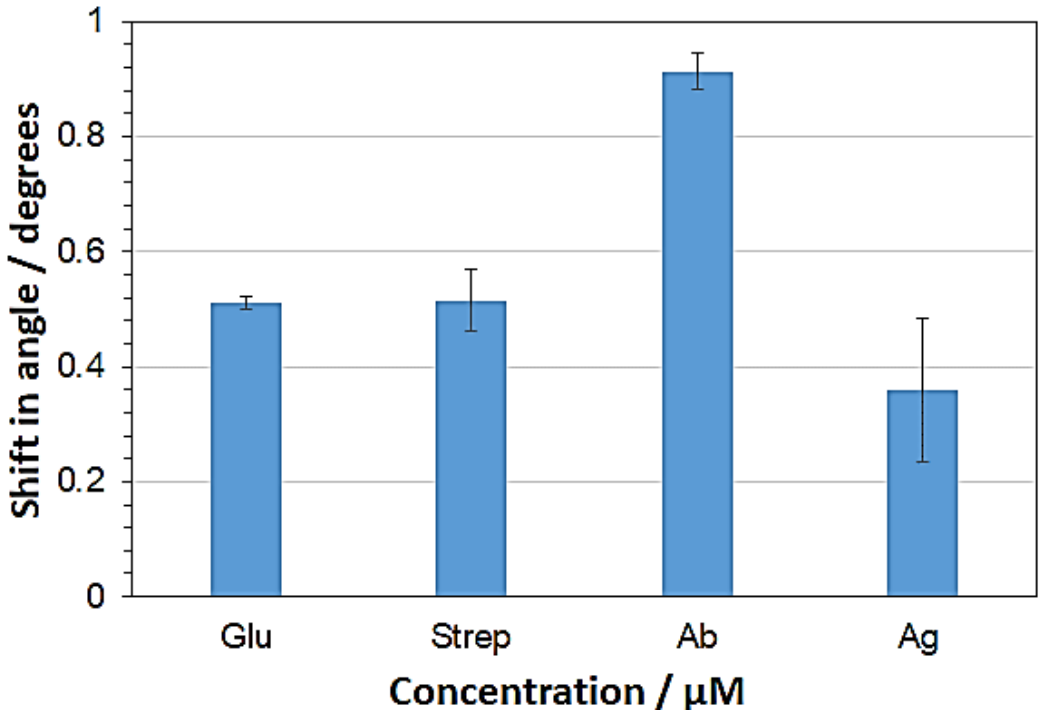

Figure 7.8: Variation of shift in angle according to change the concentration of Biotinylated anti-goat human coagulation Factor (III) 0.1 µM.

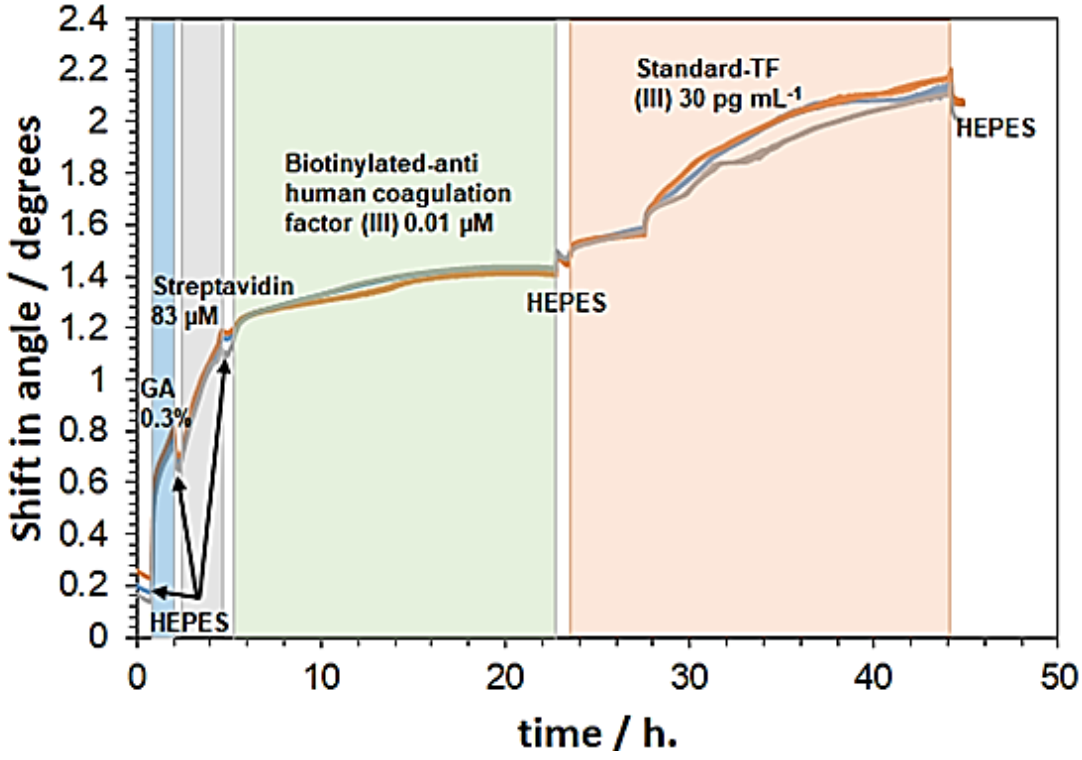

Figure 7.9: Changing in the reflectivity dip angle versus time using different solutions HEPES buffer pH 7.4, 0.3% of glutaraldehyde as a linker for the waveguide layer, Streptavidin 83 µM, Biotinylated goat anti-human coagulation Factor (III) 0.01 µM overnight. Then recombinant human coagulation Factor (III) 30 pg mL^{-1} overnight. The surface initially incubated with the RB4 dye (0.1 µM) for 5 min.

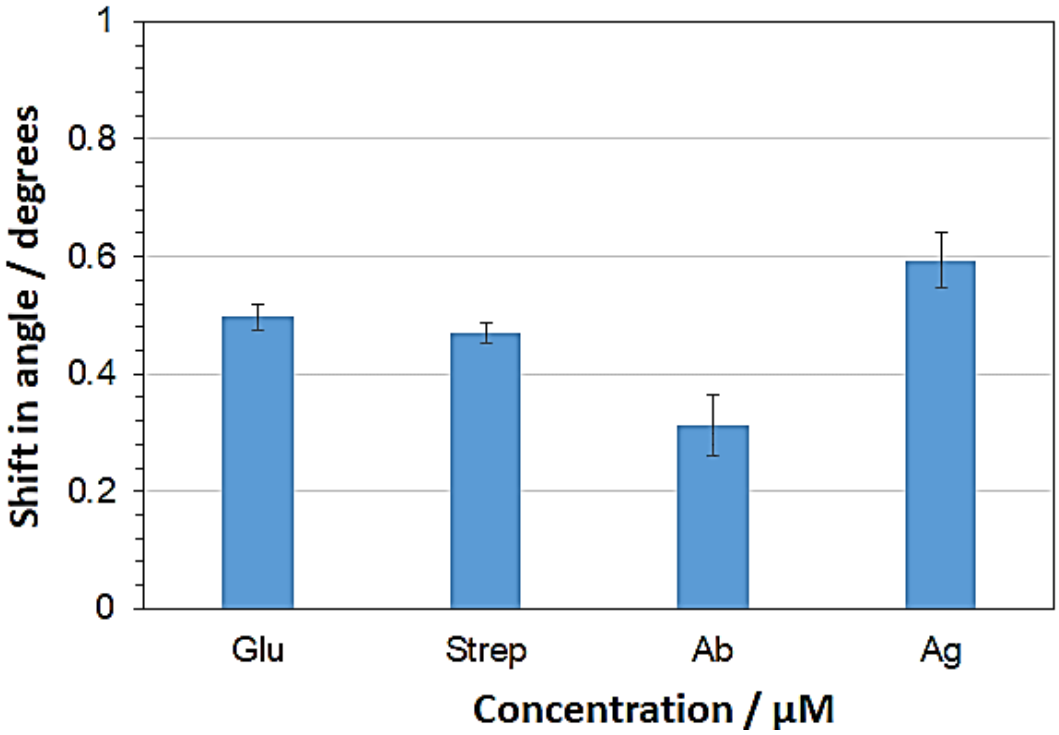

Figure 7.10: Variation of shift in angle according to change the concentration of Biotinylated anti-goat human coagulation Factor (III) 0.01 µM.

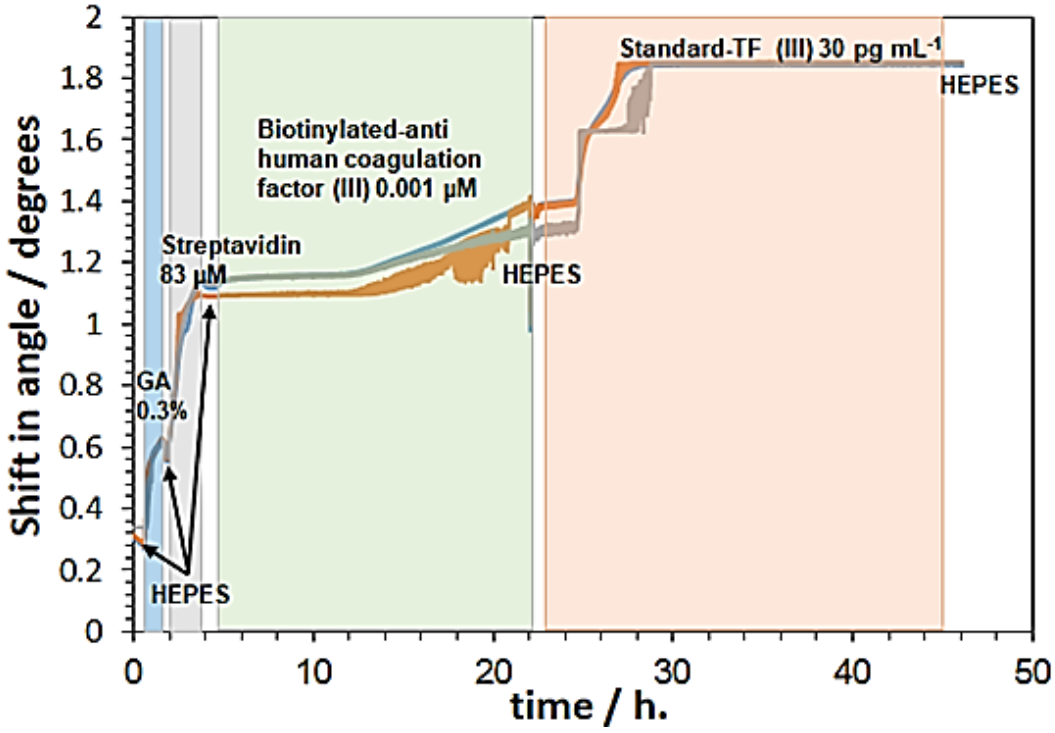

Figure 7.11: Changing in the reflectivity dip angle versus time using different solutions HEPES buffer pH 7.4, 0.3% of glutaraldehyde as a linker for the waveguide layer, Streptavidin 83 µM, Biotinylated goat anti-human coagulation Factor (III) 0.001 µM overnight. Then recombinant human coagulation Factor (III) 30 pg mL^{-1} overnight. The surface initially incubated with the RB4 dye (0.1 µM) for 5 min.

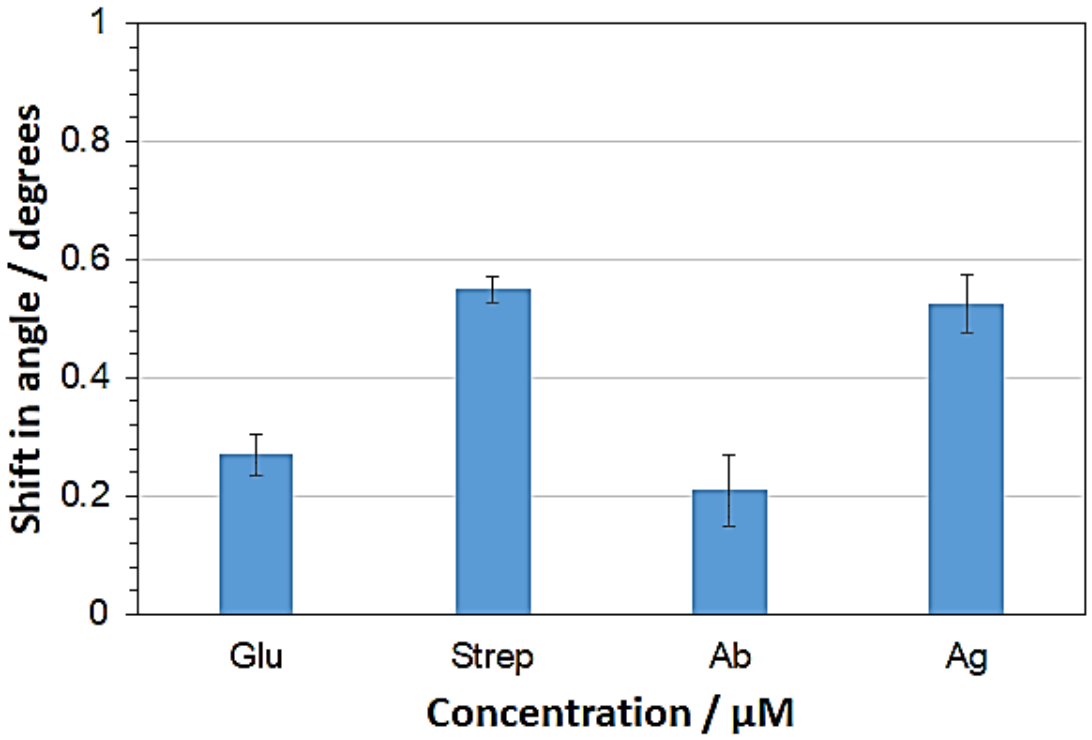

Figure 7.12: Variation of shift in angle according to change the concentration of Biotinylated anti-goat human coagulation Factor (III) 0.001 µM.

Fig.7.13 shows the degree of shifting in angle upon applying different concentrations of Biotinylated anti-goat human coagulation Factor (III) as shown in figs.7.5, 7.7, 7.9, and 7.11. Each concentration of antibody was performed on different chitosan chip that was initially treated with glutaraldehyde, streptavidin. It can be seen from the figs.7.6, 7.8, 7.10, and 7.12, the concentration of antibody is decreased, the degree of shifting in angle is increased which indicates more antigen bound to immobilized antibody. Each bar represented the average of the three reading from different boxes. And have been found that when using a concentration of 0.01 µM of the antibody leads to bind more of standard TF to the surface.

When leave the antibody for an overnight, more shifting in the dip position that was obtained which means that more antibody bound to the surface. Also this applied for an antigen as it is bound to the surface more and more once it leaves for an overnight.

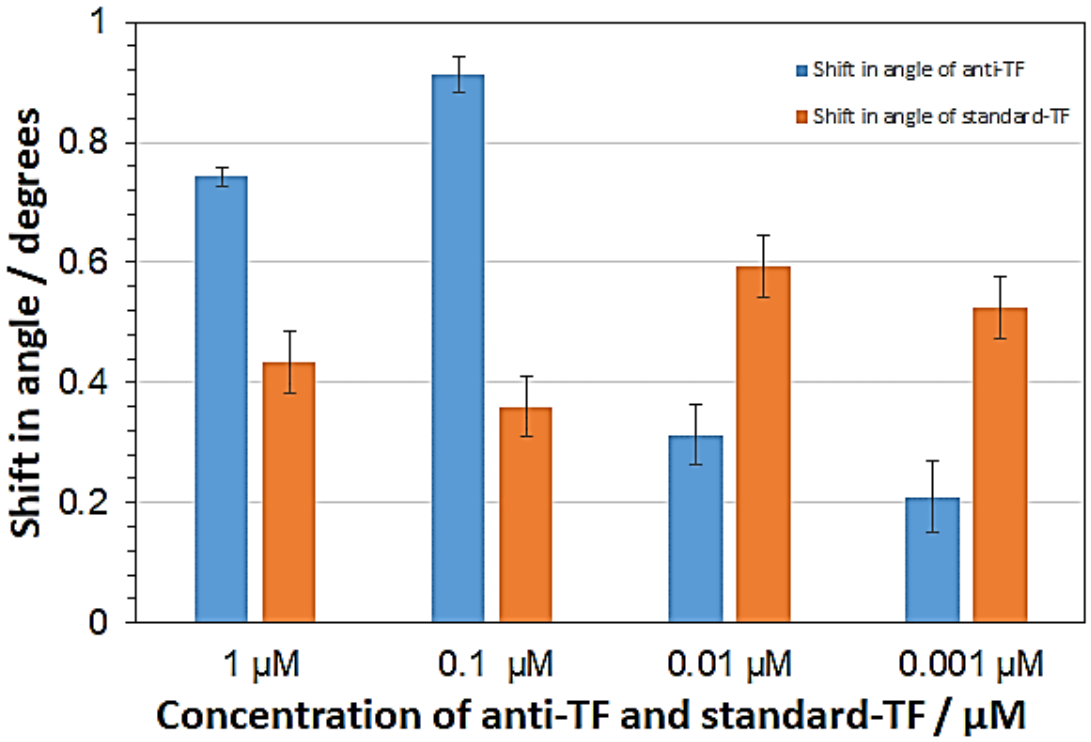

Figure 7.13: Variation of shift in angle according to change the concentration of Biotinylated anti-goat human coagulation Factor (III) 1, 0.1, 0.01, and 0.001 µM.

The blue bar represents the average shift obtained from the different antibody concentrations for the orange bar represents the average shift obtained from flushing the standard tissue factor (III) which is always at the same concentration (30 pg mL^{-1}).Each bare represented the average of the three reading from different boxes and have been found out that using a concentration of 0.01 µM of the antibody leads to bind more of standard TF to the surface. So, this concentration (0.01 µM) of biotinylated anti human coagulation factor will be used with different concentrations of the antigen (standard tissue factor (III).

7.4 Optimise concentration of standard Tissue Factor (III)

The aim of these experiments are to find out which concentration of the antibody that can provide a high degree of shifting by applying standard TF, and to investigate the reaction between the right concentration of antibody biotinylated anti-goat human coagulation factor (III) using different concentrations of standard-TF (III) 30, 3, 0.3, 0.03, and 0.03 pg mL^{-1}. This will lead to make a calibration curve and hence calculate the limit of detection. Signals obtained for TF standard solutions of 0.003, 0.03, 0.3, 3, and 30 pg mL^{-1} are shown in figs.7.14, 7.16, 7.18, 7.20, and fig.7.22.

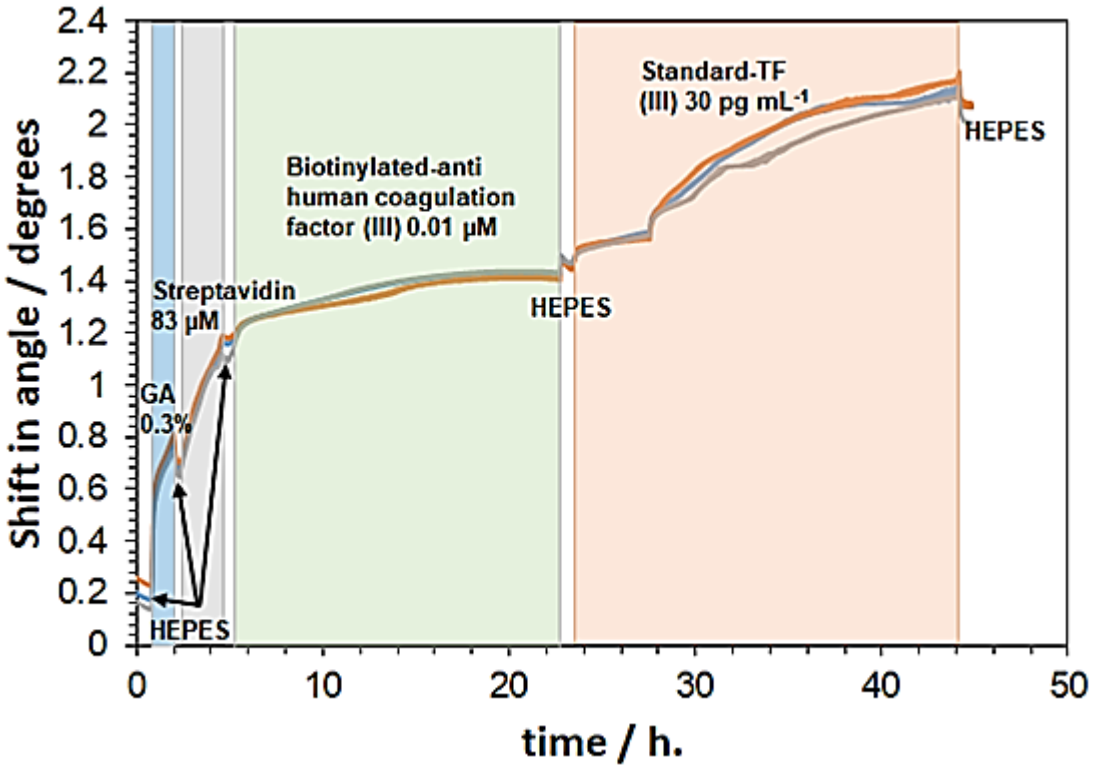

Figure 7.14: Changing in the reflectivity dip angle versus time using different solutions HEPES buffer pH 7.4, 0.3% of glutaraldehyde as a linker for the waveguide layer, Streptavidin 83 µM, Biotinylated goat anti-human coagulation Factor (III) 0.01 µM overnight, . Then recombinant human coagulation Factor-(III) 30 pg mL^{-1} overnight. The surface initially incubated with the RB4 dye (0.1 µM) for 5 min.

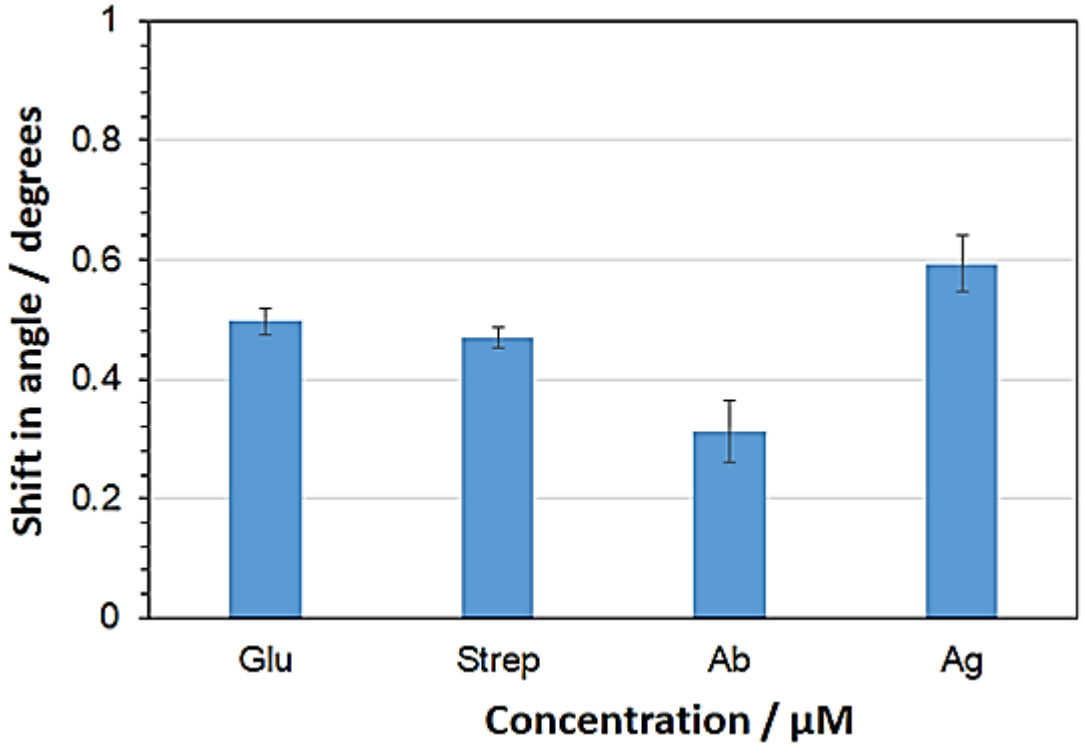

Figure 7.15: Variation of shift in angle according to change the concentration of standard Factor (III) 30 pg mL^{-1}.

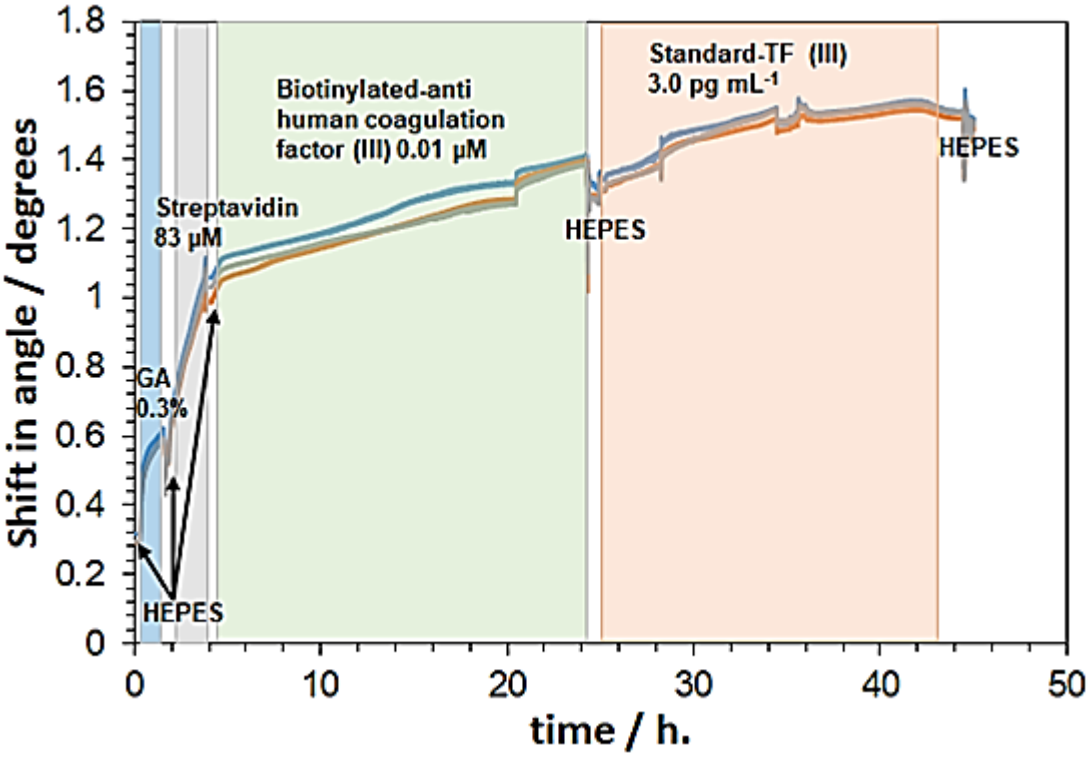

Figure 7.16: Changing in the reflectivity dip angle versus time using different solutions HEPES buffer pH 7.4, 0.3% of glutaraldehyde as a linker for the waveguide layer, Streptavidin 83 µM, Biotinylated goat anti-human coagulation Factor (III) 0.01 µM overnight, . Then recombinant human coagulation Factor (III) 3 pg mL^{-1} overnight. The surface initially incubated with the RB4 dye (0.1 µM) for 5 min.

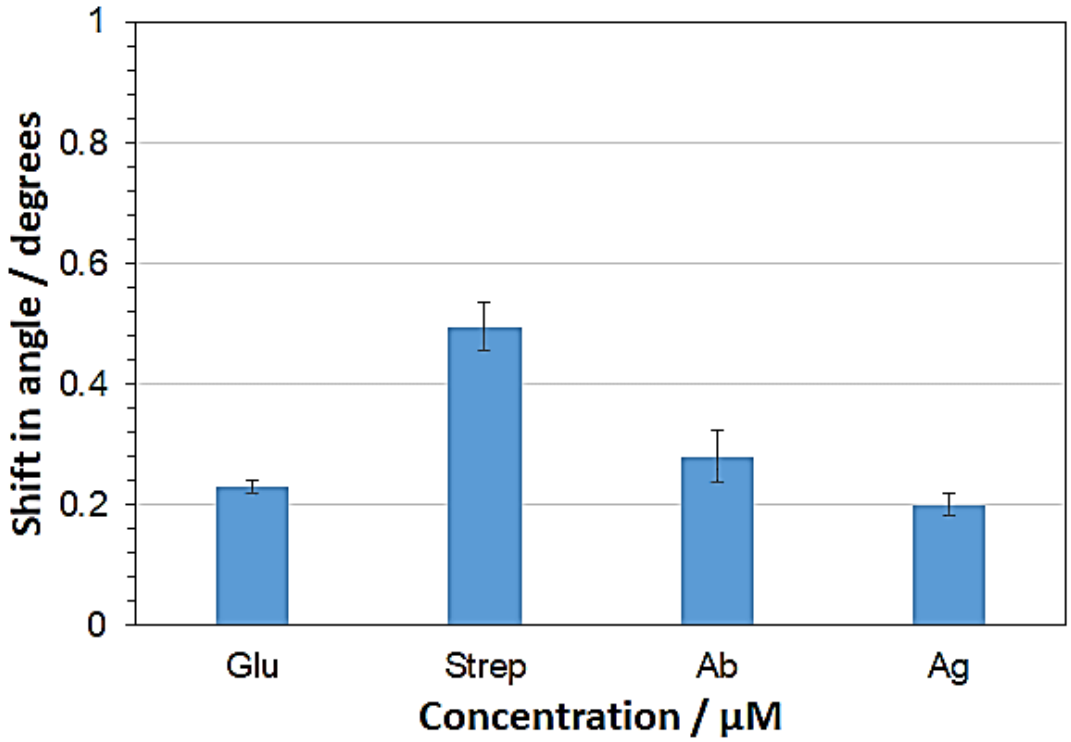

Figure 7.17: Variation of shift in angle according to change the concentration of standard Factor (III) 3 pg mL^{-1}.

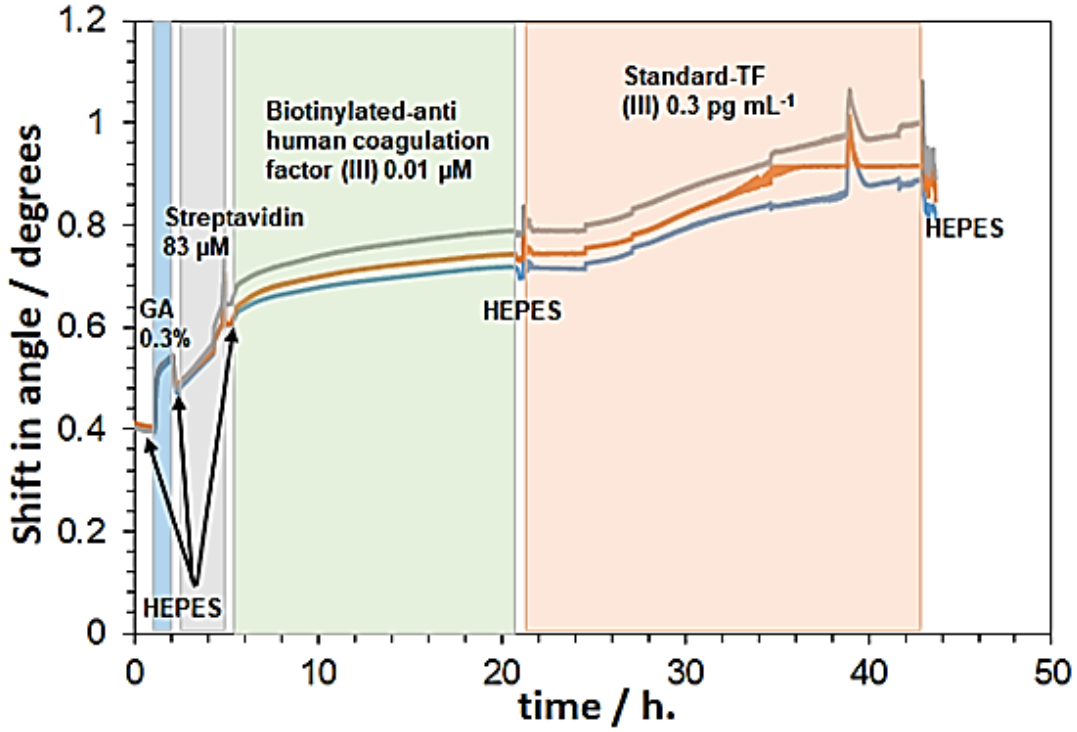

Figure 7.18: Changing in the reflectivity dip angle versus time using different solutions HEPES buffer pH 7.4, 0.3% of glutaraldehyde as a linker for the waveguide layer, Streptavidin 83 µM, Biotinylated goat anti-human coagulation Factor (III) 0.01 µM overnight. Then recombinant human coagulation Factor (III) 0.3 pg mL^{-1}overnight. The surface initially incubated with the RB4 dye (0.1 µM) for 5 min

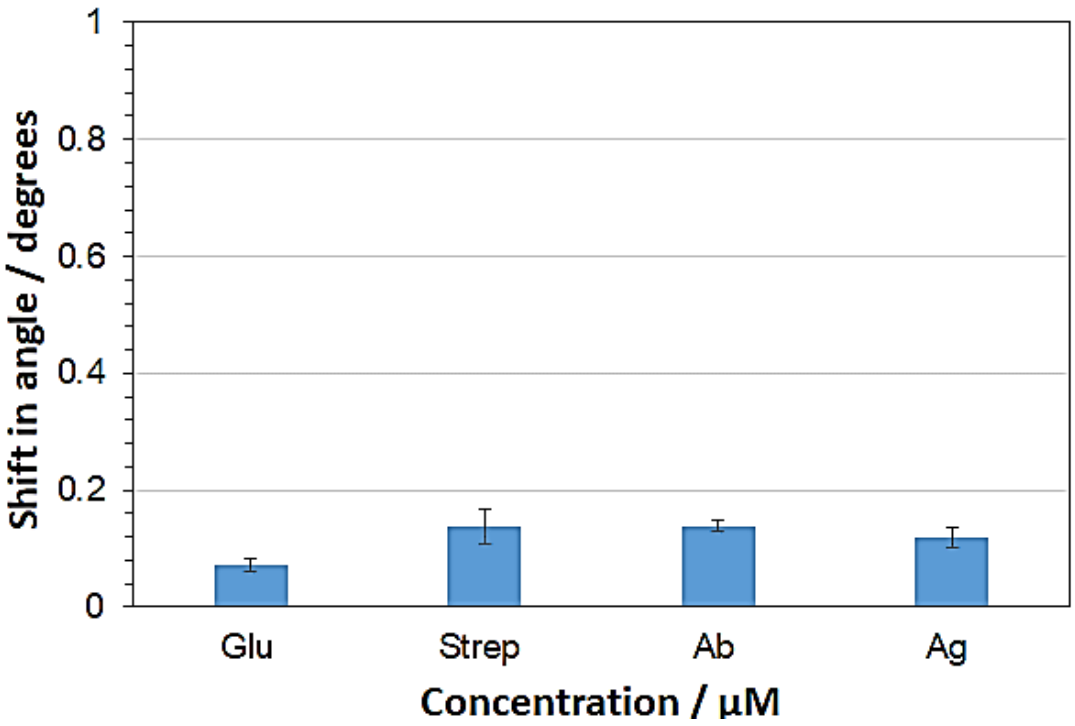

Figure 7.19: Variation of shift in angle according to change the concentration of standard Factor (III) 0.3 pg mL^{-1}.

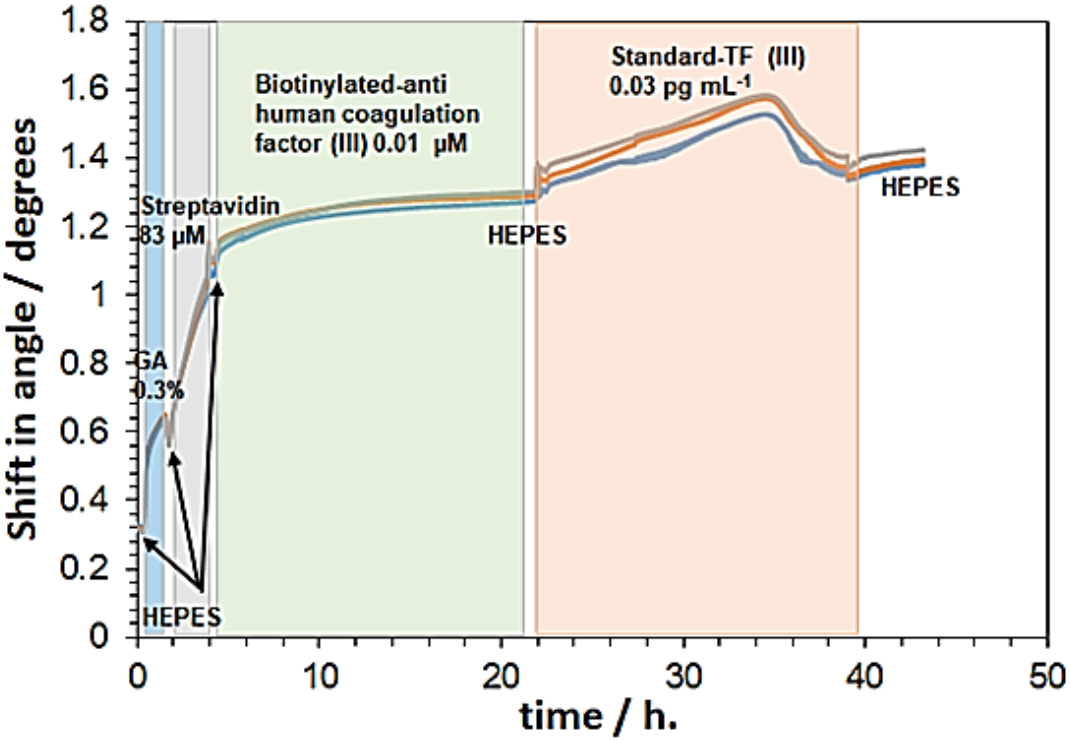

Figure 7.20: Changing in the reflectivity dip angle versus time using different solutions HEPES buffer pH 7.4, 0.3% of glutaraldehyde as a linker for the waveguide layer, Streptavidin 83 µM, Biotinylated goat anti-human coagulation Factor (III) 0.01 µM overnight. Then recombinant human coagulation Factor (III) 0.03 pg mL^{-1}overnight. The surface initially incubated with the RB4 dye (0.1 µM) for 5 min.

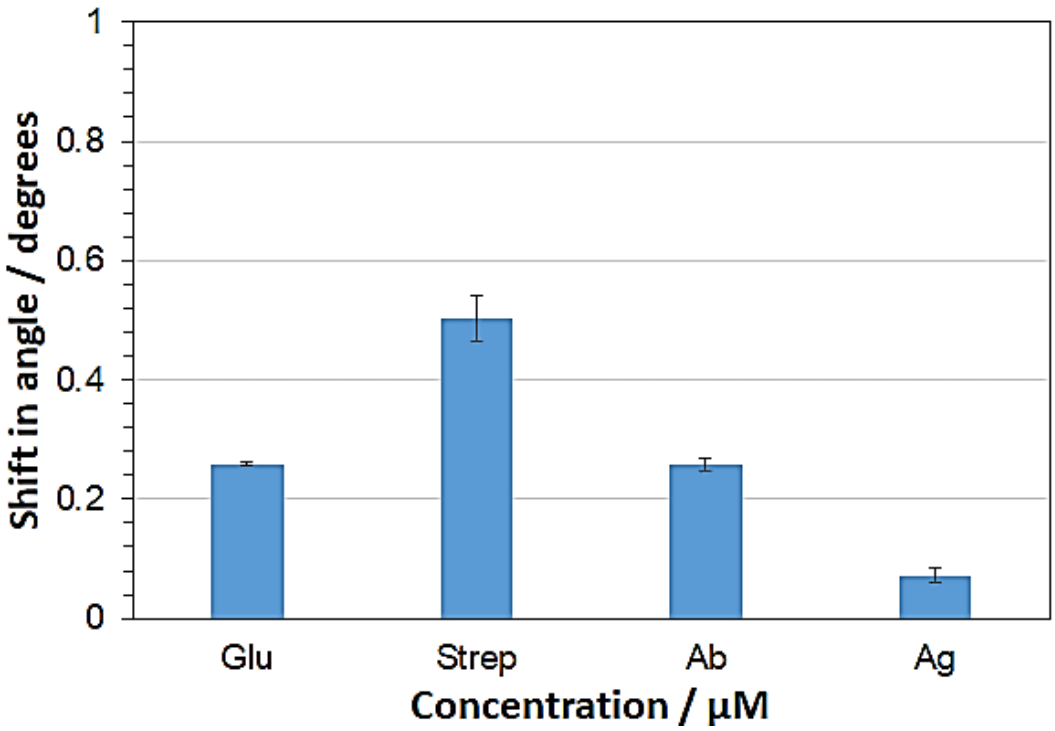

Figure 7.21: Variation of shift in angle according to change the concentration of standard Factor (III) 0.03 pg mL^{-1}.

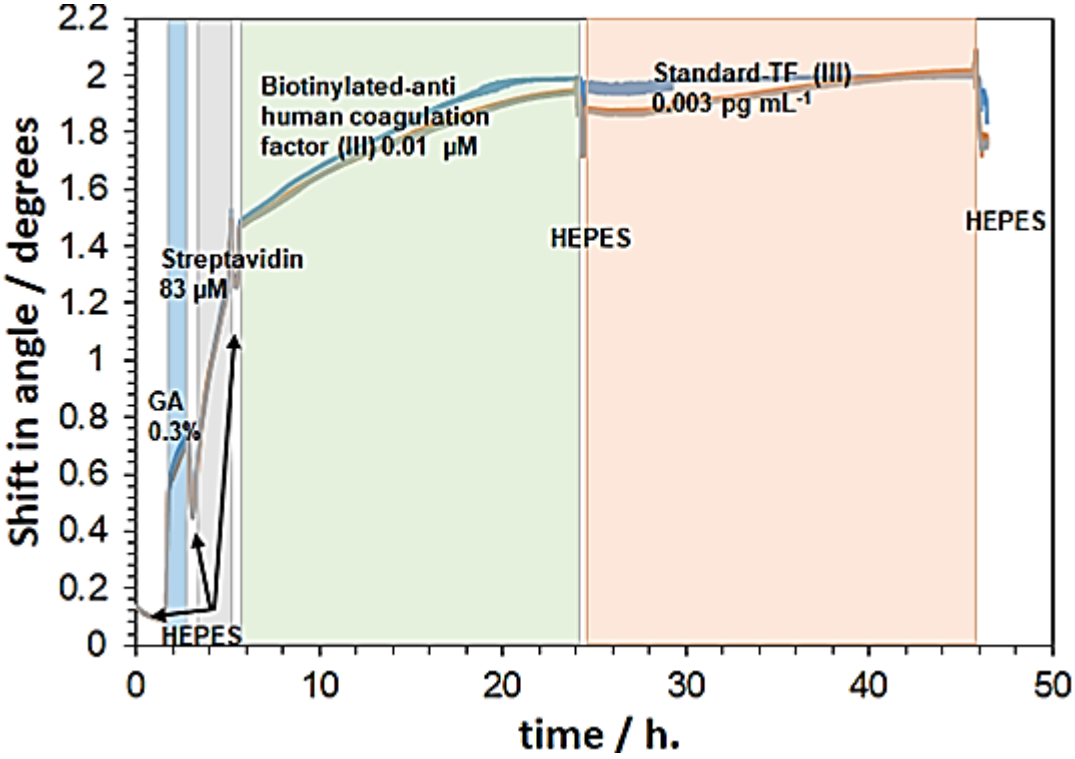

Figure 7.22: Changing in the reflectivity dip angle versus time using different solutions HEPES buffer pH 7.4, 0.3% of glutaraldehyde as a linker for the waveguide layer, Streptavidin 83 µM, Biotinylated goat anti-human coagulation Factor (III) 0.01 µM overnight. Then recombinant human coagulation Factor (III) 0.003 pg mL^{-1}overnight. The surface initially incubated with the RB4 dye (0.1 µM) for 5 min.

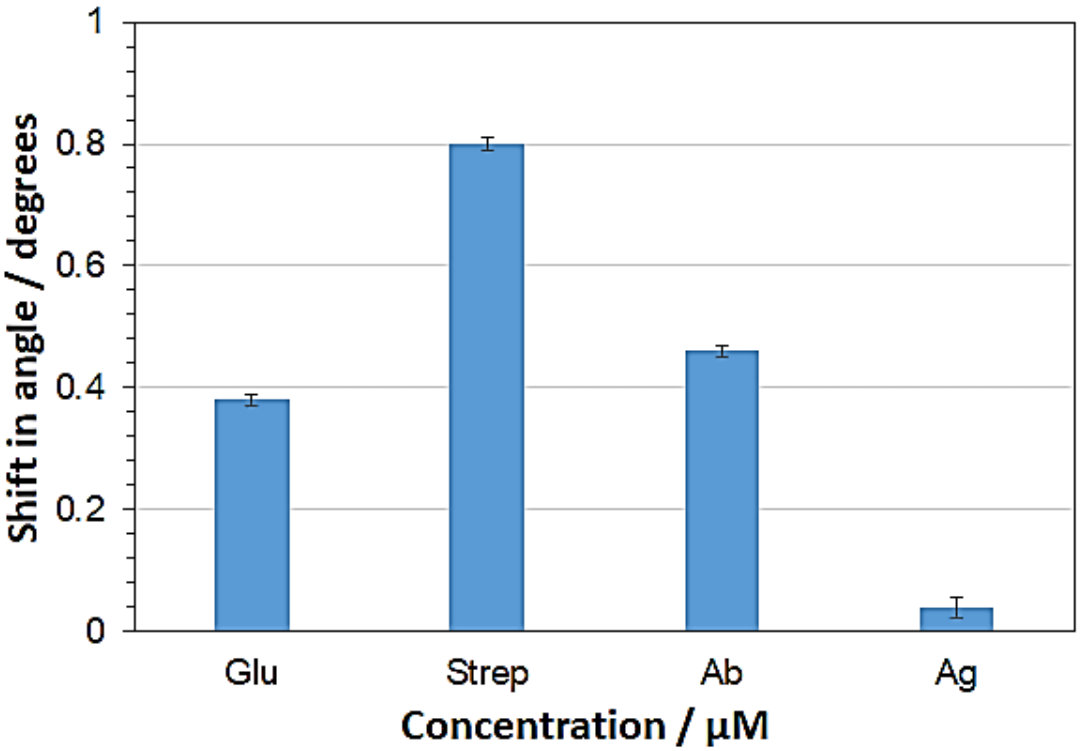

Figure 7.23: Variation of shift in angle according to change the concentration of standard Factor (III) 0.003 pg mL^{-1}.

Fig.7.24, shows the degree of shifting in angle upon applying different concentrations of antigen. Each concentration of antigen was performed on different chitosan chip that was initially treated with 0.3% glutaraldehyde, 83 µM streptavidin and 0.01 µM of biotinylated antibody. It can be seen from the figure that summarizes figs.7.15, 7.17, 7.19, 7.21, and 7.23, the concentration of antigen is increased, the degree of shifting in angle is increased which indicates more antigen bound to immobilized antibody. The lowest concentration of antigen was 0.003 pg mL^{-1}.

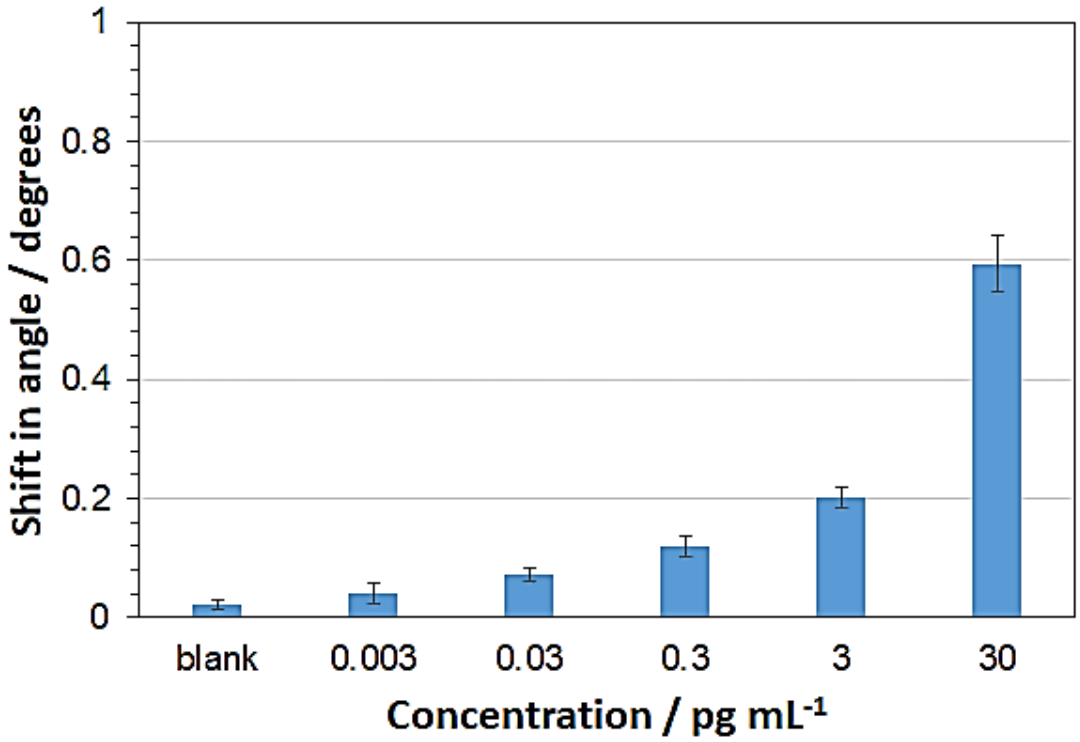

Figure 7.24: Variation of shift in angle according to change of the concentration of Standard Factor (III) 30, 3, 0.3, 0.03, and 0.003 pg mL^{-1}.

7.5 Blank experiment (Immobilisation of Biotinylated-anti human coagulation factor (III) without standard (TF)

The aim of this experiment is to obtain a shift in angle (degrees) when immobilisation of biotinylated-anti human coagulation Factor (III) 0.01 µM into the waveguide film without standard TF (III) as indicated in fig.7.25, and 7.26. For the pancreatic cell line samples, measurement of TF from both the Aspc-1 and Miapaca-2 media on the DDLW showed a value close to the reading for 3 pg mL-1 standard TF solution, compared to 7.86 pg mL^{-1} and 6.89 pg mL-1 measured via ELISA, respectively. The results demonstrate a proof-of-concept that label-free detection of real samples from cell effluent can be studied.

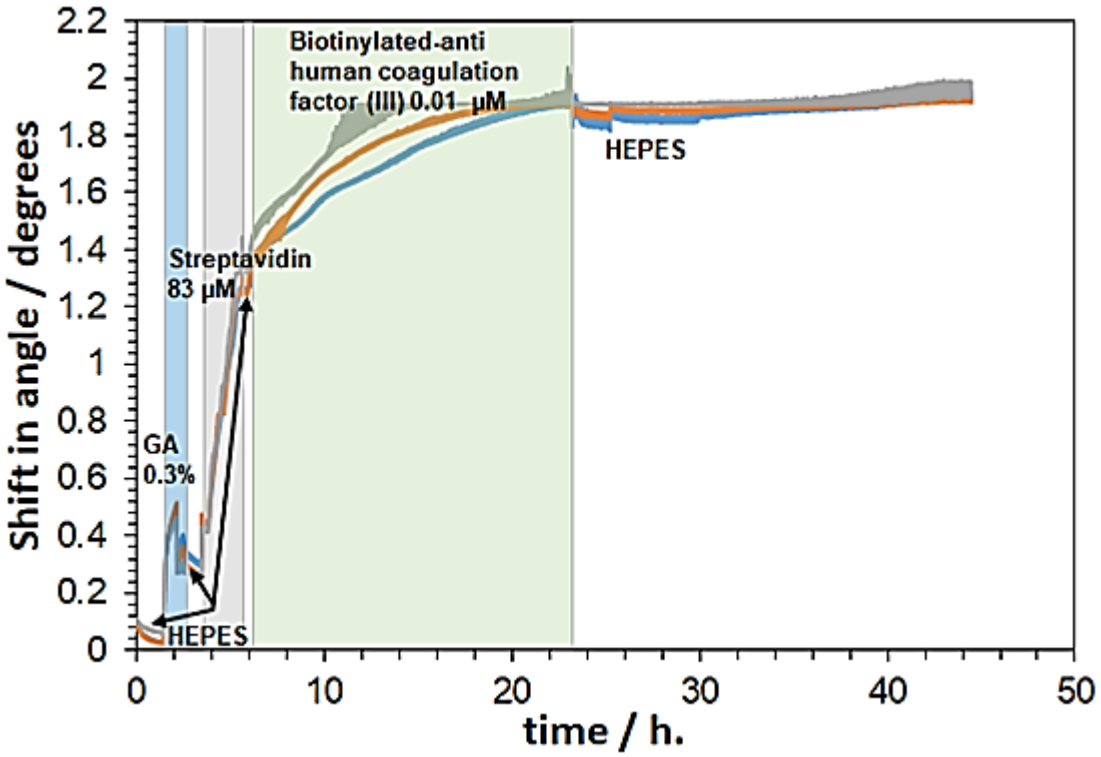

Figure 7.25: Changing in the reflectivity dip angle versus time using different solutions HEPES buffer pH 7.4, 0.3% of glutaraldehyde as a linker for the waveguide layer, Streptavidin 83 µM, Biotinylated goat anti-human coagulation Factor (III) 0.01 µM overnight, . Then HEPES buffer was flushed. The surface initially incubated with the RB4 dye (0.1 µM) for 5 min.

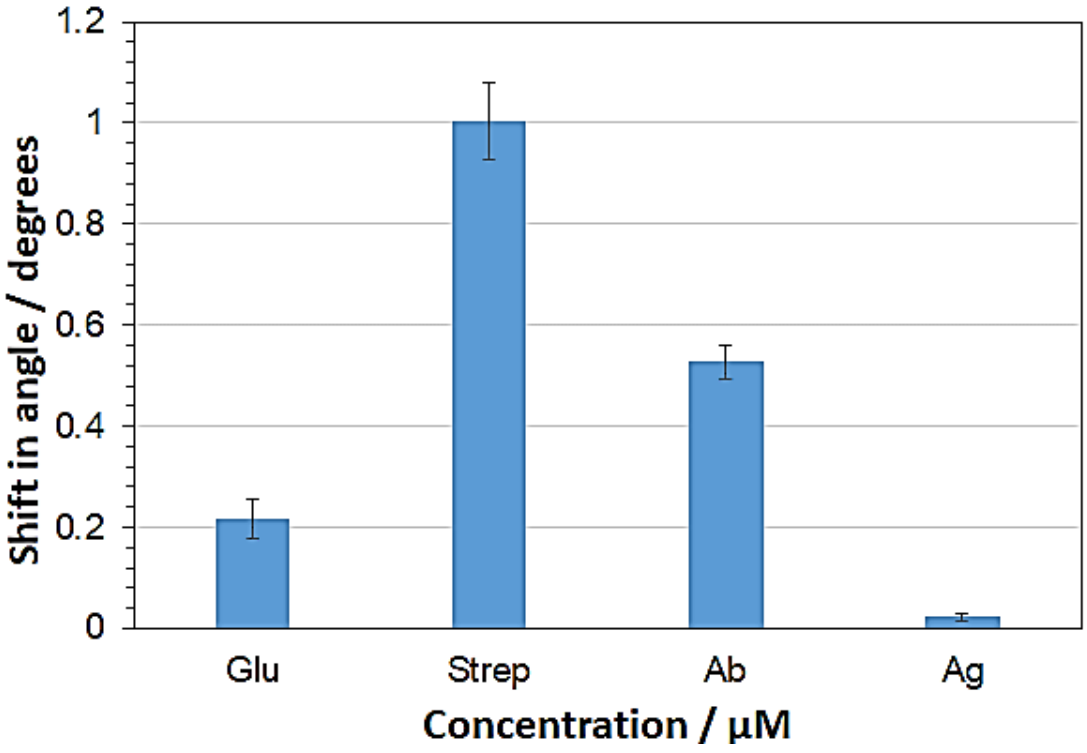

Figure 7.26: Variation of shift in angle according to change the concentration of biotinylated anti goat-TF without applying standard Factor (III).

7.6 Detection of Tissue Factor (III) in a culture media using DDLW sensor

For the pancreatic cell line samples, measurement of TF from both the Aspc-1 and Miapaca-2 media on the DDLW. These experiment were performed in order to measure the concentration of Tissue Factor (III) expressed from pancreatic cell lines of Aspc-1 and Miapaca-2 cells (7.86, and 6.89 pg mL^{-1}) respectively on the Dye doped leaky waveguide sensor.

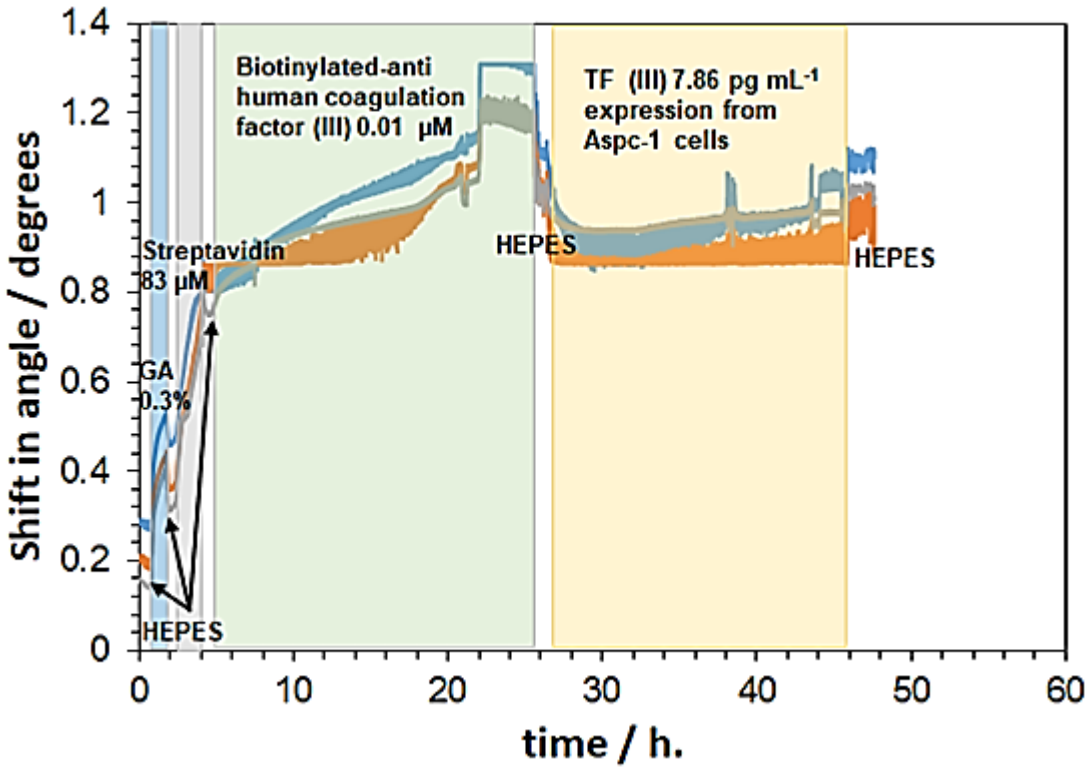

Figure 7.27: Changing in the reflectivity dip angle versus time using different solutions HEPES buffer pH 7.4, 0.3% of glutaraldehyde as a linker for the waveguide layer, Streptavidin 83 µM, Biotinylated goat anti-human coagulation Factor (III) 0.01 µM overnight, . Then recombinant human coagulation Factor (III) was expressed on Aspc-1 cells (7.86 pg mL^{-1}) overnight. The surface initially incubated with the RB4 dye (0.1 µM) for 5 min.

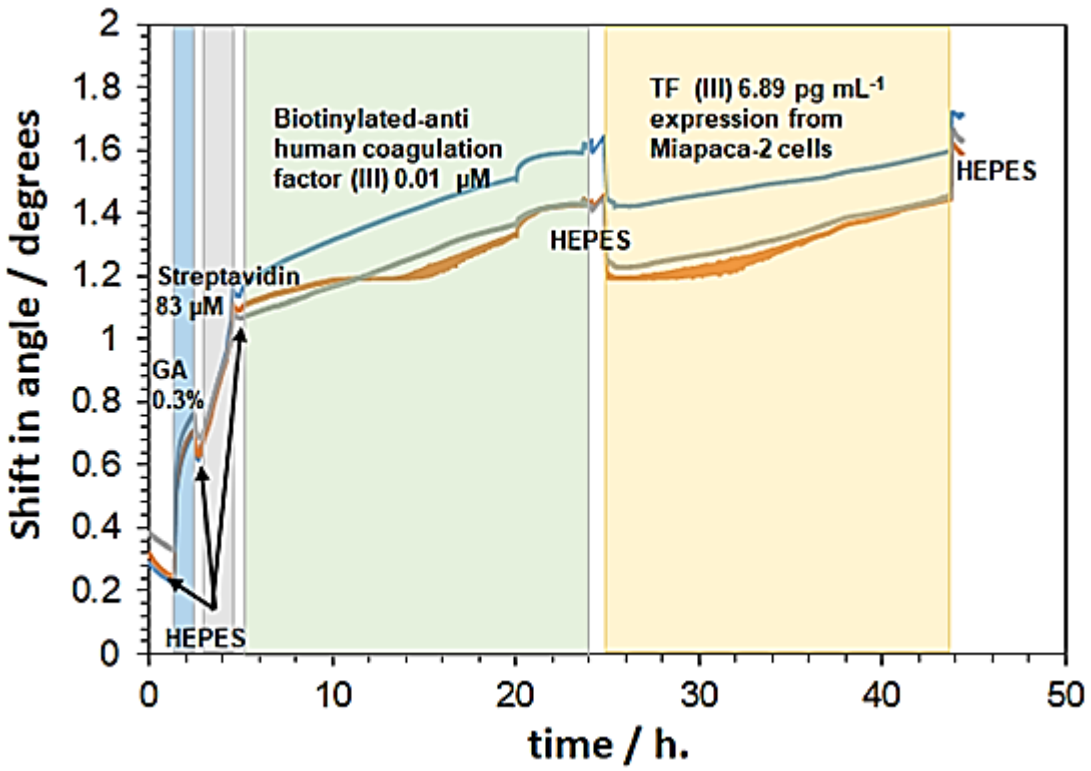

Figure 7.28: Changing in the reflectivity dip angle versus time using different solutions HEPES buffer pH 7.4, 0.3% of glutaraldehyde as a linker for the waveguide layer, Streptavidin 83 µM, Biotinylated goat anti-human coagulation Factor (III) 0.01 µM overnight, . Then recombinant human coagulation Factor (III) was expressed on Miapaca-2 cells (6.89 pg mL^{-1}) overnight. The surface initially incubated with the RB4 dye (0.1 µM) for 5min.

Figs.7.27 and 7.28 are indicate the degree of shifting in angle upon applying 7.86, and 6.89 pg mL^{-1} concentration of Tissue Factor (III) that was expressed from pancreatic cell lines (Aspc-1, and Miapaca-2 cells) respectively showed a value close to the reading for 3 pg mL^{-1} standard TF solution, compared to 7.86 pg mL^{-1} and 6.89 pg mL^{-1} measured via ELISA, respectively. This concentration of antigen was performed on chitosan chip that was initially treated with glutaraldehyde 3%, streptavidin 83 µM and Biotinylated anti-goat human coagulation Factor (III) 0.01 µM . It can be seen from the figure the degree of shifting in angle is about 0.17 º and 0.19º when applied 7.86, and 6.89 pg mL^{-1} of Tissue Factor (III) that was expressed from Pancreatic cell lines (Aspc-1, and Miapaca-2 cells) as indicated in fig.7.29 and table 7.3. In conclusion, when applying lowest concentrations of TF were expressed on unknown sample solutions of (Aspc-1 and Miapaca-2 cell lines) the degrees of shifting in angles were very close to the shifting in angles of standard solutions TF that were prepared to investigate the detection limit.

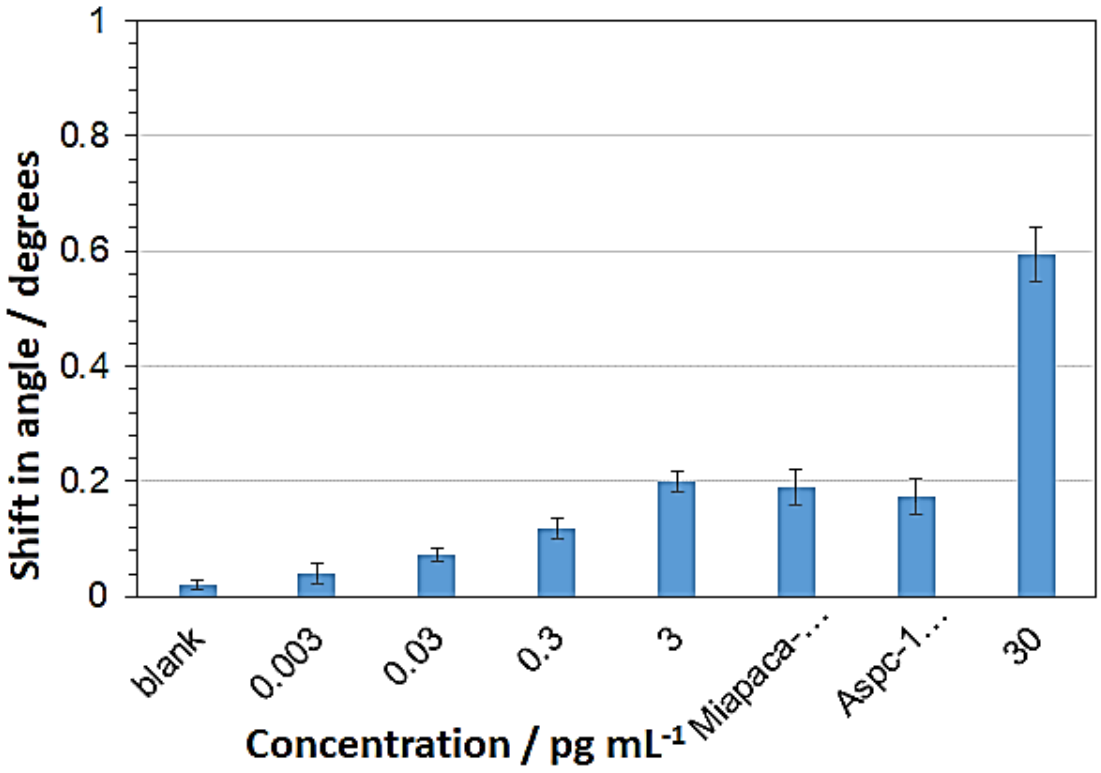

Figure 7.29: The correlation between the concentration of Tissue factor (TF) and shift in angle.

Table 7.3: Correlation between the Concentration of Tissue Factor (TF) standards and shift in angle.

Concentration / pg mL^{-1}	Shift in angle / degrees
Blank	0.02
Standard-TF 0.003	0.04
Standard-TF 0.03	0.07
Standard-TF 0.3	0.11
Standard-TF 3	0.2
TF expression from Aspc-1 cells	0.17
TF expression from Miapaca-2 cells	0.19
Standard-TF 30	0.59

The results demonstrate a proof-of-concept that label-free detection of real samples from cell effluent can be studied.

7.7 Conclusion

The current study has involved investigating the concentration of Tissue Factor expressed on pancreatic cell lines. Two types of cell lines were used, Aspc-1 and Miapaca-2, to optimize the methodology application by ELISA, a conventional setup. A leaky waveguide system was also used to determine the release of TF from pancreatic cell lines and compare the results of the two setups.

From previous results, a range of TF standard solutions were prepared at 450 nm and centrifuged at 400 rpm to create a calibration curve recorded by ELISA plate reader to investigate the concentration of Tissue Factor expressed from real samples from cell effluent. TF release from pancreatic cell lines (Aspc-1 and Miapaca-2 cells) into the cell culture media was studied over a period of 72 h and quantified via ELISA with a calibration curve in the concentration range of 7.825 to 500 pg mL^{-1}. Cell numbers were established via haemocytometer. From the ELISA data it could be estimated that, for the Aspc-1 cells, TF release raised for the first 24 h and then dropped to about after 72 h. whereas, for the Miapaca-2 cells, TF release rose over the first 10 h and then rained at this level.

Moreover, there were a strong correlations between the level of TF antigen and activity in these cells, showing that the TF present on the cancer cells was active as approved in the literature.

Therefore, the concentration of Tissue Factor was increased when the number of cells was increased over time, due to the generation of each pancreatic cell line. As can be seen from the results that were obtained on the DDLW sensor, the degree of shifting in angle is about 0.17 º and 0.19º of Tissue Factor (III) that was expressed from pancreatic cell lines (Aspc-1, and Miapaca-2 cells), and showed a value close to the reading for 3 pg mL^{-1} standard TF solution, compared to 7.86 pg mL^{-1} and 6.89 pg mL^{-1} measured via ELISA, respectively. In conclusion, the results have been demonstrated that label-free detection (DDLW) sensor can be used to detect of real samples from cell effluent.

CHAPTER 8

Conclusion and Future work

8.1 Conclusion

The primary objective of this research work has been to develop, implement and apply effectively a dye-doped leaky waveguide sensor to optimise and characterize label free optical biosensors for detection of various biomolecular interactions. The dye-doped leaky waveguide is an evanescent wave sensing mechanism for detection of biomolecular interactions. The leaky waveguide sensor was investigated because it is a relatively inexpensive and easy to use tool for scientific analysis and detection. It was designed to have sensitivity as biomarkers are usually present in biofluids at very low levels. The design goal for realizing high sensitivity was to design a structure that created a large pore size hydrogel as the waveguide which can allow a greater amount of biomolecules to be sensed inside the waveguide region.

In chapter one the theory behind label free optical biosensors was discussed including their underlying principles, mechanisms, architectures and the immobilization techniques used. This chapter included a literature review of the current state of immunobiosensors and the need for high sensitivity, low cost measurement methods. A key component of the optical biosensors is the binding between the sensor surface and the chemical or a biological system. The physical and chemical properties of the functionalized surface play an important role in achieving optimal recognition of the target and limiting the nonspecific adsorption. Immobilizations of biorecognition elements such as antibodies, enzymes, proteins, nucleic acids on the functionalized surface are discussed. The high performance of an optical biosensor comes from its ability to immobilize biomolecules while maintaining their natural activity. A successful sensor must target the biomolecule in solution with low nonspecific adsorption to the solid support. These specifications govern the specificity and sensitivity of such devices and can be tailored by appropriate choice of the interface where the biomolecules are immobilized.

In Chapter 2 the experimental details were discussed including the equipment and materials used, the processes to optimise the waveguide layer, and experimental methods for the enhancement of the thin polymer waveguide film porosity. This chapter also includes a description for the experiments to optimise the immobilisation of the biorecognition element.

In chapter 3 the optimisation and characterisation of the chitosan waveguide is described. It was found that 2% of chitosan solution coated a on cleaned glass at a spin speed 3000 rpm represented the optimum conditions to get a thin waveguide film to confine the light

inside the waveguide layer. After that, to characterise the leaky waveguide layer the number of moles of amine groups in the whole volume of the chitosan film that was available to bind with the recognition species (antibody) was determined and the highest amount of amine groups for 1%, 1.5% and 2% of chitosan were measured using two different UV-visible spectrophotometric set ups. The range number of moles of the RB4 concentrations obtained through the UV/vis spectrophotometer from 18 to 183 femtomoles, whereas the number of moles of amino groups the RB4 concentration values obtained from the custom-built optical setup were higher values range from 36 to 456 fmol. By comparison data for each setup a slightly higher concentration of Reactive blue 4 dye is shown at custom-built setup with the same chitosan chip with different concentrations 1, 1.5, and 2% of chitosan film respectively. That's due to when increasing the concentration of chitosan will increase the number of moles of amines groups Additional experiments investigated the incubation time of the reactive blue 4 dye with 2% of chitosan. It was found that 10 min resulted in the highest sensitivity compared with the other incubation times.

The research then moved to investigate the porosity of the chitosan layer. Initial experiments utilised glycerol and the sensitivity of the chitosan waveguide to using different buffer in which to dissolve the glycerol was investigated, however water had the higher RI. In addition the size of the pores in the waveguide film was investigated by studying the diffusion into the waveguide of molecules of different sizes including BSA (bovine serum albumin), and different molecular weights of polymers of PEG (polyethylene glycol) and PEO (polyethylene oxide). It was concluded that none of these larger molecules were diffusing inside the waveguide film to the small pore size.

Chapter 4 focused on enhancing the porosity of the chitosan film. Therefore, different methodologies were used to increase the pore size of chitosan film. Firstly, silica beads were incorporated into the chitosan layer to provide pores, this proved promising initially for experiments with different concentrations of BSA molecules (0.5, 1, 2, 3, 4, and 5%) with high the shift of degrees. The beads however needed to be then dissolved with NaOH to leave the pores behind and, the stability of chitosan film was effected by the NaOH treatment. Another approach that was effective was to control the dry time and use of 1% of chitosan and this provided improved results.

Following this protocol, a crosslinker N hydroxysuccinimide-polyethylene glycol-N hydroxysuccinimide (NHS-PEG-NHS) with different lengths was used in order to control the pore size on the dried chitosan film. However, no enhancements were observed using

this approach. In obtaining all these results it became clear that the quality of the coverage of the waveguide layer was very important. In chapter 5 the use of different techniques were utilised to optimise and characterize the waveguide. Different concentrations of the chitosan solution with different spin speeds were investigated to ensure a good thin film was obtained. A white light interferometer technique was used for examining surface thickness of the spin-coated chitosan layer. By increasing the chitosan concentrations (0.5%, 1% and 1.5% of chitosan investigated) the viscosity of chitosan solution increased which led to a change in the thickness of the waveguide (119.7, 663.9, and 1046.8 nm) respectively. A Bruker Dektak XT profilometer 3D was also utilized to measure the thin film thickness and uniformity by scanning over features fluctuating in height between 1 mm to 5 nm. The surface roughness of the chitosan waveguide film was measured on both flat and curved surfaces. For the flow cells the values obtained for the blue channel were compared (before and after) for 0.5, 1 and 2 % of chitosan film incubated in 100 mM of reactive blue 4 dye solution. These experiments indicated removal of reactive blue 4 dye and the instability of the waveguide thin film during a waveguide run as indicated in table 5.2 the average measurements for different concentrations of chitosan thin film at different spin coating speeds, these experiments were repeated three times.

Confocal Scanning Microscope was used to study the porosity of chitosan waveguide film. Porosity measurements indicated that the chitosan deposited on the substrate (glass slides) was thicker around the edges when spin coated at 900 rpm (range = 2-50 μm) compared to the centre of the substrate (range = 2-10 μm).

Chapter 6 describes the investigation of different immobilisation methods to bind a model biorecognition molecule, rabbit IgG to the waveguide such that anti-rabbit IgG could be measured, First, EDC-Sulpho-NHS was utilized to crosslink the Anti-IgG antibody into the chitosan waveguide layer at a normal pH 7.4. The mechanism of this immobilization depends on the activation of a carboxyl group which is conjugate to the antibody by using a different ratio, 1:4, 1:1 and 4:1, of EDC-Sulpho-NHS. The present study indicated that EDC-Sulpho-NHS based crosslinking of Anti-IgG had a low attaching efficiencies, which is contrary to the literature stating that the binding efficiencies were enhanced when EDC-Sulpho-NHS was used[141]. That may be due to the molecular interactions between EDC and Sulpho-NHS, which might be interfering with the binding of EDC-Sulpho-NHS activated Anti-IgG to the amino groups of chitosan waveguide layer. To overcome the problem glutaraldehyde which is a homo-bifunctional cross-linker t was investigated. But there was a high reactivity of glutaraldehyde toward chitosan amine groups but no

interaction for Anti-IgG with detection IgG. That may be due to the orientation of the antibody, which means that the aldehyde group of glutaraldehyde reacted with the amino groups of the antibody and affected the orientation of the antibody. Lastly, the biotin-streptavidin system was used to immobilize the antibody. Streptavidin was bound to the amine groups within the chitosan layer using glutaraldehyde. Then biotinylated anti-rabbit IgG was immobilised by binding between streptavidin and biotin. Finally, the binding of rabbit-IgG and the immobilised anti-rabbit IgG was studied. This approach proved very successful and a calibration curve as obtained for anti-IgG with a limit of detection of 6 ± 1 pg mL^{-1}.

In Chapter 7 an application of the leaky waveguide detection method was studied. This focused on the investigation of the concentration of Tissue Factor expressed from pancreatic cell lines. Two types of cell lines were used, Aspc-1 and Miapaca-2, and the TF was initially measured by a conventional ELISA protocol.

This method was carried out in a 96-well microtitre plate (more depending on the samples being analysed) a method that has been used for many years due to its ease and sensitivity. A typical assay ELISA can take in excess of 24 hours due to the number of steps and the size of the wells.

Using standard conditions[155] a calibration curve was obtained for TF and then the TF expressed from unknown sample solutions was determined. TF release from pancreatic cell lines (Aspc-1 and Miapaca-2 cells) into the cell culture media was studied over a period of 72 h and quantified via ELISA with a calibration curve in the concentration range of 7.825 to 500 pg mL^{-1}. Cell numbers were established via haemocytometer. From the ELISA data it could be estimated that, for the AsPC-1 cells, TF release raised for the first 24 h and then dropped to about after 72 h. whereas, for the Miapaca-2 cells, TF release rose over the first 10 h and then rained at this level.

Furthermore, it was shown that there were a strong correlations between the level of TF antigen and activity in these cells, showing that the TF present on the cancer cells was active. Moreover, it was shown that the concentration of TF increased when the number of cells was increased over time, due to the generation of each pancreatic cell line.

The Miapaca-2 cells had been generated from a patient with a primary adenocarcinoma tumour and have epithelial cell-like morphology with abundant cytoplasm, and low to no TF expression); Aspc-1 cells were generated from pancreas ascites from an adenocarcinoma patient, with low to moderate TF expression. The results were then

compared with those obtained for the leaky waveguide detection method. The antibody was immobilised using the protocol developed for the anti-IgG. A calibration was obtained for different TF concentrations (0.003, 0.03, 0.3, 3, and 30 pg mL^{-1}) with a limit of detection of 0.003 pg mL^{-1}. The results obtained for the samples of Aspc-1and the Miapaca-2 cell lines were 7.86 ± 1, and 6.89 ± 1 pg mL^{-1} and this was comparable with the results obtained for the ELISA. These label-free biosensors have potential for continuous measurement for healthcare monitoring.

Other studies that have reported high concentrations of TF in platelets and blood cells and the presence of TF in plasma have used commercial assays such as ELISA, Flow cytometer, and Confocal laser scanning microscopy, etc as indicated in table (1.3).

The continuous measurement of biomarkers such as proteins and hormones in blood and serum are the cornerstone of healthcare monitoring and optimising treatment plans. Often such biomarkers are present in minute concentrations. Conventional analysis methods involve assays with costly labelled antibodies and lengthy protocols on microtitre well plates. To measure antibodies by florescence technique is requires to clean the sample because (it contains interfering materials such as other proteins, salts, etc.), and also if using an optical based labelled sensor needs to prepare the sample, that's lead to consume time and lost sample.

Label-free biosensors are therefore an attractive alternative to improve biomarker analysis. These label-free biosensors (table 1.3) have potential for continuous measurement for healthcare monitoring. Therefore, dye-doped leaky waveguide sensor technique discussed in the thesis can be used to detect other of cancer biomarkers in future to enhance the sensitivity of the leaky waveguide sensor.

8.2 Future Work

Once the immobilisation chemistry has been developed, it is intended that the leaky waveguide system should be used to study the release of tissue factor (TF) from pancreatic cells in real time, and that its results will be compared to those of the conventional microwell-based ELISA system. These label-free biosensors have potential for continuous measurement for healthcare monitoring.

Key factors that will effect measurements will be temperature and humidity. In future work these will need to be controlled. This could be achieved by using an enclosed box where the temperature can be fixed and the humidity maintained by utilised a saturated salt solution inside the box.

Once the immobilisation chemistry is developed, the waveguide system is intended to be used to study the release of tissue factor (TF) from pancreatic cells (Aspc-1 and Miapaca-2 cells) in real-time, and compared to the conventional microwell-based ELISA system. Different TF concentrations (0.003-30 pg mL^{-1}) were investigated.

CHAPTER 9

Conferences & Memberships

Appendix

9.1 Conferences

- 5th PhD Experience Conference, (14-15th) April 2014, University of Hull, attending.
- 6th PhD Experience Conference, (7-8th) April 2015, University of Hull, attending.
- Chemistry Department Colloquium, 21st July 2016, Hull University, poster presentation.
- Analytical Research Forum (ARF) conference, 8th July 2016, Burlington House, Piccadilly, London, poster presentation.
- Chemistry Department Colloquium, 24th Jan 2018, Hull University, presentation.
- The 22 International Conference on Miniaturized Systems for Chemistry and Life Sciences (μTAS 2018), Kaohsiung Exhibition Center in Kaohsiung, Taiwan (11th - 15th) November, 2018.

9.2 Memberships

- Royal Society of Chemistry (RSC).

References

1. Ligler, F. S.; Taitt, C. R., *plasmonic sers molecular sentinels: a new biosensing approach*. 2008; p 385.
2. Cooper, J.; Cass, T., *Biosensors*. Oxford University Press, USA: 2004.
3. Turner, A. P. F., *Biosensors: Fundamentals and applications – Historic book now open access*. 2015; Vol. 65, p A1.
4. Avraham Rasooly, K. E. H., *Biosensors and biodetection : methods and protocols*. Humana Press: New York :, 2009.
5. Vo-Dinh, T.; Cullum, B., *Biosensors and biochips: advances in biological and medical diagnostics*. 2001/02/28 ed.; 2000; Vol. 366, p 540-51.
6. Taitt, C. R.; Anderson, G. P.; Ligler, F. S., Evanescent wave fluorescence biosensors: Advances of the last decade. *Biosensors & bioelectronics* **2016,** *76*, 103-112.
7. Garipcan, B.; Çağlayan, M.; Demirel, G., *New Generation Biosensors based on Ellipsometry*. 2011.
8. Prasad, P. N., *Introduction to biophotonics*. John Wiley & Sons: 2004.
9. Grieshaber, D.; MacKenzie, R.; Voeroes, J.; Reimhult, E., Electrochemical biosensors-sensor principles and architectures. *Sensors* **2008,** *8* (3), 1400-1458.
10. Sadik, O. A.; Aluoch, A. O.; Zhou, A., Status of biomolecular recognition using electrochemical techniques. *Biosensors and Bioelectronics* **2009,** *24* (9), 2749-2765.
11. Bosch, M. E.; Sánchez, A. J. R.; Rojas, F. S.; Ojeda, C. B., Recent development in optical fiber biosensors. *Sensors* **2007,** *7* (6), 797-859.
12. Smith, L. M.; Sanders, J. Z.; Kaiser, R. J.; Hughes, P.; Dodd, C.; Connell, C. R.; Heiner, C.; Kent, S. B.; Hood, L. E., Fluorescence detection in automated DNA sequence analysis. *Nature* **1986,** *321* (6071), 674.
13. Martellucci, S.; Chester, A. N.; Mignani, A. G., Optical sensors and microsystems. *New York, Boston, London* **2002**.
14. Cooper, M. A., *Label-free biosensors: techniques and applications*. Cambridge University Press: 2009.
15. Dzydevich, S. V.; Shul'ga, A. A.; Soldatkin, A. P.; Hendji, A. M. N.; Jaffrezic‐Renault, N.; Martelet, C., Conductometric biosensors based on cholinesterases for sensitive detection of pesticides. *Electroanalysis* **1994,** *6* (9), 752-758.
16. Ramanathan, K.; Danielsson, B., Principles and applications of thermal biosensors. *Biosensors and Bioelectronics* **2001,** *16* (6), 417-423.
17. Damjanovic, D., Materials for high temperature piezoelectric transducers. *Current Opinion in Solid State and Materials Science* **1998,** *3* (5), 469-473.
18. Cooper, M. A., Label-free screening of bio-molecular interactions. *Analytical and bioanalytical chemistry* **2003,** *377* (5), 834-842.
19. Cooper, M. A., Non-optical screening platforms: the next wave in label-free screening? *Drug discovery today* **2006,** *11* (23-24), 1068-1074.

20. Isola, N. R.; Stokes, D. L.; Vo-Dinh, T., Surface-enhanced Raman gene probe for HIV detection. *Analytical chemistry* **1998,** *70* (7), 1352-1356.

21. Passaro, V.; Dell'Olio, F.; De Leonardis, F., Electromagnetic field photonic sensors. *Progress in quantum electronics* **2006,** *30* (2-3), 45-73.

22. Chao, C.-Y.; Guo, L. J., Biochemical sensors based on polymer microrings with sharp asymmetrical resonance. *Applied Physics Letters* **2003,** *83* (8), 1527-1529.

23. Jang, B.; Hassibi, A., Biosensor systems in standard CMOS processes: Fact or fiction? *IEEE Transactions on Industrial Electronics* **2009,** *56* (4), 979-985.

24. Frederix, F.; Friedt, J.-M.; Choi, K.-H.; Laureyn, W.; Campitelli, A.; Mondelaers, D.; Maes, G.; Borghs, G., Biosensing based on light absorption of nanoscaled gold and silver particles. *Analytical chemistry* **2003,** *75* (24), 6894-6900.

25. Steel, A. B.; Herne, T. M.; Tarlov, M. J., Electrochemical Quantitation of DNA Immobilized on Gold. *Analytical Chemistry* **1998,** *70* (22), 4670-4677.

26. Baldini, F.; Chester, A. N.; Homola, J.; Martellucci, S., *Optical chemical sensors*. Springer Science & Business Media: 2006; Vol. 224.

27. Donahue, A. C.; Albitar, M., Antibodies in biosensing. In *Recognition Receptors in Biosensors*, Springer: 2010; pp 221-248.

28. Phillips, K. S.; Cheng, Q., Recent advances in surface plasmon resonance based techniques for bioanalysis. *Analytical and bioanalytical chemistry* **2007,** *387* (5), 1831-1840.

29. Potyrailo, R. A.; Hobbs, S. E.; Hieftje, G. M., Optical waveguide sensors in analytical chemistry: today's instrumentation, applications and trends for future development. *Fresenius' journal of analytical chemistry* **1998,** *362* (4), 349-373.

30. Homola, J., Present and future of surface plasmon resonance biosensors. *Analytical and bioanalytical chemistry* **2003,** *377* (3), 528-539.

31. Boyd, R. W.; Heebner, J. E., Sensitive disk resonator photonic biosensor. *Applied Optics* **2001,** *40* (31), 5742-5747.

32. Densmore, A.; Xu, D.-X.; Waldron, P.; Janz, S.; Cheben, P.; Lapointe, J.; Delge, A.; Lamontagne, B.; Schmid, J.; Post, E., A silicon-on-insulator photonic wire based evanescent field sensor. *IEEE Photonics Technology Letters* **2006,** *18* (23), 2520-2522.

33. Chao, C.-Y.; Guo, L. J., Design and optimization of microring resonators in biochemical sensing applications. *Journal of Lightwave Technology* **2006,** *24* (3), 1395.

34. White, I. M.; Zhu, H.; Suter, J. D.; Hanumegowda, N. M.; Oveys, H.; Zourob, M.; Fan, X., Refractometric sensors for lab-on-a-chip based on optical ring resonators. *IEEE Sensors Journal* **2007,** *7* (1), 28-35.

35. van Gent, J.; Lambeck, P. V.; Kreuwel, H. J.; Gerritsma, G. J.; Sudhölter, E. J.; Reinhoudt, D. N.; Popma, T. J., Optimization of a chemooptical surface plasmon resonance based sensor. *Applied optics* **1990,** *29* (19), 2843-2849.

36. Almeida, V. R.; Xu, Q.; Barrios, C. A.; Lipson, M., Guiding and confining light in void nanostructure. *Optics letters* **2004,** *29* (11), 1209-1211.

37. Kahn, K.; Plaxco, K. W., Principles of biomolecular recognition. In *Recognition receptors in biosensors*, Springer: 2010; pp 3-45.

38. Choi, M. M., Progress in enzyme-based biosensors using optical transducers. *Microchimica Acta* **2004,** *148* (3-4), 107-132.

39. Kuswandi, B.; Andres, R.; Narayanaswamy, R., Optical fibre biosensors based on immobilised enzymes. *Analyst* **2001,** *126* (8), 1469-1491.

40. Ginsburg, G. S.; McCarthy, J. J., Personalized medicine: revolutionizing drug discovery and patient care. *trends in Biotechnology* **2001,** *19* (12), 491-496.

41. Eguchi, M.; Kahn, M., Design, synthesis, and application of peptide secondary structure mimetics. *Mini reviews in medicinal chemistry* **2002,** *2* (5), 447-462.

42. Lam, K. S.; Renil, M., From combinatorial chemistry to chemical microarray. *Current opinion in chemical biology* **2002,** *6* (3), 353-358.

43. Sadler, K.; Tam, J. P., Peptide dendrimers: applications and synthesis. *Reviews in Molecular biotechnology* **2002,** *90* (3-4), 195-229.

44. Sawyer, T.; Chorev, M., Peptide revolution: genomics, proteomics and therapeutics. *BioTechniques* **2003,** *34* (3), 594-599.

45. Lu, Y.; Zhang, T.-F.; Shi, Y.; Zhou, H.-W.; Chen, Q.; Wei, B.-Y.; Wang, X.; Yang, T.-X.; Chinn, Y. E.; Kang, J., PFR peptide, one of the antimicrobial peptides identified from the derivatives of lactoferrin, induces necrosis in leukemia cells. *Scientific reports* **2016,** *6*, 20823.

46. Tothill, I. E., Peptides as molecular receptors. In *Recognition Receptors in Biosensors*, Springer: 2010; pp 249-274.

47. Shrivastava, A.; Gupta, V., Methods for the determination of limit of detection and limit of quantitation of the analytical methods. *Chronicles of Young Scientists* **2011,** *2* (1), 21-25.

48. Welling, G. W.; Geurts, T.; Van Gorkum, J.; Damhof, R. A.; Drijfhout, J. W.; Bloemhoff, W.; Welling-Wester, S., Synthetic antibody fragment as ligand in immunoaffinity chromatography. *Journal of Chromatography A* **1990,** *512*, 337-343.

49. Nakamura, C.; Inuyama, Y.; Shirai, K.; Sugimoto, N.; Miyake, J., Detection of porphyrin using a short peptide immobilized on a surface plasmon resonance sensor chip. *Biosensors and Bioelectronics* **2001,** *16* (9-12), 1095-1100.

50. Tong, L.; Hu, L.; Zhang, J.; Qiu, J.; Yang, Q.; Lou, J.; Shen, Y.; He, J.; Ye, Z., Photonic nanowires directly drawn from bulk glasses. *Optics Express* **2006,** *14* (1), 82-87.

51. Barrelet, C. J.; Greytak, A. B.; Lieber, C. M., Nanowire photonic circuit elements. *Nano Letters* **2004,** *4* (10), 1981-1985.

52. Bures, J.; Ghosh, R., Power density of the evanescent field in the vicinity of a tapered fiber. *JOSA A* **1999,** *16* (8), 1992-1996.

53. Foster, M. A.; Turner, A. C.; Lipson, M.; Gaeta, A. L., Nonlinear optics in photonic nanowires. *Optics Express* **2008,** *16* (2), 1300-1320.

54. Poulton, C.; Schmidt, M.; Pearce, G.; Kakarantzas, G.; Russell, P. S. J., Numerical study of guided modes in arrays of metallic nanowires. *Optics letters* **2007,** *32* (12), 1647-1649.

55. Chalyan, T.; Guider, R.; Pasquardini, L.; Zanetti, M.; Falke, F.; Schreuder, E.; Heideman, R. G.; Pederzolli, C.; Pavesi, L., Asymmetric Mach–Zehnder interferometer based biosensors for aflatoxin M1 detection. *Biosensors* **2016,** *6* (1), 1.

56. Homola, J.; Yee, S. S.; Gauglitz, G., Surface plasmon resonance sensors. *Sensors and Actuators B: Chemical* **1999,** *54* (1-2), 3-15.

57. Ekgasit, S.; Tangcharoenbumrungsuk, A.; Yu, F.; Baba, A.; Knoll, W., Resonance shifts in SPR curves of nonabsorbing, weakly absorbing, and strongly absorbing dielectrics. *Sensors and Actuators B: Chemical* **2005,** *105* (2), 532-541.

58. Le Person, J.; Colas, F.; Compere, C.; Lehaitre, M.; Anne, M.-L.; Boussard-Plédel, C.; Bureau, B.; Adam, J.-L.; Députier, S.; Guilloux-Viry, M., Surface plasmon resonance in chalcogenide glass-based optical system. *Sensors and Actuators B: Chemical* **2008,** *130* (2), 771-776.

59. Gentleman, D. J.; Obando, L. A.; Masson, J.-F.; Holloway, J. R.; Booksh, K. S., Calibration of fiber optic based surface plasmon resonance sensors in aqueous systems. *Analytica Chimica Acta* **2004,** *515* (2), 291-302.

60. Sharma, A. K.; Gupta, B., Absorption-based fiber optic surface plasmon resonance sensor: a theoretical evaluation. *Sensors and Actuators B: Chemical* **2004,** *100* (3), 423-431.

61. Jianrong, C.; Yuqing, M.; Nongyue, H.; Xiaohua, W.; Sijiao, L., Nanotechnology and biosensors. *Biotechnology advances* **2004,** *22* (7), 505-518.

62. Zynio, S. A.; Samoylov, A. V.; Surovtseva, E. R.; Mirsky, V. M.; Shirshov, Y. M., Bimetallic layers increase sensitivity of affinity sensors based on surface plasmon resonance. *Sensors* **2002,** *2* (2), 62-70.

63. Sharma, A. K.; Gupta, B., On the performance of different bimetallic combinations in surface plasmon resonance based fiber optic sensors. *Journal of applied physics* **2007,** *101* (9), 093111.

64. Homola, J.; Slavik, R., Fibre-optic sensor based on surface plasmon resonance. *Electronics Letters* **1996,** *32* (5), 480.

65. Lin, H.-Y.; Tsai, W.-H.; Tsao, Y.-C.; Sheu, B.-C., Side-polished multimode fiber biosensor based on surface plasmon resonance with halogen light. *Applied optics* **2007,** *46* (5), 800-806.

66. Lin, Y.-C.; Tsao, Y.-c.; Tsai, W.-H.; Hung, T.-S.; Chen, K.-S.; Liao, S.-C., The enhancement method of optical fiber biosensor based on surface plasmon resonance with cold plasma modification. *Sensors and Actuators B: Chemical* **2008,** *133* (2), 370-373.

67. Suter, J. D.; White, I. M.; Zhu, H.; Fan, X., Thermal characterization of liquid core optical ring resonator sensors. *Applied optics* **2007,** *46* (3), 389-396.

68. Armani, A. M.; Kulkarni, R. P.; Fraser, S. E.; Flagan, R. C.; Vahala, K. J., Label-free, single-molecule detection with optical microcavities. *science* **2007,** *317* (5839), 783-787.

69. Serpengüzel, A.; Griffel, G.; Arnold, S., Excitation of resonances of microspheres on an optical fiber. *Optics Letters* **1995,** *20* (7), 654-656.

70. Milosevic, M., Internal reflection and ATR spectroscopy. *Applied Spectroscopy Reviews* **2004,** *39* (3), 365-384.

71. Schmitt, K.; Oehse, K.; Sulz, G.; Hoffmann, C., Evanescent field sensors based on tantalum pentoxide waveguides–a review. *Sensors* **2008,** *8* (2), 711-738.

72. Maims, C.; Hulme, J.; Fielden, P. R.; Goddard, N. J., Grating coupled leaky waveguide micro channel sensor chips for optical analysis. *Sensors and Actuators B: Chemical* **2001,** *77* (3), 671-678.

73. Zourob, M.; Mohr, S.; Brown, B. J. T.; Fielden, P. R.; McDonnell, M. B.; Goddard, N. J., Bacteria detection using disposable optical leaky waveguide sensors. *Biosensors and Bioelectronics* **2005,** *21* (2), 293-302.

74. Gupta, R.; Goddard, N. J., A novel leaky waveguide grating (LWG) device for evanescent wave broadband absorption spectroscopy in microfluidic flow cells. *Analyst* **2013,** *138* (6), 1803-1811.

75. Goddard, N. J.; Mohr, S.; Singh, K.; Holmes, R.; Joyce, K.; Hulme, J.; Bounaria, A.; Fielden, P. R. In *Leaky Waveguide Devices as Simple Sensitive Optical Detectors for use in μTAS Applications*, Proceedings of the MicroTech 2000 Conference, Springer-Verlag: 2000; pp 27-3.

76. Kissinger, P. T., Biosensors—a perspective. *Biosensors and Bioelectronics* **2005,** *20* (12), 2512-2516.

77. Qiu, Y.; Park, K., Environment-sensitive hydrogels for drug delivery. *Advanced drug delivery reviews* **2001,** *53* (3), 321-339.

78. Nayak, S.; Lyon, L. A., Soft nanotechnology with soft nanoparticles. *Angewandte chemie international edition* **2005,** *44* (47), 7686-7708.

79. Frenot, A.; Chronakis, I. S., Polymer nanofibers assembled by electrospinning. *Current opinion in colloid & interface science* **2003,** *8* (1), 64-75.

80. Koev, S.; Dykstra, P.; Luo, X.; Rubloff, G.; Bentley, W.; Payne, G.; Ghodssi, R., Chitosan: an integrative biomaterial for lab-on-a-chip devices. *Lab on a Chip* **2010,** *10* (22), 3026-3042.

81. Murthy, C. R.; Armani, A. M., Mass transport effects in suspended waveguide biosensors integrated in microfluidic channels. *Sensors* **2012,** *12* (11), 14327-14343.

82. Law, M.; Sirbuly, D. J.; Johnson, J. C.; Goldberger, J.; Saykally, R. J.; Yang, P., Nanoribbon waveguides for subwavelength photonics integration. *Science* **2004,** *305* (5688), 1269-1273.

83. Tothill, I.; Turner, A., New developments and opportunities in the diagnosis of livestock diseases. *towards livestock disease diagnosis and control in the 21st century* **1998**, 79.

84. Emili, A. Q.; Cagney, G., Large-scale functional analysis using peptide or protein arrays. *Nature biotechnology* **2000,** *18* (4), 393.

85. Jelinek, R.; Kolusheva, S., Carbohydrate biosensors. *Chemical reviews* **2004,** *104* (12), 5987-6016.

86. Turkova, J., Oriented immobilization of biologically active proteins as a tool for revealing protein interactions and function. *Journal of Chromatography B: Biomedical Sciences and Applications* **1999,** *722* (1-2), 11-31.

87. Homola, J.; Koudela, I.; Yee, S. S.; Slavík, R.; Čtyroký, J.,. *Sensors & Actuators: B. Chemical* **1999,** *54*, 1-2.

88. Knopp, D.; Tang, D.; Niessner, R., Bioanalytical applications of biomolecule-functionalized nanometer-sized doped silica particles. *Analytica Chimica Acta* **2009,** *647* (1), 14-30.

89. Homola, J., Electromagnetic theory of surface plasmons. In *Surface plasmon resonance based sensors*, Springer: 2006; pp 3-44.

90. Norde, W., Adsorption of proteins from solution at the solid-liquid interface. *Advances in colloid and interface science* **1986,** *25*, 267-340.

91. Dugas, V.; Elaissari, A.; Chevalier, Y., Surface sensitization techniques and recognition receptors immobilization on biosensors and microarrays. In *Recognition Receptors in Biosensors*, Springer: 2010; pp 47-134.

92. Frederix, F.; Bonroy, K.; Reekmans, G.; Laureyn, W.; Campitelli, A.; Abramov, M. A.; Dehaen, W.; Maes, G., Reduced nonspecific adsorption on covalently immobilized protein surfaces using poly (ethylene oxide) containing blocking agents. *Journal of biochemical and biophysical methods* **2004,** *58* (1), 67-74.

93. Dugas, V.; Elaissari, A.; Chevalier, Y., *Surface Sensitization Techniques and Recognition Receptors Immobilization on Biosensors and Microarrays*. 2009; p 47-134.

94. Zourob, M., *Recognition receptors in biosensors*. Springer: 2010.

95. Ye, J.; Gestwicki, J. E.; Norris, T. B.; Baker Jr, J. R.; Bersano-Begey, T. F., Analytical system with photonic crystal sensor. Google Patents: 2013.

96. Brogan, K. L.; Wolfe, K. N.; Jones, P. A.; Schoenfisch, M. H., Direct oriented immobilization of F (ab′) antibody fragments on gold. *Analytica chimica acta* **2003,** *496* (1-2), 73-80.

97. Bagiyan, G.; Koroleva, I.; Soroka, N.; Ufimtsev, A., Oxidation of thiol compounds by molecular oxygen in aqueous solutions. *Russian chemical bulletin* **2003,** *52* (5), 1135-1141.

98. Savage, M. D., *Avidin-biotin chemistry*. Pierce Chemical Co.: 1992.

99. Holmberg, A.; Blomstergren, A.; Nord, O.; Lukacs, M.; Lundeberg, J.; Uhlén, M., The biotin‐streptavidin interaction can be reversibly broken using water at elevated temperatures. *Electrophoresis* **2005,** *26* (3), 501-510.

100. Spicer, E. K.; Horton, R.; Bloem, L.; Bach, R.; Williams, K. R.; Guha, A.; Kraus, J.; Lin, T.-C.; Nemerson, Y.; Konigsberg, W. H., Isolation of cDNA clones coding for human tissue factor: primary structure of the protein and cDNA. *Proceedings of the National Academy of Sciences* **1987,** *84* (15), 5148-5152.

101. Khorana, A. A.; Fine, R. L., Pancreatic cancer and thromboembolic disease. *The lancet oncology* **2004,** *5* (11), 655-663.

102. Drake, T. A.; Morrissey, J.; Edgington, T., Selective cellular expression of tissue factor in human tissues. Implications for disorders of hemostasis and thrombosis. *The American journal of pathology* **1989,** *134* (5), 1087.

103. Khorana, A. A.; Kuderer, N. M.; Culakova, E.; Lyman, G. H.; Francis, C. W., Development and validation of a predictive model for chemotherapy-associated thrombosis. *Blood* **2008,** *111* (10), 4902-4907.

104. Nemerson, Y., Tissue factor and hemostasis [published erratum appears in Blood 1988 Apr; 71 (4): 1178]. *Blood* **1988,** *71* (1), 1-8.

105. Bazan, J. F., Structural design and molecular evolution of a cytokine receptor superfamily. *Proceedings of the National Academy of Sciences* **1990,** *87* (18), 6934-6938.

106. Dorfleutner, A.; Ruf, W., Regulation of tissue factor cytoplasmic domain phosphorylation by palmitoylation. *Blood* **2003,** *102* (12), 3998-4005.

107. Peppelenbosch, M. P.; Versteeg, H. H., Cell biology of tissue factor, an unusual member of the cytokine receptor family. *Trends in cardiovascular medicine* **2001,** *11* (8), 335-339.

108. Wolf, P., The nature and significance of platelet products in human plasma. *British journal of haematology* **1967,** *13* (3), 269-288.

109. Freyssinet, J. M., Cellular microparticles: what are they bad or good for? *Journal of Thrombosis and Haemostasis* **2003,** *1* (7), 1655-1662.

110. Taraboletti, G.; D'Ascenzo, S.; Borsotti, P.; Giavazzi, R.; Pavan, A.; Dolo, V., Shedding of the Matrix Metalloproteinases MMP-2, MMP-9, and MT1-MMP as Membrane Vesicle-Associated Components by Endothelial Cells. *The American Journal of Pathology* **2002,** *160* (2), 673-680.

111. Hussein, M. N. A.; Meesters, E. W.; Osmanovic, N.; Romijn, F. P. H. T. M.; Nieuwland, R.; Sturk, A., Antigenic characterization of endothelial cell‐derived microparticles and their detection ex vivo. *Journal of Thrombosis and Haemostasis* **2003,** *1* (11), 2434-2443.

112. Lechner, D.; Kollars, M.; Gleiss, A.; Kyrle, P. A.; Weltermann, A., Chemotherapy‐induced thrombin generation via procoagulant endothelial microparticles is independent of tissue factor activity. *Journal of Thrombosis and Haemostasis* **2007,** *5* (12), 2445-2452.

113. Giesen, P. L. A.; Rauch, U.; Bohrmann, B.; Kling, D.; Roqué, M.; Fallon, J. T.; Badimon, J. J.; Himber, J.; Riederer, M. A.; Nemerson, Y., Blood-borne tissue factor: Another view of thrombosis. *Proceedings of the National Academy of Sciences* **1999,** *96* (5), 2311.

114. VanWijk, M. J.; VanBavel, E.; Sturk, A.; Nieuwland, R., Microparticles in cardiovascular diseases. *Cardiovascular Research* **2003,** *59* (2), 277-287.

115. Turner, S. L.; Blair-Zajdel, M. E.; Bunning, R. A. D., adams and adamtss in cancer. *British Journal of Biomedical Science* **2009,** *66* (2), 117-128.

116. Kirwan, C. C.; Nath, E.; Byrne, G. J.; McCollum, C. N., Prophylaxis for venous thromboembolism during treatment for cancer: questionnaire survey. *BMJ : British Medical Journal* **2003,** *327* (7415), 597-598.

117. Sproul, E. E., Carcinoma and Venous Thrombosis: The Frequency of Association of Carcinoma in the Body or Tail of the Pancreas with Multiple Venous Thrombosis. *The American Journal of Cancer* **1938,** *34* (4), 566.

118. Mandalà, M.; Reni, M.; Cascinu, S.; Barni, S.; Floriani, I.; Cereda, S.; Berardi, R.; Mosconi, S.; Torri, V.; Labianca, R., Venous thromboembolism predicts poor prognosis in irresectable pancreatic cancer patients. *Annals of Oncology* **2007,** *18* (10), 1660-1665.

119. Nalluri, S.; Chu, D.; Keresztes, R.; Zhu, X.; Wu, S., Risk of venous thromboembolism with the angiogenesis inhibitor bevacizumab in cancer patients: A meta-analysis. *JAMA* **2008,** *300* (19), 2277-2285.

120. Tesselaar, M.; Romijn, F.; Van der Linden, I.; Prins, F.; Bertina, R.; Osanto, S., Microparticle-associated tissue factor activity: A link between cancer and thrombosis? AACR: 2006.

121. Muller, I.; Klocke, A.; Alex, M.; Kotzsch, M.; Luther, T.; Morgenstern, E.; Zieseniss, S.; Zahler, S.; Preissner, K.; Engelmann, B., Intravascular tissue factor initiates coagulation via circulating microvesicles and platelets. *The FASEB Journal* **2003,** *17* (3), 476-478.

122. Welsh, J.; Smith, J.; Yates, K.; Greenman, J.; Maraveyas, A.; Madden, L., Tissue factor expression determines tumour cell coagulation kinetics. *International journal of laboratory hematology* **2012,** *34* (4), 396-402.

123. Ettelaie, C.; Collier, M. E.; Featherby, S.; Benelhaj, N. E.; Greenman, J.; Maraveyas, A., Analysis of the potential of cancer cell lines to release tissue factor-containing microvesicles: correlation with tissue factor and PAR2 expression. *Thrombosis journal* **2016,** *14* (1), 2.

124. Marquette, C. A.; Blum, L. J., Chemiluminescent enzyme immunoassays: a review of bioanalytical applications. *Bioanalysis* **2009,** *1* (7), 1259-1269.

125. Canziani, G.; Zhang, W.; Cines, D.; Rux, A.; Willis, S.; Cohen, G.; Eisenberg, R.; Chaiken, I., Exploring biomolecular recognition using optical biosensors. *Methods* **1999,** *19* (2), 253-269.

126. Lakshmanan, R. S.; Efremov, V.; O'Donnell, J. S.; Killard, A. J., Measurement of the viscoelastic properties of blood plasma clot formation in response to tissue factor concentration-dependent activation. *Analytical and bioanalytical chemistry* **2016,** *408* (24), 6581-6588.

127. Chu, A. J., Tissue factor, blood coagulation, and beyond: an overview. *International journal of inflammation* **2011,** *2011*.

128. Gupta, R.; Goddard, N. J., A proof-of-principle study for performing enzyme bioassays using substrates immobilized in a leaky optical waveguide. *Sensors and Actuators B: Chemical* **2017,** *244*, 549-558.

129. Ibrahim, I. A.; Zikry, A.; Sharaf, M. A., Preparation of spherical silica nanoparticles: Stober silica. *J. Am. Sci* **2010,** *6* (11), 985-989.

130. Stöber, W.; Fink, A.; Bohn, E., Controlled growth of monodisperse silica spheres in the micron size range. *Journal of colloid and interface science* **1968,** *26* (1), 62-69.

131. Hoyt, L., New table of the refractive index of pure glycerol at 20 C. *Industrial & Engineering Chemistry* **1934,** *26* (3), 329-332.

132. Zhang, Y.; Zhang, M., Calcium phosphate/chitosan composite scaffolds for controlled in vitro antibiotic drug release. *Journal of Biomedical Materials Research Part A* **2002,** *62* (3), 378-386.

133. Rao, K. S.; El-Hami, K.; Kodaki, T.; Matsushige, K.; Makino, K., A novel method for synthesis of silica nanoparticles. *Journal of colloid and interface science* **2005,** *289* (1), 125-131.

134. Webb, C. E.; Jones, J. D., *Handbook of Laser Technology and Applications: Laser design and laser systems*. CRC Press: 2004; Vol. 2.

135. Hariharan, P., Interferometers in handbook of optics. McGraw-Hill Companies, Inc., New York: 1996.

136. Wen, Y.; Qu, W.; Cheng, H.; Asundi, A. In *Three-dimensional imaging of microstructures by an improved compact digital holographic microscope (ICDHM) with dual wavelength*, International Conference on Optical and Photonic Engineering (icOPEN 2015), International Society for Optics and Photonics: 2015; p 95242M.

137. Bobinger, M.; Angeli, D.; Colasanti, S.; La Torraca, P.; Larcher, L.; Lugli, P., Infrared, transient thermal, and electrical properties of silver nanowire thin films for transparent heaters and energy‐efficient coatings. *physica status solidi (a)* **2017,** *214* (1).

138. Wood, S.; Kirkham, J.; Marsh, P.; Shore, R.; Nattress, B.; Robinson, C., Architecture of intact natural human plaque biofilms studied by confocal laser scanning microscopy. *Journal of Dental Research* **2000,** *79* (1), 21-27.

139. Alirezaei, S.; Monirvaghefi, S.; Saatchi, A.; Ürgen, M.; Kazmanlı, K., Novel investigation on tribological properties of Ni–P–Ag–Al2O3 hybrid nanocomposite coatings. *Tribology International* **2013,** *62*, 110-116.

140. Vashist, S. K., Comparison of 1-ethyl-3-(3-dimethylaminopropyl) carbodiimide based strategies to crosslink antibodies on amine-functionalized platforms for immunodiagnostic applications. *Diagnostics* **2012,** *2* (3), 23-33.

141. Akkoyun, A.; Bilitewski, U., Optimisation of glass surfaces for optical immunosensors. *Biosensors and Bioelectronics* **2002,** *17* (8), 655-664.

142. Dou, Y. H.; Haswell, S. J.; Greenman, J.; Wadhawan, J., Voltammetric immunoassay for the detection of protein biomarkers. *Electroanalysis* **2012,** *24* (2), 264-272.

143. East, D. A.; Mulvihill, D. P.; Todd, M.; Bruce, I. J., QD-antibody conjugates via carbodiimide-mediated coupling: a detailed study of the variables involved and a possible new mechanism for the coupling reaction under basic aqueous conditions. *Langmuir* **2011,** *27* (22), 13888-13896.

144. Zhang, D.; Zhou, W.; Wei, B.; Wang, X.; Tang, R.; Nie, J.; Wang, J., Carboxyl-modified poly (vinyl alcohol)-crosslinked chitosan hydrogel films for potential wound dressing. *Carbohydrate polymers* **2015,** *125*, 189-199.

145. Teste, B.; Vial, J.; Descroix, S.; Georgelin, T.; Siaugue, J.-M.; Petr, J.; Varenne, A.; Hennion, M.-C., A chemometric approach for optimizing protein covalent immobilization on magnetic core–shell nanoparticles in view of an alternative immunoassay. *Talanta* **2010,** *81* (4-5), 1703-1710.

146. Nandanan, E.; Jana, N. R.; Ying, J. Y., Functionalization of gold nanospheres and nanorods by chitosan oligosaccharide derivatives. *Advanced Materials* **2008,** *20* (11), 2068-2073.

147. Jung, Y.; Jeong, J. Y.; Chung, B. H., Recent advances in immobilization methods of antibodies on solid supports. *Analyst* **2008,** *133* (6), 697-701.

148. Davies, D. R.; Padlan, E. A.; Sheriff, S., Antibody-antigen complexes. *Annual review of biochemistry* **1990,** *59* (1), 439-473.

149. Dancil, K.-P. S.; Greiner, D. P.; Sailor, M. J., A porous silicon optical biosensor: detection of reversible binding of IgG to a protein A-modified surface. *Journal of the American Chemical Society* **1999,** *121* (34), 7925-7930.

150. Viola, R. E.; Cleland, W., Use of pH studies to elucidate the chemical mechanism of yeast hexokinase. *Biochemistry* **1978,** *17* (20), 4111-4117.

151. Kiernan, J. A., Formaldehyde, formalin, paraformaldehyde and glutaraldehyde: what they are and what they do. *Microscopy today* **2000,** *1* (5), 8-12.

152. Öztop, H. N.; Saraydin, D.; Cetinus, Ş., pH-sensitive chitosan films for baker's yeast immobilization. *Applied biochemistry and biotechnology* **2002,** *101* (3), 239-249.

153. Helm, C. A.; Knoll, W.; Israelachvili, J. N., Measurement of ligand-receptor interactions. *Proceedings of the National Academy of Sciences* **1991,** *88* (18), 8169-8173.

154. Haas, S. L.; Jesnowski, R.; Steiner, M.; Hummel, F.; Ringel, J.; Burstein, C.; Nizze, H.; Liebe, S.; Löhr, J. M., Expression of tissue factor in pancreatic adenocarcinoma is associated with activation of coagulation. *World journal of gastroenterology: WJG* **2006,** *12* (30), 4843.

155. Ueno, T.; Toi, M.; Koike, M.; Nakamura, S.; Tominaga, T., Tissue factor expression in breast cancer tissues: its correlation with prognosis and plasma concentration. *British journal of cancer* **2000,** *83* (2), 164.